NASA CR-120877

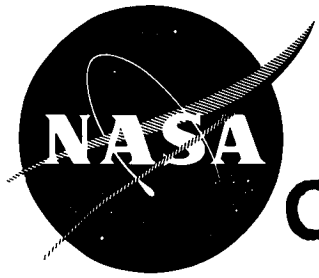

MODIFIED FUSED SILICIDE COATINGS FOR TANTALUM (Ta-10W) REENTRY HEAT SHIELDS

by

C. M. Packer and R. A. Perkins

LOCKHEED MISSILES & SPACE COMPANY, INC.

prepared for

NATIONAL AERONAUTICS AND SPACE ADMINISTRATION

NASA Lewis Research Center
Contract NAS 3-14316
John. P. Merutka, Project Manager

NOTICE

This report was prepared as an account of Government-sponsored work. Neither the United States, nor the National Aeronautics and Space Administration (NASA), nor any person acting on behalf of NASA:

A.) Makes any warranty or representation, expressed or implied, with respect to the accuracy, completeness, or usefulness of the information contained in this report, or that the use of any information, apparatus, method, or process disclosed in this report may not infringe privately-owned rights; or

B.) Assumes any liabilities with respect to the use of, or for damages resulting from the use of, any information, apparatus, method or process disclosed in this report.

As used above, "person acting on behalf of NASA" includes any employee or contractor of NASA, or employee of such contractor, to the extent that such employee or contractor of NASA or employee of such contractor prepares, disseminates, or provides access to any information pursuant to his employment or contract with NASA, or his employment with such contractor.

Requests for copies of this report should be referred to

National Aeronautics and Space Administration
Scientific and Technical Information Facility
P.O. Box 33
College Park, Md. 20740

1. Report No.	2. Government Accession No.	3. Recipient's Catalog No.
NASA CR-120877		

4. Title and Subtitle	5. Report Date
Modified Fused Silicide Coatings for Tantalum (Ta-10W) Reentry Heat Shields	April 15, 1973
	6. Performing Organization Code O/52-31
7. Author(s)	8. Performing Organization Report No.
Charles M. Packer and Roger A. Perkins	D316824
	10. Work Unit No.
9. Performing Organization Name and Address	
Lockheed Palo Alto Research Laboratory 3251 Hanover St. Palo Alto, Calif. 94304	11. Contract or Grant No. NAS 3-14316
	13. Type of Report and Period Covered Final Technical
12. Sponsoring Agency Name and Address	
National Aeronautics and Space Administration Washington, D.C. 20546	14. Sponsoring Agency Code

15. Supplementary Notes

Project Manager, John P. Merutka, NASA Lewis Research Center, Cleveland, Ohio

16. Abstract

This report presents the results of a program of research to develop a reliable, high-performance, fused slurry silicide coating for Ta-10W alloy. The effort was directed toward developing new and improved formulations for use at 2600° to 2800° F (1700° to 1811° K) in an atmospheric reentry thermal protection system with a 100-mission capability. Based on a thorough characterization of isothermal and cyclic oxidation behavior, bend transition temperatures, room- and elevated-temperature tensile properties, and creep behavior, a 2.5Mn-33Ti-64.5Si coating (designated MTS) provides excellent protection for the Ta-10W alloy in simulated reentry environments. An extensive analysis of the oxidation behavior and characteristics of the MTS coatings in terms of fundamental mechanisms is also presented.

17. Key Words (Suggested by Author(s))	18. Distribution Statement
Silicide Coatings Ta-10W Alloy Thermal Protection Systems Cyclic Oxidation Behavior Mechanical Properties Protective Mechanisms	Unclassified - unlimited

19. Security Classif. (of this report)	20. Security Classif. (of this page)	21. No. of Pages	22. Price*
Unclassified	Unclassified	195	$3.00

* For sale by the National Technical Information Service, Springfield, Virginia 22151

FOREWORD

This report covers work performed under Contract NAS 3-14316 for the period 16 June 1970 through 15 April 1973. The work was administered by the NASA-Lewis Research Center, Mr. John P. Merutka as Project Manager.

The report was prepared by Dr. Charles M. Packer and Mr. Roger A. Perkins of the Metallurgy and Composites Laboratory, Material Sciences Directorate, Lockheed Palo Alto Research Laboratory, Palo Alto, California. Research tasks were performed under the direction of Dr. Packer as Principal Investigator and Mr. Perkins as Program Manager. Dr. Henry W. Lavendel assisted in the formulation of coatings, and Mr. Earl K. Montgomery was responsible for specimen preparation and environmental exposures.

ABSTRACT

This report presents the results of a program of research to develop a reliable, high-performance, fused slurry silicide coating for the Ta-10W alloy. The effort was directed toward developing new and improved formulations for use at 2600° to 2800° F (1700° to 1811° K) in an atmospheric reentry thermal protection system with a 100-mission capability. Based on a thorough characterization of isothermal and cyclic oxidation behavior, bend transition temperatures, room- and elevated-temperature tensile properties, and creep behavior, a 2.5 Mn-33Ti-64.5Si coating (designated MTS) provides excellent protection for the Ta-10W alloy in simulated reentry environments. An extensive analysis of the oxidation behavior and characteristics of the MTS coating in terms of fundamental mechanisms also is presented.

CONTENTS

ILLUSTRATIONS

TABLES

SUMMARY

The objective of this program was to develop a reliable, high-performance fused slurry silicide coating for the Ta-10W alloy for use in an atmospheric reentry thermal protection system at temperatures of 2600° to 2800° F (1700° to 1811° K).

Initially, consideration of principles related to coating/substrate and coating/environment reactions led to the selection of 75 different compositions for evaluation. Of these, 21 were effectively applied to Ta-10W and their oxidation resistance was studied in cyclic oxidation tests at 2600° F (1700° K), 10 torr (13.33 hN/m^2) (1-hr cycle, 37 min at maximum temperature).

Two excellent coatings were produced from the 75 compositions studied. These were within the range of 2.5 to 10 Mn – 31 to 41 Ti – 54 to 57 Si. Although all compositions studied within this range had lifetimes exceeding 100 cycles at 2600° F (1700° K), 10 torr (13.33 hN/m^2), the best compositions for use in the temperature range of interest in this program were 2.5Mn-33Ti-64.5Si and 8Mn-31Ti-61Si. Of these, the 2.5Mn-33Ti-64.5Si composition had the better characteristics for the specific requirements of the program and was selected for extensive characterization. This composition was designated the MTS coating. Cobalt was added to the MnTiSi coatings with the objective of improving performance at higher temperatures and lower pressures. The composition 2.5Co-2.5Mn-32Ti-63Si was selected for characterization and was designated the CMTS coating.

Extensive oxidation characterization of the MTS and CMTS coatings showed that they have lifetimes of more than 200 hr under isothermal conditions at 2600° F (1700° K), 1.0 to 10 torr (1.33 to 13.33 hN/m^2) and cyclic lifetimes of over 100 cycles under these conditions. At 2600° F (1700° K), 1.0 torr (1.33 hN/m^2), 13 of 13 MTS specimens had lifetimes of more than 400 cycles. At higher temperatures and lower pressures, the coatings had more limited lifetimes. Statistical analyses of cyclic lifetime showed that the performance of both coatings was highly reliable (Figures I, II). The high reliability is shown by the steep slopes of the Weibull curves in these plots. These curves show the performance of the MTS and CMTS coatings at 2600° to 2800° F (1700° to 1811° K), 0.1 to 10 torr (0.13 to 13.33 hN/m^2).

The tensile strength and bend ductility are not influenced significantly by the environment during the lifetime of the coatings. The bend ductile-brittle transition temperature is below the liquid nitrogen temperature after exposure to temperatures and pressures in the range of interest to the program. In general, the bend, tensile, and creep properties of the MTS-coated Ta-10W in all conditions of exposure within the protective lifetime of the coating are comparable to those of the uncoated Ta-10W alloys. The tensile elongation data for Ta-10W as-coated and after cyclic oxidation exposure are summarized in Figures III and IV. The good ductility relative to the baseline data for uncoated Ta-10W illustrates the excellent protection afforded by these coatings.

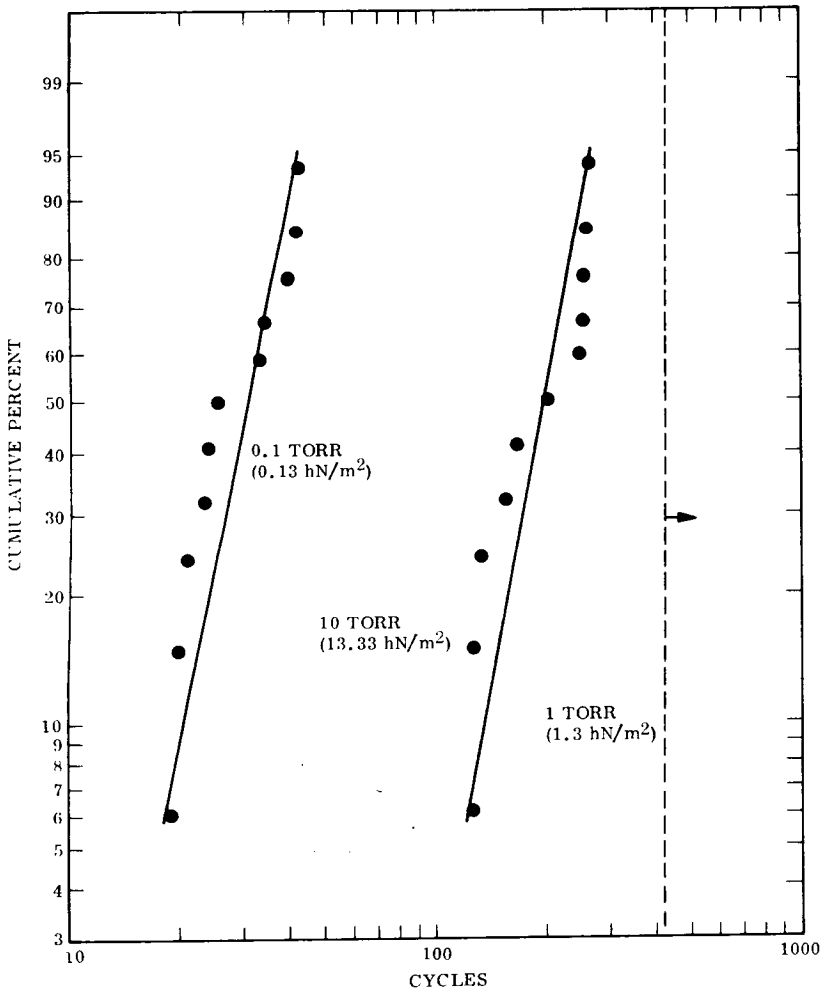

(a) At 2600°F (1700°K)

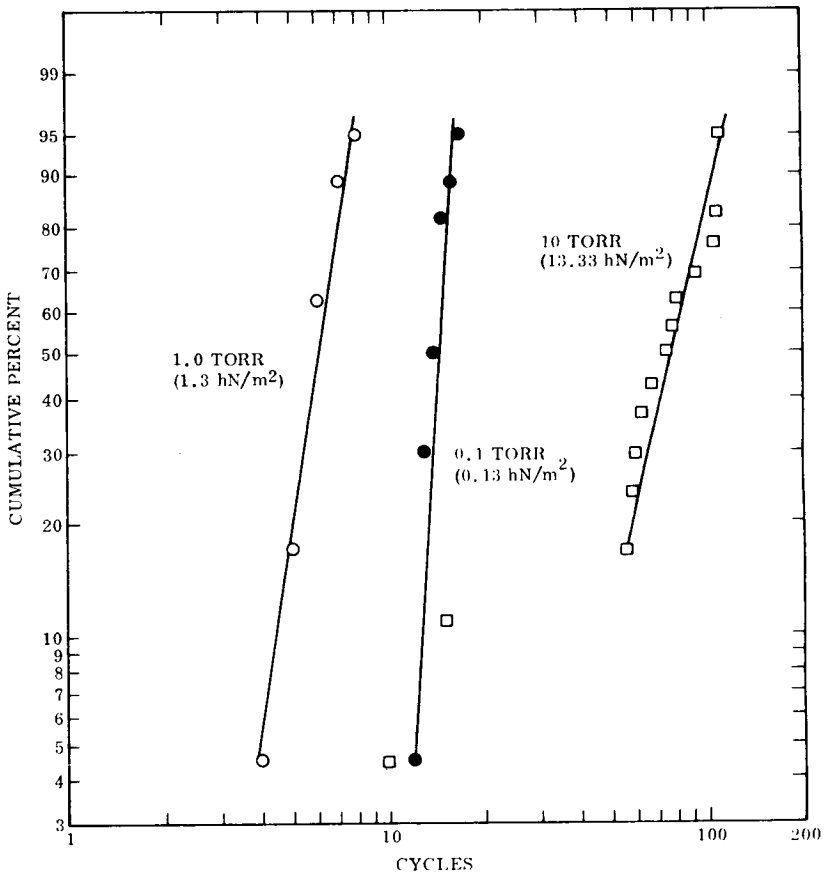

(b) At 2800°F (1811°K)

Figure I Weibull Plot of MTS Coating Performance

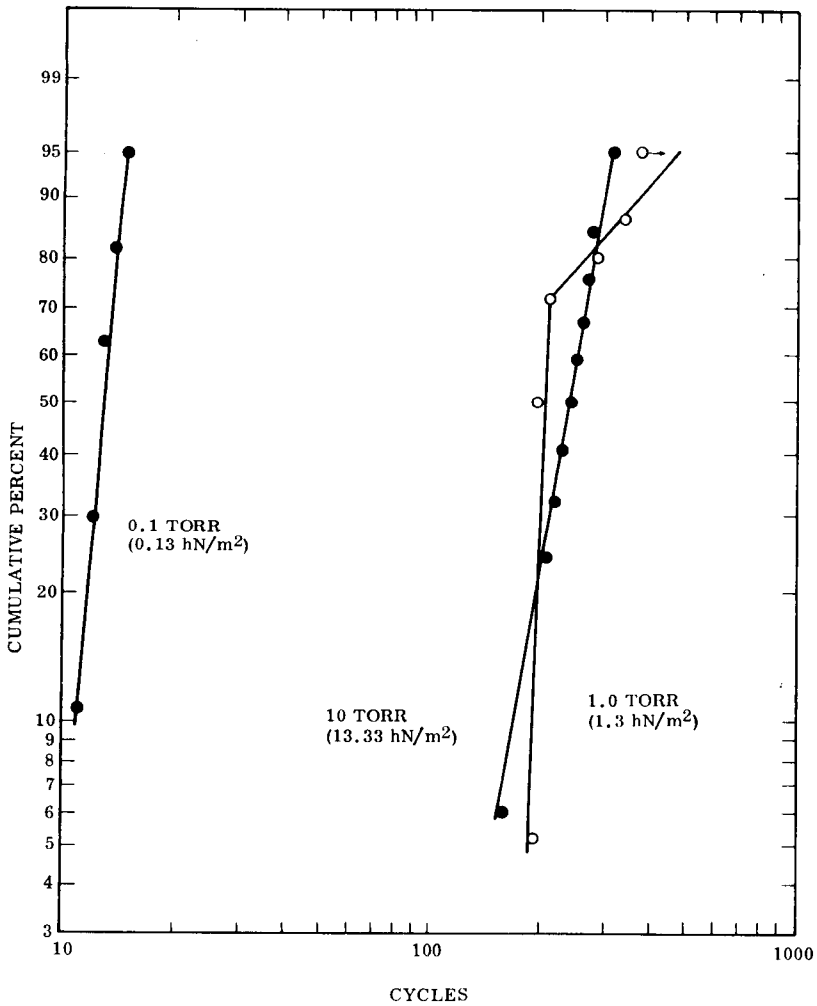

(a) At 2600°F (1700°K)

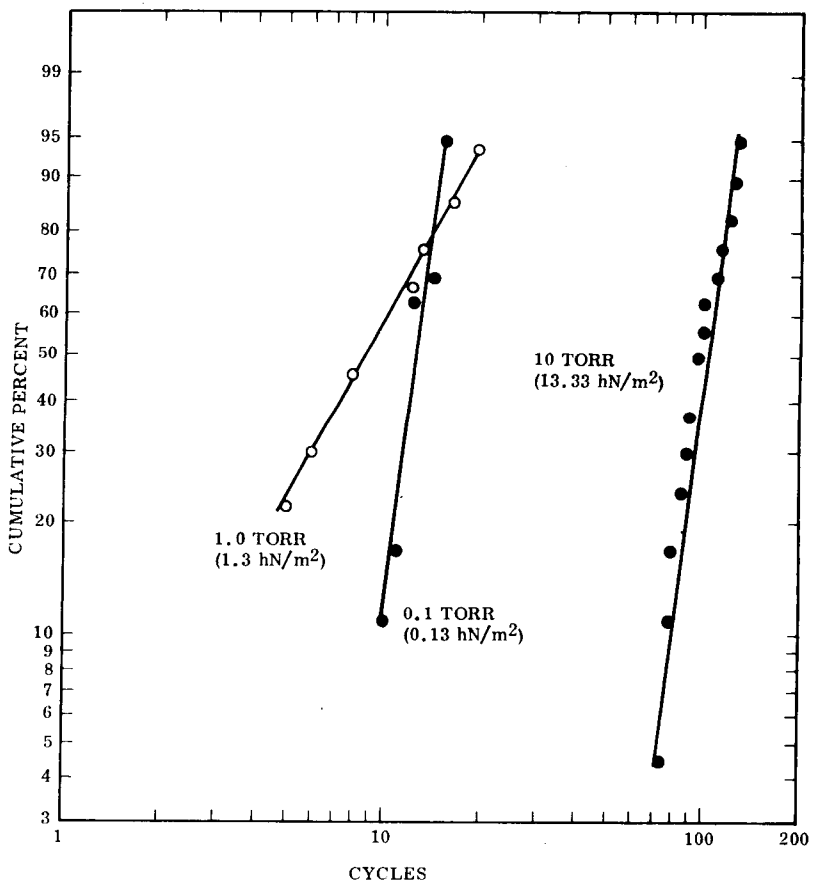

(b) At 2800°F (1811°K)

Figure II Weibull Plot of CMTS Coating Performance

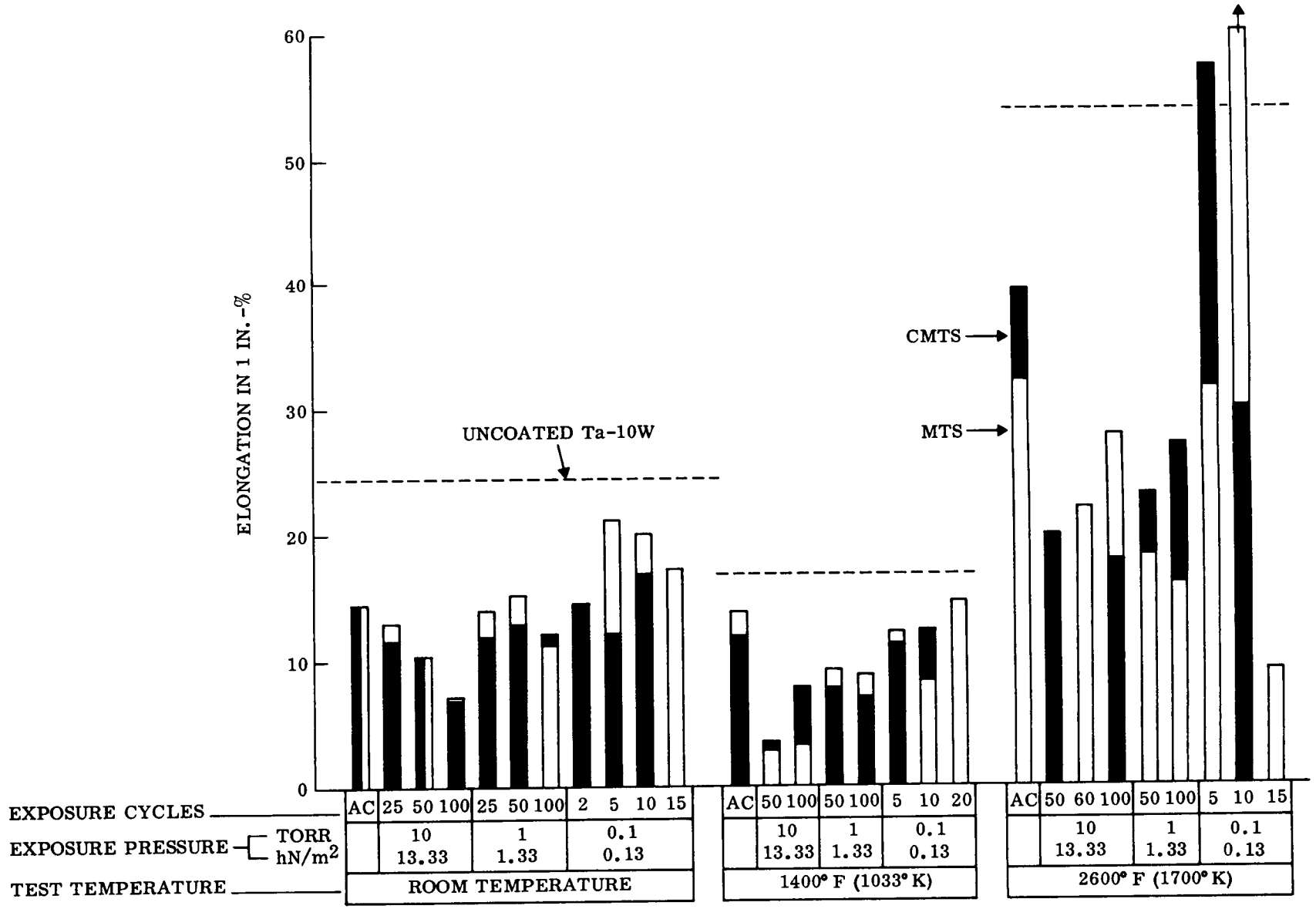

Figure III Effect of 2600° F (1700° K) Cyclic Exposure on Tensile Ductility of Coated Ta-10W.

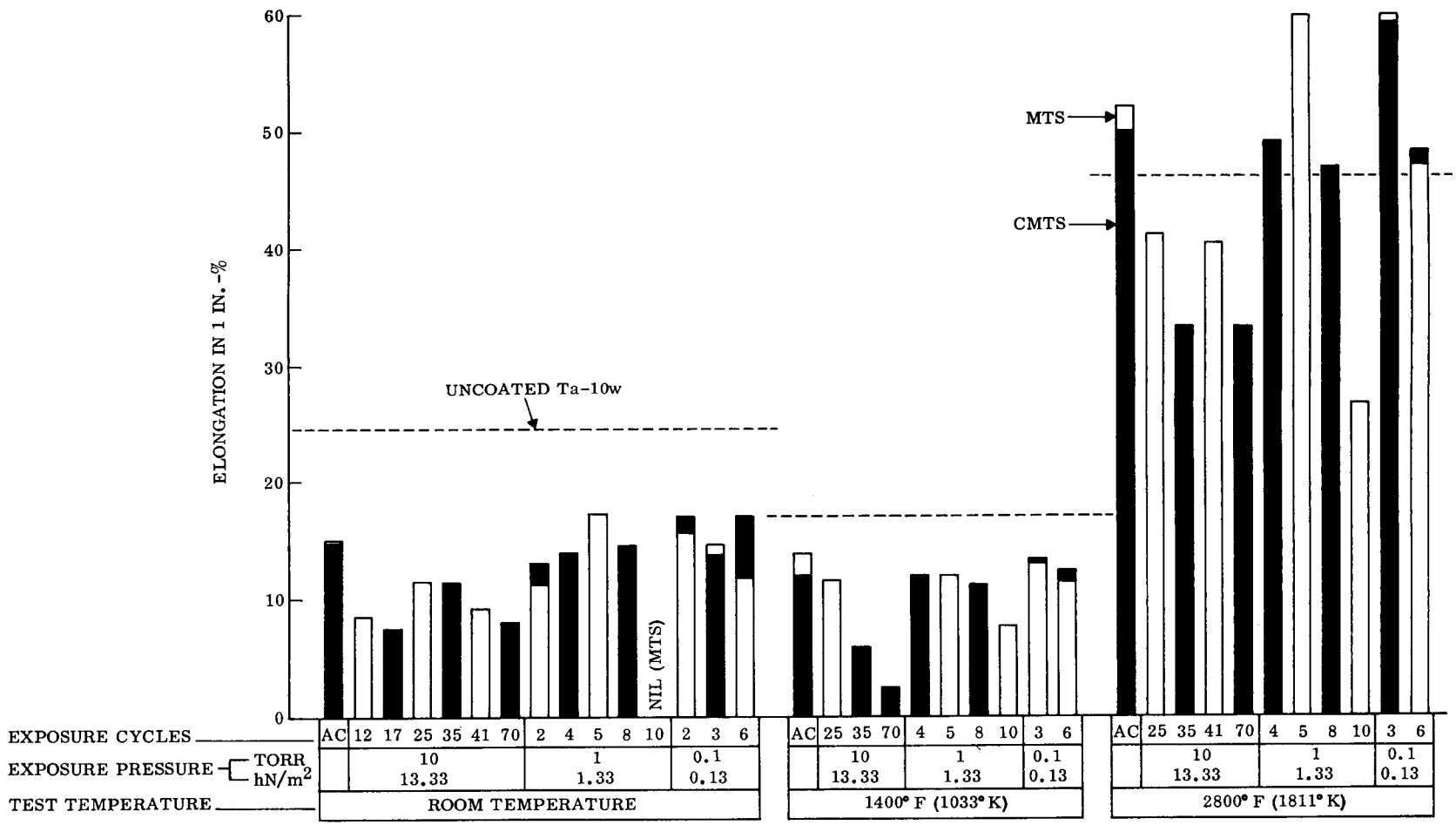

Figure IV Effect of 2800° F (1811° K) Cyclic Exposure on Tensile Ductility of Coated Ta-10W.

The emittance of both coatings reaches a high value of 0.85 to 0.95 early in the first cycle under environmental exposures in the 2600° to 2800° F (1700° to 1811° K) temperature range at pressures of 0.1 to 10 torr (0.13 to 13.33 hN/m^2). After initial exposure, the emittance of both coatings remains high and is not affected greatly by continued exposure or variations in the environment.

Both coatings can be applied conveniently to structural components having complex configurations in a single-step process using conventional slurry fusion coating technology. Miniature rib-stiffened heat-shield panels protected with these coatings were subjected to simulated atmospheric reentry exposures, and the performance of the coatings was the same as that during cyclic oxidation exposures with simple test specimens. Stress had no influence on the performance of coatings in the simulated reentry exposures. These coatings provide the same reliable protection for complex structural elements as they do for laboratory test coupons.

Detailed metallurgical analysis correlated the performance of the coatings with fundamental protection mechanisms. The coatings develop a thick, protective film of silica on the surface during the first few minutes of exposure and an outer layer of (Ti, Mn) O_2 that provide improved performance and high emittance in low-pressure environments. The as-coated structure and the oxide layer that has formed on the MTS coating after 30 min at 2600° F (1700° K), 10 torr (13.33 hN/m^2), are shown in Figure V. The early formation of a thick oxide layer is significant in the performance of these coatings because it provides a self-healing cover for the hairline fissures that exist in silicide coatings. Oxidation within these fissures on cyclic heating has a controlling effect on coating life. The thick oxide film provides an effective barrier which is responsible for the greatly increased cyclic life of these coatings.

A comparative analysis showed that the MTS coating is the better of the two coatings in that it provides more reliable protection at the edges of thin-gage sheet material. This coating provides absolute protection of the substrate until visible evidence of substrate oxidation appears on the surface. Once substrate oxidation appears on the surface, however, the coating protection degrades rapidly at the site and can no longer prevent or stop substrate oxidation.

Conventional fusion coating equipment and procedures can be used in the application of the MTS and CMTS coatings. Limited process development work will be required for scale-up to full-size structural components.

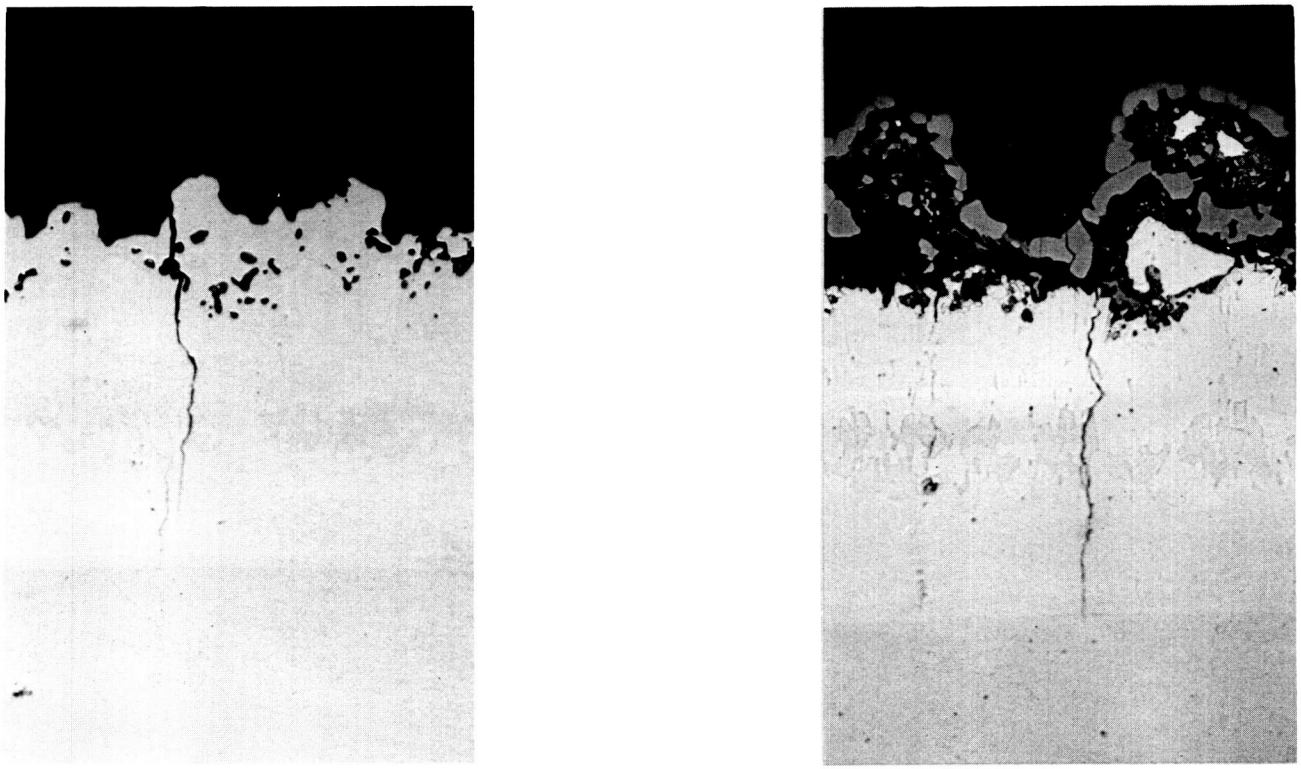

As-Coated

30 min, 2600° F (1700° K),
10 torr (13.33 hN/m^2)

Figure V Structure of the MTS Coating in the As-Coated Condition and After Oxidation Exposure. 500 ×. Note the amount of oxide layer that has formed in 30 min.

INTRODUCTION

A radiative thermal-protection system attached to a load-carrying substructure is an attractive design concept for a reusable, economical Space Shuttle vehicle. From the standpoint of cost effectiveness and performance, the entire system must be designed for maximum use with minimum repair and refurbishment. Currently, a goal of 100 missions (reentry cycles) is sought for all major components of the thermal-protection system.

A large portion of the structure will operate in a temperature range where conventional high-temperature metals and alloys can be used effectively to meet such a requirement. In many regions, however, temperatures will exceed limits for these materials, and higher melting point metals such as columbium and tantalum alloys will be required. Although most of these requirements can be handled effectively by coated columbium alloys, temperatures in a few areas will exceed 2500° F (1643° K); in such cases, the alloys of tantalum become attractive candidates. Like columbium, these materials must be protected by oxidation-resistant coatings.

Although considerable effort has been expended over the past 10 years to develop suitable coatings for tantalum and its alloys, no satisfactory solution to the problem of oxidation protection by coating has been found. The few coating systems currently available either do not offer an adequate lifetime during Space Shuttle reentry conditions or are not particularly adaptable to the manufacture of heat-shield components. The latter factor is of major concern because complex assemblies must be coated reproducibly with a uniform, high-quality coating to achieve required levels of reliability. On the basis of extensive studies with columbium alloys and limited experience with tantalum, the fused slurry silicide coatings appear to offer the best potential for meeting basic requirements.

Background

The first generation of coatings for tantalum alloys was based on $TaSi_2$ applied by pack cementation techniques (refs. 1 and 2). Limited lifetimes in intermediate temperature ranges were a problem that could not be solved, however, because only simple disilicide coatings could be applied by the pack cementation process. The subsequent development of fused slurry processes provided a means for composition adjustment needed to solve this problem.

Stetson et al. (refs. 3, 4, and 5) postulated that different thermal expansivities of the coating and the substrate were responsible for many of the problems with silicide coatings on tantalum and attempted to design coatings with more compatible thermal expansivities. Their approach was to apply, by slurry-sinter techniques, a metallic surface modifier that subsequently was siliconized to produce an alloy silicide coating with greatly improved behavior. These second-generation silicide coatings were based on Mo-W-Ti-V modifier alloys. The results indicated that vanadium was useful for improved performance at intermediate temperatures and that titanium improved the high-temperature oxidation resistance. The role of tungsten and molybdenum was postulated to be one of reducing the differences in thermal expansitivity.

These coatings provide good slow-cycle oxidation resistance at 1600° and 2600° F (1144° and 1700°K). The behavior of these coating systems in simulated reentry environments has not yet been characterized adequately, but the major limitation appears to be the method of application. The final step is pack siliconizing, a technique that is not adaptable to the manufacture of large and complex heat-shield assemblies.

The Vitro Laboratories have developed a somewhat different family of coatings for tantalum, based on electrophoretic deposition of mixed silicides (refs. 6, 7, and 8). Vitro found that $MoSi_2$ in conjunction with VSi_2 and $TiSi_2$ or $CrSi_2$ provided the best protection for tantalum at 1500° and 2400° F (1089° and 1589°K). Coatings based on WSi_2 were found to have limited performance at intermediate temperatures. Vanadium disilicide was judged to be the best addition for improving intermediate temperature performance. Best results were obtained by applying a VSi_2 undercoating with an $MoSi_2$+$TiSi_2$ or $CrSi_2$ overlayer in a two-step process. The VSi_2 layer is dense; the overlayer is porous. The comparative roles of coating composition and coating structure in providing protection were not defined clearly. Performance was evaluated on visual evidence of coating wearout. Although substrate oxidation was not visible in 400 hr, sufficient leakage of oxygen through the coating occurred to embrittle the substrate. Excessive porosity of the coating may be a contributing factor in this aspect of behavior.

The first fused slurry coatings for tantalum were based on the Sn-Al system (refs. 9, 10, and 11). Although good resistance to oxidation over a very broad temperature and pressure range was achieved, the rapid interdiffusion of aluminum and tantalum at high temperature, the high volatility of tin, surface fluidity, and the reactivity of molten tin place undesirable limitations on the use of this system in reentry heat-shield applications. As a result, effort was shifted to development of a fused slurry silicide coating for tantalum (ref. 12). A Si-20Ti-10Mo formulation evolved as the most promising system for tantalum. The effort applied to the development was minor compared with the effort for development of a coating of columbium (ref. 12). As a result, the existing formulation is not necessarily optimum, and the coating system has not been adequately characterized.

A third type of slurry coating that has been proposed for tantalum is based on an overlay of oxidation-resistant elements or alloys. Major interest has centered on the Hf-20Ta alloys (refs 13, 14, and 15). These coatings, in general, have shown rather poor performance in screening tests and do not appear to have sufficient potential for further consideration at this time. The slurry process employed by Hill and Rausch for applying these coatings (ref. 14) is of some interest, however. These investigators used a fugitive Cu-Al molten vehicle to carry the Hf-Ta particles. The vehicle was slowly withdrawn, by heating in a vacuum, to leave a dense sintered coating.

It is significant that by and large the rationale for development of coatings for tantalum is based on what has happened with columbium. With one or two exceptions, fundamental considerations of coating behavior, coating substrate interactions, and service requirements have not been taken into account in developing most of the existing formulations. There is, in fact, no sound fundamental basis for the current compositions of fused slurry silicide coatings on either columbium or tantalum alloys; the rationale for these coatings is principally "persuasive empirical evidence such as the success of the duplex vacuum pack Ti-Cr-Si coating for columbium" (ref. 11).

Objective

The objective of this program was to improve the oxidation resistance and reliability of fused slurry silicide coatings for the tantalum alloy Ta-10W. Efforts were directed toward developing a coating usable from 2600° to 2800° F (1700° to 1811° K) in a thermal protection system for the proposed Space Shuttle with a 100-mission capability. Specifically, the program was designed to (1) provide a comparative evaluation of a variety of coating compositions with respect to oxidation and mechanical behavior, (2) further evaluate the most promising systems under cyclic oxidation conditions, and (3) demonstrate the applicability and performance of these coatings on miniature heat-shield panels under simulated environmental reentry conditions.

Technical Approach

Initially, a series of experimental coating compositions was selected on the bases of several coating application and coating protection concepts. These concepts were based on fundamental principles related to coating/substrate and coating/environment reactions. Evaluation of these experimental coating compositions included the practicality of application; the structure of the coating; and, for coatings that were appropriately applicable, oxidation screening tests under cyclic temperature conditions. These screening tests were conducted in air at 10 torr (13.33 hN/m^2) at a maximum temperature of 2600° F (1700° K).

Analysis of the results of evaluation of the experimental coatings led to the selection of three developmental coating systems. Adjustments were made to the composition of these developmental systems, and the influence of coating application process variables on coating structure and performance was studied. The performance was evaluated under cyclic temperature conditions at temperatures in the range of 2600° to 2800° F (1700° to 1811° K) and air pressures in the range of 0.1 to 10 torr (0.13 to 13.33 hN/m^2). An analysis of the structure and performance of all the compositions and process variable combinations provided the basis for selection of the two best coating compositions and optimized coating application procedures for extensive characterization.

The extensive characterization of the two best coatings included the oxidation resistance and emittance of the coatings, the mechanical properties of the substrate/coating composites, the applicability of the coatings to structural components, the performance of coated structural components in simulated reentry environments, and detailed metallurgical analyses. Specifically, the performance of the coatings was evaluated under isothermal and cyclic temperature conditions at 2600° to 2800° F (1700° to 1811° K), 0.1 to 10 torr (0.13 to 13.33 hN/m^2). The cyclic temperature exposures included a sufficient number of test specimens for a statistical analysis of the performance of the coatings. The coating emittance and substrate/coating composite mechanical properties were determined as a function of exposure time at these temperatures and pressures. The mechanical properties included room-temperature and elevated-temperature tensile properties and bend ductile-brittle transition temperature. In addition, creep properties were determined with as-coated material. Further characterization included the evaluation of coating tolerance to intentional damage. Coatings were applied to structural components in the form of miniature heat-shield panels, and the structure of the coatings was analyzed, with emphasis on the regions of the panels that contained complex configurations. These panels were subjected to simulated reentry environmental exposures where temperature as well as stress was cycled.

Metallurgical studies defined the composition and phase distribution of the coatings before and after exposure to environmental conditions. In addition, the influence of several environmental variables on the structure of the coatings was evaluated. In these studies, the effects of temperature, pressure, and level of cyclic exposure were analyzed in terms of fundamental considerations of coating behavior, to establish a rationale for coating performance.

Finally, a comparative analysis of the performance of the two coatings reviewed all the experimental results and metallurgical studies. On the basis of this comparative analysis, one coating was selected as the best coating for tantalum alloys developed during this program.

MATERIALS AND TEST SPECIMENS

Substrate Material

The substrate material was the alloy Ta-10W* which was in sheet form, 0.013 in. (0.033 cm) thick. Four different lots of Ta-10W were used during the course of the investigation. The range of ingot compositions of the Ta-10W is presented in Table 1.

TABLE 1. – COMPOSITION RANGE OF Ta-10W
(Ingot Composition)

[Values in weight percent.]

Element	Top	Bottom
W	9.6–10.6	10.4
Ta	Balance	Balance
	Ingot analysis, ppm	
Cb	283–597	344–709
Co	<10	<10
Fe	240	<40
H	<5	<5
Mo	<20	<20
Ni	<20	<20
O	<50	<50
N	8–25	8–25
C	<30	<30

Coating Input Powders

The powders used in slurry preparation were both elemental materials and compounds. In most cases the powders were -325 mesh; however, a few elemental powders were somewhat larger, up to -200 mesh. Formulations containing titanium were prepared using TiH because studies showed that, similar to the conclusions reached in other investigations, the use of the hydride led to better coatings. The hydride dissociates during the fusion heat treatment, leaving a clean, highly reactive titanium powder. Some studies required the use of prealloyed powders. The preparation of these materials consisted of pressing elemental powders into a compact and arc melting several times in a helium atmosphere. A mortar and pestle enabled the comminution of the resulting ingot into -325 mesh powder.

*Obtained from Teledyne Wah Chang Albany, Albany, Oregon.

Specimen Preparation

Specimens included those for screening tests, statistical and baseline studies, tensile and creep tests, bend ductile-brittle transition temperature determinations, and emittance measurements. Two groups of miniature heat shield panels were prepared, one group for testing and the other for delivery to NASA. In addition, two types of plasma arc test samples were prepared for testing by NASA.

The screening, statistical, baseline, and bend specimens were 1/2 by 4 in. (1.3 by 10.2 cm). Tensile specimens were 4 in. (10.2 cm) long with 3/4 in. (1.9 cm) wide shoulders and a 1-1/4 by 1/4 in. (3.2 by 0.6 cm) gage length. The tensile axis was parallel to the sheet rolling direction. Emittance specimens were 1/4 by 4 in. (0.6 by 10.2 cm). The designs of the miniature heat shield panels are shown in Figures 1 and 2, and the designs of the plasma arc test samples in Figures 3 and 4.

Electron-beam welding was the method used to fabricate the miniature heat shield panels. Specially designed molybdenum fixtures supported panel components and an electron beam passed along the top of T-sections. The voltage was 15 kV; the current, 50 mA; the beam travel speed, 30 in. (76.2 cm)/min; and the pressure, 10^{-4} torr (0.013 N/m^2). The cross sections of the weld region before and after welding are shown schematically in Figure 5.

Coatings will wear out prematurely if edges and corners are not properly prepared; therefore, particular attention was given to the preparation of these regions. All corners were rounded by hand, and edges were rounded by vibratory finishing with Al_2O_3 triangular shapes. Chemical etching was the final step in preparing edges as well as surfaces; the etchant was 2 parts H_2SO_4, 2 parts HNO_3, and 1 part HF. Weights and dimensions were recorded for all specimens after etching.

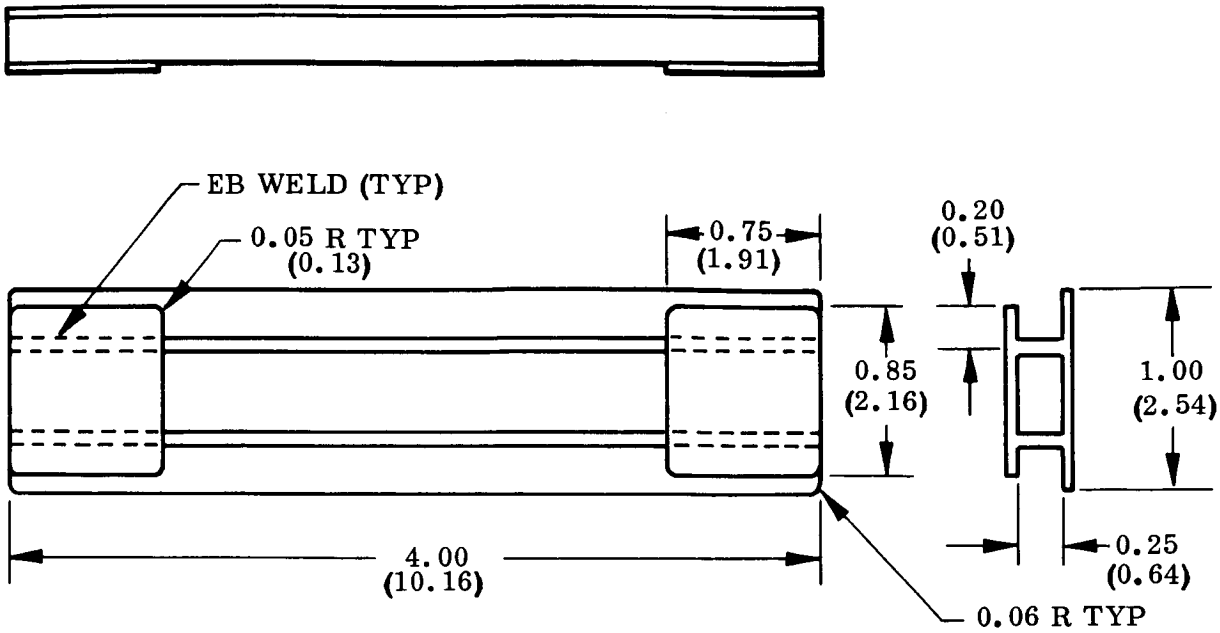

DIMENSIONS IN INCHES (CENTIMETERS)

Figure 1 Miniature Rib-Stiffened Heat Shield Panel for Delivery to NASA.

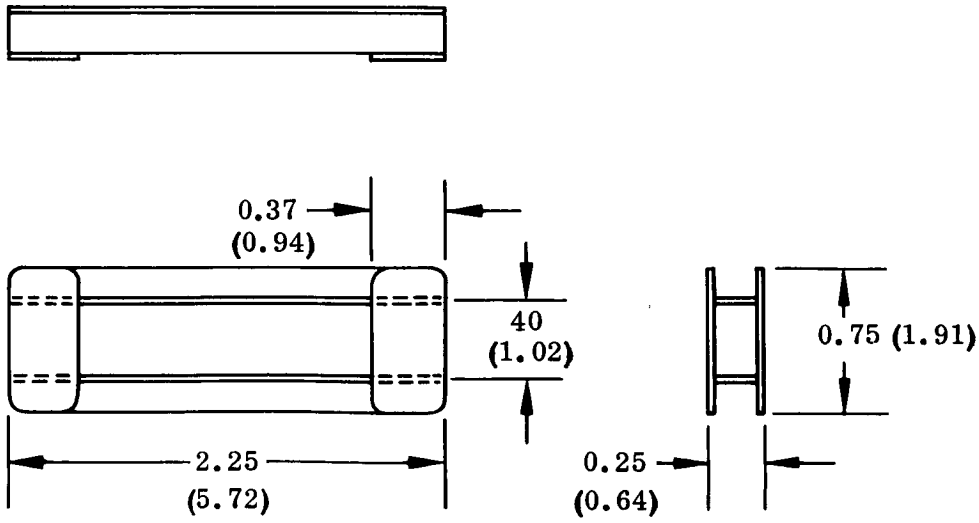

DIMENSIONS IN INCHES (CENTIMETERS)

Figure 2 Miniature Rib-Stiffened Heat Shield Panel for Oxidation Testing.

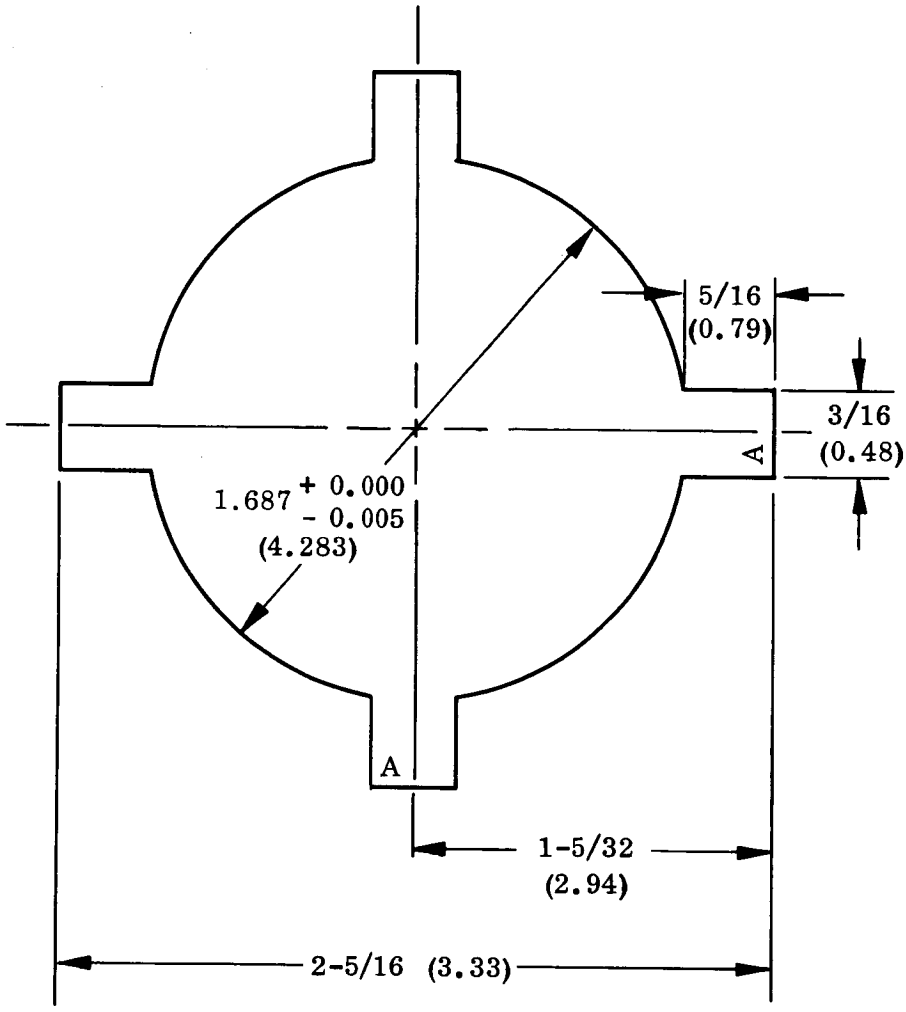

DIMENSIONS IN INCHES (CENTIMETERS)

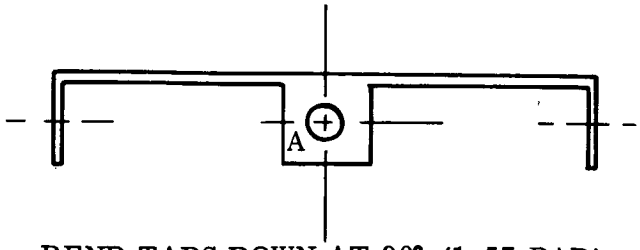

BEND TABS DOWN AT 90° (1.57 RAD)
EDGE VIEW

Figure 3 Plasma-Arc Test Sample for Delivery to NASA (Single-Piece Stagnation Model).

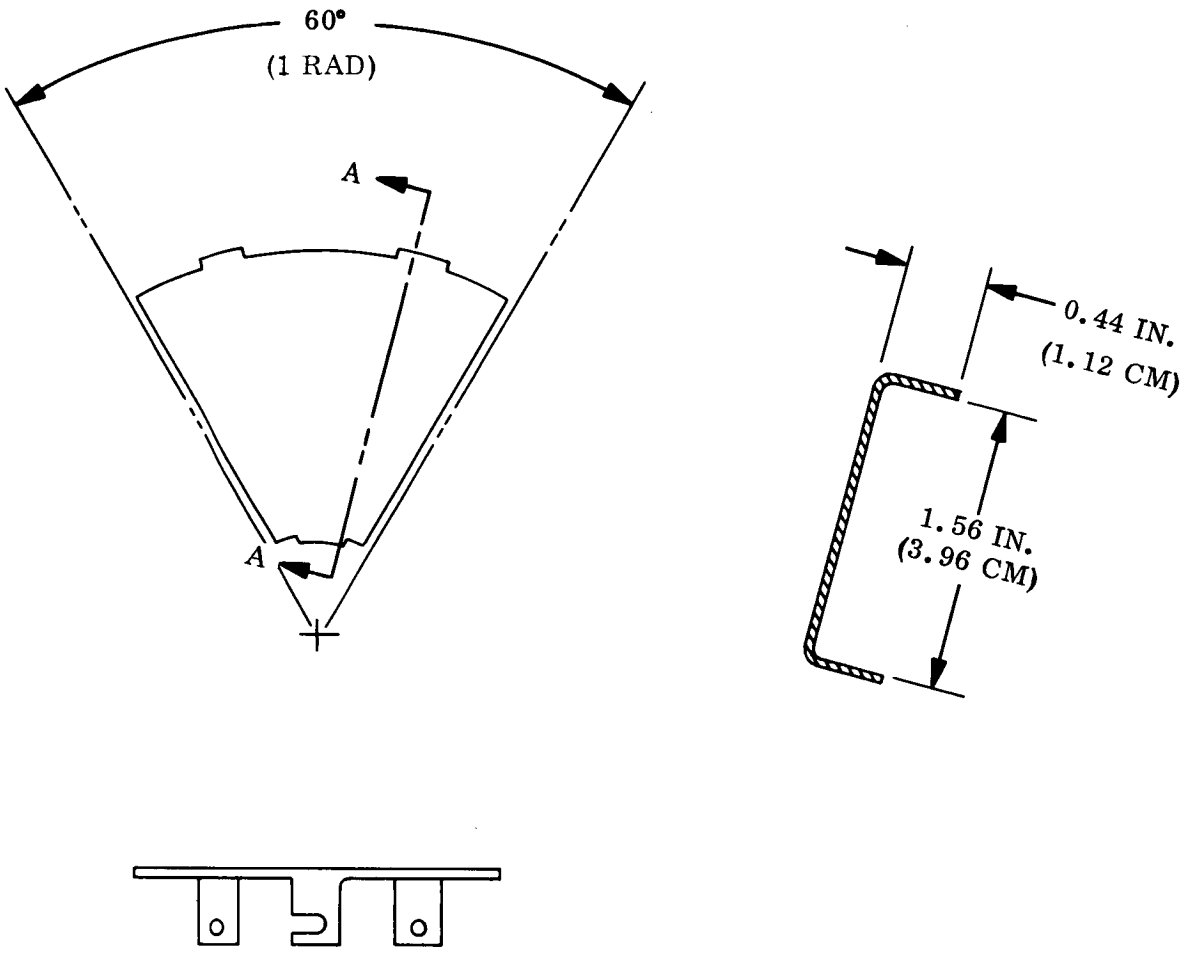

Figure 4 Plasma-Arc Test Sample for Delivery to NASA.

(a) Before Welding

(b) After Welding

DIMENSIONS IN INCHES (CENTIMETERS)

Figure 5 Cross Section of the Weld Region Before and After Welding.

PROCEDURES AND EQUIPMENT

Coating Application

In this section, the procedures for slurry preparation, as well as slurry application, fusion, and coating inspection, are discussed in general terms applicable to all the coatings evaluated during the program. In Appendix A, a specification is presented which describes in detail the application of the best coatings developed in this program.

- Slurry Preparation

Slurry preparation consisted of blending appropriate proportions of powders of the desired coating constituents with an organic vehicle. The viscosity and stability of viscosity of the slurry, as well as the uniformity of the slurry, were the significant criteria in developing a procedure for slurry preparation. The organic vehicle initially used was the Solar E-4 vehicle (ref. 4) but the viscosity decreased rapidly and settling of the powders occurred within 12 hr after preparation. Further studies led to use of the Raffi and Swanson L-18 vehicle (ref. 5). These studies showed that the stability of slurries prepared with this vehicle was excellent and that an additive of Baker MPA mineral spirits prevented settling.

Additional studies included the variation of solid-to-liquid ratios to establish a ratio for the proper slurry viscosity for the application of slurries by dipping or by spraying. The results showed that a solid:liquid ratio of 1:2 (by weight) provided a viscosity of 3,500 to 5,000 cps (3.5 to 5 Nsec/m^2), suitable for dipping, and a ratio of 1:1 provided a viscosity of 1,000 cps (1 Nsec/m^2), suitable for spraying.

A planetary ball mill provided the means of blending slurries. The blending time was 1 hr. Some preliminary studies showed that use of a conventional ball mill was unsatisfactory because some powder agglomerates remained in the slurry.

- Slurry Application

In the early part of the program, dipping with a controlled withdrawal rate was the method used to apply slurries to specimens. A withdrawal rate of 5 in./min (12.7 cm/min) provided a coating thickness of about 0.003 in. (0.008 cm). The dipping method has certain disadvantages, however. The withdrawal rate is highly dependent upon the slurry viscosity, and if the green coating is too thin, it is difficult to redip the specimens and withdraw at the proper rate to increase the thickness to the desired values. If the green coating is too thick, the slurry must be removed and reapplied. Furthermore, and more important, the dipping process is less effective than spraying when coating some complex configurations, particularly those having right-angle corners.

Consequently, for the major part of the program, coating application consisted of spraying the slurry on specimens with an airbrush. The number of passes per side was 10 to

15. The coating weight was an index of the coating thickness, and by weighing the specimen periodically between passes, the gradual application of the slurry furnished a means of attaining the appropriate thickness efficiently.

Green coating thickness uniformity was determined by means of nondestructive testing instruments, using eddy current techniques. A Dermitron Nondestructive Thickness Tester was used during most of the program. In the early stages of the program, an Inductotest Thickness Tester provided measurements of thickness uniformity.

- Slurry Fusion

A cold-wall, vacuum or inert gas, induction furnace served as a facility for fusion of the coatings. The furnace included a 12 in. (30 cm) by 4 in. (10 cm) diameter tantalum susceptor which had in its central region a 4 in.(10 cm) long, uniform-temperature hot zone. Alumina rods supported the specimens within the susceptor. A Pt-Pt Rh thermocouple, which was in a thin-wall Al_2O_3 tube within the susceptor, measured the temperature and provided input to a Datatrak controller that, with the use of a programmed time-temperature schedule, controlled the heating rate, fusion temperature, time of temperature, and cooling rate. The environment during fusion was either vacuum, $\sim 10^{-5}$ torr (0.0013 N/m^2), or helium, depending upon the coating system. With coating formulations containing highly volatile elements, such as manganese, the use of helium minimized the loss of these constituents.

- Coating Inspection

Inspection of all samples after fusion included macroscopic observation using a binocular microscope and nondestructive testing using either the Dermitron or Inductotest eddy current instruments. The principal factors observed were coating uniformity, completion of fusion, the nature of the coating at the edges, and, in the case of panels and plasma-arc specimens, the quality of the coating at joints and corners. Weighing of all specimens furnished data for the determination of coating weight per unit area. In addition, the dimensions of all specimens were measured after coating.

Metallographic analyses provided a further means of coating evaluation after application of the coating as well as after exposure to oxidation. Small pieces of a phenolic material adjacent to the specimen, which was in a Bakelite mount, afforded excellent edge preservation. Use of the phenolic material made possible clear examination of the coating structure at the surface at magnifications up to 3,000×. Metallographic samples were prepared by conventional metallographic practices through the step of polishing with 1-μm diamond paste. Final polishing included the use of an automatic polishing device containing a slurry of Finish-Pol metallographic polishing abrasive and 35 g of potassium ferrocyanide, $K_3Fe(CN)_6$; 2 g of sodium hydroxide, NaOH; and 150 ml of water. The etchant was 7.5 parts hydrofluoric acid, HF; 2.5 parts nitric acid, HNO_3; and 100 parts water; the etching time was 10 to 60 sec.

Oxidation Testing

Initially, the furnace for oxidation screening tests, which required temperature cycling, consisted of a 15 in. (38 cm) diameter by 12 in. (31 cm) deep cold-wall chamber with specimens heated radiatively from an inductively heated susceptor. The susceptor was

tantalum with a SnAl protective coating and was 3 in. (8 cm) in diameter by 10 in. (25 cm) long. A shaped induction coil heated the susceptor in a band about 2 in. (5 cm) wide at the middle of the susceptor. This configuration provided a temperature gradient along the length of the susceptor and consequently in specimens that were tested within the susceptor. The specimens were positioned so that the temperature increased from top to bottom. Kanthal hooks supported the specimens. A Datatrak programmer and a Thermal controller coupled to a magnetic amplifier controlled the temperature automatically.

These susceptors wore out in less than ten 30-min cycles, however, at 2600° F (1700° K) (specimen temperature). The temperature of the susceptor was probably 2800° to 3000° F, (1811° to 1922° K), considering heat losses in the system. Use of a TiMoSi fused slurry silicide coating (R512C class) extended the susceptor lifetime to only about 20 cycles and undesirable oxide deposits (SiO_2 and MoO_2) deposited on the test specimen surfaces when the susceptor wore out.

To eliminate these problems, the tantalum susceptor was replaced by a Pt-Rh susceptor, but there was considerable vaporization of the Pt which deposited on the test specimens. Therefore, a thin-wall Al_2O_3 sleeve was installed inside the susceptor to prevent the Pt vapor from reacting with the specimens. The system worked well at 2600° F (1700° K) except when a sudden power surge occurred. The susceptor was operating at a temperature so close to the melting point that such surges caused melting of the susceptor. For these reasons, it was also unlikely that this system would be adequate for 2800° F (1811° K) exposures.

Additional modifications of the oxidation test equipment included the use of a tantalum susceptor with the Co-Ti-Si formulation developed during this program in the hope that the high performance capabilities of this substrate-coating system would permit a greater coating lifetime at the high temperatures of the susceptor. Again, however, power surges caused overheating that resulted in localized wearout in the susceptor. This susceptor was made of tantalum sheet that was formed and spot welded. Notably, this coating flowed into the spot-welded joint well, producing a uniform coating on faying surfaces that had a separation of less than 1 mil (0.003 cm).

Because of the impracticality of frequently replacing the susceptors, an additional modification was made: the test apparatus was converted to a double-vacuum-chamber furnace in which a 2-7/8 in. (7.3 cm) inside diameter, 27 in. (69 cm) long mullite tube served as the inner test chamber. Air flowed through the test chamber at reduced pressure [0.1 to 100 torr (0.13 to 133 hN/m^2)] and at subsonic velocity. The outer chamber contained helium at a pressure balanced with that of the air in the inner chamber to prevent deformation of the tube at high temperature. A sacrificial mullite liner inside the tube prevented any reaction between the tube wall and the specimens, the supporting brackets, or volatile products. Coated tantalum hooks supported the specimens, and a tantalum susceptor in the outer chamber heated the hot zone.

Initially, temperature cycling consisted of changing the temperature of the hot zone. Thermal cycling, however, limited the lifetime of the mullite tube and premature failure of the tubes became a problem. Consequently, a hydraulically operated piston was incorporated in the system to move specimens in and out of the hot zone. A programmed Datatrak controller controlled the movement of specimens to conform with the appropriate time/temperature schedule.

A second furnace with a 5 in. (12.5 cm) diameter by 18 in. (45 cm) long hot zone placed in operation increased testing capabilities. This furnace had an Al_2O_3 tube heated by a graphite element. It was also a double-vacuum-chamber system, with N_2 on one side to protect the graphite and on the other for test exposures. The pressures of the two gases were balanced across the tube wall to minimize creep of the tube at high temperature. The thermal lag in this furnace was too great for temperature cycling by changing furnace temperature; therefore all temperature cycling was accomplished by withdrawing specimens from the hot zone. A program-controlled lead screw system provided a linear change of specimen temperature with time.

Modifications to two additional furnaces supplied an increased testing capacity. These were vertical, molybdenum-wound, resistance-heated tube furnaces, which are shown schematically in Figure 6. Each furnace was equipped with a screw drive mechanism to move specimens in and out of the hot zone automatically to provide temperature cycling from about 200°−300°F (366°−422°K) to the maximum desired temperature. A programmed Datatrak controller regulated the movement of the specimens. A water-cooled copper push rod supported coated tantalum hooks, which, in turn, supported the specimens. Up to 17 specimens could be tested simultaneously. Temperature control consisted of shielded Pt-PtRh thermocouples and West temperature controllers. The length-to-diameter ratio of these furnaces was sufficiently high to provide blackbody conditions. Therefore, the use of a calibrated single-color Microoptical Pyrometer enabled reliable temperature calibration.

Adjustment of a controlled leak valve at the top of the furnace and throttling of the vacuum system at the bottom of the furnace controlled the rate of air flow through the furnace, as well as the air pressure. In addition to maintaining proper temperatures and pressures during all oxidation exposures, a principal concern was maintaining an adequate air flow past the test specimens. If the air flow is too little, the environment immediately surrounding the specimens becomes depleted in oxygen and the effective oxygen pressure is decreased. Consequently, because the pressure in the region near the specimens is lower than the desired value, the results of oxidation tests can be markedly distorted. A sight port and prism at the bottom of the furnace permitted the observation of specimens during oxidation exposure.

These furnaces proved so successful that they were used for some of the screening tests and all the exposures of statistical, baseline, tensile, bend, defect, and emittance samples. In addition, as will be later discussed, one furnace was further modified for miniature heat shield panel testing.

Temperature and Pressure Measurements

During oxidation testing as well as other experiments that required optical pyrometers (e.g., determination of normal spectral emittance), a National Bureau of Standards (NBS) certified calibration lamp served as a facility for calibrating the pyrometers. In all cases, the calibration apparatus included any sight glasses or prisms required in the test system to correct for any effects on the output of the pyrometer. The calibration of each instrument was checked routinely throughout the program.

At pressures of 0.1 to 1 torr (0.13 to 1.3 hN/m^2), an Alphatron Vacuum Gauge measured the pressures. At pressures of 1 to 10 torr (1.3 to 13.33 hN/m^2), a Dubrovin Gauge measured the pressure. In addition, a McCleod Universal Vacuum Gauge connected to the test system served as a standard for routine calibration of the other pressure gages.

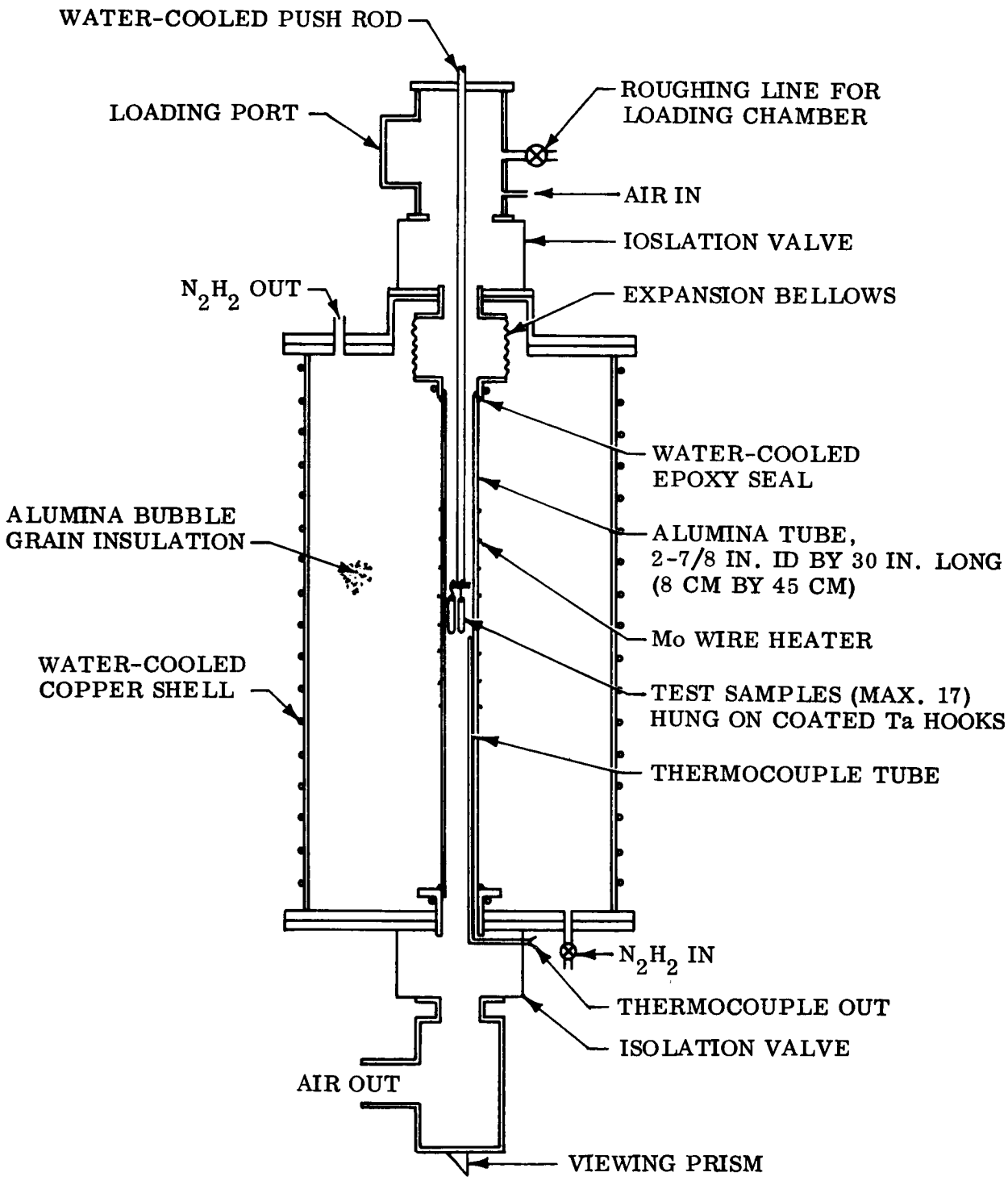

Figure 6 Schematic of Test Furnace Used for Cyclic Oxidation Exposures.

Screening Tests

Experimental and developmental coating systems were evaluated by means of screening tests. As previously mentioned, specimen dimensions for these tests were 4 by 1/2 by 0.013 in. (6 by 1-1/4 by 0.033 cm). The screening tests consisted of cyclic temperature exposures at an air pressure of 10 torr (13.33 hN/m^2). During each cycle, specimens were heated to 2600°F (1700°K) in 15 min, held at this temperature for 30 min, and cooled in 15 min. Appropriate positioning of the specimens within the hot zone of the test furnace provided a temperature gradient of 1800° to 2600°F (1255° to 1700°K) along the length of the specimen. With the temperature gradient, coating performance was evaluated over a broad range in temperature. This is significant because experience has shown that some coating systems can show reduced performance in a low-temperature range where insufficient oxide is formed to heal hairline fissures in the coating. In such cases, an evaluation based solely on high-temperature tests could be misleading. During the screening tests, the test specimens were periodically examined and the cyclic exposure was continued until the first observable indication of substrate oxidation.

Isothermal Baseline Tests

As part of the characterization of the best coating systems developed during the course of the program, isothermal baseline oxidation exposures were conducted. In these tests, specimens 4 by 1/2 by 0.013 in. (6 by 1-1/4 by 0.033 cm) were positioned in the vertical, molybdenum-wound resistance furnace so as to have a uniform temperature along their length. The specimens remained at constant temperature until evidence of coating wear-out appeared. During the oxidation exposure, the sight prism at the bottom of the furnace enabled routine examination of the coating performance. Isothermal baseline exposures were conducted at 2600°, 2700°, and 2800°F (1700°, 1589°, and 1811°K) and at air pressures from 0.1 to 10 torr (0.13 to 13.33 hN/m^2).

Exposure of Statistical, Emittance, Tensile, and Bend Specimens

Cyclic exposures were conducted with statistical, emittance, tensile, and bend specimens. A cycle consisted of heating specimens from about 200°F (366°K) to the maximum temperature in 15 min, holding at the maximum temperature for 30 min, and cooling in 15 min. This schedule was maintained by programming the movement of the specimens in and out of the hot zones of the vertical molybdenum-wound resistance furnaces. Two temperature/time schedules were followed; one with a maximum temperature of 2600°F (1700°K) and the other with a maximum temperature of 2800°F (1811°K). With each temperature, exposures were conducted at three air pressure levels – 0.1, 1.0, and 10 torr (0.13, 1.3, and 13.33 hN/m^2). At each pressure, there was adequate airflow past the specimens to prevent depletion of oxygen in the immediate proximity of the test specimens.

For the exposure in statistical studies, 15 specimens were exposed at each temperature/pressure combination. This number was selected to provide an appropriate specimen population for a Weibull analysis of the coating performance under each temperature/pressure condition. Routine inspections were conducted during exposures, and the exposure of each specimen continued until evidence of substrate oxidation appeared.

The emittance, tensile, and bend specimens were exposed in duplicate for prescribed fractions of the coating lifetime that had been established on the basis of the statistical

analyses. Duplicate emittance specimens were removed for emittance determinations after 10, 25, 50, and 100 cycles. Duplicate tensile and bend specimens were removed for test after 25, 50, and 100 cycles. Under conditions where statistical analyses indicated lifetimes less than 100 cycles, duplicate specimens were removed for test at corresponding fractions of the coating lifetime. Emittance specimens of a given coating system were exposed independently to prevent any minor contamination from another coating system, which might cause subtle effects that would influence the emittance.

Duplicate emittance specimens of each system were also exposed under each set of conditions for 1 cycle. The objectives of these tests were to follow the change in emittance with time during the first cycle and to determine the emittance after 1 cycle. These tests were conducted by heating the specimen by self-resistance in the emittance test apparatus (described in the section on emittance determination).

Tensile Tests

All tensile tests were conducted in accordance with MAB 216-M, "Evaluation Test Methods for Refractory Metal Sheet Materials." Pin-loaded specimens of the general configuration shown in Figure 7 were used for tests at all temperatures. The pin hole support regions were reinforced with two additional sheet thicknesses of tantalum T-222 alloy. As Shown in Figure 7, the tabs were spot welded to opposite sides of each shoulder, which gives three sheet thicknesses of material in the pin support region. The specimen shoulders were grit blasted to remove the coating, and the two tabs were spot welded to the bare metal in at least 10 different locations surrounding the pin hole.

Shoulder reinforcement permitted the use of cross-head motion for strain measurement in the high-temperature tests. No deformation was observed in the pin support region in any of the tests conducted at 1400°, 2600°, and 2800°F (1033°, 1700°, and 1811°K). The sample in Figure 7 was strained over 45 percent in the gage section at 2600°F with no measurable strain in either the pin holes or shoulders. The effective gage length was taken as the total length [1.20 in. (3.05 cm)] of the 0.25 in. (0.633 cm) wide reduced section. The deformation within this region was very uniform, as shown by the pattern of parallel fissures in the coating which opened up during tensile straining. All coated samples tested at elevated temperature had very uniform deformation and none necked down at high strain levels. This unique aspect of behavior is discussed in the section on analysis of results.

Tests at all temperatures were conducted at a constant rate of cross-head travel of 0.05 in. (0.127 cm)/min. Strain to the ultimate strength in the elevated-temperature tests was determined with a recording LVDT extensometer system which measured the movement of the lower pull rod. Extension past the ultimate was taken from the readings of a dial gage which also followed pull rod motion. The total measured extension was divided by 1.2 to obtain the strain in a 1 in. (2.54 cm) gage section. Strain in the tests at room temperature was measured directly over a 1 in. (2.54 cm) gage section using an Instron clip-on strain gage extensometer for the full range of the test. In all tests, a load strain curve was measured and recorded by a Class C (or better) extensometer for use in determining the 0.2-percent offset yield strength.

The room-temperature tensile tests were conducted in a 10,000 lb (4,540 kg) Instron tester at a temperature between 70° and 85°F (294°−303°K). The elevated-temperature tests were conducted in a 60,000 lb (27,250 kg) Riehle tensile test machine using an Instron 1,000-lb load cell to measure and record loads. Use of the large tensile machine was required to accommodate an Astro Industries cold-wall vacuum furnace in which the hot tensile tests were conducted. The more sensitive Instron load cell was incorporated in the load train to provide an accurate measurement of loads at the low levels required to test the specimen. The same load cell was used for the room-temperature tensile tests in the Instron frame. Each day of testing, the cell was calibrated by dead weight loading with calibrated 20 lb (9.1 kg) weights. The LVDT cross-head follower and the strain gage extensometers also were calibrated daily using a Templin calibrator with a sensitivity of 20 μ-in. (50.8×10^{-6} cm) per division.

Hot tensile tests were conducted in vacuum using an Astro Industries cold-wall furnace. The specimens were heated by radiation from a tungsten mesh heater of 2 in. (5.08 cm) diameter and 7 in. (17.72 cm) length. Temperature was measured and controlled by a Pt-Pt-10Rh thermocouple attached to the center of the gage section with a tantalum clip.

(a) Shoulders Grit Blasted for Spot Welding to Tabs

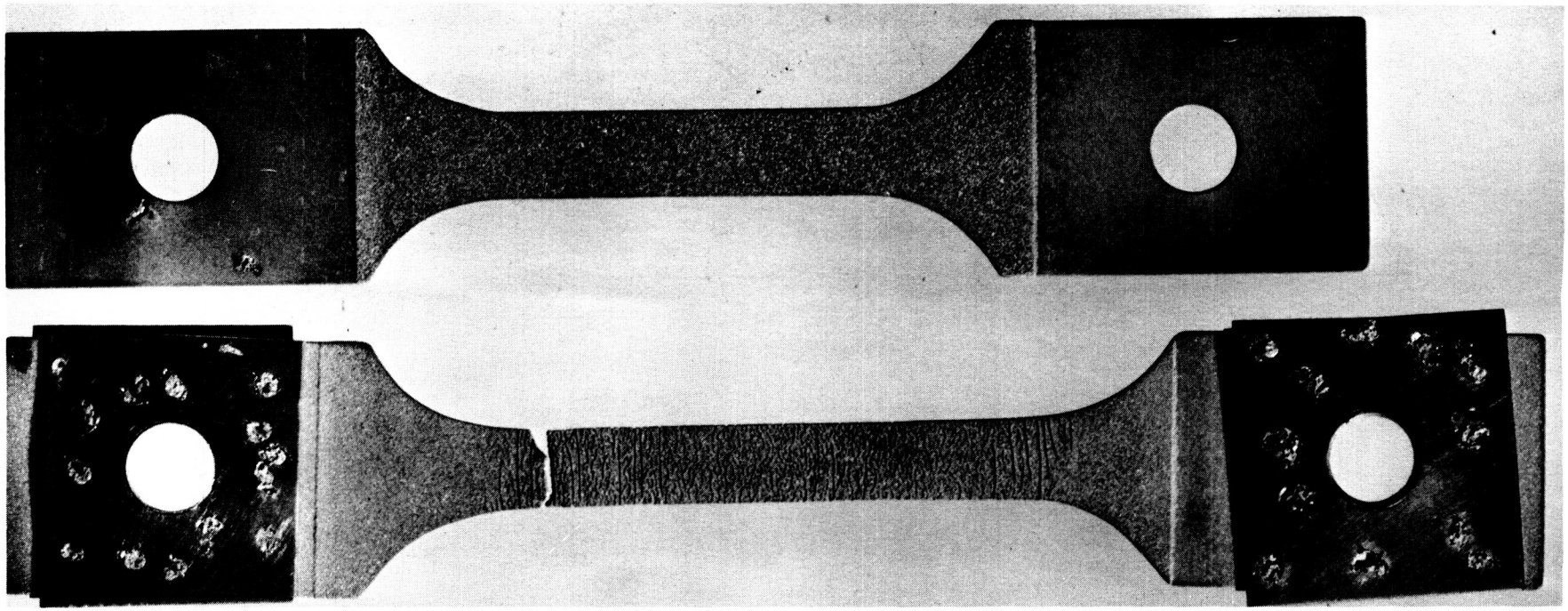

(b) Shoulders Reinforced With Spot-Welded T-222 Alloy Tabs, Ta-10 W/MTS As-Coated, 2600°F (1700°K) Tensile Test, 46-Percent Elongation

Figure 7 Shoulder Reinforcement of Pin-Loaded Hot Tensile Specimens, 2×.

Temperature within the gage section was within ±5 percent of the control temperature at all test temperatures. The samples were heated to temperature in 30 min and were equilibrated 15 min at temperature before testing. All tests were in vacuum at 10^{-4} torr (0.013 N/m^2) or less. Specimens were held with molybdenum grips using 0.25 in. (0.65 cm) tungsten pins to transmit the load. Axiality was maintained by means of a universal connection in the upper (stationary) pull rod.

Creep Tests

Creep tests at 2600° and 2800°F were conducted in air using tensile samples with a 0.25 by 1.2 in. (0.635 by 3.05 cm) gage section. The samples were loaded at 6 ksi (41.4 MN/m^2), with the stress calculation based on residual substrate thickness after coating. Tests were conducted in an Arc-Weld 10,000 lb (4,540 kg) creep frame with a 20:1 lever arm ratio.

The samples were heated by direct resistance using a 17-kVA SCR power supply. Water-cooled copper grips were used to load the samples and provide electrical contact. The specimens were centered with steel pins through the shoulders and were rigidly clamped in the water-cooled copper blocks. Only the center 2 in. (5.08 cm) of the specimen was heated. The temperature distribution along the gage section is shown in Figure 8. Temperature within a 0.6 in. (1.52 cm) zone is within 30°F (54°C) of the set temperature. At a gage of 0.75 in. (1.9 cm), the temperature is within 70°F (126°C) of the set temperature. With increasing distance from the center, the temperature drops rapidly. Since creep rate is an exponential function of temperature, the total creep strain that will occur outside the center 0.75 in. (1.9 cm) zone can be neglected for all practical purposes, and the effective gage length of the sample can be assumed to be 0.75 in. (1.9 cm).

To check the validity of this assumption, two samples of coated Ta-10W were tested in air by resistance heating and in vacuum by radiant heating procedures. In the latter case, a Brew cold-wall furnace with a 2.5 in. (6.35 cm) diameter by 6 in. (15.2 cm) long tantalum element heated the specimen by radiation. The effective 1.2 in. (3.05 cm) long gage section in this case was within ±5°F of the control temperature. Creep curves based on the assumed 0.75 in. (1.9 cm) gage section for air tests and a 1.2 in. (3.05 cm) gage section for vacuum tests are shown in Figure 9 . Strain in both cases was measured from cross-head (pin) motion, using a Collins direct-current linear transducer with a scale factor of 212 mV/mil extension. The results of creep tests by both methods at 2600° and 2800°F (1700° and 1811°K) were in excellent agreement (Figure 9). Based on this correlation, the direct resistance heating method in air was qualified for use in characterizing the creep behavior of coated samples in this program.

Temperature in all tests was measured and controlled by a Pyro Eye two-color optical pyrometer. This instrument reads true temperature directly without an emittance correction for materials that are gray bodies. Since most coated refractory metals have a reasonably flat curve for spectral emittance versus wavelength, a gray-body assumption is valid and a two-color pyrometer can be used. Temperature was also checked with a single-color optical pyrometer using emittance correction factors established in the course of this program. The check temperatures were within 2 percent of the two-color pyrometer temperature. Both instruments were calibrated periodically against an NBS-certified tungsten ribbon lamp.

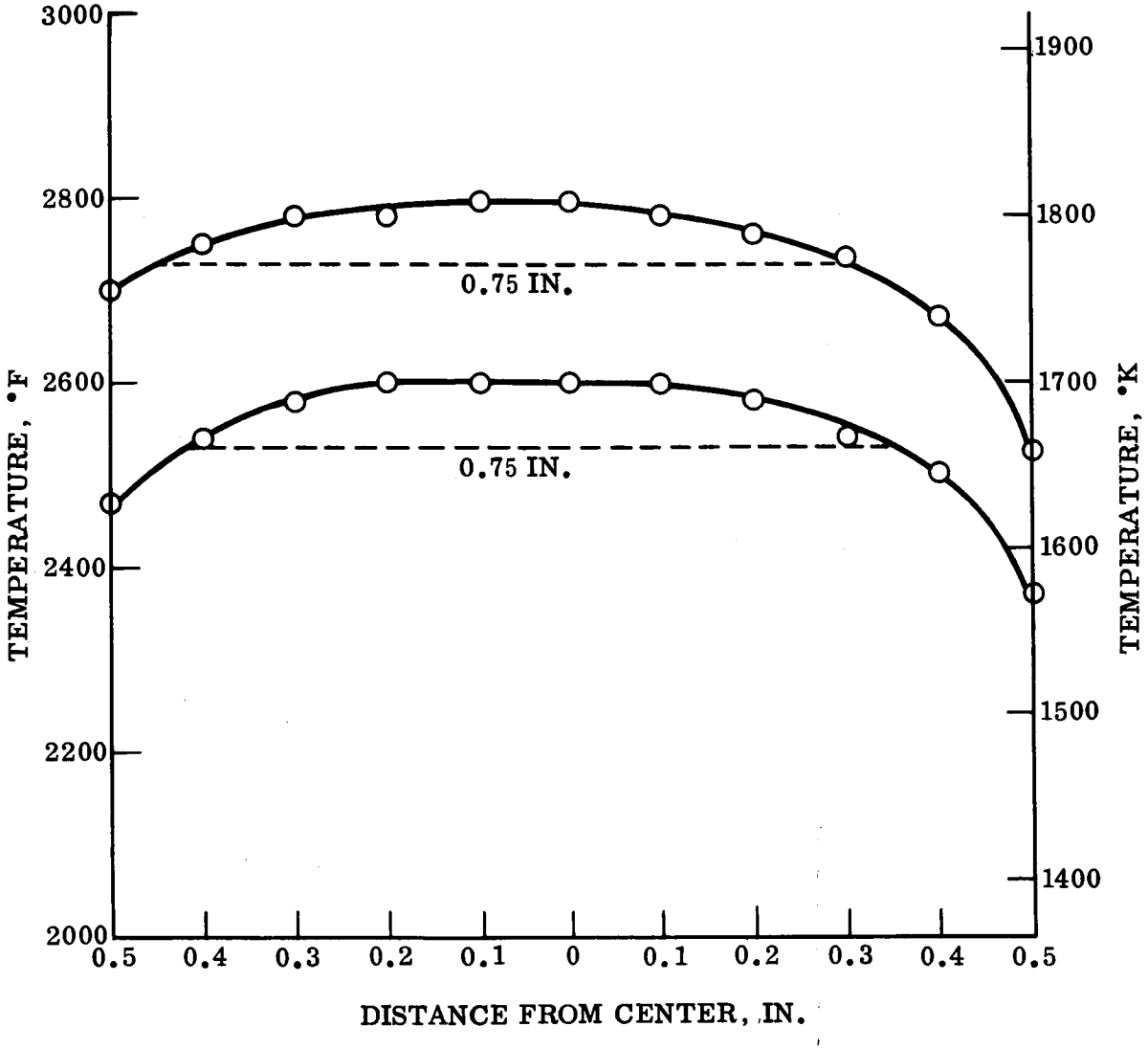

Figure 8 Temperature Distribution Along the Length of Resistance-Heated Creep Samples.

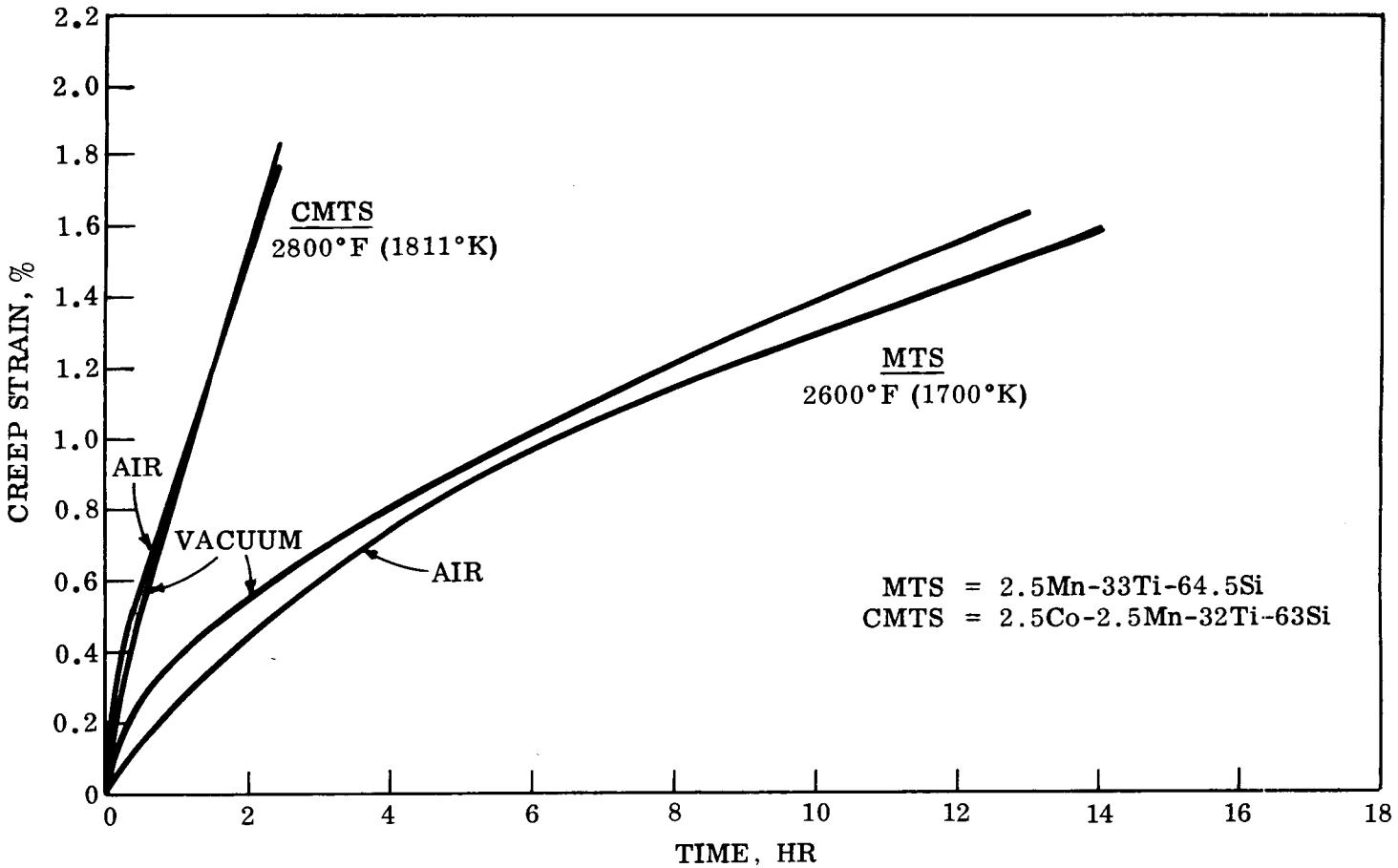

Figure 9 Comparison of Creep Curves Obtained by Self-Resistance (Air) Versus Radiant Heating (Vacuum) of Samples.

The output of the two-color pyrometer was put into a feedback control system that maintained the sample temperature at any desired point. Temperature/time and strain/time curves were recorded continuously by means of dc millivolt recorders. The time to 1-percent strain, total primary creep strain, time to end of primary creep, and steady-state creep rate were obtained from the creep curves.

Bend Ductile-to-Brittle Transition Tests

Bend tests were performed with the equipment and procedures specified in "Evaluation Test Methods for Refractory Metal Sheet Materials" (MAB216-M), with one exception: the samples prepared for determination of the bend ductile-to-brittle transition temperature were limited to a maximum length of 1.5 in. by the configuration of the environmental test furnace. This constraint precluded use of a 1 in. (2.54 cm) span for sample support, as specified in MAB216-M for sheet 0.009−0.030 in. (0.023−0.076 cm) thick; instead, the specimen was supported on a 0.5 in. (1.275 cm) span. This procedure resulted in an increase in the rate of bending and is a somewhat more severe test than the one specified. At a ram speed of 1 in./min (2.54 cm/min), a 90-deg bend is completed in 30 sec with a 1 in. (2.59 cm) span and in 15 sec with 0.5 in. (1.27 cm) span. The increased strain rate could result in higher ductile-to-brittle transition temperatures.

The bend sample was supported on a stainless steel channel die with a 0.5 in. (1.27 cm) span. The support points had a 0.050 in. (0.127 cm) radius. A stainless steel punch with a 0.1 in. (0.254 cm) diameter molybdenum loading pin was used to make the bend by moving down between the supports at a fixed cross-head speed of 1.0 in./min (2.54 cm/min). The punch and support were completely submerged in liquid nitrogen or dry ice and acetone in an insulated stainless steel can for bend tests at subzero temperatures. All tests were conducted in a 200-lb-capacity Instron tensile test machine. Loads were measured with a 200-lb-capacity load cell, and a load-deflection curve was plotted for each test.

In preliminary tests, a large drop in load was observed when the coating on the compression side adjacent to the loading ram ruptured and spalled from the surface. A typical load deflection curve with a large load spike is shown in Figure 10. With continued bending, further crushing of the coating material occurred on the compression side and a serrated load-deflection curve was produced.

Coating spall has two undesirable effects on the bend test. With this portion of the coating in compression, deformation of the sample is resisted and a large load – considerably in excess of the normal bending load – builds up on the surface. A load-deflection curve for the same material with the coating removed from the compression side is shown in Figure 10. Note that the two curves are identical except for the initial loading spike and the serrations in the curve associated with the breakup of the coating in the compression region under the ram.

When compressive breakup occurs, the excess load on the sample is relieved by rapid deformation of the substrate. The thin sheet kinks and pulls away from the ram, forming a bend radius much sharper then desired. This effect is illustrated by cross-section photographs of actual bend samples in Figure 11. The actual bend radius is 1.6t instead of the 4t desired. The net result is an uncontrolled bend test in which the strain rate is variable and too fast and the bend radius is variable and too sharp.

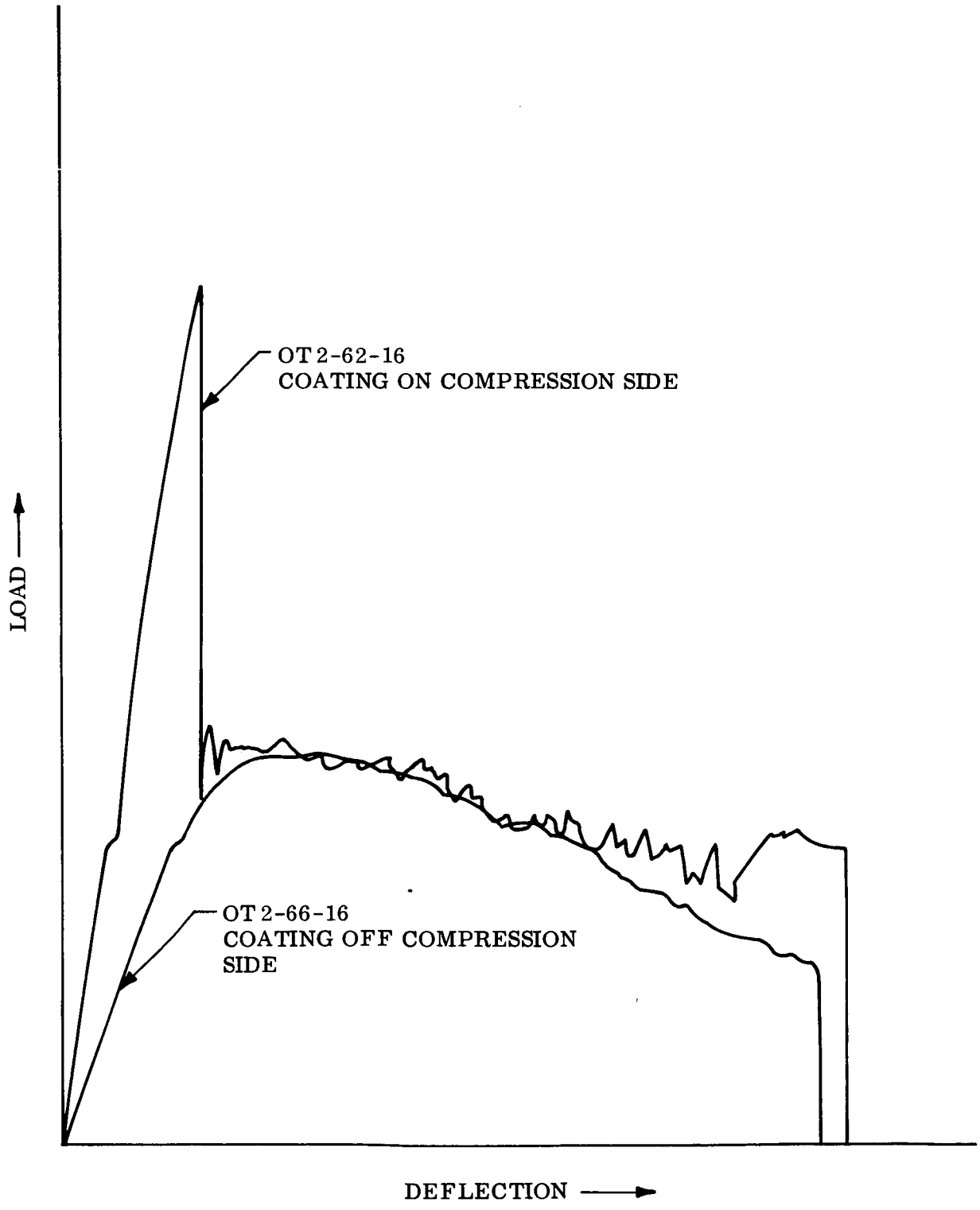

Figure 10 Effect of Removing Coating From Compression Side on Load-Deflection Curves in Bending, Ta-10W/MnTiSi, 2600°F (1700°K)/1 Torr (1.33 hN/m^2)/100 Cycles, Liquid Nitrogen Test.

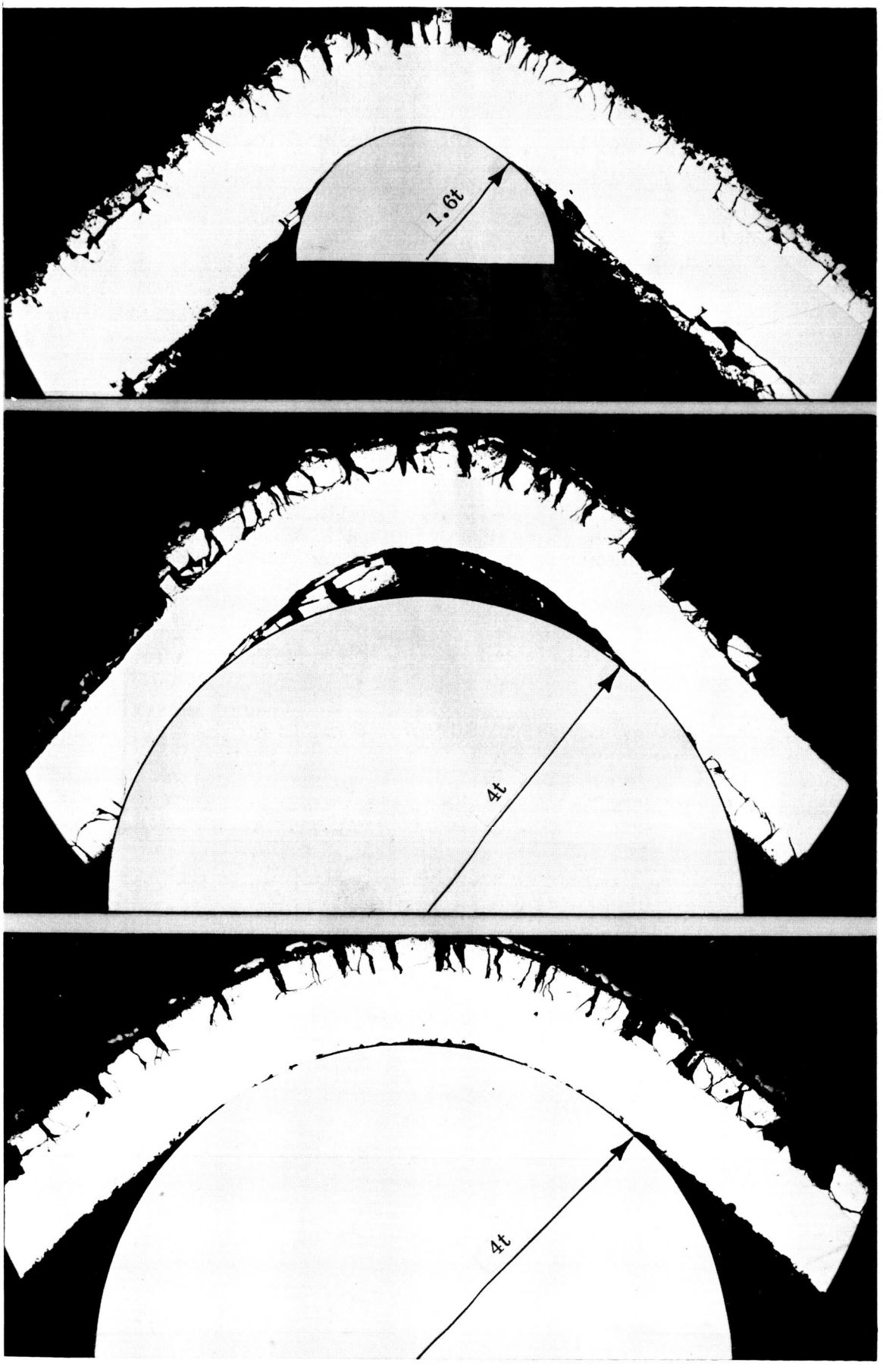

B-2917
50×

(a)
OT 2-119-10
AS-COATED
COATING ON COMPRESSION SIDE

B-2919
50×

(b)
OT 2-36-12
2600°F – 10 TORR
100 CYCLES
COATING ON COMPRESSION SIDE

B-2920
50×

(c)
OT 2-36-12
2600°F – 10 TORR
100 CYCLES
COATING OFF COMPRESSION SIDE

Figure 11 Effect of Removing Coating From Compression Side on Effective Bend Radius With a 4t Mandrel.

As shown in Figure 11, the bend radius conforms exactly to the punch radius when the coating is removed from the compressive side before bending. This is a controlled bend with respect to both bend rate and bend radius. The results are reproducible from test to test. Since the primary purpose of this test is to compare materials behavior, this procedure was used in all bend testing. Removal of the coating from the compression side does not affect the behavior on the tension side. The stress concentrations generated by fissures in the coating under tension still exist, and the stress conditions that govern deformation and fracture of the substrate are unchanged. The DBTT should not be affected by removing the coating from the compression side per se. This was confirmed with several different samples by bending as-coated and exposed samples in liquid nitrogen with and without the coating on this compressive side. All samples had ductile 90 deg-4t bends. The two curves in Figure 10 are 90 deg-4t bends in liquid nitrogen for duplicate MTS-coated samples exposed for 100 cycles at 2600°F (1700°K) – 1 torr (1.33 hN/m^2).

Emittance Measurements

The normal spectral emittance was determined at a wavelength, λ, of 0.65 μm with specimens coated with the two best coating systems developed during the program. Test specimens were heated by self-resistance in a cold-wall furnace, shown schematically in Figure 12. Manually controlled current passing through 1/4 in. by 4 in. (0.6 cm by 10 cm) specimens resistively heated them to the desired temperature. Air flowed past the specimens subsonically; air pressure was held constant by regulating a controlled leak valve and throttling the vacuum line. At 0.1 torr (0.13 hN/m^2) an Alphatron Vacuum Gauge measured the pressure and at 1 and 10 torr (1.33 and 13.33 hN/m^2) a Dubrovin Vacuum Gauge measured the pressure. In addition, a McCleod Universal Vacuum Gauge connected to the system provided a calibration standard for the other vacuum gages. A Microoptical Pyrometer calibrated with an NBS-certified lamp measured the brightness temperature and a Milletron two-color pyrometer (also calibrated with an NBS-certified lamp) measured the color temperature.

Determination of emittance included the assumption of graybody conditions, which entailed the further assumption that the color temperature was equal to the true temperature. The emittance, ϵ_λ, was calculated using the relationship

$$\ln \epsilon_\lambda = \frac{c_2}{\lambda}\left(\frac{1}{T} - \frac{1}{\theta}\right)$$

where c_2 is a constant equal to 1.43×10^{-4} °Kμm, λ is the wavelength equal to 0.65 μm, T is the true temperature in degrees Kelvin, and θ is the brightness temperature in degrees Kelvin.

Coating emittances were measured after various levels of oxidation exposure at 2600° and 2800°F (1700° and 1811°K) and air pressures of 0.1, 1.0, and 10 torr (0.13, 1.3, and 13.33 hN/m^2). For specimens exposed at 2600°F (1700°K), the emittance was measured at 1870°, 2200°, and 2600°F (1294°, 1478°, and 1700°K) on heating and cooling; for those exposed at 2800°F (1811°K), the emittance was measured at 2000°, 2400°, and 2800°F (1366°, 1589°, and 1811°K) on heating and cooling. The air pressure during emittance measurements of an exposed specimen was the same as that during exposure of the specimen. For each set of exposure conditions, emittance measurements were made on duplicate specimens.

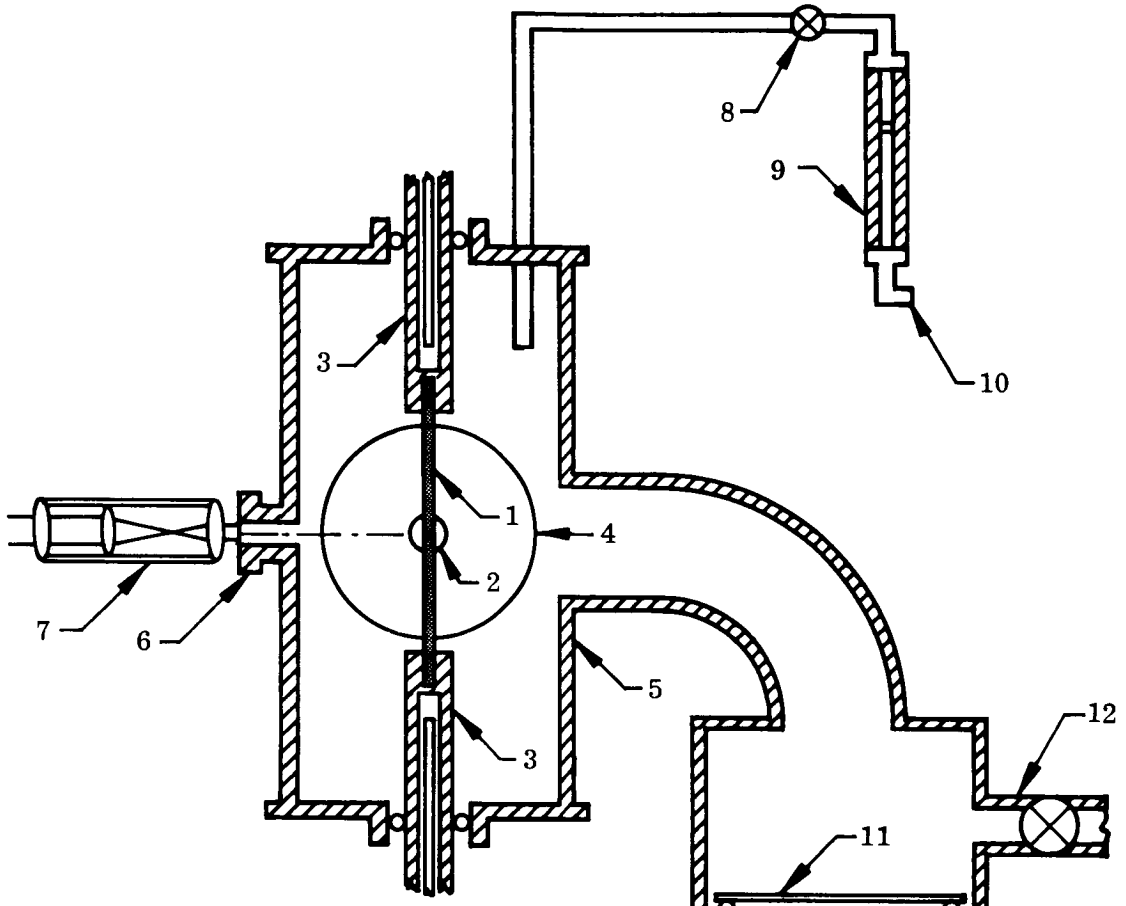

1 Emittance Specimen
2 Pressure-Gage Port
3 Water-Cooled Electrode
4 Access Door
5 Water-Cooled Chamber
6 Observation Port (3)
7 Pyrometer
8 Leak-Rate Control Valve
9 Flowmeter
10 Gas Inlet
11 High-Vacuum Valve
12 Roughing Valve
13 Fore Line
14 Diffusion Pump

Fig. 12 Cold-Wall Test Furnace Used for Emittance Determinations.

In addition, duplicate specimens in the as-coated condition were heated rapidly (<30 sec) to each of the exposure temperatures [2600° and 2800°F (1700° and 1811°K)] at each air pressure level, 0.1, 1.0, and 10 torr (0.13, 1.3, and 13.33 hN/m^2)], and the emittance was measured continually for 30 min to determine the change in emittance during the equivalent of the first cycle of oxidation exposure. On cooling, the emittance of these specimens was measured at the same lower temperatures as for the exposed specimens.

Further tests included emittance measurements of as-coated specimens in a helium environment. The temperatures for these measurements were 1870°, 2000°, 2200°, 2400°, 2600°, and 2800°F (1294°, 1366°, 1478°, 1589°, 1700°, and 1811°K).

Intentional Damage Studies

Coated specimens were intentionally damaged and then exposed to cyclic oxidation exposure to assess the effect of the exposure on damage sites. The types of intentional damage were 1/2t-, 2t-, and 4t-diameter holes in the coating and 4t-diameter holes through the specimen (where t = substrate thickness). A high-speed jeweler's drill press with tungsten carbide dental burrs produced the holes.

Simulated Reentry Environmental Exposures

The simulated reentry environmental exposures consisted of cycling both temperature and bending stress with miniature rib-stiffened heat-shield panels. The temperature/stress/time schedule is presented in Figure 77 in the Applicability to Structural Components section. In these tests the stress on the panel decreased as the temperature increased; remained constant during the period of the cycle at constant temperature; and increased as the temperature decreased during the final phase of the cycle. As with the exposure of other types of samples, movement of the miniature heat-shield panel in and out of the hot zone of a molybdenum-wound resistance furnace provided temperature cycling. Three-point loading of the panel with a variable load served to cycle the stress.

A specially designed fixture afforded the means for applying the variable load to the panel. This fixture is shown schematically in Figure 13. The panel was supported by Ta-10W U-shaped hangers, coated with the MTS coating – one of the two best coating systems developed during this program. These hangers were secured with molybdenum pins to a water-cooled copper block which was brazed to a water-cooled copper push rod. A stainless steel tube transmitted the load through the push rod from externally applied weights to a coated Ta-10W load bar, which, in turn, transmitted the load to the panel. A coated Ta-10W bar positioned across the panel served to distribute the load uniformly across the midsection of the panel.

The push-rod assembly at the top of one of the vertical furnaces was modified to accommodate the apparatus for automatically varying the load applied to the test panel during the cyclic exposures. This apparatus is shown schematically in Figure 14. (Each series of weights consisted of four balanced weights to avoid any bending moment on the load system.) In the figure, the apparatus is shown in the highest position – that is, during exposure conditions where the panel is high in the furnace, out of the hot zone, in the lowest temperature region of the furnace. Under these conditions, the stress is at its highest level; all the weights are being supported by the stainless steel tube that transmits the load through the push rod to the coated Ta-10W load rod. When the panel is lowered into the hot zone of the furnace, the push rod sequentially releases the series of weights as they come to rest on the weight support platform, thus reducing the load on the panel. After exposure at the maximum temperature, a condition where both temperature and stress are constant, the process is reversed; the weights are picked up from the weight support platform, and the load on the panel increases as the panel temperature decreases.

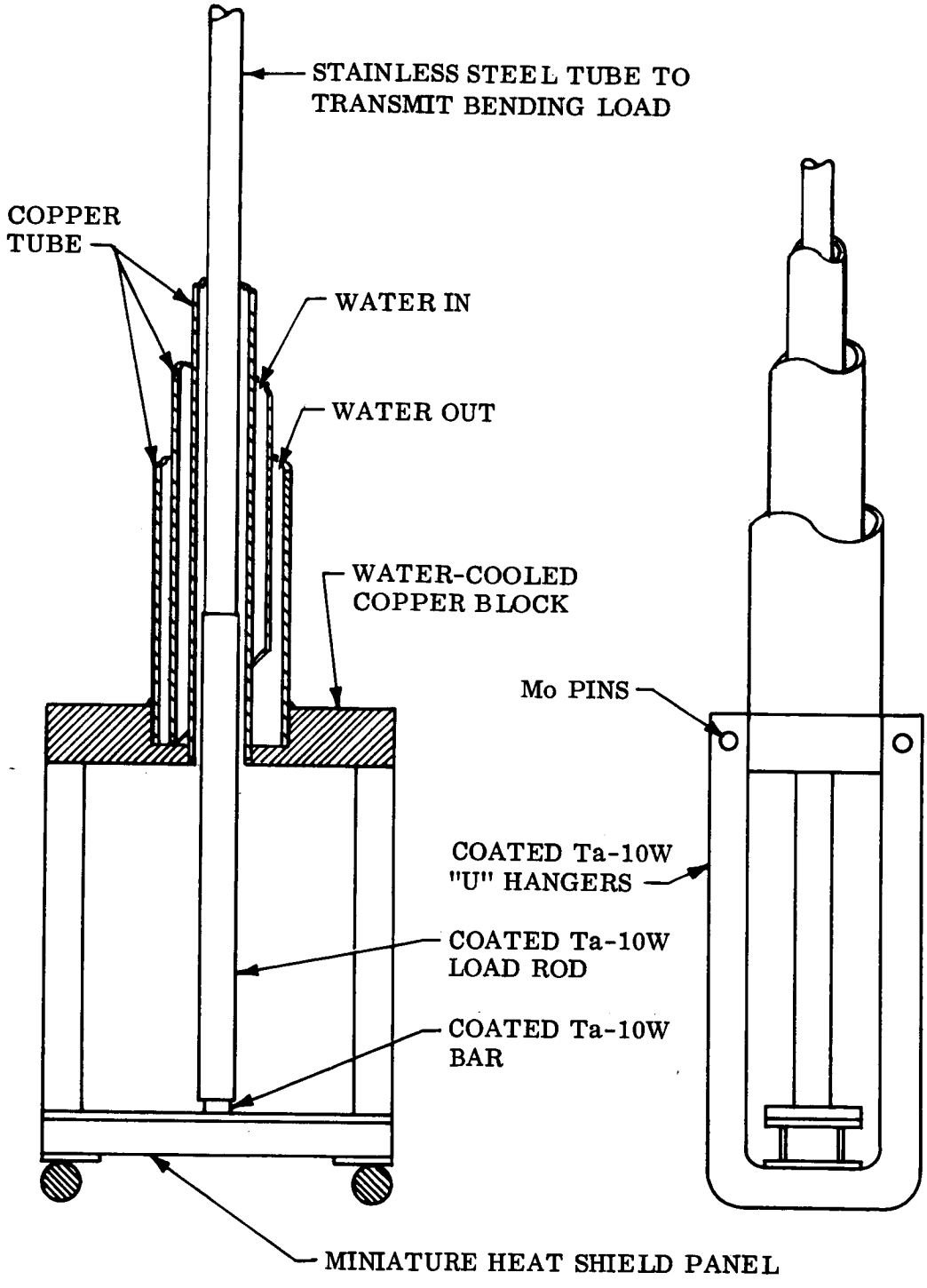

Figure 13 Fixture for Simulated Reentry Environment Testing of Miniature Heat Shield Panels (Full Scale).

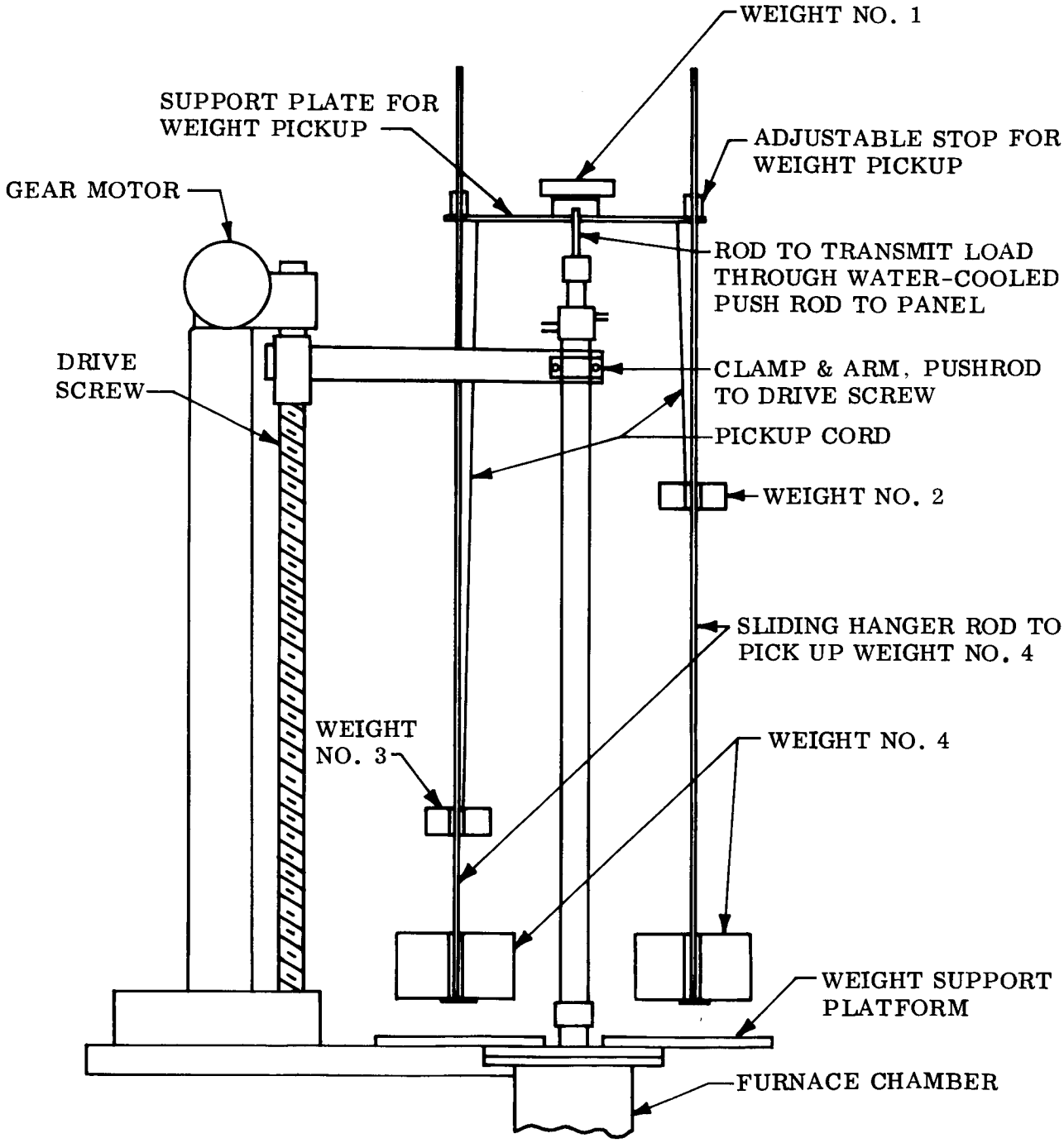

Figure 14 Load Application System for Simulated Reentry Environmental Testing of Miniature Heat Shield Panels.

The prescribed temperature/stress/time schedule dictated the magnitude of each weight series, the distance between weights, and the rate of push-rod movement.

Determination of the weights to provide the appropriate stresses in the outer fibers of the ribs in the miniature heat-shield panels was based on the following analysis:

The stress, s , can be calculated from the flexural formula

$$S = \frac{Mc}{I} \tag{1}$$

where M is the bending moment, c is the distance between the outer fibers and the neutral plane, i.e., that plane where the stress in the ribs is zero, and I is the moment-of-inertia.

To analyze the stress in the miniature panel, consider the following diagram, which represents this panel cross-section.

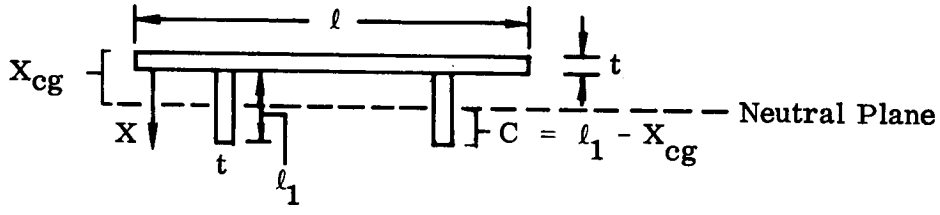

To solve for X_{cg}, the distance from the top of the panel to the center-of-gravity or the neutral plane, the moments of areas are balanced as follows:

$$\ell t X_{cg} + 2\,\frac{\left(X_{cg} - \frac{t}{2}\right)\left(X_{cg} - \frac{t}{2}\right)}{2} = 2\,t\,\frac{\left[\ell_1 - \left(X_{cg} - \frac{t}{2}\right)\right]\,t\,\left[\left(\ell_1 - (X_{cg} - \frac{t}{2})\right)\right]}{2} \tag{2}$$

where

ℓ = 0.75 in. (1.91 cm)
ℓ_1 = 0.25 in. (0.635 cm)
t = 0.011 in. (0.028 cm) (t = residual substrate thickness after coating.)

From Eq. (2), X_{cg} = 0.053 in. (0.135 cm).

For the configuration

$$I = \ell t X_{cg}^2 + 2\left[t\frac{\ell_1^3}{12} + \ell_1 t\left(\frac{\ell_1}{2} + \frac{t}{2} - X_{cg}\right)^2\right] \tag{3}$$

and for the dimensions of the panels evaluated

$$I = 8.5 \times 10^{-5}\ \text{in.}^4\ (3.54 \times 10^{-3}\ \text{cm}^4)$$

Since

$$M = \frac{PL}{4} \tag{4}$$

where P is the applied load and L is the distance between the supports on the lower side of the panel [2 in. (5.08 cm)] , Eq. (1) can be rearranged as

$$P = \frac{4IS}{Lc} \tag{5}$$

and since I, L, and c are now known, the load for any stress in the outer fibers of the ribs on the rib-stiffened miniature panels can be calculated.

COATING DEVELOPMENT

Analysis of Coating Behavior

- Protective Mechanisms

The development of improved silicide-base coatings for tantalum should be guided by an understanding of the metallurgical and environmental factors that govern the performance of existing coating systems. A comprehensive review of the fundamentals of coating behavior prepared by the Materials Advisory Board provides most of the needed background information (ref. 15). The mechanism of protection in simple silicide coatings is based on the selective oxidation of silicon to form a protective film of silica (SiO_2) on the surface. The concurrent oxidation of both the metal and the silicon constituents can produce an oxide film that is less protective, resulting in more rapid wearout of the coating (refs. 16–20).

Selective oxidation in silicides is a function of the metal (M) to silicon (Si) ratio, the relative free energies of the metal and silicon oxides, temperature, and pressure. A low metal-to-silicon ratio facilitates selective oxidation of silicon. The disilicides (MSi_2) readily form protective silica films on heating in air. In general, these compounds are more resistant to oxidation than the intermediate (M_5Si_3) or lower (M_3Si, M_4Si) silicides over a broad temperature/pressure range.

In addition, the disilicides of molybdenum, tungsten, and rhenium are more resistant to oxidation than those of columbium, tantalum, chromium, and titanium (refs. 17, 18). As shown in Table 2 , the free energy of tungsten and molybdenum oxides is half that of silica. Hence, the formation of SiO_2 is favored thermodynamically during oxidation of tungsten and molybdenum silicides. Furthermore, the oxides of molybdenum and tungsten have a high vapor pressure and tend to evaporate from the silica film if concurrent oxidation does occur. Columbium and tantalum, on the other hand, have about the same potential for oxidation as silicon. Concurrent oxidation of both constituents is much more likely to occur with the silicides of these metals. The oxides of columbium and tantalum have a low vapor pressure and remain in the oxide films. These more complex $(Cb,Ta)_2O_5$-SiO_2 films tend to be less protective. Consequently, the disilicides of columbium and tantalum oxidize more rapidly, and coatings based on these compounds may have a shorter life (ref. 18)

The data of Table 2 indicated that the metallic constituent of the silicides of titanium, zirconium, hafnium, and yttrium should be oxidized preferentially to silicon. These materials should provide more stable refractory oxide scales that may improve performance at low pressures and high temperatures, where the silica or silica-rich films form volatile reaction products (SiO) or become too fluid.

- Temperature and Pressure Effects

In addition to metal-to-silicon ratios and thermodynamic considerations, two other factors – temperature and pressure – govern the formation of protective silica films on

TABLE 2. – THERMODYNAMIC PROPERTIES OF METAL OXIDES

Oxide	ΔF at 1800°F, kcal/g atom O	Melt point, °K	Boiling point, °K
MoO_3	-31.0	1068	1428
WO_3	-32.3	1743	2500
Fe_3O_4	-33.2	1870	–
V_2O_5	-42.0	943	2325
Cr_2O_3	-53.6	2553	73273
Cb_2O_5	-54.6	1785	>2500
Ta_2O_5	-61.2	2150	>2500
SiO_2	-66.5	2000	–
TiO_2	-74.5	2123	3273
Al_2O_3	-87.7	2313	–
ZrO_2	-90.5	2950	4570
HfO_2	-93.0	3063	–
Y_2O_3	-108.5	2500	4570

silicides. Every silicide phase in which silicon is the most active element (most negative free energy for oxide formation) has a region of temperature and pressure in which the silicon can be oxidized preferentially. Each silicide also has a temperature/pressure region in which both the metal and the silicon will be oxidized simultaneously. The temperature/pressure boundary that defines the regions of active (rapid) and passive (protective) oxidation behavior for $MoSi_2$ is illustrated in Figure 15. The transition temperature for the formation of a protective (passive) silica film increases with increasing pressure of the oxidants (O_2, H_2O, CO_2). In general, high temperatures and low pressures favor selective oxidation to form protective silica films.

It should be noted, however, that a second transition, this time from passive to active behavior, will occur with increasing temperature beyond the boundary at any pressure. This transition results from the formation of a volatile oxide of silicon, SiO. The boundary characteristic for this transition in $MoSi_2$ also is shown in Figure 15. The consumption of silicon is accelerated to the right of this boundary as a result of vaporization of the oxidation products. The central passive area is the region of temperatures and pressures within which a silicide coating will have its best resistance to oxidation and, hence, its maximum useful life.

The behavior of all silicide phases will be similar with respect to these active/passive/active transitions as a function of temperature and pressure. The boundary locations, however, will vary widely for different silicide compositions. The greatest effect is in the left boundary of Figure 15, which defines the minimum temperature at which a protective silica film can be found. For example, in air at 1 atm, $MoSi_2$, Mo_5Si_3, and $TaSi_2$ (or $CbSi_2$) can be oxidized to form protective silica films at 1750°, 2650°, and 3000°F (1228°, 1728°, and 1922°K), respectively (refs. 17,18,20). At lower temperatures, both the metal and silicon constituents are oxidized.

As previously mentioned, the position of this boundary is governed by the metal-to-silicon ratio in the silicide and the relative differences in the free energy of formation of the oxides of the metal and silicon. Coating composition must be adjusted to move this boundary as far to the left as possible for good coating performance. If temperatures much above 2000°F are required to develop protective oxide films, coating life will be shortened significantly by rapid oxidation at low temperatures during cyclic exposures.

The low-pressure passive-to-active transition boundary also depends on coating composition, but to a lesser extent. This boundary is defined by the free energy of the reaction between silicon (Si) and silica (SiO_2) to form silicon monoxide (SiO) vapor. Its respective position, therefore, depends on the free energy of formation of the silicide compounds. Using available free energy and heat of reaction data, Bartlett et al. have estimated these boundaries for various silicides, as shown in Figure 16 (ref. 17). Since the thermodynamic properties of the silicides are similar, the differences are not too great. They are significant, however, with a 250°C range between the outer limits ($MoSi_2$ versus Ta_5Si_3).

This boundary defines the maximum temperature at any pressure to which a coating can be exposed without disrupting the protective silica film. At higher temperatures, volatile SiO will form and coating life will be reduced. Thus, it is important to adjust the coating composition to move this boundary as far to the right as possible. A coating of Ta_5Si_3 would have the highest temperature capability on the basis of these calculations.

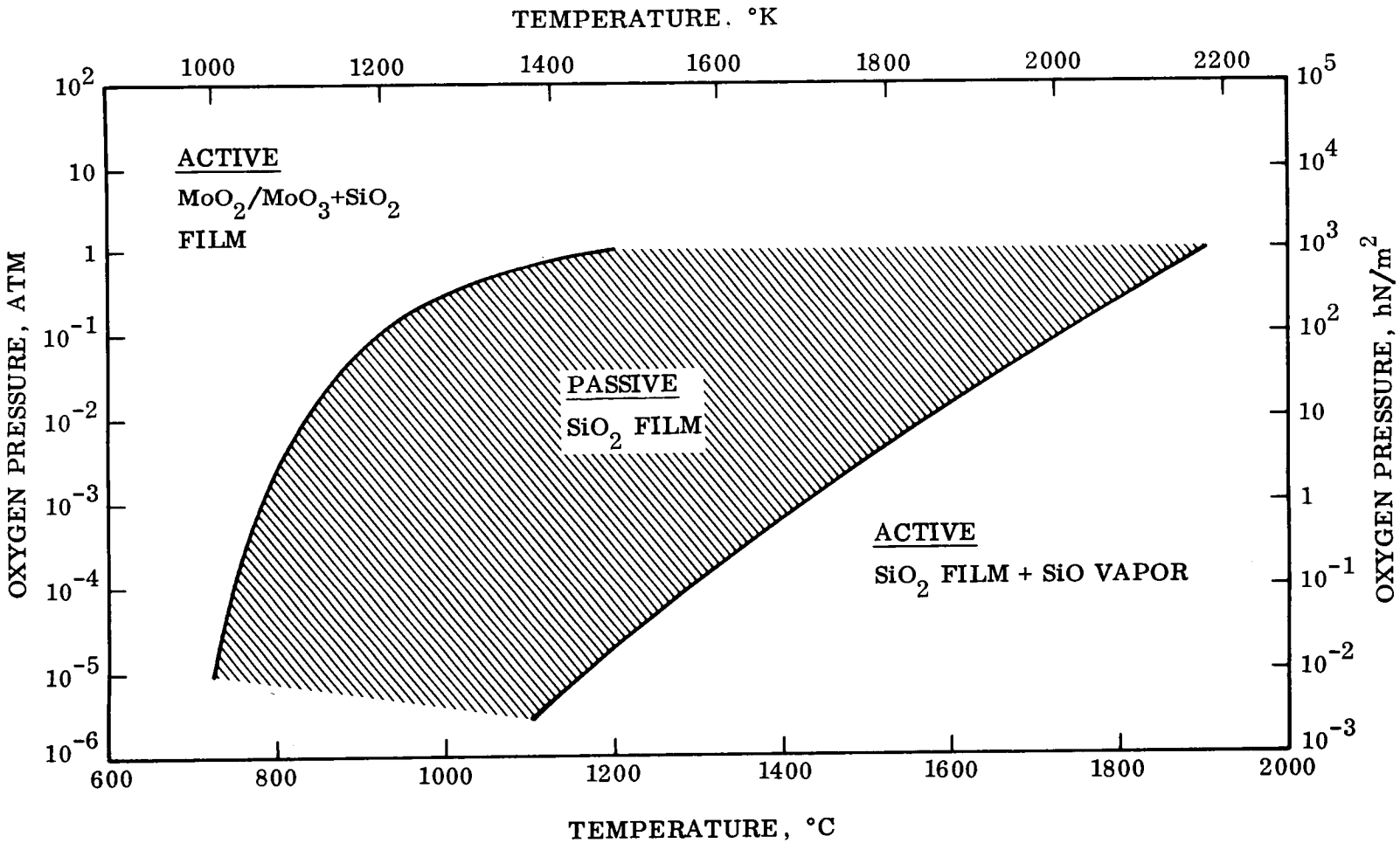

Figure 15 Transitions in the Oxidation Behavior of $MoSi_2$ (Ref. 17).

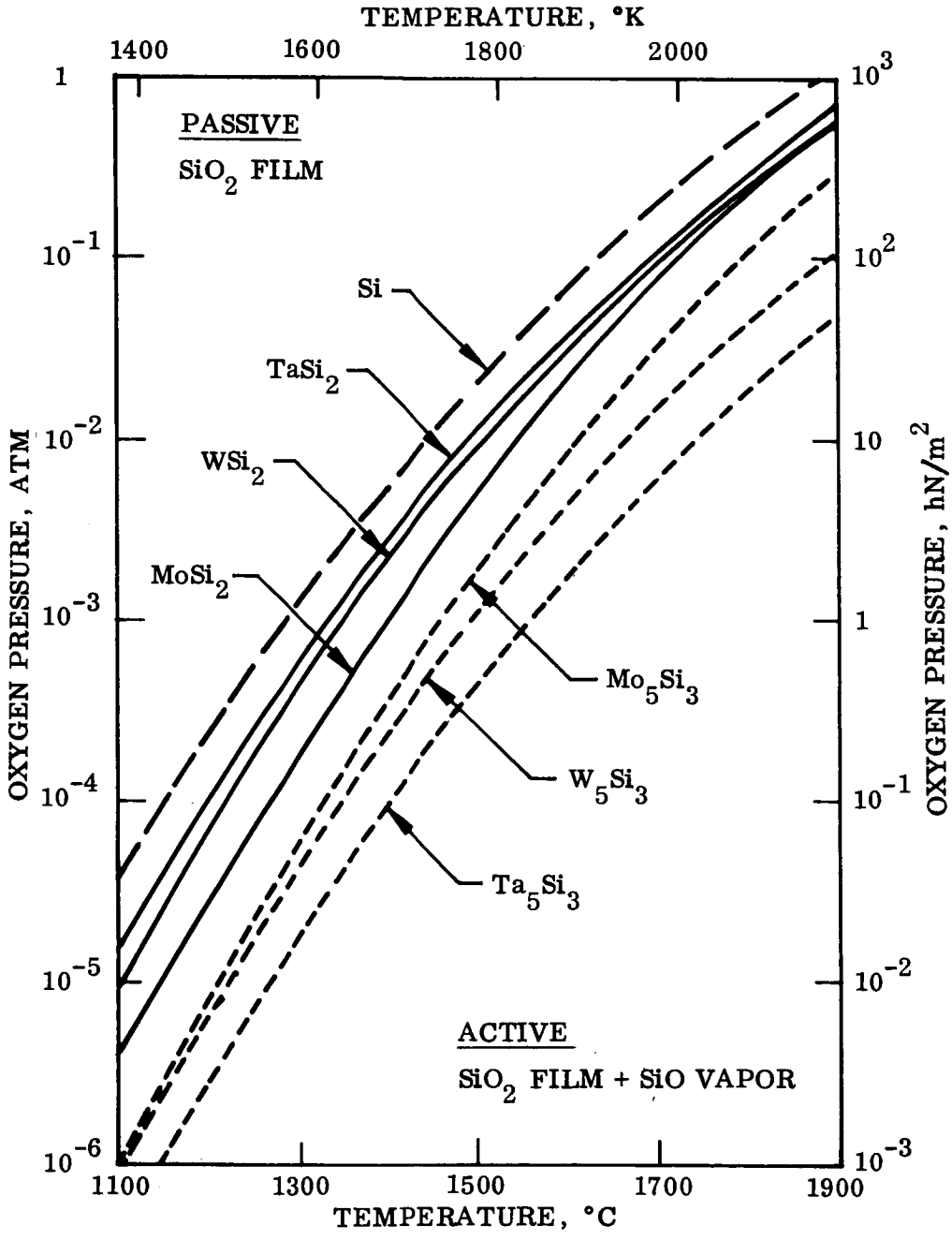

Figure 16 Effect of Silicide Composition on the Theoretical Boundary for Passive to Active Transition in Low-Pressure Oxidation (Ref. 17).

Unfortunately, this compound has a very high transition temperature [>3000°F (1922°K)] at 1 atm for the formation of a protective silica film.

Extensive modification of the coating is needed to provide a major shift of this boundary to lower pressures. Since the boundary represents a limitation of silica as a protective oxide, one logical approach would be to introduce more stable oxides into the protective scale. Addition of more reactive elements, such as titanium, zirconium, hafnium, and yttrium that are selectively oxidized, might provide a modified silica scale that is more resistant to volatilization effects at low pressures. Silicides that form complex oxide scales can provide good protection and may serve as the basis for improved coatings. The Materials Advisory Board study indicated that coatings that form complex oxides, spinels, or dense glasses are needed for a major advance in performance (ref. 15).

- Substrate/Coating Interdiffusion

It can be seen from the foregoing discussion that a coating will experience accelerated oxidation and wearout largely as the result of silicon depletion. As the metal-to-silicon ratio in the coating is increased, the boundary for protective film formation will shift to higher temperatures and lower pressures. In most instances, coating life will be governed by the time required to shift this boundary into the operating temperature/pressure range. Unfortunately, this time is not governed solely by oxidation reactions at the surface that consume silicon; if it were, coating life would be several orders greater than that obtained with present systems. Silicide coatings do not have a fixed composition and structure. The coatings are changing continuously during service, as a function of the total environment. Silicon continues to diffuse to the substrate, forming an ever-widening zone of intermediate and lower silicides at the coating/substrate interface. This process is very rapid at high temperatures relative to the rate of silicon loss from the surface by oxidation. The net effect,however, is the same – depletion of the silicon reservoir and an increase in the ratio of metal to silicon in the coating. In many instances, diffusion of silicon to the substrate, rather than surface oxidation, is the life-controlling factor.

Diffusion studies of many systems indicate that the rate of conversion to lower silicides by this process depends largely on the substrate composition and is comparatively independent of coating composition. This relationship results from the fact that the process tends to be controlled by the diffusion of silicon through M_5Si_3 and M_3Si compounds formed at the interface by reaction with the substrate. The "M" in these compounds includes all the silicide-forming metal constituents of the substrate. Little, if any, of the metal constituents in the coating appear in these new phases developed during use at elevated temperatures.

When coating wearout is controlled by silicon diffusion to the substrate, life will depend solely on temperature and coating thickness. Since the process is diffusion controlled, life will be an exponential function of temperature and will be proportional to the square of coating thickness. Silicide coatings on molybdenum follow this relationship closely, and useful life can be predicted with reasonable accuracy from diffusion data (refs. 15, 20,21). Control of coating thickness provides a simple means for significantly extending coating life under these conditions.

- Hairline Fissures

The protective oxide films and silicide phases are strong and ductile at high temperatures. Ductility at low temperatures is negligible. Generally, the silicides have a high coefficient of expansion relative to that of the substrate and are placed in tension on cooling. The tensile stresses are relieved by the formation of hairline fissures in the coating perpendicular to the substrate. These tiny cracks extend to the coating interface or intermediate silicide layer at one end and through the protective oxide film on the surface at the other. On reheating, the fissures are closed by thermal expansion and heal by diffusion. They may reopen or new fissures may form during cooling.

During the heating cycle, oxidants can have access to the interior of the coating along these fissures. Oxides may form in the fissures, preventing complete healing at high temperatures. With repeated cycling, many of the fissures remain open and allow oxidation to continue within the coating. With time or repeated cycling, they widen and often they are the sites for initial wearout of the coating. Fissures formed at the edges of thin sheet are most subject to this type of oxidation because of the geometrical configurations and are most difficult to protect from internal oxidation.

Internal oxidation along fissures is simply another cause of removal of silicon from the coating and acceleration of wearout. Fissures increase the effective surface area for oxidation. In addition, oxygen pressure within the fissure may be considerably less than that at the surface, which can cause a transition to active oxidation and formation of SiO within the fissured region. Oxidation rates may be significantly higher than those at the surface (ref. 23).

It is generally recognized that the protective silica film must provide an effective seal for fissures at the surface to minimize this effect and assure long coating life. Control of the thickness and structure of the surface oxide is essential. The formation of thick, dense oxide layers that are plastic or viscous at moderate temperatures is needed to provide major advances in the performance of silicide-base coatings (ref. 15).

Coating Development Criteria

- Coating Concepts

The foregoing discussion suggests four different approaches to the development of improved silicide coatings for tantalum:

- Class I – Tantalum-free silicides without readily oxidizable metallic constituents
- Class II – Tantalum-free silicides with readily oxidizable metallic constituents to control the amount and characteristics of the oxidation products
- Class III – Alloyed silicides containing tantalum and readily oxidizable metallic elements designed to produce double oxides or spinels
- Class IV – Alloyed silicides that are low in tantalum and rich in metallic constituents that will control the softening point and plasticity of the oxide films

The first two are envisioned as stable, oxidation-resistant silicides (e.g., $MoSi_2$ or WSi_2) that have been modified by the addition of elements that will enhance the ability of the silica film to seal coating fissures and inhibit volatilization at low pressures.

A prime requirement for these coatings will be complete exclusion of oxygen from the substrate over a wide range of temperatures and gas pressures. Available thermodynamic data, knowledge of failure-protection mechanisms, thermal expansion data, and oxidation studies clearly indicate that $MoSi_2$ is the best base for such a coating system. There is evidence, however, that such a system may not be adequately self-healing in selected temperature/pressure ranges and may be susceptible to accelerated oxidation. Modification of a basic $MoSi_2$ coating will be required to achieve the desired properties. Selecting and balancing coating compositions to control the oxidation products and improve surface healing of fissures will be of prime concern in coating development studies.

- Molybdenum Disilicide Coatings

$MoSi_2$ coatings have been evaluated on tantalum in previous studies (ref. 24). The coatings had an open structure (porous, cracked), however, and performance was not up to the level attainable from fully dense molybdenum disilicide. Attainment of a fully dense, sound coating is considered to be a prerequisite for good performance, and new approaches must be devised for producing the desired structures on tantalum.

The application of dense $MoSi_2$ coating compositions that are free of tantalum will require a new approach to the application of fused slurry silicides. As used today, the slurries are usually composed of 65 to 75 weight percent silicon, with the addition of a metal or metals chosen to form a eutectic or near-eutectic liquid with the silicon at the fusion temperature. This silicon-rich liquid reacts with the refractory metal substrate to form silicides of the substrate metals. As these compounds are formed, the liquid is gradually consumed, and the result is a solid layered structure that is composed, as a rule, of a surface layer of the substrate metal disilicide backed up by a zone of the substrate's next lower silicide (M_5Si_3), containing in solution most of the eutectic-forming additions. The final bond to the substrate is usually a thin diffusion band of a low-silicon phase.

This mechanism of the fused-coating formation intrinsically restricts the composition of the coating to the silicides of the substrate and offers little, if any, control over composition. The basic chemistry is modified only to a very limited degree by judicious choice of the eutectic former and minor additions of other metals. When it is desired to shift the composition of the principal coating-forming silicide from that of the substrate to another that may be more stable under service conditions, the silicon-eutectic slurry technique is not applicable.

An approach that has been used with mixed success is the deposition of an alloy modifier on the surface of the part to be coated. The modifier is then reacted with a fused silicon-eutectic slurry to produce the desired coating, free of substrate elements (ref. 24). This process was the basis for the Cr-Ti-Si coating initially developed for columbium in the 1960's, with the exception that the Cr-Ti alloy overlay was siliconized by a pack process rather than by a slurry process (ref. 25). In current practices, alloy modifiers, including Mo and W, are applied by slurry fusion, slurry sinter, or vapor deposition processes. The alloy overlays are then converted to silicides by slurry-fusion or vacuum-pack processes (refs. 24,26).

Although encouraging results have been achieved with both tungsten and molybdenum silicide-base coatings, all the approaches have a weakness in common that limits the overall reliability of coated hardware: the control of coating thickness, composition, and structure of such coatings becomes increasingly difficult as the complexity of the part to

be coated increases. If the alloy modifier layer is not deposited uniformly or if the subsequent siliconizing step does not proceed uniformly, gross variations in composition and structure will occur. The most common variation is the result of penetrating the alloy modifier layer by over-siliconizing thin spots. Substrate elements will appear in these regions of the coating, and random sites for early wearout are created (ref. 23). While it is possible to control this behavior on small coupons or samples in the laboratory, it is virtually impossible to achieve adequate control in the production coating of complex parts. Nonuniform deposits are likely to occur as a result of blind spots, temperature gradients, and inadequate or excessive flow in many areas. Past experience clearly indicates that a single-step coating process or a duplex process in which the second layer is a duplicate of the first will produce the most reliable coating system for large, complex, sheet-metal parts.

The two-step processes in which an alloy modifier is applied for subsequent conversion by an overlayer have another limitation with respect to manufacture, assembly, and repair: these coatings do not, in general, lend themselves readily to recoating or local repair of damaged areas. Recoating of fasteners is particularly difficult. In general, stripping and recoating of the entire part may be necessary to effect sound repairs.

- Fugitive Vehicle Slurries

A new approach to the application of silicides free of substrate elements by slurry-fusion techniques has been conceived. This approach entails the use of a low-melting-temperature fugitive vehicle that will contain silicon and perhaps one or more of the other coating elements in solution. Elements that do not dissolve are dispersed as fine powders in the liquid alloy. The process is predicated on the occurrence, within the liquid vehicle, of the chemical reactions to form the silicides.

When a coating is desired in a situation that requires that the silicide formation and growth be confined to the fused slurry layer (i.e., between the components of the slurry), the chemical transfer through the interface between the fused slurry and the tantalum substrate has to be controlled. Operating with a slurry wherein the fused silicon is put in contact with a high-surface-area powder of the desired silicide former, at a temperature at which the reaction rate is controlled by the interface transfer, the powder/liquid reaction will be favored simply because the area of the powder exposed to the liquid is much greater than that of the substrate surface. To lower the fusion temperature, a low-melting-temperature silicon solvent will be used as the fugitive carrier. Depending on its nature, this solvent will be removed from the coating during the fusion by volatilization, or will enter the composition of the coating as one of the silicide formers. From the chemical point of view, the reagents that have a high solubility for silicon are of two types: (1) those that are inert to most or all other components in the slurry system, including the refractory metal substrate and (2) those that have a tendency to react with the substrate and other slurry components.

Metals such as magnesium and calcium belong to the first category. At 2000°F (1366°K) the magnesium-silicon system is completely liquid at all silicon concentrations up to about 65 weight percent silicon; in the calcium-silicon system, a liquid phase exists at concentrations of 75-percent silicon above 2300° F (1533° K). Both magnesium and calcium form eutectics at about 60 weight percent silicon which melt near 1800°F (1255°K). Magnesium and calcium are inert to refractory metals, and both have low boiling points and high vapor pressures, so they can readily be removed by volatilization from the fused coating.

Tin and antimony were considered for the second category of fugitive vehicles in this program. Both have complete liquid solubility for silicon above 2600°F (1700°K) and can be used as liquid solvents for most of the alloy modifiers for silicide coatings. Neither will dissolve molybdenum or tungsten, but both will alloy with tantalum. The melting points and vapor pressures are high compared with those of calcium and magnesium, giving a wider latitude for controlled evaporation of the fugitive vehicle as the coating is formed. Because of the toxicity of antimony vapor and safety problems involved in using this element for slurry coatings, only tin was selected for use in this program.

- Control of Oxide Films

The third approach to design of a fused coating for tantalum was to allow tantalum to enter the coating as a silicide but to modify the composition with readily oxidizable elements that will control the structure and properties of the protective oxide films. This is a variation of the basic fused slurry process currently in use. The main departure from conventional fused coatings (e.g., Si-20Ti-10Mo) is the adjustment of composition to provide the balanced atom ratios of alloy additions needed to produce double oxides or spinels in the oxidation products. It is known that minimum oxidation rates occur in many alloy systems at atom ratios where unique oxides are formed. The formation of Cr_2O_3 spinels, for example, is important in the oxidation resistance of iron-, nickel-, and cobalt-base alloys. Certain binary refractory metal alloys have rate minima at atom ratios where complex double oxides are formed. Recent studies at the Lockheed Palo Alto Research Laboratory show that the minimum rates of oxidation in Cb-Hf-Ti and Ta-Hf-Ti alloys occur at Cb:Hf and Ta:Hf ratios (atom) of 2:1, which would correspond to $HfO_2 \cdot Cb_2O_5$ or $HfO_2 \cdot Ta_2O_5$ if both elements were oxidized into the scale.

This approach is based on controlled atom ratios to yield double oxides with tantalum or spinels with iron and chromium, aluminum, or yttrium if all elements are oxidized into the scale. It is believed that such a balance will provide the most stable oxide phases with the best resistance to oxidation. All of these coatings contain an appreciable amount of tantalum as a coating constituent. In order to control chemistry, tantalum was added to the coating formulation prior to its fusion on the substrate. The process did not rely on reaction of the substrate with the slurry to create the desired coating formulation. Ultrafine metal powders and prealloyed slurries having a low melting point were used to produce the desired reactions within the slurry over a large surface area. No fugitive vehicle was used in this case, and a complete reaction between liquid and solid phases to form compounds was employed to solidify the coating.

In the fourth class of coatings, modifiers were employed to control the amount, softening point, and plasticity of the oxide films that form. Particular attention was given to increased oxide formation and oxide stability at low pressure. Internal oxidation along coating fissures can be minimized by forming a thicker layer of a more stable and protective oxide film. A pure amorphous silica softens (melts) at about 3100°F (1978°K). In the service range of 2600°−2800°F (1700°−1811°K), the silica film is soft but very viscous. Formation of large blisters has been observed in silica films on $MoSi_2$ in air at low pressure at 2850°F (1834°K) (ref. 22). As the viscosity of silica films decreases with increasing temperature, their ability to protect surface irregularities and fissures in the coating is increased. Electrical resistance measurements of oxide films on $MoSi_2$ made by LMSC reveal that silica films formed in air at 3000°F (1922°K) are impervious and completely insulating, whereas those formed at 2600°F (1700°K) have minute breaks at sharp edges or corners of coating fissures and surface irregularities. It was the aim of

this approach to coating improvement to reduce the softening temperature of the oxide films for improved protection at lower temperatures. This reduction must be done, of course, without decreasing the viscosity to the point where the oxides become fluid and can be washed off by a high-velocity flow.

Many metal oxides form low-melting eutectics with silica and were considered as additives to control oxide softening and viscosity. Table 3 summarizes the minimum melting temperatures and compositions for the M_xO_y-SiO_2 systems that might be considered in this program.

TABLE 3. – M_xO_y-SiO_2 EUTECTICS

[Pure SiO_2 = 3115°F (1986°K).]

M_xO_y	Weight percent M_xO_y	Melting temperature	
		°F	°K
FeO	62, 77	2147	1448
MnO	63	2192	1473
CoO	58, 75	2336	1553
TiO_2	10	2804	1813
Al_2O_3	10	2822	1823

Oxides of iron, manganese, and silicon have the greatest fluxing effect but may produce an oxide that is too fluid at high metal oxide concentrations. Oxides of titanium and aluminum have a more moderate softening effect and can be used at higher concentrations without an excessive reduction in viscosity. Combinations of FeO, MnO, and CoO, and TiO_2 with SiO_2 are of particular interest, since all form double oxides with silica and with each other. Basically, a $TiSi_2$ coating modified with iron, cobalt, or manganese should form protective oxides with an improved ability to protect surface irregularities and coating fissures at moderate temperatures.

- Eutectic Vehicle Slurries

The Class III and IV coatings proposed for this program represent a marked departure from current fusion coating technology. They do not constitute further development or continued minor modification of existed fused slurry coatings. The current generation of fusion coatings is produced from slurries rich in silicon (65–75 percent silicon). These coatings are predominantly lightly alloyed silicides that are rich in substrate elements owing to substrate reaction with the large excess of silicon in the slurry. Formation of the coating normally consumes about 1 mil (0.00254 cm) per side of the substrate during the fusion/diffusion cycle.

The basic process is one of MSi_2-Si eutectic fusion in which the range of compositions is limited. Figures 17 a and b illustrate the basic approach used to date in the design of

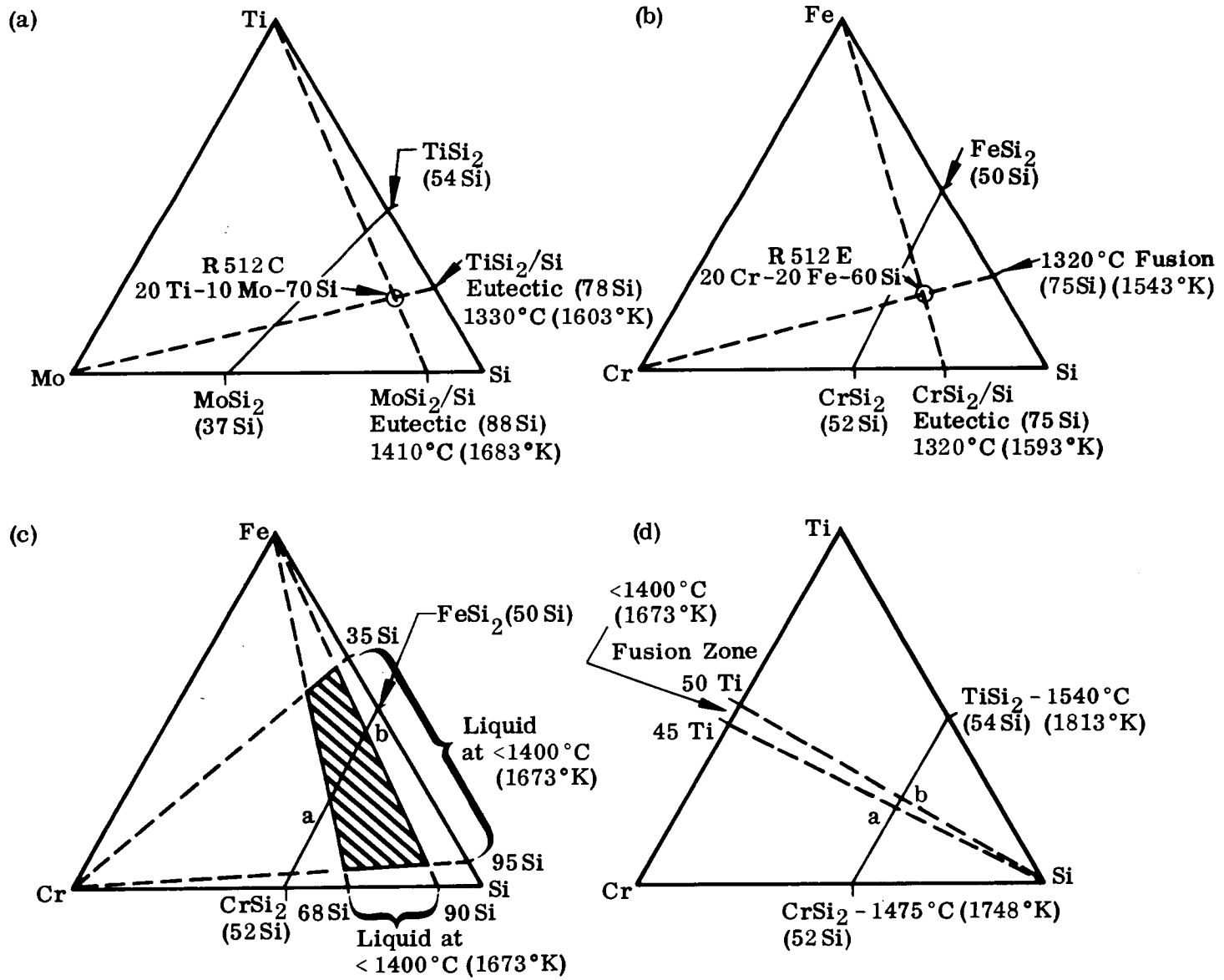

Figure 17 Possible Approaches to the Design of Fusion Silicide Coatings.

such coatings. The Si-20Ti-10Mo coating for Ta (R512C), for example, is formulated by the intersection of two tielines to the $TiSi_2$-Si and $MoSi_2$-Si eutectics (Figure 17a). With this formulation, eutectic melting will occur between titanium and silicon at 1330°C (1603°K) followed by melting of the balance of the coating at 1410°C (1683°K). If all the silicon reacts to form $MoSi_2$ and $TiSi_2$, a large excess will remain to react with the substrate; hence, this coating will be rich in silicides of tantalum.

A slightly different approach is used to formulate the Si-20Cr-20Fe coating for columbium (R512E). Here, the chromium and silicon are balanced for eutectic melting at 1320°C (1593°K), whereas the iron and silicon are balanced to form a hypoeutectic composition ($FeSi_2$-Si system) with complete melting at the same temperature. [Note: Eutectic melting in $FeSi_2$-Si occurs at 1208°C (1481°K).] This coating will have a fusion temperature of 1320°C (1593°K), and all constituents will fuse simultaneously. As with the Si-20Ti-10Mo coating, this composition has excess silicon and will form $CbSi_2$ (or Cb_5Si_3) in the coating. The formulation, however, is closer to the $CrSi_2$-$FeSi_2$ mixed disilicide tieline, and the coating would contain less of the substrate silicides.

Most fused slurry coating formulations are variations of composition around tieline intercepts such as these. In general, the compositions are at the silicon-rich end of the diagram, with quaternary or higher additions to improve performance. It is doubtful if further variations of this type will produce significant changes in performance. Instead, a major change in compositions of the fused slurry type should be sought. As has been discussed, this change should promote the formation of surface oxidation products containing controlled metal oxide additions. This will require the deposition of coatings with a predetermined composition that will dissolve a minimum of the substrate during fusion. The slurries for these coatings will have a higher metal-to-silicon ratio than those currently used and will be balanced in composition to produce mixed disilicides by reaction of the constituent elements in the coating with each other.

The design of such coatings must take into account the requirement for nearly complete fusion of the slurry deposit to obtain a dense, uniform coating well bonded to the substrate. In the past, it has been found that coatings designed with partial fusion tend to be loosely bonded or nonuniform. On the other hand, complete fusion can result in excessive flow of the coating. Best results appear to be achieved when a small amount of silicon or silicide remains solid to retain the liquid phases on the surface until reactions to form all the silicide phases are complete. In some cases, this can be accomplished by utilizing eutectic melting between the two metallic constituents to form a liquid phase that will react with solid silicon. For example, as shown in Figure 17d, Cr-Ti-Si can be produced by using a Cr-Ti alloy that melts below 1400°C (1673°K) to react with silicon which has a melting point above 1400°C (1673°K). This permits the coating to be formed completely at a temperature below the melting point of silicon without a substrate/silicon reaction. With this approach, based on a fusible metallic phase, coatings lean in silicon can readily be produced.

The metallic fusion approach will permit coatings to be formulated over a much wider area of the diagram, since it does not rely on eutectic fusion with silicon to form the coating. The shaded area in Figure 17c shows the range of compositions that can be fused at temperatures below 1400°C (1673°K), based on Fe-Cr silicide system eutectics. If Fe-Cr had a eutectic region with melting below 1400°C, this region could be extended to cover a much greater area of the ternary system.

A survey of binary eutectics indicates that cobalt, iron, manganese, yttrium, titanium, and chromium form many eutectics that melt below 1400°C (1673°K). These six elements provide the best basis for metal eutectic fusion coatings as a replacement for the current generation of silicon eutectic systems. It is significant that, as previously discussed, all of these elements are attractive constituents of silicide coatings for the control of oxide structure and properties.

Metallic fusion systems can be designed to produce a solid solution or mixture of the respective disilicides of the constituent elements. The majority of metal disilicides will form continuous or extended solid solutions with each other. Close control of slurry composition will be required, however, to produce the desired structure. The solid solubility range of silicides is wide with respect to metal:silicon ratio. This is illustrated by the ternary diagram for the Mo-V-Si system (Figure 18). Minor changes in silicon content will introduce new phases. If silicon reacts with the substrate during fusion, the Mo, V:Si ratio in the coating will increase and cause formation of intermediate silicides. In eutectic fusion systems, this effect is minimized by selection of compositions that have fusion temperatures below the fusion temperature of silicon. The liquid-metal phases may react with the substrate, which would decrease the metal:silicon ratio in the slurry. This is a more desirable direction in which to shift compositions. In general, the metal-eutectic slurries will fuse at low temperatures [<1400°C (1673°K)] and substrate reactions should be minimized. Metal eutectic fusion offers the ability to produce truly alloyed silicides of a closely controlled composition that should be relatively independent of substrate composition.

Screening of Experimental Coatings

- Experimental Approach

The experimental coating compositions were first screened for fusion behavior. Small tabs of Ta-10W sheet, 0.5 in. (1.27 cm) wide by 0.75 in. (1.91 cm) long by 0.013 in. (0.033 cm) thick were dip coated with 20 to 30 mg/cm^2 of the slurry to be evaluated. In some cases, drop tests were conducted with only a drop of the slurry placed on the tab to evaluate the surface wetting and flow characteristics for a given fusion temperature.

All coated samples were given the same initial fusion treatment. They were heated to 2550°F (1672°K) in 5 min in vacuum. The samples were diffusion annealed for 1 hr, furnace cooled to 1200°F (922°K) in 5 min, stress relieved 10 min at 1200°F (922°K), and furnace cooled to room temperature. The melting and flow behavior of each sample was observed through a sight port during the heatup and diffusion anneal.

The fired samples were inspected visually at low-power magnification for general quality. Factors such as density, surface texture, edge coverage, and coating fissures were considered in the visual examination. A 90 deg-4t bend was made at one end to check for coating adhesion and overall ductility. Selected samples were cross sectioned and examined by optical metallography to determine coating thickness, density, and general structure. Particular attention was devoted to the uniformity of thickness and structure on flat surfaces and edges.

When the coating did not fuse properly at 2550°F (1672°K), additional samples were fused at appropriately higher or lower temperatures. Coatings that did not melt or flow adequately at 2750°F (1783°K) were rejected as unsuitable for further evaluation. This

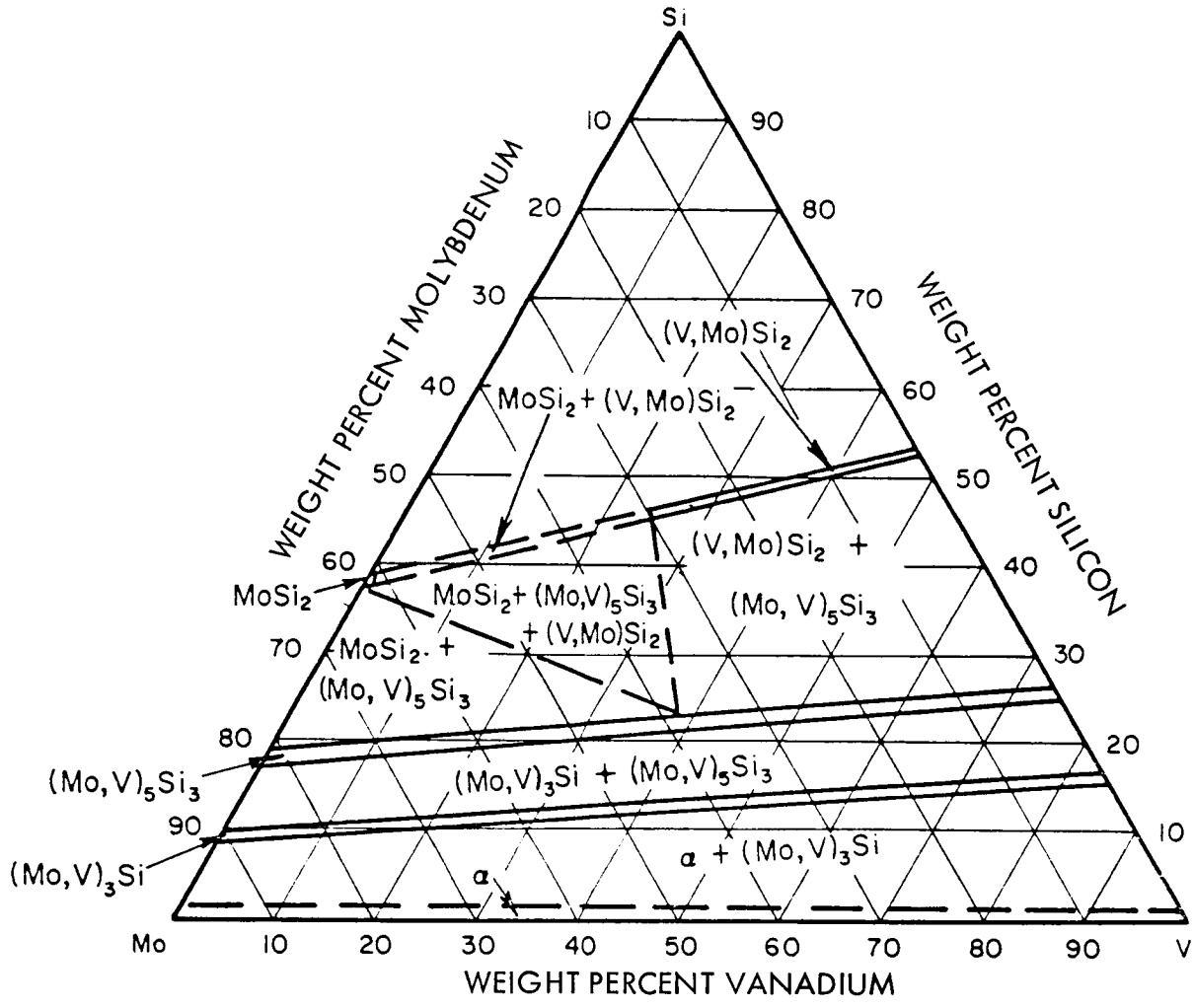

Figure 18 Mo-Si-V Ternary System at 800° C (1073° K) (Ref. 27).

decision was based on the consideration of 2570°F (1683°K) as the maximum practical temperature for the application of fusion silicide coatings. Silicon loss by evaporation is very high above this temperature, resulting in formation of porous and irregular deposits of varying chemistry.

Coatings that were too fluid at 2550°F (1672°K) were fused at 100°F (55.5°C or K) intervals lower until a temperature was reached at which flow was proper or fusion did not occur. In all tests, a suitable temperature was sought at which the coatings would fuse completely and flow over the surface to smooth out irregularities in the green deposit. Excessive flow to the bottom or edges was unacceptable, and attempts were made to correct this behavior by changes in fusion temperature or, in some cases, the rate of heating through the fusion range.

Coatings which, on the basis of fusion characteristics, overall quality, and structure, appeared to have the ability to protect the substrate were then screened for oxidation resistance. Test samples 0.5 in. (1.27 cm) wide by 4 in. (10.16 cm) long by 0.013 in. (0.033 cm) thick were coated with 20 to 30 mg/cm of green slurry and fused by the procedure previously established. The samples were then tested by slow cyclic exposure to a 2600°F (1700°K), 10 torr (13.33 hN/m^2) environment. The cycle consisted of 15 min to temperature, 30 min at temperature, and 15 min to 1200° F (922° K). Only the lower 3 in. of the specimens was heated in order to establish a temperature gradient for evaluating possible low-temperature limitations for each coating. The gradient was 800° F (444° C or K), with the top at 1800° F (1255° K) and the bottom at 2600° F (1700° K). Samples were inspected at 1, 5, and 10 cycles and every 10 cycles thereafter. They were removed from test on the first appearance of substrate oxide at the surface.

- Results of Fusion Studies

Fifteen coating compositions selected on the basis of the criteria presented in the previous subsection were evaluated for fusion behavior. The compositions proposed, arranged by classes, are given in Table 4 . Coating 1 is an unmodified $MoSi_2$ coating which was to be deposited by a fugitive-vehicle process using $CaSi_2$. Coatings 2 through 6 are modified $MoSi_2$ coatings produced by reacting molybdenum or $MoSi_2$ powders with a small amount of liquid silicon eutectic vehicle. Coatings 7 through 13 are basically $TaSi_2$ coatings, modified with large additions of titanium, hafnium, aluminum, chromium, iron, and yttrium to produce double oxides or spinels in the protective oxide films. Coatings 14 and 15 are baseline systems of existing coatings for tantalum. The Solar TNV-13 coating is normally produced by siliciding a metallic alloy overlay; in this program, an attempt was made to produce this coating by a direct fusion process using the Ti-Si eutectic as a liquid vehicle to react with the tungsten, molybdenum, and vanadium in the slurry.

Of these initial compositions, only compositions 11 and 15 fused to form acceptable coatings on Ta-10W. Many variations of the different coating systems were tried without success. The approaches based on the use of $CaSi_2$ (or $MgSi_2$) as fugitive vehicles were found to be completely impractical. The vapor pressure of the carrier element is too high and the liquid vehicle cannot be retained in the coating for a sufficient time to form dense, sound deposits. $CaSi_2$ works much better than $MgSi_2$ but still could not be used to produce a dense $MoSi_2$ coating by reacting the liquid with molybdenum powder. The resultant deposits were porous and loosely sintered. It is interesting to note that a sound, dense coating of $TaSi_2$ can be formed by reacting a $CaSi_2$ slurry with the substrate. An example is shown in Figure 19a. An excellent coating was obtained on flat surfaces. The fused slurry,

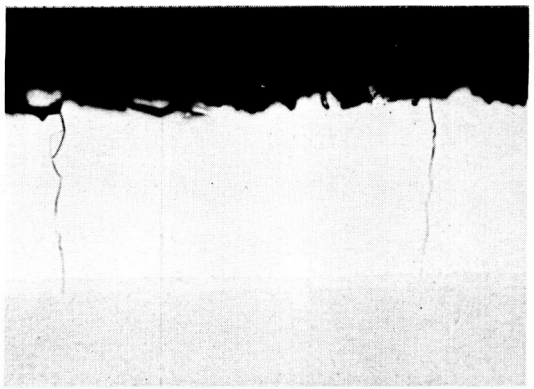

B3159

(a) $CaSi_2$ (1)

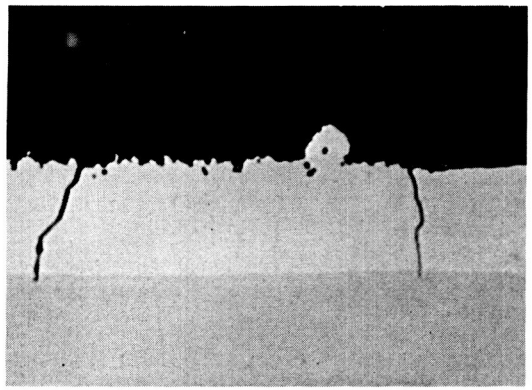

B3158

(b) 11 Al-39 Si-50 Sn (9)

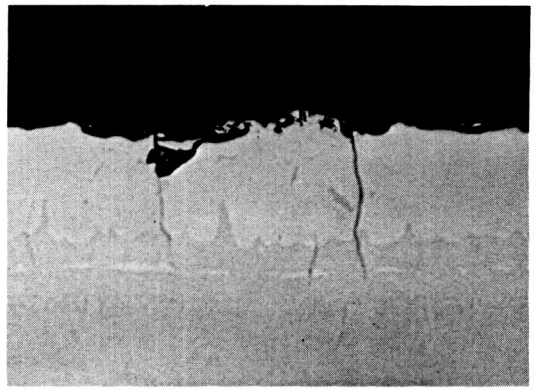

B3155

(c) 20 Al-20 Fe-60 Si (13)

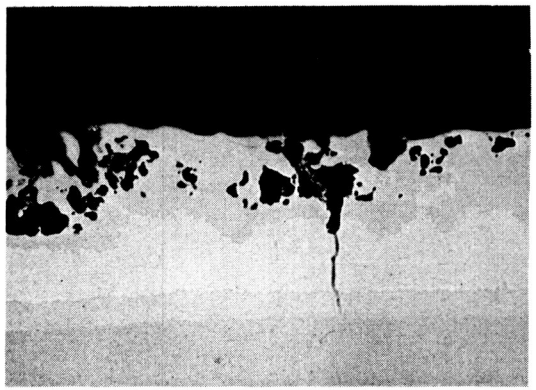

B3138

(d) 50 Hf-50 Si (8)

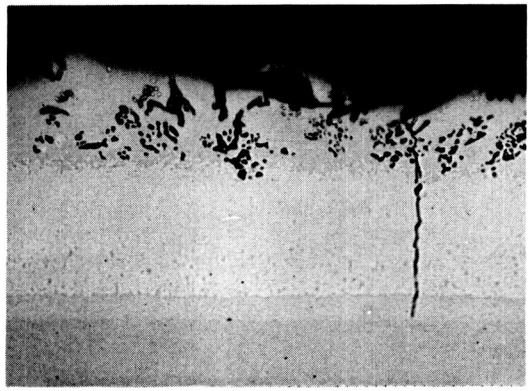

B3139

(e) 95 (50 Hf-50 Si)-5$TiSi_2$ (8)

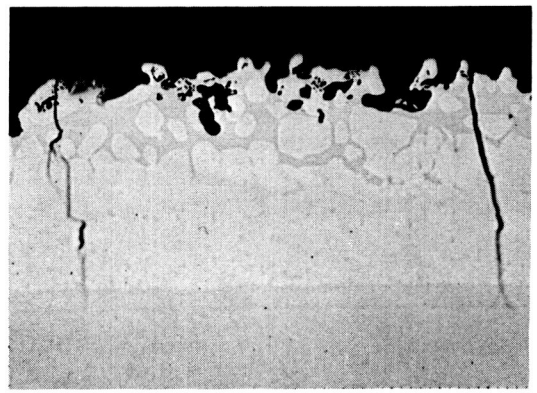

B3131

(f) 22.5 Ti-77.5 Si (7)

Figure 19 Structure of Experimental Coating Systems 1, 7, 8, 9, and 13, As-Deposited, Not Etched, 500×.

TABLE 4. – PROPOSED COATINGS FOR FUSION STUDIES

Class	No.	Type	Slurry composition	Liquid vehicle
I	1	Ta-free, fugitive vehicle	63Mo-37Si	$CaSi_2$
II	2	Ta-free, silicon eutectic	50$MoSi_2$-22.5Ti-27.5Si	45Ti-55Si
II	3	Ta-free, silicon eutectic	50$MoSi_2$-23.5Cr-26.5Si	47Cr-53Si
II	4	Ta-free, silicon eutectic	50$MoSi_2$-23.5V-26.5Si	47V-53Si
II	5	Ta-free, silicon eutectic	29Mo-34Zr-37Si	48Zr-52Si
II	6	Ta-free, silicon eutectic	66Mo-15Al-19Si	44Al-56Si
III	7	Ta-rich, silicon eutectic	60Ta-9Ti-31Si	22.5Ti-77.5Si
III	8	Ta-lean, silicon eutectic	50Hf-50Si	50Hf-50Si
III	9	Ta-rich, fugitive vehicle	29(78Ta-5Al-17Si)-71Sn	Sn
III	10	Ta-rich, silicon eutectic	28.2Y-71.8Si	28.2Si-71.8Y
III	11	Ta-rich, silicon eutectic	20Cr-10Fe-70Si	22Cr-78Si
III	12	Ta-rich, silicon eutectic	7Fe-20Y-73Si	21.5Y-78.5Si
III	13	Ta-rich, silicon eutectic	20Al-20Fe-60Si	25Al-75Si
–	14	Solar TNV-13	31W-12Mo-9.5Ti-9.5V-38Si	Si
–	15	Sylvania R512C[a]	20Ti-10Mo-70Si	22Ti-78Si

[a]Developed by the High Temperature Composites Laboratory, Chemical and Metallurgical Division, Sylvania Electric Products, Inc., now known as HiTEMCo, a subsidiary of DeWiant Corporation, Hicksville, N.Y.

however, tended to draw to the edges and formed unacceptably thick coatings with large fissures at all edges.

Attempts to produce fusion coatings with less than 50-percent silicon in the slurry were equally unsuccessful. Coatings 2 through 7 and coating 14 showed, in general, incomplete fusion and consisted of loosely sintered powders or porous deposits. The intent in these systems was to limit reaction with the substrate for better control of coating composition by reducing the amount of liquid carrier and having it react completely with fine powders of molybdenum, $MoSi_2$ or tantalum dispersed in the slurry. In all cases, the fusion and flow of the coating were insufficient. The liquid reacted rapidly with the powders but left a porous sintered deposit because of insufficient liquid phase. Only slurries having more than 50-percent silicon produced dense, sound silicide coatings (Nos. 8, 10 through 13, and 15).

It was concluded from this initial experiment that a large amount of liquid phase is required to produce a satisfactory coating. This, in terms of conventional technology, requires a high silicon content. Coatings 1, 3, 7, and 9 were reformulated to produce modified compositions in which excess silicon was provided. These coatings contain tantalum because of substrate reaction with the excess silicon. In addition, 13 new compositions based on metal-metal eutectic fusion to increase the amount of liquid phase without increasing substrate reactions were added for screening evaluation. Six of these were Class III, containing zirconium, hafnium, titanium, iron, and chromium, to form double

oxides or spinels; six were Class IV, containing cobalt, manganese, and vanadium, to control the softening points and viscosity of oxide films.

With few exceptions, the metal-eutectic coatings had excellent fusion characteristics and produced sound, high-quality coatings. In many cases, lower fusion temperatures were needed to limit coating flow. Low fusion temperatures and good surface flow proved to be major advantages of the metal eutectic systems. Slurries having as little as 45-percent silicon fused completely at a temperature of 2550°F (1672°K) or less.

With these additional compositions and variations of the original 15, a total of 74 different coating formulations were evaluated for fusion behavior and general quality. The results are summarized in Table 5 and Figures 19 through 23. As indicated in Table 5, 21 of these coatings showed sufficient promise to be recommended for oxidation behavior screening evaluation. A discussion of the fusion behavior and general characteristics of the various types of coatings evaluated in the fusion study follows.

(1) Coating 1 – $MoSi_2$ and Modified $MoSi_2$

As previously discussed, the fugitive vehicle approach for deposition was unsuccessful. Attempts to apply $MoSi_2$ by silicon eutectic fusion with 55-percent silicon were equally unsuccessful. It was concluded that lower melting point eutectics or a higher fusion temperature was needed to provide an adequate reaction between molybdenum, or $MoSi_2$, and the liquid phases in the coating. Iron, manganese, and cobalt were added in modifications 1b, 1c, and 1d to effect a fluxing action of the molybdenum and $MoSi_2$. The degree of fusion increased in direct proportion to the amount of low-melting constituents added. Good fusion was obtained with 33- to 34-percent iron or cobalt and 45- to 46-percent silicon, with the balance molybdenum. In all cases where $MoSi_2$ was added, with a resultant decrease in the free silicon content to 28 to 30 percent, fusion was incomplete. It appears that at least 45-percent silicon is required in the slurry for adequate fusion and flow. Coatings 1b with 20Mo-34Fe-45Si and 1d with 22Mo-33Co-46Si had excellent fusion and flow characteristics. Coverage was uniform, and edges were sound.

(2) Coating 2 – $(Mo,Ti)Si_2$

This coating was an attempt to fuse $MoSi_2$ with $TiSi_2$; titanium and silicon were added as elemental powders. Trial fusions were made at $MoSi_2$:$TiSi_2$ ratios of 50:50, 40:60, and 30:70 without success. In all cases, fusion was incomplete and a porous sintered deposit was formed.

(3) Coating 3 – $(Mo,Cr)Si_2$

This coating is similar to Coating 2 except that $CrSi_2$, as elemental chromium and silicon, was used as the liquid vehicle. The same ratios of $MoSi_2$:$CrSi_2$ were studied, and similar results were achieved. An attempt was made to produce a mixed Mo-Cr silicide coating from elemental powders of molybdenum, chromium, and silicon. Fusion characteristics were poor, with the silicon content as high as 56 percent and fusion temperatures to 2730°F (1772°K). Typical structures of a 28Cr-25Mo-47Si coating are shown in Figures 20E and F. The coating was variable, with thick edges and spots, and little, if any, flow occurred. The outer portion of the coating was granular, with many large voids. Only a thin inner region, about 0.8 mil (0.002 cm) thick, of dense, uniform coating was produced.

TABLE 5. – SUMMARY OF EXPERIMENTAL COATING STUDIES

No.	Coating type	Liquid vehicle		Slurry composition	Coating quality			Comments	Selected for screening tests
		Class	Composition Weight percent	Weight percent	Good	Fair	Poor		
1a	$MoSi_2$	Fugitive	$CaSi_2$	$80MoSi_2$-$20CaSi_2$			X	Loosely sintered.	
				$50MoSi_2$-$50CaSi_2$			X	Loosely sintered.	
				50Mo-$50CaSi_2$			X	Loosely sintered.	
			$86CaSi_2$-$14MgSi_2$	49Mo-$44CaSi_2$-$7MgSi_2$			X	Spalled on heating.	
		Silicon eutectic	Si	45Mo-55Si			X	Incomplete fusion, porous.	
1b	$(Mo,Fe)Si_2$		25Fe-75Si	$80MoSi_2$-15Si-5Fe			X	Loosely sintered.	
			44Fe-56Si	$50MoSi_2$-22Fe-28Si		X		Little flow.	
			42.5Fe-57.5Si	20Mo-34Fe-46Si	X			Good flow, sound edges.	X
1c	$(Mo,Mn)Si_2$		50Mn-50Si	$90MoSi_2$-5Mn-5Si			X	Loosely sintered.	
				$74MoSi_2$-13Mn-13Si			X	Incomplete fusion.	
				$50MoSi_2$-25Mn-25Si			X		
				$40MoSi_2$-30Mn-30Si			X		
1d	$(Mo,Co)Si_2$	Metal eutectic	60Co-40Mo	33Co-22Mo-45Si	X			Good flow, smooth edges.	X
2	$(Mo,Ti)Si_2$	Silicon eutectic	45Ti-55Si	$50MoSi_2$-22.5Ti-27.5Si			X	Incomplete fusion.	
				$40MoSi_2$-27Ti-33Si			X		
				$30MoSi_2$-31.5Ti-38.5Si			X		
3	$(Mo,Cr)Si_2$		47Cr-53Si	$50MoSi_2$-23.5Cr-26.5Si			X		
				$40MoSi_2$-28.2Cr-31.8Si			X		
				$35MoSi_2$-30.5Cr-34.5Si			X		
			37Cr-63Si	25Mo-28Cr-47Si		X		Thin, poor flow, granular.	
			44.5Cr-55.5Si	10Mo-40Cr-50Si			X	Incomplete fusion.	
			30Cr-70Si	20Mo-24Cr-56Si		X		Poor flow, granular.	
4	$(Mo,V)Si_2$		47V-53Si	$50MoSi_2$-23.5V-26.5Si			X	Incomplete fusion.	
				$40MoSi_2$-28.2V-31.8Si			X		
				$30MoSi_2$-32.9V-37.1Si			X		
5	$(Mo,Zr)Si_2$		48Zr-52Si	29Mo-34Zr-37Si			X	Incomplete fusion.	
			53Zr-47Si	19Mo-43Zr-38Si			X	Incomplete fusion.	
6	$(Mo,Al)Si_2$		44Al-56Si	66Mo-15Al-19Si			X	Porous, loosely sintered.	
7a	$(Ti,Ta)Si_2$		22.5Ti-77.5Si	60Ta-9Ti-31Si		X		Fissured edges.	
			22.5Ti-77.5Si	22.5Ti-77.5Si	X			Good flow, sound edges.	X
7b	$(Ti,Cr)Si_2$	Metal eutectic	53Ti-47Cr	25Ti-22Cr-53Si	X			Good flow, sound edges.	X
7c	$(Ti,Fe)Si_2$		50Ti-50Fe	24Ti-24Fe-52Si	X				X
7d	$(Ti,Mn)Si_2$		42.5Mn-57.5Ti	20Mn-27Ti-53Si	X				X
7e	$(Ti,Co)Si_2$		50Ti-50Co	24Ti-24Co-52Si	X				X
8a	$(Hf,Ta)Si_2$	Silicon eutectic	50Hf-50Si	50Hf-50Si		X		Flows to edges, coarse crystals.	
			40Hf-60Si	40Hf-60Si		X		Flows to edges, fine crystals.	
8b	$(Hf,Ti,Ta)Si_2$		49Hf-51Si	48Hf-2Ti-50Si		X		Flows to edges, coarse crystals.	
			52.5Hf-47.5Si	50Hf-5Ti-45Si	X			Uniform coating, fine crystals.	X
		Silicon eutectic	50Hf-50Si	95(50Hf-50Si)-$5TiSi_2$	X			Uniform coating, fine crystals.	

TABLE 5 (Cont.)

No.	Coating type	Liquid vehicle		Slurry composition	Coating quality			Comments	Selected for Screening tests
		Class	Composition Weight percent	Weight percent	Good	Fair	Poor		
8c	$(Hf,Cr)Si_2$	Metal eutectic	90Hf-10Cr	65Hf-7Cr-28Si	X			Uniform coating, good edges.	X
8d	$(Hf,Fe)Si_2$		85Hf-15Fe	60Hf-10Fe-30Si	X			Uniform coating, good edges.	X
8e	$(Zr,Cr)Si_2$		82Zr-18Cr	48Zr-11Cr-41Si			X	Spalled on heating.	
8f	$(Zr,Fe)Si_2$		70Zr-30Fe	41Zr-17Fe-42Si			X	Loosely sintered.	
8g	(Zr,Mn)Si		45.5Zr-54.5Mn	25Zr-30Mn-45Si	X			Uniform coating, good edges.	X
9a	$(Ta,Al)Si_2$	Fugitive vehicle	Sn	29(78Ta-5Al-17Si)-71Sn			X	Porous	
			27Sn-73Si	21Ta-14Al-16Sn-44Si		X		Large edge fissures.	
			56Sn-44Si	11Al-39Si-50Sn	X			Very thin, uniform.	
		Silicon eutectic	23Al-77Si	78Ta-5Al-17Si			X	Porous.	
			23Al-77Si	33.7Ta-15.5Al-51.2Si			X	Attacks substrate.	
			23Al-77Si	50Ta-11.3Al-38.7Si			X	Loosely sintered.	
			23Al-77Si	23Al-77Si			X	Spalls on heating.	
			20Al-80Si	20Al-80Si			X	Severe attack of substrate.	
			10Al-90Si	10Al-90Si			X	Severe attack of substrate.	
		Fugitive vehicle	$CaSi_2$	$15Al-85CaSi_2$			X	Penetrated substrate.	
9b	$(Ta,Ti,Al)Si_2$	Silicon eutectic	23Al-77Si	22Al-5Ti-73Si			X	Penetrated substrate.	
9c	$(Ta,Fe,Al)Si_2$		23Al-77Si	22Al-5Fe-73Si		X		Local reactions at edges.	
10a	$(Ta,Y)Si_2$		28.2Y-71.8Si	28.2Y-71.8Si		X		Flows to edges, edge fissures.	
10b	$(Ta,Mo,Y)Si_2$		28.2Y-71.8Si	90(28.2Y-71.8Si)-10Mo		X		Flows to edges, no fissures.	
			28.2Y-71.8Si	85(28.2Y-71.8Si)-15Mo	X			Uniform, good edges.	X
11a	$(Ta,Fe,Cr)Si_2$		22Cr-78Si	20Cr-10Fe-70Si	X			Uniform, good edges.	X
			30Cr-70Si	23Cr-23Fe-54Si	X			Uniform, good edges.	X
11b	$(Co,Cr)Si_2$	Metal eutectic	58Co-42Cr	29Co-21Cr-50Si		X		Nonuniform, good edges.	X
11c	$(Mn,Cr)Si_2$		70Mn-30Cr	35Mn-14Cr-51Si	X			Flows to edges, low fusion temp.	X
11d	$(Co,V)Si_2$		62Co-38V	19V-31Co-50Si	X			Uniform, good edges.	X
11e	$(Fe,V)Si_2$		65Fe-35V	17V-32Fe-51Si			X	Nonuniform, segregates.	X
11f	$(Mn,V)Si_2$		50V-50Mn	24V-24Mn-52Si	X			Uniform, good edges.	X
11g	(Mn,Fe)Si		50Mn-50Fe	24Mn-24Fe-52Si		X		Nonuniform, edge fissures.	X
11h	(Mn,Co)Si		50Co-50Mn	25Co-25Mn-50Si		X		Nonuniform, edge fissures.	X
12	$(Ta,Fe,Y)Si_2$	Silicon eutectic	21.5Y-78.5Si	7Fe-20Y-73Si			X	Flows to edges, edge splits.	
13	$(Ta,Fe,Al)Si_2$		25Al-75Si	20Fe-20Al-60Si			X	Flows to edges, edge splits.	
			20.5Al-79.5Si	17Fe-17Al-66Si		X		Edge fissures.	
			11Al-89Si	10Fe-10Al-80Si		X		Incomplete reaction.	
14	Solar TNV		Si	31W-12Mo-9.5Ti-9.5V-38Si			X	No fusion to 2800°F (1811°K).	
15	Sylvania R512C	Silicon eutectic	22Ti-78Si	20Ti-10Mo-70Si	X			Uniform, good edges.	X

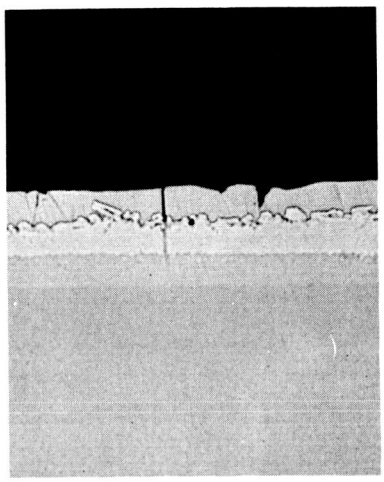

B3140

(a) 28Y-72Si(10)

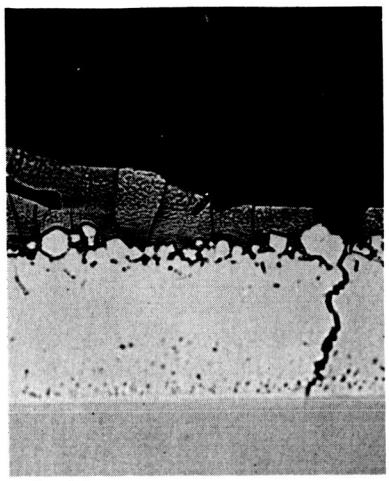

B3141

(b) 20Y-7Fe-73Si(12) Fused at 2460°F (1622°K)

B3156

(c) 20Y-7Fe-73Si(12) Fused at 2550°F (1672°K)

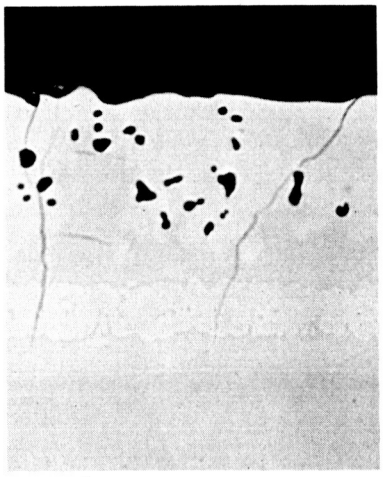

B3153

(d) 20Cr-10Fe-70Si(11)

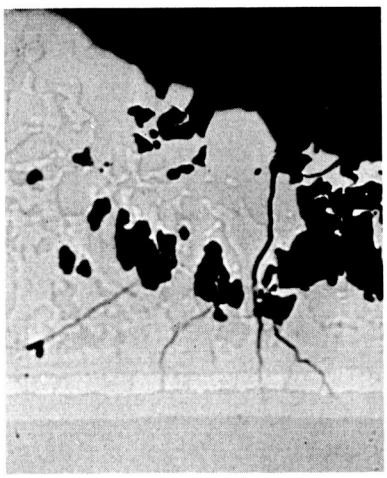

B3157

(e) 28Cr-25Mo-47Si(3) Fused at 2550°F (1672°K)

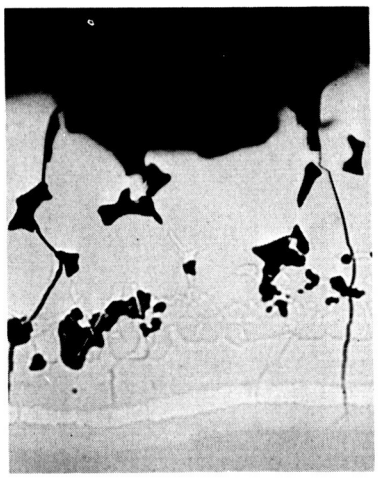

B3142

(f) 28Cr-25Mo-47Si(3) Fused at 2730°F (1772°K)

Figure 20 Structure of Experimental Coating Systems 3, 10, 11, and 12, As-Deposited, Not Etched, 500×.

(4) Coating 4 – $(Mo,V)Si_2$

This coating is also similar to Coating 2 but VSi_2 was used instead of $TiSi_2$ to fuse the $MoSi_2$ phase. The results were identical, with incomplete fusion at all temperatures to 2730°F (1772°K) and ratios of $MoSi_2$:VSi_2 as low as 30:70.

(5) Coating 5 – $(Mo,Zr)Si_2$

A Zr-Si eutectic melt was used as the liquid vehicle to react with molybdenum powder in this coating. Fusion was incomplete with a silicon content of 37 to 38 percent. As before, insufficient liquid phase was generated to produce adequate flow and a dense coating.

(6) Coating 6 – $(Mo,Al)Si_2$

The Al-Si eutectic was used to react with molybdenum in this system. Again, insufficient liquid was generated to form a dense coating.

(7) Coating 7 – $(Ti,Ta)Si_2$

This coating was predicated initially on the addition of tantalum powder to the slurry for reaction with excess silicon. It was believed that this would minimize the amount of reaction with the substrate and result in a more uniform and reproducible composition. In the first trial of this system, flow was limited and the edges of the coating were deeply fissured. It appears that the reactions with the powder are too rapid and the coating does not adequately wet, or flow over, the surface. The coating was reformulated, omitting the tantalum powder, and much better results were obtained. A standard Ti-Si eutectic produces an excellent coating on Ta-10W, as shown in Figure 19f. The coating is uniform and dense, with a slightly roughened or textured surface. An intermediate silicide (M_5Si_3) is present as a second phase, with higher concentrations near the surface. Fissures in the coating are fairly wide, indicating a moderate difference in thermal expansion coefficients between coating and substrate. Coatings ranging in thickness from 1 to 4 mils were readily produced by controlling the amount of green slurry applied.

The coating was modified further by additions of chromium, iron, manganese, and cobalt to introduce oxide modifiers into the protective films. Formulations 7b through e were based on metal-eutectic fusion systems and were designed to give double silicides (e.g., $TiSi_2 \cdot CrSi_2$). Compositions were selected from the intercept of the metal-metal eutectic melting tieline with the disilicide tieline in a ternary diagram constructed from binary systems. All systems had excellent fusion characteristics and produced dense uniform coatings and good edge coverage. These coatings, including the binary Ti-Si slurry, are very fluid at 2550°F (1672°K) and have some tendency to flow to edges, particularly if applied heavily. A slow rate of heating through the fusion range 2400°–2550°F (1589°–1672°K) or fusion at 2400°–2450°F (1589°–1616°K) will eliminate this problem.

(8) Coating 8 – $(Ta,Hf)Si_2$

The 50Hf-50Si slurry fuses readily at 2550°F (1672°K) but forms large primary dendritic crystals on the surface. As shown in Figures 19d and e the outer portion of the coating is very porous, with many large voids. By changing the Hf:Si ratio to 40:60, a finer structure and denser coating was produced. However, it was desired to maintain a lower silicon content for a controlled mixture of phases. In addition, the straight Hf-Si slurry had a

pronounced tendency to flow to the edges in both ranges studied. It was found, however, that these problems could be eliminated by the addition of 5-percent titanium or $TiSi_2$. Addition of 2-percent titanium had little effect, whereas 5-percent titanium produced a fine, dense structure, with uniform surface and edge coverage. A typical structure with a 5-percent $TiSi_2$ addition is shown in Figure 19e. The outer zone appears to be a continuous layer of the M_5Si_3 intermediate silicide, with random fine porosity. The dense inner zone has a two-phase structure, with M_5Si_3 islands dispersed in a MSi_2 matrix.

This coating was modified further by the addition of chromium and iron, in the place of titanium, to control oxide film structure and properties. Uniform, dense coatings with fine grain structures and good edge coverage were produced in both cases.

A further modification was made with zirconium substituted for hafnium in chromium- and iron-containing slurries. Although low-melting eutectics are formed by zirconium and chromium or iron, good fusion could not be obtained. The Zr-Cr-Si slurries invariably spalled from the surface upon heating to fusion temperature. The reason for this behavior was not apparent. The Zr-Fe-Si slurry did not fuse at all, and only a loosely sintered coating was formed.

By reducing the zirconium content and substituting manganese for iron, excellent fusion was achieved with as little as 45-percent silicon. This coating was very uniform, with good edge coverage.

(9) Coating 9 – $(Ta,Al)Si_2$

The combination of aluminum and silicon in a slurry produces an exothermic reaction that results in local attack of the substrate during fusion. Good coatings were achieved by fusion of either pure aluminum or pure silicon on Ta-10W. However, whenever the elements were combined in varying ratios from 10Al:90Si to 23Al:77Si, substrate attack resulted. The reactions occurred mainly at edges, with large splits and flowers of intermetallic compounds growing out from the edge. In one attempt, the silicon was added as $CaSi_2$ (fugitive vehicle) and the coating that was put on only one side of the sheet completely penetrated the substrate. The addition of 5-percent titanium to an Al-Si slurry produced a similar result. A 5-percent addition of iron reduced the reactivity but local edge attack still occurred.

The only method by which substrate attack could be prevented and a fused Ta-Al-Si coating produced was to use tin as a fugitive vehicle. A slurry of 11Al-39Si-50Sn produced a thin, uniform, dense coating. The coating was fused at 2550°F (1672°K) in helium, and the tin was subsequently removed by vacuum evaporation. A typical structure is shown in Figure 19b. The coating is about 1 mil thick and has very wide fissures penetrating to the substrate. Large fissures also formed at the edges. A large difference in thermal expansion coefficients is indicated, and the fissures produced in the coating are unacceptably wide.

(10) Coating 10 – $(Ta,Y)Si_2$

A Y-Si eutectic was used to apply a mixed $TaSi_2$-YSi_2 coating on Ta-10W. The slurries were prepared from prealloyed Y-Si powders, since yttrium is not stable in the presence of oxygen in powder form. The slurry fused well at 2550°F (1672°K) but had a pronounced tendency to flow to the edges. A large buildup of coating, with wide fissures, formed at

all edges. The structure of the Y-Si coating on flat surfaces is shown in Figure 20a. The coating is thin – about 1 mil thick – with two outer layers of equal thickness and two thinner inner layers of equal thickness. The outermost layer appears to be a low-melting yttrium-rich silicide phase.

Molybdenum (10–15 percent) was added to the coating in an attempt to reduce the tendency to flow to edges. Good results were achieved with a 15-percent molybdenum addition, and a uniform, dense coating with sound edges was produced.

(11) Coating 11 – (Ta, Fe, Cr)Si_2

Chromium and iron were added to this coating to introduce oxides that would form spinels in the protective film. Excellent coatings were produced by the fusion of silicon eutectics with 54- to 70-percent silicon. A typical structure of a 20Cr-10Fe-70Si coating is shown in Figure 20d. A 1.5-mil-thick coating with a uniform layered structure was produced. The thick outer layer appears to be an intermediate silicide phase (M_5Si_3) and contains a few random pores. A variety of modifications in which cobalt and manganese were substituted for iron and vanadium was substituted for chromium were also evaluated. All of these systems were based on metal/eutectic fusion and were designed to give mixed disilicides of the coating constituents with minimum substrate reaction. All slurries were formulated low in silicon (50–52 percent) to achieve this result. The Co-Cr and Mn-Cr silicide coatings tended to flow to the edges during fusion. The Mn-Fe and Mn-Co silicide systems fused nonuniformly and had large edge fissures. The Fe-V-Si coating segregated during fusion and produced an irregular coating. Excellent results were achieved with the V-Co and V-Mn silicide systems. All systems except the V-Fe-Si coating were recommended for oxidation screening tests to assess the relative behavior of the various combinations of oxide film modifiers in silicides.

(12) Coating 12 – (Ta, Fe, Y)Si_2

This coating is a variation of Coating 10; iron has been added to introduce a spinel-forming oxide into the protective scale. The coating fused well but had a strong tendency to flow to the edges. Deep, wide fissures formed in the thickened edge deposits. Decreasing the fusion temperature to 2460°F (1622°K) improved the edge condition but did not produce a satisfactory coating. Like the Y-Si coating, it probably needs an addition of molybdenum to control surface flow. The structures of this coating, as fused at 2460°F (1622°K) and 2550°F (1672°K), are shown in Figures 20b and c. The outermost layer appears to be a very low melting yttrium-rich silicide. At fusion temperature, this phase filled the large edge fissures that formed during growth of the coating. The higher fusion temperature increased the amount of intermediate silicides within the coating, probably as a result of increased reaction of silicon with the substrate. The metal : silicon ratio appears to be higher overall in this coating.

(13) Coating 13 – (Ta, Al, Fe)Si_2

The 20Al-20Fe-60Si slurry tended to spall on heating and flowed to the edges, forming deep splits when it fused. Prealloying of the powders prevented spalling but did not reduce edge buildup. Adjusting the Al-Si ratio and reducing the iron content had little effect. A typical structure of the 20Al-20Fe-60Si coating on flat surfaces is shown in Figure 19c.

(14) Coating 14 – $(W, Mo, Ti, V)Si_2$

As previously mentioned, this composition (Solar TNV-13) cannot be applied as a direct fusion slurry because of an inadequate volume of liquid phases. Based on experience with Coatings 1 through 5, a silicon content in excess of 60 percent is probably needed for adequate fusion and flow.

(15) Coating 15 – $(Ta, Ti, Mo)Si_2$

This formulation is the Sylvania R512C coating as applied by LMSC. The coating fuses well at 2550°F (1672°K) with little flow. A uniform, dense coating with good edge coverage is produced. The structure of the coating as deposited by Sylvania and LMSC is shown in Figures 21a and b, respectively. The general microstructural features are identical. The coating deposited by LMSC has a slightly thicker Ta_5Si_3 zone at the interface, indicating a slightly higher diffusion temperature or longer diffusion time than that used for the coating deposited by Sylvania. In addition, the LMSC-deposited coating had random deposits of spongy, unfused material on the surface, as shown in Figures 21c and d. Large edge fissures were also formed.

Three additional samples were fused in vacuum at 2370°, 2640°, and 2820°F (1573°, 1723°, and 1823°K) and given a 1-hr diffusion anneal at those temperatures to determine the effect on general structure and quality. Typical microstructures are shown in Figure 22. The sample fused at 2370°F (1573°K) has about the same Ta_5Si_3 layer thickness at the interface as the Sylvania sample. The outer portion of the coating has a much more columnar structure, however. (Compare Figure 21a with Figure 22a.) The outer structure becomes equiaxed and coarse grained with increasing fusion temperature. A 90°F increase in fusion temperature from 2550°F (1672°K) to 2640°F (1723°K) leads to pronounced grain growth in the outer portion of the coating. At still higher temperatures [2820°F (1823°K)] the outer layer appears to disintegrate and becomes very porous. It was concluded from these studies that the coating should be fused at about 2450°F (1617°K) to reproduce most closely the structure developed by Sylvania in depositing the R512C composition.

The change in structure and density of the outer layer with increasing temperature is probably the result of increased evaporation of silicon during fusion. A similar effect with respect to structural changes is observed when the coating is fused in vacuum or helium at the same temperature. As shown in Figure 23, fusion at 2570°F (1683°K) in helium at atmospheric pressure produces a columnar grain structure with a thin layer of equiaxed crystals at the surface. (Note polarized-light photographs.) The structure is similar to that obtained by fusing in vacuum at a lower temperature. As shown in Figure 23, the same coating fused in vacuum at 2570°F (1683°K) has a thick layer of coarse equiaxed grains at the surface.

Weight change measurements indicate a 2 mg/cm^2 weight loss when a 30 mg/cm^2 green slurry is fused at 2550°F (1672°K) in helium at atmospheric pressure for 1 hr. The same coating loses 5 mg/cm^2 on fusing in vacuum (10^{-5} torr, 1.33×10^{-5} hN/m^2). The 2 mg/cm^2 is the nominal loss due to evaporation of the organic binders. By difference, therefore, 3 mg/cm^2 of metallics (presumably silicon) also evaporate from the coating. Assuming that all the loss is silicon, the slurry composition would shift from 20Ti-10Mo-70Si to 22.4Ti-11.2Mo-66.4Si. Although this is not a drastic change in composition, it does cause a significant change in the outer structure of the coating. Most of this loss

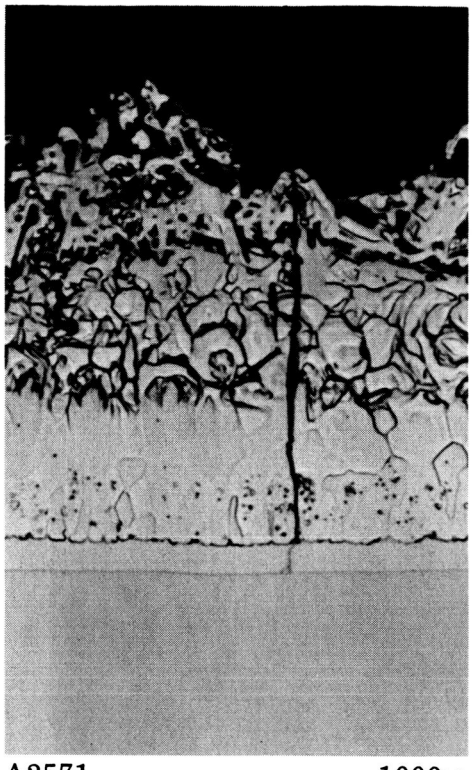

A2571 1000×

(a) Coated by Sylvania, 2 Mils/Side

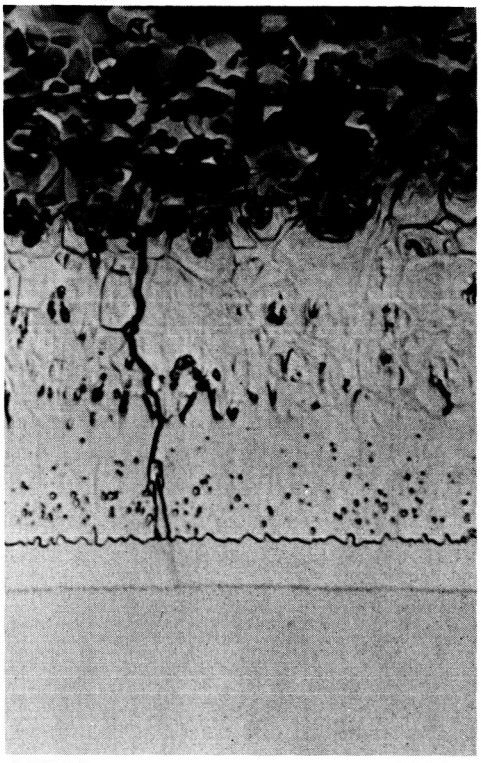

A2583 1000×

(b) Coated by LMSC, 2 Mils/Side

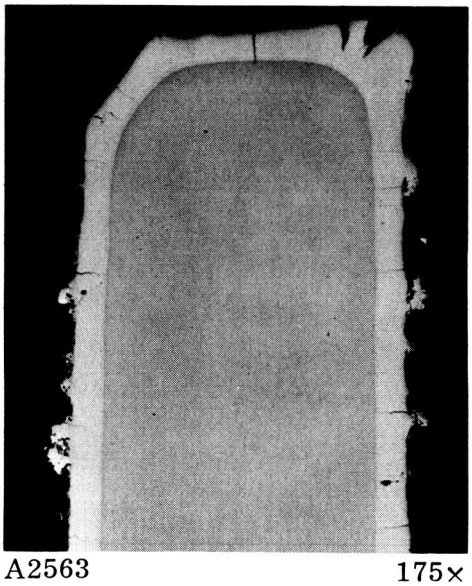

A2563 175×

(c) Coated by LMSC, 2 Mils/Side

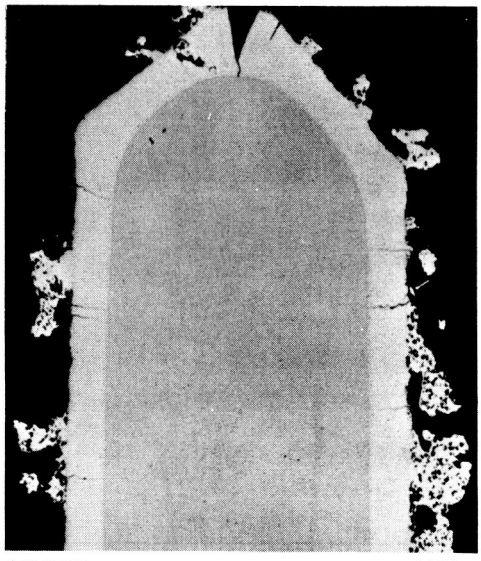

A2562 175×

(d) Coated by LMSC, 3.5 Mils/Side

Figure 21 Structure of Si-20 Ti-10 Mo (R512C-Type) Coating (No. 15, Experimental Series).

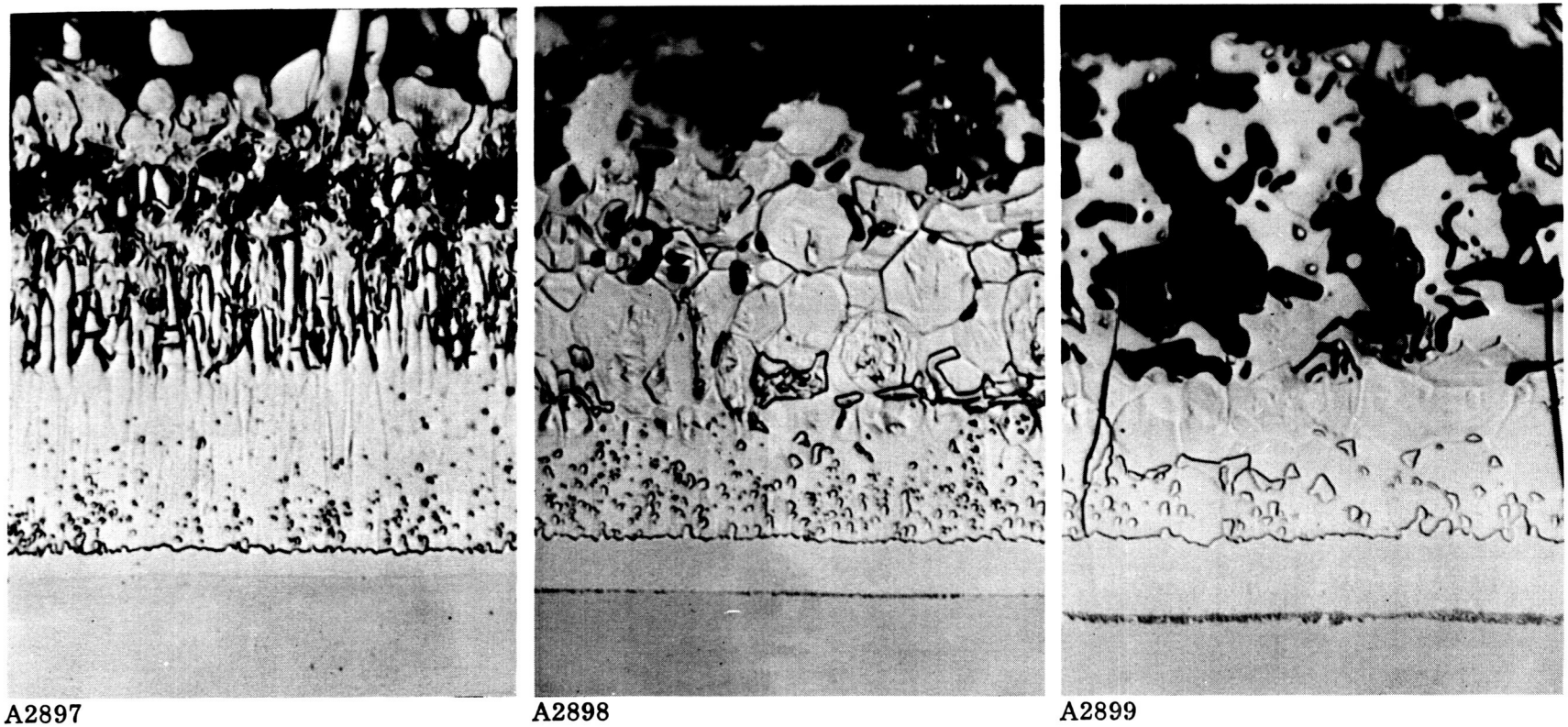

A2897 (a) 2370° F (1573° K)

A2898 (b) 2640° F (1723° K)

A2899 (c) 2820° F (1823° K)

Figure 22 Effect of Fusion Temperature on Structure of Vacuum-Fused Si-20Ti-10Mo, Etched, 1000×.

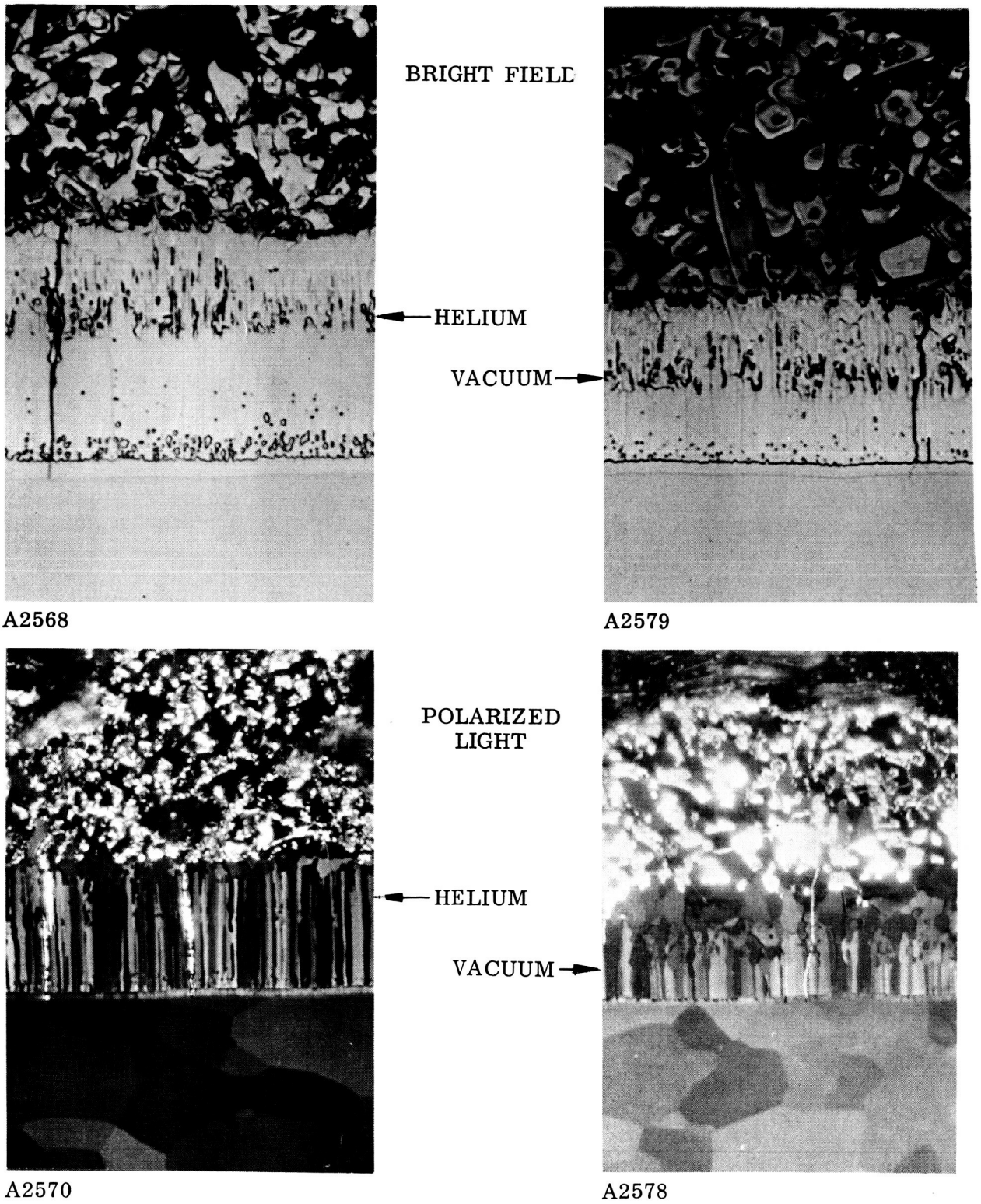

Figure 23 Effect of Vacuum Fusion on Structure of Si-20Ti-10Mo Coatings Fused at 2570°F (1683°K), 500×.

probably occurs on fusion, when liquid phases are present at the surface. Vacuum volatility studies with silicide coatings on molybdenum and columbium alloys reveal a net weight loss of 1 mg/cm^2 in 1 hr at 2600° F (1700° K) in vacuum (ref. 23) Visual observation of the R512C coating during fusion indicates that liquid phases are present for at least 30 min, accounting for the higher silicon loss. This coating should be fused in helium or at low temperatures [2450° F (1616° K)] in vacuum.

Coating weight studies indicate that a maximum thickness of 2 mils per side can be applied to 13-mil sheet without causing serious edge fissures. Thicker coatings tend to develop wide edge fissures, as shown in Figures 21c and d.

- Results of Cyclic Oxidation Tests

At least two samples from each of the 21 coating systems selected for oxidation screening test were exposed to the 2600° F (1700° K), 10 torr (13.33 hN/m^2) slow cycle. The results are summarized in Table 6 , with the coating systems listed in order of decreasing cyclic lifetime. Three coating systems – (MnTi)Si_2, (Mn, Zr)Si_2, and (Co, Ti)Si_2 – met the program goal of a 100-cycle life under these conditions. Five out of six samples of the (Mn, Ti)Si_2 coating had a 100 or more cycle life. This coating developed an extremely protective glassy black oxide film on the surface that effectively healed all fissures and surface irregularities. The oxide film was 1 to 1.5 mils (0.00254–0.00381 cm) thick over the entire surface and edges after 100 cycles of exposure.

It is significant that the only coating systems capable of providing protection for more than 30 cycles of exposure were of the Class IV type. These coatings were modified with either cobalt or manganese to control the softening point and viscosity of the oxide films. Eight out of the 10 Class IV coatings evaluated had lifetimes in excess of 30 cycles. The two systems that did not survive 30 cycles were (Co, Mn)Si_2 and (Co, Cr)Si_2. Both systems appeared to have generally poor resistance to oxidation and wore out between 10 and 21 cycles.

The other 11 coatings are of the Class III type, modified with elements to form double oxides or spinels. Cyclic lifetimes ranged from 5 to 25 cycles. Coatings rich in highly oxidizable metals such as hafnium and yttrium produced refractory oxide films and had the shortest cyclic lifetimes. The baseline R512C system – 20Ti-10Mo-70Si – wore out after about 10 cycles.

The results of this study clearly indicate that oxide film characteristics comprise the key factor governing coating life under cyclic exposure. Metallographic examination of exposed samples revealed that in all cases the initial wearout was caused by widening of fissures in the coating as a result of internal oxidation. A typical example is shown in Figure 24. Four different modifications of a $TiSi_2$ coating on Ta-10W are shown. In three cases (Figures 24a , b, and c) fissures that were of hairline proportions in the as-coated condition widened considerably after as little as 10 to 25 cycles of exposure. The oxide films on the surface are not dense, and oxygen has direct access to the fissure. The appearance of a M_5Si_3 zone along both edges of the fissure is evidence of oxidation in this region. The 2.5Mn-33Ti-64.5Si coating (Figure 24d), on the other hand, has a 1 to 1.5 mil (0.00254 to 0.00381 cm) thick,dense oxide film on the surface. After 245 cycles, the fissures in this coating grew to about the same size as those in the other three. Use of the modified oxide film resulted in a 10- to 20-fold increase in cyclic life due to the better surface protection at these sites. The mechanism involved in the

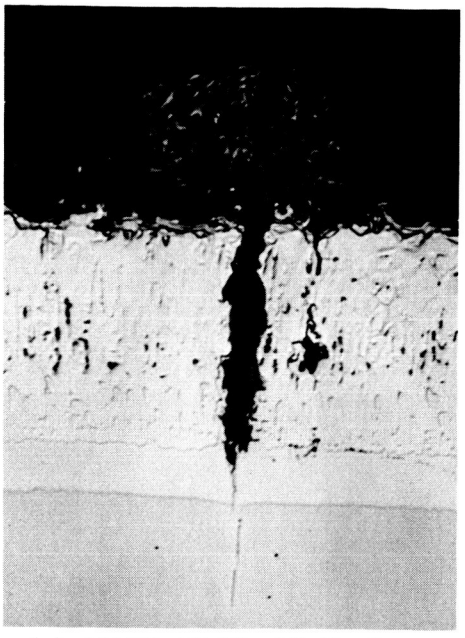

(a) 22 Ti-78 Si, 10 Cycles

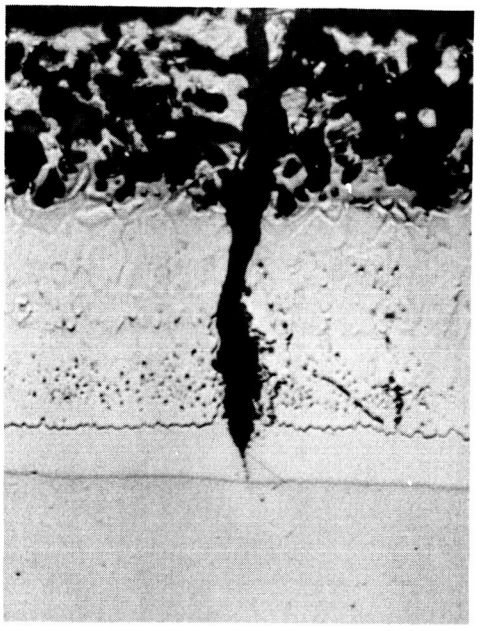

(b) 20 Ti-10 Mo-70 Si, 10 Cycles

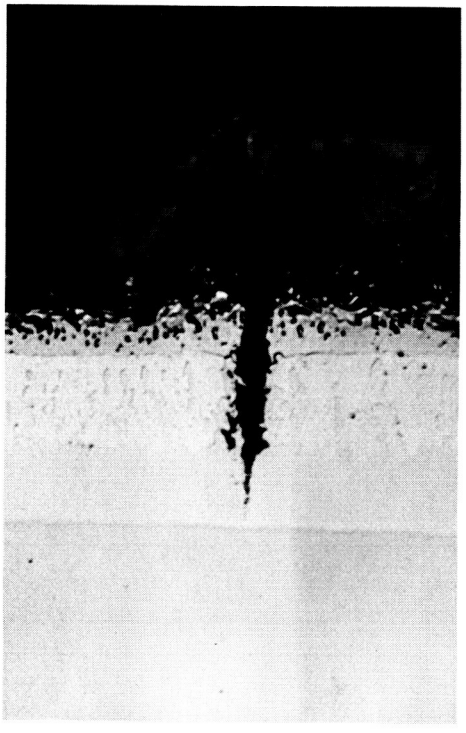

(c) 25Ti-22Cr-53Si, 25 Cycles

(d) 2.5 Mn-33 Ti-64.5 Si, 245 Cycles

Figure 24 Effect of Modifiers on Oxide Structure of Titanium Silicide Coatings Exposed at 2600°F (1700°K), Not Etched, 500×

TABLE 6. – RESULTS OF CYCLIC OXIDATION TESTS ON EXPERIMENTAL COATING SYSTEMS

Coating class	No.	Coating type	Liquid vehicle	Slurry composition, weight percent	Coating weight, mg/cm^2	Coating lifetime, cycles[a]	Wearout location
IV	7d	$(Mn,Ti)Si_2$	Metal-eutectic	20Mn-27Ti-53Si	20-22	50, 100, 100, 100+, 100+, 100+	Edge
IV	8g	$(Mn,Zr)Si_2$		25Zr-30Mn-45Si	28-29	100+, 100+	General
IV	7e	$(Co,Ti)Si_2$		24Ti-24Co-52Si	28-30	100, 100+	Edge
IV	1d	$(Co,Mo)Si_2$		33Co-22Mo-45Si	30-32	<40, <40, 59, 84, 100+	Edge
IV	11d	$(Co,V)Si_2$		31Co-19V-50Si	33-34	64-88, 40-69	Surface
IV	11g	$(Mn,Fe)Si_2$		24Mn-24Fe-52Si	18-20	17, 57, 64	Surface
IV	11c	$(Mn,Cr)Si_2$		14Cr-35Mn-51Si	18-27	30, 30, 40	Surface
IV	11f	$(Mn,V)Si_2$		24V-24Mn-52Si	30	<40, <40	Surface
III	7b	$(Cr,Ti)Si_2$		25Ti-22Cr-53Si	19-20	20, 25, 37	General
III	11a	$(Ta,Cr,Fe)Si_2$	Silicon-eutectic	20Cr-10Fe-70Si	25-26	20, 23	General
III	11a	$(Ta,Cr,Fe)Si_2$		23Cr-23Fe-54Si	24-25	10, 20, 20	General
IV	11h	$(Co,Mn)Si_2$	Metal-eutectic	25Co-25Mn-50Si	24-25	<21, <21	Surface
IV	11b	$(Co,Cr)Si_2$		29Co-21Cr-50Si	22	<21, <21	Surface
III	7c	$(Ti,Fe)Si_2$		24Ti-24Fe-52Si	19-24	10, 10, 15	General[b]
III	7a	$(Ta,Ti)Si_2$	Silicon-eutectic	22Ti-78Si	19-20	10, 10	Edge
Baseline	15	R512C		20Ti-10Mo-70Si	24-26	8, 10	Edge
III	10b	$(Ta,Y,Mo)Si_2$		85(28Y-72Si)-15Mo	–	5, 10, 10	Edge
III	8c	$(Hf,Cr)Si_2$	Metal-eutectic	65Hf-7Cr-28Si	19-25	6, 6, 11	Edge
III	8d	$(Hf,Fe)Si_2$		60Hf-10Fe-30Si	27-29	6, 6, 6	Edge
III	1b	$(Mo,Fe)Si_2$	Silicon-eutectic	34Fe-20Mo-46Si	17-18	5, 5, 5	Edge[c]
III	8b	$(Hf,Ti,Ta)Si_2$	Silicon-eutectic	50Hf-5Ti-45Si	20-23	4, 5	Edge

[a] 2600°F (1700°K), 10 torr (13.33 hN/m^2) – 15-min heat, 30-min hold, 15-min cool.
[b] 2300°–2500°F (1533°–1644°K) range.
[c] 2150°–2350°F (1450°–1561°K) range.

oxidation and protection of these sites is discussed in detail in the section on analysis of results.

- Damage Tolerance Assessment

The effect of local damage to a coating that may expose the substrate to oxidation is an important consideration in evaluating behavior. The main consideration is the rate at which oxidation in this area spreads to protected areas and broadens the damage site. It is desirable that the coating heal small sites and minimize their rate of growth.

The behavior of an initial group of 10 coatings screened for oxidation resistance was assessed by intentionally damaging the coating in a local area prior to oxidation testing. The coating was removed completely in a 0.060 in. (0.152 cm) diameter area by grit blasting to expose the substrate below. The samples were then exposed to the 2600°F (1700°K), 10 torr (13.33 hN/m^2) slow-cycle test and visually inspected after every cycle. In all but one sample, a 0.125 in. (0.318 cm) hole was oxidized clear through the sheet and coating on the reverse side after 1 exposure cycle (Figure 25b). In grit blasting the small site, it was difficult to determine whether all traces of the coating had been removed. On the second cycle, however, a hole was oxidized through the substrate and the thin coating layer did not remain protective. The hole oxidized through the specimens continued to enlarge with each cycle of exposure. Metal and coating were converted to oxide and physically removed. The outline of the oxidized portion of the sample at various cycles of exposure is shown in Figure 26. The material below this boundary has been converted to oxide and physically removed. Testing was stopped at 9 to 10 cycles – when 0.75 to 1.5 in. (1.9 to 3.8 cm) of the specimen had been consumed by oxidation.

In all tests, substrate oxidation was rapid and the coatings could not develop an adequate oxide film to protect the damage sites. Significant differences in the rate of recession by oxidation were noted, however. The hafnium-rich coatings (8b, c, and d) had the highest recession rates; the coatings rich in titanium and chromium (7a and b and 11a) had the lowest rates. The Fe-Mo-Si coating (1b) wore out at the edges in the cooler regions of the samples and established a secondary recession pattern.

The results of this study suggest that in coatings that form refractory oxide scales the spread of a damaged area will increase with continued oxidation. Coatings that contain cobalt or manganese as modifiers to soften the oxide films and control viscosity should be more resistant to local damage. The damage tolerance of such coatings is discussed in detail in the section on characterization of the best coating systems. The initial spread of a damage site (4t hole through coating) is slow by comparison, but a hole is still oxidized through the substrate in one cycle at 2600° F (1200° K), 10 torr (13.33 hN/m^2). The hole is about half the size of that formed in the alloys that do not contain cobalt or manganese. The growth rates on continued cycling are similar to those for the Ti-Si coating (No. 7a), and no major increase in healing tendencies exists.

The original intent of this study was to determine the effect of continued cyclic exposure on the bend ductility and tensile strength of intentionally damaged samples. This was

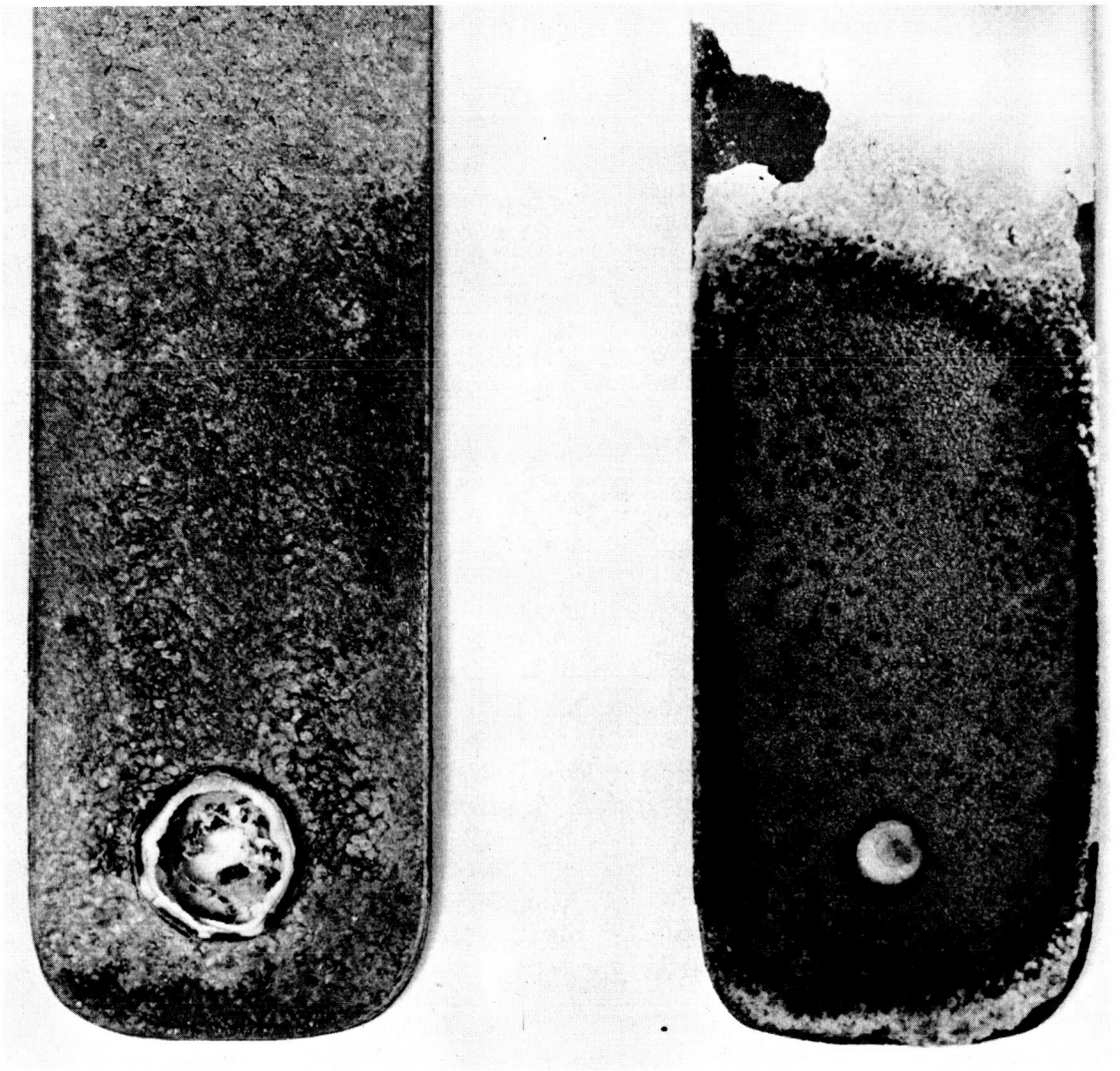

(a) Coating 10b, Y-Mo-Ta-Si. Coating removed to expose substrate; substrate oxidized.

(b) Coating 7c, Fe-Ti-Si. Incomplete removal of coating; substrate protected.

Figure 25 Representative Damage Test Samples After 1-Cycle Exposure, 2600° F (1700° K), 10 Torr (13.33 hN/m^2). [0.050 in. (0.125 cm) hole in coating.].

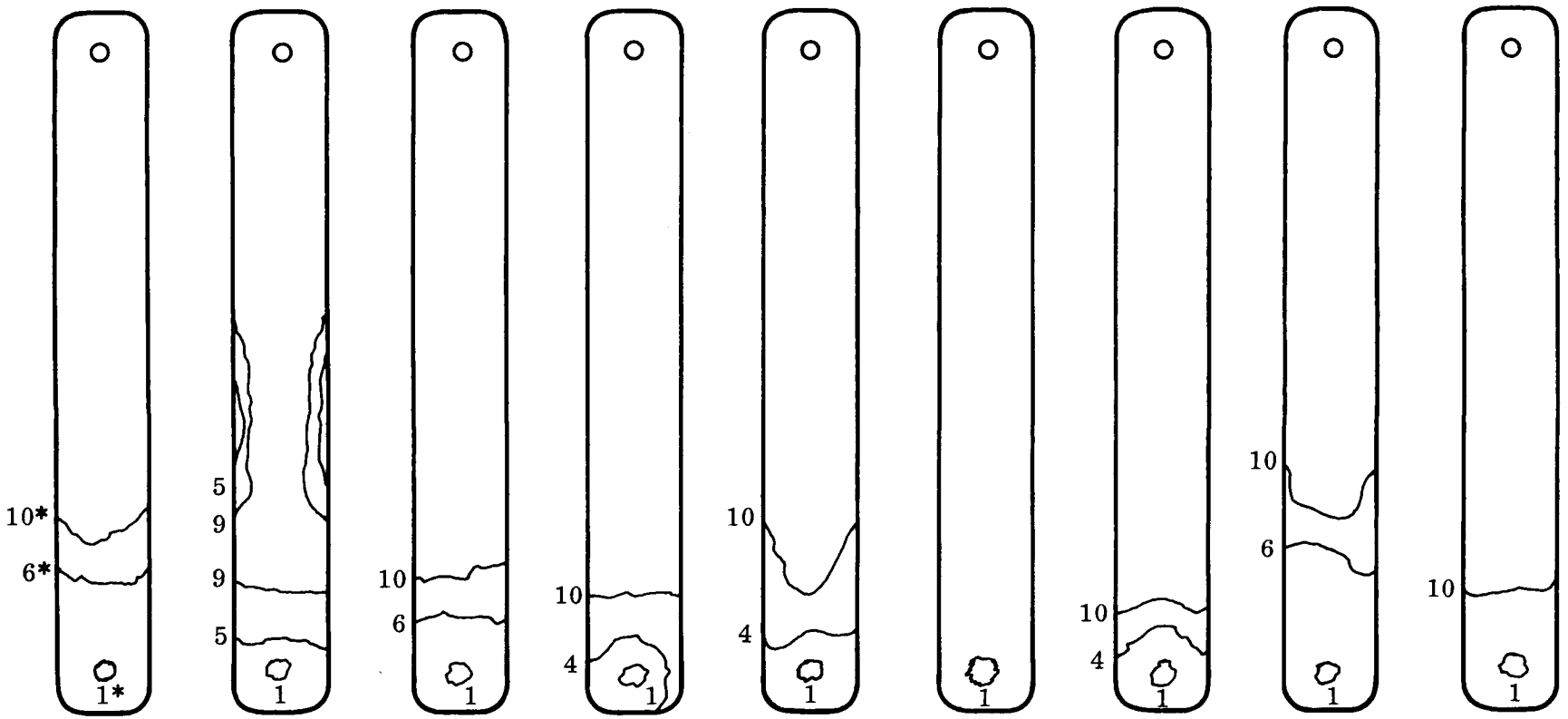

*Number of 2600° F (1700° K). 10 Torr (13.33hN/m^2) Oxidation Cycles.
Line indicates extent of oxidized substrate region.

Figure 26 Effect of Cyclic Exposure on Substrate Oxidation of Intentionally Damaged Experimental Coating Systems. [0.060 in. (0.152 cm) hole in coating to substrate.].

predicated on a behavior like that of columbium, in which the damage extends out from the site as a zone of interstitial hardening and embrittlement of the substrate. In Ta-10W, however, the substrate is converted rapidly to a voluminous oxide, and nothing remains to be tested. The surface recession by oxidation almost keeps pace with the inward diffusion of oxygen, so that only a narrow, hard, embrittled zone borders on the advancing oxidation front. Bend tests have shown good ductility to within about 0.050 in. (0.127 cm) of the oxide/metal interface. Since conversion of the metal to oxide is so rapid under these conditions, no further tests of damage tolerance were made. It is sufficient to conclude that local removal of any coating on Ta-10W will result in rapid penetration of the substrate by conversion to oxide but that the rate of oxidation is not catastrophic at 2600°F (1700°K).

- Basis for Selection of Development Coatings

An evaluation of fusion behavior, coating quality, and cyclic oxidation screening test results indicated that the following three coating systems of the six most promising systems have the best potential as improved fusion silicide coatings for tantalum:

(1) 20Mn-27Ti-53Si
(2) 24Co-24Ti-52Si
(3) 30Mn-25Zr-45Si

These coatings had a demonstrated capability to protect the substrate for over 100 cycles in air at 2600°F (1700°K) and 10 torr (13.33 hN/m^2). In each case, a protective oxide film developed on the surface early in the exposure and remained as an effective barrier to oxidation throughout 100 cycles. The as-coated thickness for all systems was 2 to 2.5 mils (0.00507 to 0.00635 cm), and the thickness after test of the silicide portion of the coating was 3 to 4 mils (0.00762 to 0.0102 cm) in the case of Systems 1 and 2, with an oxide layer approximately 1 mil thick (0.00254 cm). The silicide layer was thinner in the case of System 3 – about 1 to 1.5 mils (0.00254–0.00381 cm) – but the glassy layer was about 2.5 mils thick (0.00635 cm). In all cases, there was evidence of enhanced resistance to oxidation in fissures in the lower silicide zones that exist near the coating/substrate interface. This evidence is particularly clear in the case of Systems 1 and 2, in which a marked decrease is evident in the wideness of fissures at the boundary between silicides, about midway through the thickness of the coating. The remaining substrate thickness after 100 cycles was about 9.5 mils (0.0241 cm) in all cases, indicating that less than 2 mils (0.00508 cm) per side of substrate material were consumed during the coating process and the subsequent oxidation exposure [62 hr cumulative time at 2600°F (1700°K)].

Excellent bend ductility of the substrate was retained in specimens coated with each of these three coating systems. Samples of each system were ductile, with a 90 deg-4t bend at room temperature. It was also possible to reverse-bend these samples 90 deg. The material was ductile at both the cold end and the hot end of the gradient-heated sample, which demonstrates the effectiveness of these coatings over a broad temperature range.

Other candidates for selection as developmental coatings included the 31Co-19V-50Si, 24Mn-24Fe-52Si, and 22Mo-33Co-45Si systems. The 31Co-19V-50Si coating showed promise by surviving between 64 and 88 screening test cycles, but the oxide film that formed on the surface, although good in some regions, was nonuniform in thickness and quality. It was concluded that further compositional modifications of this system were necessary.

The 24Mn-24Fe-52Si coating demonstrated a potential of up to 64 cycles, but it was apparent that the oxide film that formed was too fluid at 2600° F (1700°K). Large globules of the oxide flowed to the lower portion of the specimen. As a result, further studies with this composition did not appear to be justified.

The 22Mo-33Co-45Si coating demonstrated a life capability of 100+ cycles in preliminary tests and was considered a leading candidate for further evaluation. It was discovered, however, that the sample tested, which had been heated by a platinum susceptor along with a manganese-base coating system, had been contaminated with platinum and manganese on the surface. Additional samples were retested in an atmosphere free of these contaminants, and the coating lifetime would not exceed 40 cycles. Additional development work appears to be needed on this system, and it was therefore not selected for further evaluation.

- Property Characterization

The three LMSC-developed coating systems and three additional fusion silicide coatings previously developed by Sylvania were evaluated for strength and ductility after cyclic oxidation. The compositions tested are listed below.

- LMSC-Developed

  (1) 20Mn-27Ti-53Si
  (2) 24Co-24Ti-52Si
  (3) 30Mn-25Zr-45Si

- Sylvania

  (1) R512A – 20Cr-15Ti-75Si
  (2) R512C – 20Ti-10Mo-70Si
  (3) R512K – 20Ti-10Mo-3V-67Si

The Sylvania coatings were prepared and applied by the High Temperature Composites Laboratory, Chemical and Metallurgical Division, Sylvania Electric Products, Inc., Hicksville, N.Y.* The LMSC developmental coatings were dip coated and fused by the same procedures as used to coat screening test samples.

The first lot of samples prepared for the three LMSC systems did not perform properly. Edge condition was poor with the CoTiSi samples, a different oxide film formed on the MnTiSi coating, and the MnZrSi coating would not fuse completely, leaving a porous deposit. These difficulties were traced to a new lot of silicon powder that was contaminated with over 1-percent aluminum. No further difficulties were encountered when a new lot of high-purity silicon powder free of aluminum was used to prepare the slurries. It was concluded that aluminum is a deleterious impurity in these coating systems.

None of the tensile and bend samples of the above six coating systems survived more than 50 cycles of exposure to the 2600° F (1700° K), 10 torr (13.33 hN/m^2) condition. The

*Now HiTEMCo.

range of cyclic life is shown below.

System	Cycles to Wearout
MnTiSi	<10 to 50
CoTiSi	3 to 50
MnZrSi	<5
R512A	>9 < 25
R512C	>5 < 15
R512K	25

The performance of all systems was disappointing and indicated that further development work was required on all systems before proceeding with the work plan. The three LMSC-developed coatings had clearly demonstrated a 100-cycle capability in the initial screening tests. The variability in coating life exhibited at this point was not acceptable.

Samples that did not wear out in the cyclic exposures at 2600°F (1700°K), 10 torr (13.33 hN/m^2) were tested for tensile properties at room temperature. The results are presented in Table 7. Tensile ductility was reduced by the CoTiSi coating but was not affected by the other coatings in the as-deposited condition. The yield and ultimate strength, based on substrate thickness before coating, is low compared with that of uncoated Ta-10W. As will be discussed in the section on analysis of results, this is due to the fact that although the coatings have significant strength at room temperature and contribute to the strength of the composite, they are not as strong as the metal removed from the substrate during the coating process. Strength values based on residual substrate at room temperature are closer to the strength of uncoated Ta-10W. The Co-Ti-Si coating protected the substrate from oxygen contamination for up to 50 cycles, as shown by the consistency of tensile properties. The MnTiSi coating also was fully protective for the 10 cycles of exposure it received. The R512A and K coatings were not fully protective, on the other hand, and permitted oxygen to contaminate the substrate gradually during cyclic oxidation. This was indicated by the increase in strength and a large decrease in ductility with increased cyclic exposure.

These test results are sufficiently encouraging to warrant further development of the three LMSC systems. Two have shown a potential for absolute protection of the substrate under cyclic oxidation at low pressure (CoTiSi, MnTiSi), and all have shown potential for a lifetime of 100+ cycles. Process and compositional studies were designed to develop the full potential of these systems.

TABLE 7. – ROOM-TEMPERATURE TENSILE PROPERTIES OF SPECIMENS COATED WITH LMSC DEVELOPMENTAL AND SYLVANIA SYSTEMS AS COATED AND AFTER EXPOSURE

Specimen No.	Slurry composition, weight percent	Exposure Condition[a]	0.2% Yield Strength				Ultimate Strength				Elongation, percent
			Original Substrate[b]		Residual Substrate[c]		Original Substrate[b]		Residual Substrate[c]		
			ksi	mN/m^2	ksi	mN/m^2	ksi	mN/m^2	ksi	mN/m^2	
–	–	Uncoated Ta-10W	73	504	–	–	86	–	–	–	18.6
OT91-5	24Co-24Ti-52Si	As-coated	66	456	78	538	76	525	90	627	8.3
OT91-1	24Co-24Ti-52Si	1 cycle	66	456	78	538	72	497	84	580	6.7
OT91-2	24Co-24Ti-52Si	25 cycles	74	511	88	607	79	545	93	642	5.7
OT91-3	24Co-24Ti-52Si	50 cycles	–	–	–	–	78	538	92	635	6.2
OT99-1	30Mn-25Zr-45Si	As-coated	62	428	76	525	80	552	95	655	18.8
OT96-2	20Mn-27Ti-53Si	As-coated	64	441	77	532	80	552	95	655	13.3
OT96-5	20Mn-27Ti-53Si	10 cycles	62	428	73	504	80	552	95	655	17.9
R512A-T2	Cr-Ti-Si	As coated	63	435	75	518	80	552	95	655	16.9
R512A-T1	Cr-Ti-Si	9 cycles	66	456	79	545	66	456	79	545	~1.5
R512C-T2	20Ti-10Mo-70Si	As coated	68	469	–	–	81	559	–	–	16.9
R512C-T1	20Ti-10Mo-70Si	Wear out in <9 cycles	–	–	–	–	–	–	–	–	–
R512K-T2	Ti-Mo-V-Si	As-coated	65	448	78	538	80	552	95	655	16.5
R512K-T1	Ti-Mo-V-Si	9 cycles	80	552	95	655	90	621	103	711	9.8
R512K-T3	Ti-Mo-V-Si	25 cycles	96	663	117	808	96	663	117	808	~1.3

[a] 2600 °F (1700 °K), 10 torr (13.33 hN/m^2) cycle.

[b] Original substrate before coating.

[c] Residual substrate, as-coated.

Developmental Coating Systems Study

The screening tests resulted in selection of the following systems for further development:

- CoTiSi
- MnZrSi
- MnTiSi

The principal objective of this study was to develop the most effective coating or coatings within these systems and to establish the best application processes for these coatings. This study included the variation of compositions to improve the capability for protecting coating discontinuities related to hairline fissures at pressures greater than about 1 torr (1.33 hN/m^2) and generally to improve the performance at lower pressures through the development of more effective silica and metal oxide barriers to oxidation. In addition, process-variable studies were conducted to develop the coating structure that would provide the most effective performance for a given coating composition. The process variables studied included the type of metallic powder used in the preparation of slurries (i.e., elemental or prealloyed powders), the coating thickness, the fusion temperature and time at fusion temperature, and the rate of heating to fusion temperature and schedule for cooling from fusion temperature. Studies of coatings prepared using elemental and prealloyed powders were conducted to determine what effect different kinds of powders have on coating structure. Coating-thickness studies were directed toward determination of the best coating thickness for thin-gage material. Heating- and cooling-rate studies, as well as studies of fusion temperature and time at temperature, were conducted to select the best combination of these variables for maximum coating performance.

The fusion temperature is, of course, dependent upon what elements the coating contains and the interactions between the constituents (e.g., eutectic reactions), as well as interactions between the coating constituents and the substrate material. Too high a fusion temperature may lead to a fluid coating with excessive flow and resultant nonuniform coverage. Also, too high a fusion temperature may cause an inordinate degree of reaction with the substrate, which can result in appreciable dissolution of the substrate and sufficient interdiffusion to cause the composition of the coating to change unfavorably. Furthermore, too high a fusion temperature can cause appreciable loss of silicon and other coating constituents through volatilization. Too low a fusion temperature can cause incomplete fusion and incomplete reactions between the coating constituents and between the coating and the substrate. In addition, if during fusion the temperature is too low, the coating will not flow over any regions not covered by the slurry (e.g., low reentrant angles associated with complex shapes). Consequently, for each coating composition a determination must be made of the best fusion temperature for that specific composition.

The heating rate during the fusion treatment is similarly dependent upon the coating composition. In some cases, eutectic reactions occur between coating constituents at temperatures lower than the fusion temperature. These reactions may be critical to the formation of the desired composition and structure of the coating. In such cases, the heating rate must be compatible with the kinetics of interdiffusion of the coating constituents in order to form the appropriate eutectic composition; and it must also be sufficiently slow to allow these reactions to occur but must not be so slow as to allow premature flow of the liquid phases that are present. Conversely, eutectic reactions or other reactions

(e.g. the formation of high-melting intermetallics) that occur at lower temperatures must be avoided in order to form the proper coating. In such cases, the heating rate must be sufficiently high to prevent these reactions from occurring.

When the fusion temperature is reached, there must be time for the coating constituents to react with one another, form a liquid, react with the substrate, and form higher melting point silicides. With the coating systems under study, most of the outer regions are disilicides, with some lower silicides interspersed in some cases. It is exceedingly important that the substrate/coating system remain at a high temperature (i.e., near the fusion temperature) long enough after the silicides have formed for adequate interdiffusion between the disilicides and the substrate to occur. This interdiffusion leads to the formation of a layer of M_5Si_3 (where "M" represents major substrate elements) at the coating/substrate interface. Previous studies (ref. 23) have shown that if the M_5Si_3 is not present or is very thin, the hairline fissures that form in silicide coatings may penetrate to the substrate, turn, and run along the coating substrate interface – a result that can cause spalling of the coating. If the M_5Si_3 layer is present, the hairline fissures terminate in this zone.

The time for formation of higher melting silicides was generally 5 to 30 min in the earlier studies of this program. The time for formation of the M_5Si_3 in the coatings studied is generally independent of coating composition because the reaction involves mainly the interdiffusion of only silicon from the coating and the substrate materials. A time of 1 hr at the fusion temperature was found to be adequate to produce a 0.0002 in. (0.0005 cm) layer of M_5Si_3, which is a sufficient thickness to arrest hairline fissures. Some studies were conducted with the TiMoSi system in which the time at fusion temperature was increased to 12 hr, causing an increase in M_5Si_3 thickness that was more than threefold the thickness resulting from a 1-hr fusion treatment. Cyclic oxidation tests conducted on these specimens showed no change in behavior from that producted by heat-treating for 1 hr. On the basis of analysis of the phenomena occurring at the fusion temperature and experimental results, a time of 1 hr was adopted for fusion treatments. This time is consistent with fusion times associated with the preparation of fused silicide coatings for columbium alloys.

Because the hairline fissures form in the coating during cooling from the fusion temperature, it could be expected that variations in the cooling rate might influence the density of these fissures. To define the influence of cooling rate, four different cooling schedules were evaluated using the Mn-Ti-Si system, as follows:

(1) 2 min to ~400° F (478° K) and ~10 min to room temperature
(2) 5 min to 1100° F (866° K), 5 min at this temperature, 5 min to ~400° F (478° K), and ~10 min to room temperature
(3) 20 min to 400° F (478° K) and ~10 min to room temperature
(4) 30 min to room temperature

The differences in cooling histories caused no differences in the size, density, or distribution of hairline fissures, nor did they influence coating performance. This is understandable because it is believed that the fissures form at relatively low temperatures – probably lower than 200° F (366° K). Nevertheless, an intermediate cooling schedule (No. 2) was selected as the schedule for fusion treatments and was included in the fusion heat-treat program on the Datatrak programmer.

- CoTiSi System

The CoTiSi system was the primary system for studies of the influence of process variables. Previous studies had been conducted with a 50Co-50Ti composition on the Co-Ti side of the Co-Ti-Si phase diagram. The overall composition of this system was 24Co-24Ti-52Si. A shift was made toward higher cobalt:titanium ratios, however, with the objective of producing a modified silica having a lower melting point that would be more effective in covering the surface irregularities associated with fissures in the coating. A coating composition of 27Co-22Ti-51Si, representing a cobalt: titanium ratio of 55:45, was selected for study. Two fusion temperatures, 2417°F and 2507°F (1598° and 1648°K), and two times, 5 and 20 min, for heating to the fusion temperature (in vacuum) were evaluated. In addition, coatings prepared with both elemental and prealloyed powders and two coating thicknesses, 0.002 and 0.004 in. (0.005 and 0.010 cm), were studied. The environment during the fusion treatment was helium.

The prealloyed powder was prepared from the compound CoTi, which represents a 55Co-45Ti weight-percent composition on the Co-Ti side of the Co-Ti-Si phase diagram. The CoTi intermetallic is ductile at room temperature. It was necessary to cool a CoTi ingot, which was formed by arc-melting cobalt and titanium, to a subzero temperature by immersing it in liquid nitrogen before it could be fractured and ground to -325 mesh powder.

The influence of these variations in process variables on the performance of the 27Co-22Ti-51Si coating was evaluated at 2600°F (1700°K), 10 torr (13.33 hN/m^2); the results are shown in Figure 27. Table 8 is a summary of all the exposures conducted during the developmental coating studies and the screening studies, and includes the results obtained with the Mn-Zr-Si and Mn-Ti-Si systems.

In the evaluation of the 27Co-22Ti-51Si coating, the maximum lifetime was 55 cycles, and the life-limiting factor was wearout of the coating at specimen edges. The specimens fused at 2507°F (1648°K) with a heating time of 5 min demonstrated the best performance; those fused at the same temperature with a heating rate of 20 min demonstrated the most limited performance. There was a suggestion that the thicker coatings provided better protection than thin coatings, but there was no clear trend. No appreciable difference in performance was found between coatings prepared with elemental powders and those prepared with prealloyed powders; and metallographic analyses showed the structure of the coatings prepared with the two kinds of powders to be identical (Figure 28).

These results, which showed shorter lifetimes with the 27Co-22Ti-51Si system than with the 24Co-24Ti-52Si system, suggested that any changes in composition should be made toward a lower cobalt:titanium ratio than 50:50. Therefore, a series of tests was conducted with specimens richer in titanium. Two compositions were prepared, using elemental powders: the original 24Co-24Ti-52Si composition, to supplement earlier results and to provide a baseline for comparison, and 21.5Co-26.5Ti-52Si. The following were used for these tests: two heating rates to fusion temperature, 5 and 20 min; two fusion temperatures, 2417°F (1598°K) and 2507°F (1648°K); and two coating thicknesses, 0.002 and 0.004 in. (0.005 and 0.010 cm).

Evaluation of these compositions and the different process variable combinations included cyclic exposures at 2600°F (1700°K), 10 torr (13.33 hN/m^2). In all cases, the coating at the edges of the specimens wore out in less than 20 cycles. These results were somewhat inconsistent with those of earlier tests in which some 24Co-24Ti-52Si coated samples

TABLE 8. – SUMMARY OF CYCLIC OXIDATION STUDIES WITH DEVELOPMENTAL COATINGS

Coating Composition	Fusion Conditions					Coating Weight mg/cm²		Specimens Prepared				Coating Lifetime Cycles[a]			
	Temperature		Time to Temperature, min	Environment				Screening	Bend	Tensile	Emittance	Screening	Bend	Tensile	Emittance
	°F	°K		Heating	1 hr Isothermal Diffusion Treatment	Green	Fused								
24 Co-24 Ti-52 Si	2552	1673	5	Vacuum[b]	1/3 atm He	21-24	20-23	3				17,17			
			5			28	28	1				66			
	2552	1673	10		1/3 atm He	35	–	1[c]							
	2507	1648	5		1 atm He	29-30	28-29	2				20			
			5			21	19-20	2				25,20			
			20			31	29-30	2				25,20			
	2507	1648	20			20-22	19-22	2				25,20			
	2417	1598	5			31	30	2				20			
			5			20	18	2				25,20			
			20			29-30	26-29	2				25,20			
	2417	1598	20		1 atm He	21	20	2				20			
	2372	1573	5		1/3 atm He	27-33	25-32	11		5	5	>100,>100 >25,>25		>50,>25 >25,>1	>50,>25,>1
27 Co-22 Ti-51 Si	2507	1648	5		1 atm He	30-32	28-31		4				55,55,50		
			5			20-22	20-21		4				50,50,25		
			20			30-32	27-29		4				10,10		
	2507	1648	20			19-21	14-20		4				10,10		
	2417	1598	5			28-31	26-29		4				25,25,25		
			5			20-21	20-21		4				55,25,25		
			20			29-31	27-30		4				50,25,25		
	2417	1598	20			18-21	18-21		4				50,25,25		
21.5 Co-26.5 Ti-52 Si	2507	1648	5			29-30	28-29		2				20		
			5			21	20		2				20		
			20			31	30		2				20		
	2507	1648	20			21	20		2				20		
	2417	1598	5			30	29		2				20		
			5			21	20		2				10		
			20			31	30		2				20		
	2417	1598	20	Vacuum[b]		21	20		2				20		
2.5 Mn-23.4 Co-23.4 Ti-50.7 Si	2372	1573	5	1 atm He		29	27		2				55,50		
2.5 Mn-22.75 Co-22.75 Co-52 Si			5			31-32	30-31						50,45,40, 40		
5 Mn-22.8 Co-22.8 Ti-49.4 Si	2372	1573	5	1 atm He		26-28	26-27		2				55,55		
30 Mn-25 Zr-45 Si	2552	1673	8	Vacuum[b]		25	18		3				5,5		
			5	Vacuum[b]		28	20		1				40		
	2552	1673		1 atm He		35	–		2[c]						
	2372	1573				27-31	26-30	3	9	7	5	>100,>100	36,36,36,36	5,5,5	36,36,36,36
14 Mn-36 Zr-50 Si	2552	1673				30	29		1[c]						
	2462	1623				32	30		1[d]				<17		
	2372	1573				29-32	28-30		4[d]				<17,<17,<17		
	2507	1648				29-32	27-31		6				90,90,76, >50,>26,26, 26		
15 Mn-30 Zr-55 Si	2507	1648		1 atm He	1 atm He	30-32	29-30		2[d]				>55<72, >55<72		
	2372	1573		Vacuum[b]	Vacuum[b]	31	24		4				45,21,21		
20 Mn-27 Ti-53 Si	2552	1673			1/3 atm He	24-27	16-22	7	8	5	5	>100,>100,>100, >100,>100,>50	>40,40,15, 10,10	50,50,50, >10	>50,>50, >25,>10
	2552	1673			3/4 atm He	30	24		2				45,45		
	2552	1673				21	17		2				21,45		
	2462	1623				30	24		2				45,45		
	2462	1623				20	17		2				45,45		
	2372	1573				31	24		2				21,45		
	2372	1573	5	Vacuum[b]	3/4 atm He	20	15		2				21,45		

Underscored values are for prealloyed powders used in the preparation of slurries.

TABLE 8 (Cont.)

Coating Composition	Fusion Conditions				Coating Weight mg/cm^2		Specimens Prepared				Coating Lifetime Cycles[a]			
	Temperature		Time to Temperature, min	Environment			Screening	Bend	Tensile	Emittance	Screening	Bend	Tensile	Emittance
				Heating	1 hr Isothermal Diffusion Treatment									
						Green / Fused								
15 Mn-32 Ti-53 Si	2552	1673	5	1 atm He	1 atm He	26-31 / 25-30		4				65,65,>17, >17		
14 Mn-29 Ti-57 Si						26-31 / 25-30		4				>65,>65, >17,>17		
10 Mn-36.5 Ti-53.5 Si						25-31 / 25-30		13				>89<111, 65,>63,>50,>17		
						25-29 / 24-28		2[e]				5,5		
8 Mn-31 Ti-61 Si						25-31 / 24-30		5				>111,>111, >100,>50, >15		
						30 / 28		2[f]				15,15		
5 Mn-41 Ti-54 Si						26-29 / 24-28		6				>104,97, >42,26,25, 23		
5 Mn-32 Ti-63 Si						24-29 / 23-28		14				>100,>100, >100,>100, >78<105, 89,>86, >65<90, >78<105, >50,>50,>50		
						29-30 / 26-28		7[f]				>100,>100, 15[f],15[f],15[f],15[f]		
						29-35 / 27-32		8[h]				52,52,29, 29[g],29[g], >29<44[g], >29<44[g], >29<44[g]		
						25-32 / 24-30		2[e]				5,5		
2.5 Mn-33 Ti-64.5 Si						24-31 / 23-29		10	3			>100,100, >87,>67, >67,>66, >66,>64, >50,>25	88,84, >25	
						29-30 / 26-28		4[f]				>100,>100, 22,16		
						30 / 26-27		2[h]				40,38		
						30-31 / 26-28		2[e]				10,4		
2.5 Co-2.5 Mn-32 Ti-63 Si						29-31 / 27-30		12				>100,>100, >100,>100 >60,>60, >60,>60		
						29-33 / 27-31		8[f]				15,15,10, 11,10,10, 10,10		
						27 / 25		2[i]				24,24		
						28-30 / 27-29		2[j]				>93,>93		
						29-30 / 27-28		4[k]				>60,46, >46<60, >46<60,		
	2552	1673	5	1 atm He	1 atm He	30 / 28-30		4[h]				65,46,46, 46		

[a] 1 Cycle – 15 min to 2600°F (1700°K), 30 min at 2600°F (1700°K), 15 min cooling.
Pressure 10 torr (13.33 hN/m^2) unless otherwise noted.
[b] Vacuum – 10^{-5} torr (1.3×10^{-4} hN/m^2).
[c] Flow to bottom of specimen.
[d] Nonuniform fusion.
[e] Exposed at 2800°F (1811°K), 0.1 torr (0.13 hN/m^2).
[f] Exposed at 2600°F (1700°K), 0.1 torr (0.13 hN/m^2).
[g] Specimens prepared with oversprayed edges.
[h] Exposed at 2800°F (1811°K), 10 torr (13.33 hN/m^2).
[i] Exposed at 2600°F (1700°K), 0.5 torr (0.65 hN/m^2).
[j] Exposed at 2600°F (1700°K), 0.75 torr (0.97 hN/m^2).
[k] Exposed at 2670°F (1739°K), 0.1 torr (0.13 hN/m^2).

FUSION TEMPERATURE		2417° F (1598° K)				2507° F (1648° K)			
COATING THICKNESS		0.002 in. (0.005 cm)		0.004 in. (0.010 cm)		0.002 in. (0.005 cm)		0.004 in. (0.010 cm)	
LIFETIME, CYCLES[a]		25 50 75		25 50 75		25 50 75		25 50 75	
ELEMENTAL POWDER	5 min[b]								
	20 min								
PREALLOWED POWDER	5 min								
	20 min								

[a] 30-MIN CYCLES AT 2600° F (1700° K), 10 TORR, 13.33 hN/m^2

[b] TIME TO FUSION TEMPERATURE

Figure 27 Summary of Influence of Process Variables on Performance of 27Co-22Ti-51Si Coating

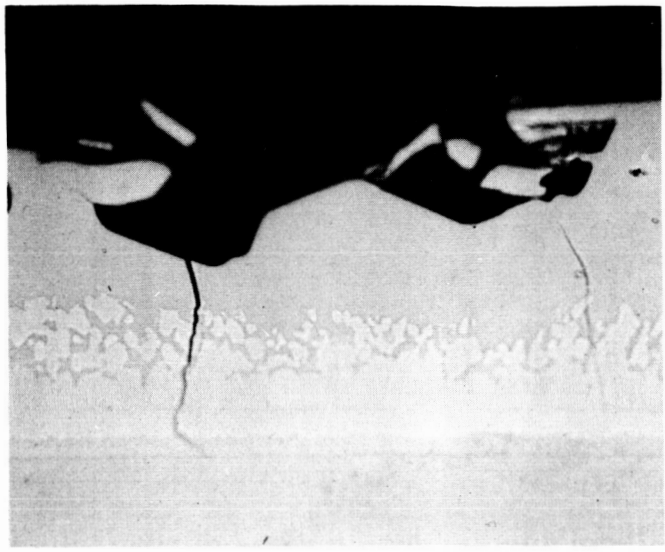

B3164

(a) Elemental Cobalt-Titanium Powders

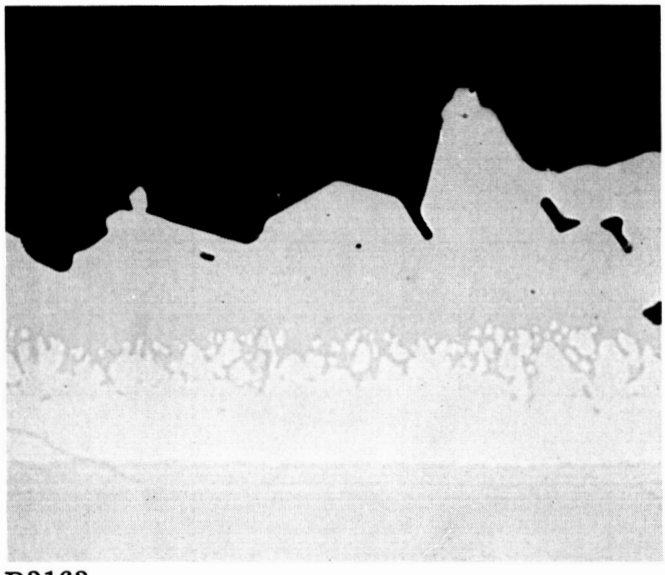

B3163

(b) Prealloyed Cobalt-Titanium Powder

Figure 28 Effect of Prealloying Cobalt and Titanium on Structure of 27Co-22Ti-52Si Coating, Not Etched, 500×.

had lifetimes in excess of 100 cycles. The earlier 24Co-24Ti-52Si specimens were fused at 2372° F (1573° K), and it was concluded that (1) small differences in fusion temperature may be important and (2) temperatures greater than 2372° F (1573° K) may be too high for effective coatings with this system. The higher temperatures – 2417° F and 2507° F (1598° and 1648° K) – were selected for the later studies to ensure that there would be fusion of all phases of the titanium-cobalt binary system. CoTi, the compound that has the highest melting point, is reported to melt at 2372° F (1573° K) (ref. 19) – but the melting point may be anywhere from 2290° to 2462° F (1527° to 1623° K).

Metallographic analyses of the Co-Ti-Si system included evaluation of coatings having three different fusion temperatures: 2372°, 2417°, and 2507° F (1573°, 1598°, and 1648° K). Photomicrographs are presented in Figure 29. For fusion temperatures of 2372° and 2417° F (1573° and 1598° K) the structures are similar, with a continuous phase along the coating/substrate interface but with a discontinuous phase that was distributed along the outer surface of the coating. This phase, which could be seen macroscopically, was found to be distributed uniformly along the flat surfaces but differently at and near the edges. Fusing at 2507° F (1648° K) produces an entirely different coating structure, which emphasizes the point previously made concerning the importance of the fusion temperature. A difference of 90° F (50° K) in fusion temperature had a significant effect on the structure of the coating. It is interesting to note that although the coating fused at 2507° F (1648° K) had more uniform microstructures than that fused at 2372° F (1573° K), the latter performed better on oxidation exposure. Microstructures of these coatings fused at 2417° F (1598° K) and 2372° F (1573° K) after exposure are shown in Figure 30a. An oxide layer is evident around the islands on the specimen fused at 2417° F (1598° K) and exposed for 10 cycles, and a thick oxide layer is apparent on the surface of the specimen fused at 2372° F (1573° K) and exposed for 100 cycles. (Figure 30b will be discussed later in this section.)

Because the CoTiSi coating systems had demonstrated a potential for long coating lifetimes but lacked consistency in their performance, consideration was given to additives that might improve the performance of these systems. In the MnTiSi and MnZrSi systems, manganese was effective as a contributor to better modified silica and metal-oxide layers at the coating surface. Therefore, manganese was selected as the additive to the CoTiSi system.

To study its influence on the behavior of CoTiSi coatings, manganese was added to this system at 2.5 and 5 weight percent, and cyclic exposures were conducted at 2600°F (1700° K), 10 torr (13.33 hN/m^2). The following compositions were evaluated:

- 2.5Mn-23.4Co-23.4Ti-50.7Si
- 2.5Mn-22.75Co-22.75Ti-52Si
- 5Mn-22.8Co-22.8Ti-49.4Si

The results of cyclic exposure tests are presented in Table 8. The lifetimes of these coatings were about 50 cycles; coating wearout at specimen edges was the life-limiting factor. Metallographic studies did not indicate that the coating was too thin at the edges, but both microscopic and macroscopic examination showed the same difference in the distribution of phases along edges compared with that on flat surfaces as that observed in the manganese-free CoTiSi coatings. An unidentified phase forms in small islands on the surface of the coating (evident in Figure 29).

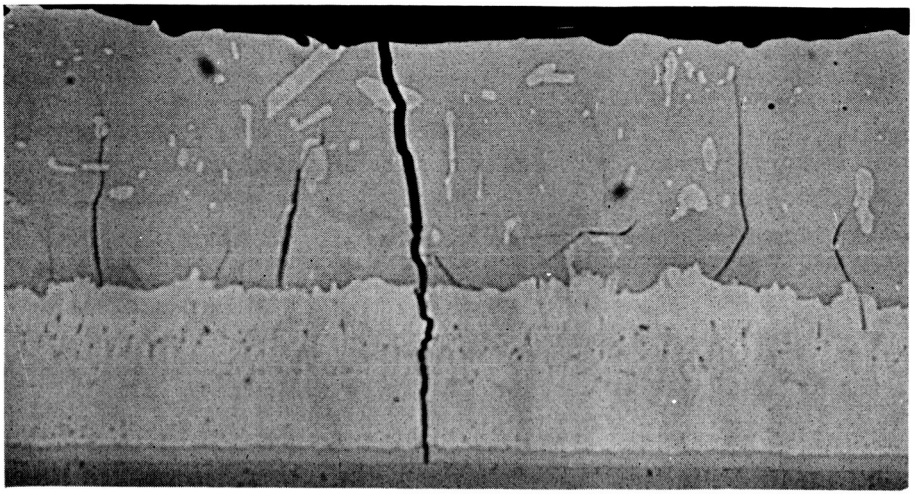

(a) 2500° F (1644° K) Fusion

B3297

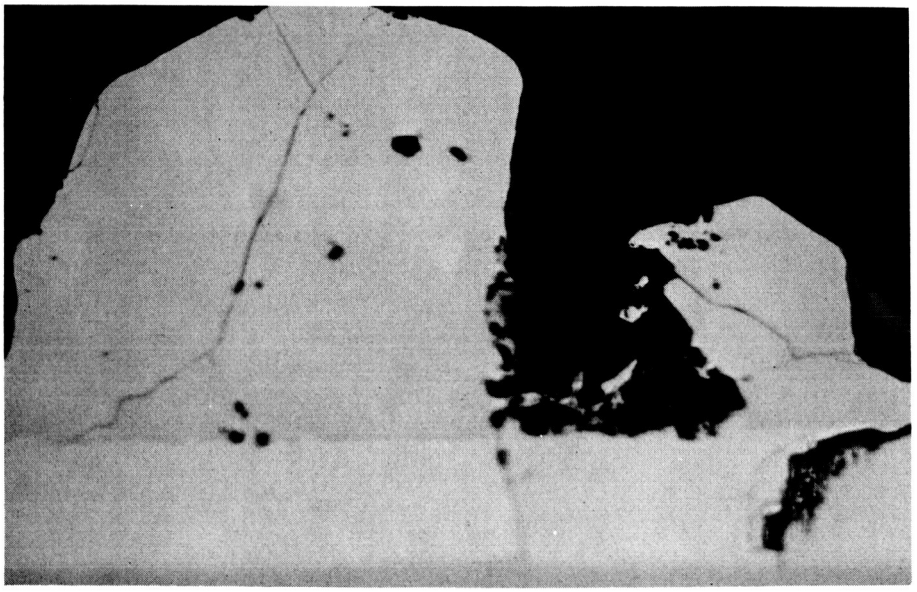

(b) 2420° F (1600° K) Fusion

B3294

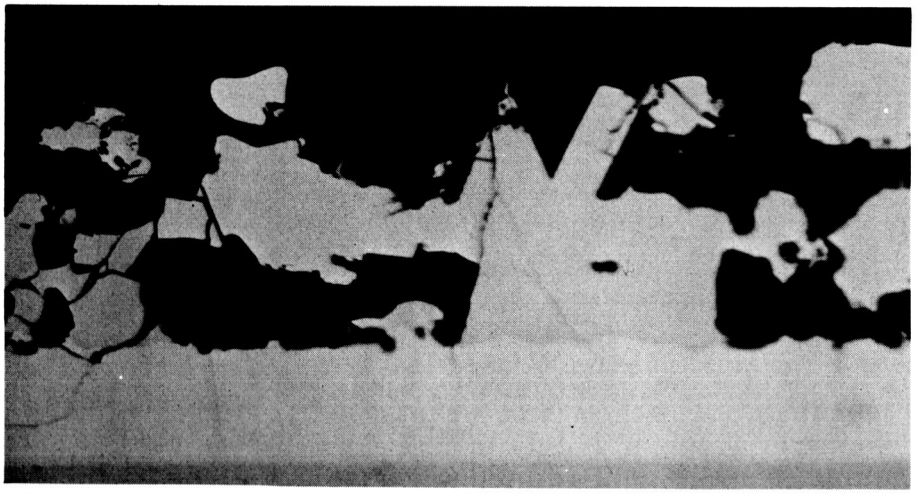

(c) 2370° F (1572° K) Fusion

B3293

Figure 29 Effect of Fusion Temperature on Structure of 24 Co-24 Ti-52 Si Coatings, Not Etched, 500×.

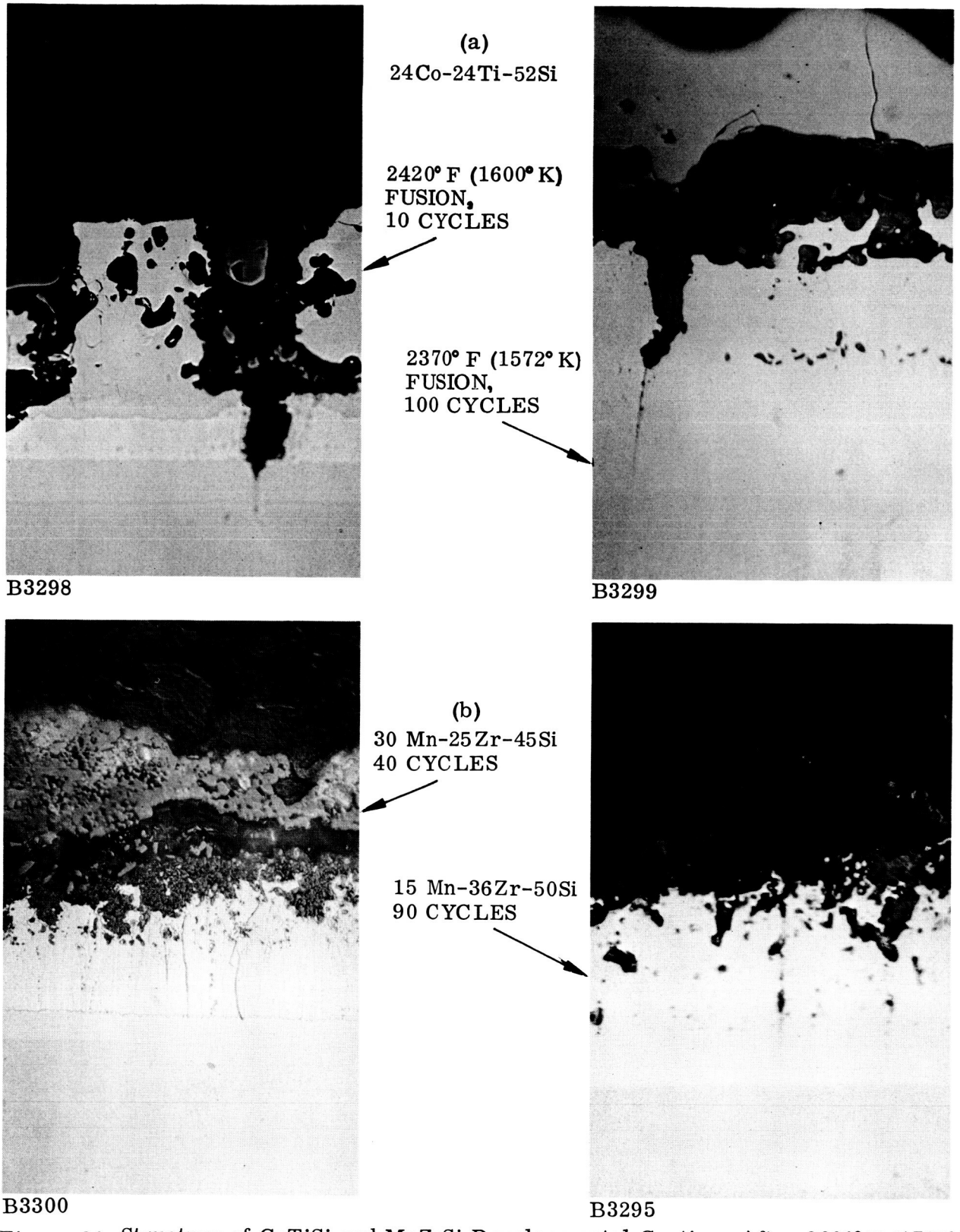

Figure 30 Structure of CoTiSi and MnZrSi Developmental Coatings After 2600° F (1700° K), 10 Torr (13.33 hN/m^2) Cyclic Exposure, Not Etched, 500×.

Near and along the edges islands of this phase were fewer than on flat surfaces; a geometric effect that influences surface tension during fusion and/or differences in the ratio of coating volume to substrate surface area are indicated. It may well be that this phase is an important factor in the performance of the coating and that the lack of an adequate amount along the edges contributed to the early coating wearout at edge sites.

The general conclusion reached regarding the CoTiSi system was that it had a potential for long lifetimes but that its overall performance was inconsistent. It may be that the system is extremely sensitive to subtle variations in processing, which would render the system impractical for scaling-up to engineering components.

- MnZrSi System

Studies with the Mn-Zr-Si system included the following compositions:

- 30Mn-25Zr-45Si
- 14Mn-36Zr-50Si
- 15Mn-30Zr-55Si

The conditions for application of the coatings and the results of cyclic exposure are presented in Table 8 . Because of the high manganese content of these coatings, a helium atmosphere was necessary to prevent excessive volatilization of the manganese. A range of fusion temperatures from 2372° to 2552° F (1573° to 1673° K) was studied for each composition, and it was found that nonuniform coatings formed at temperatures greater than 2372° F (1573° K) because of flow of the coating during fusion.

Two times to fusion – 5 and 20 min – were studied; no significant difference in structure or performance was noted between the two, and the 5-min schedule was selected.

The 30Mn-25Zr-45Si and the 14Mn-36Zr-50Si coatings fused at 2372° F (1573° K) had the best lifetimes; however, the performance of both systems was inconsistent. The lifetime of some specimens was as long as 90 to 100 cycles, but other specimens coated with the same composition had variable lifetimes in the range of 10 to 75 cycles. Furthermore, the silica-metal oxide layer that formed during the cyclic exposures appeared to have been too fluid to resist any environmental conditions that include high air flow rates. In addition, the oxide layer had a tendency to spall during temperature cycling. The loosely connected oxide layer can be seen in the photomicrographs of Figure 30b.

- MnTiSi System

In initial studies of the MnTiSi system, a 20Mn-27Ti-53Si composition was used. Three fusion temperatures – 2372°, 2462°, and 2552° F (1573°, 1623°, and 1673° K) – were evaluated, and a 5-min heating time to 2552° F (1673° K) was found to produce an excellent, uniform coating. Specimens coated with this composition were heated to fusion temperature in vacuum and held at fusion temperature in helium. An analysis of the coating weights before and after fusion indicated a loss of manganese during heating to fusion temperature. This result dictated that the entire fusion treatment be conducted in an inert atmosphere such as helium. Because of the loss of manganese, the estimated composition was 10Mn-30Ti-60Si.

As shown in Table 8 , when this coating composition was fused at 2552° F (1673° K), it demonstrated potential for effectively protecting Ta-10W for 100 cycles at 2600° F (1700° K), 10 torr (13.33 hN/m^2). An evaluation of several specimens withdrawn from test after 100 cycles indicated a potential for even greater lifetimes. A sound, uniform protective layer was evident on the surface of the specimen, and coating discontinuities associated with hairline fissures were well protected.

Because of the excellent performance demonstrated by this coating, a series of coatings with varying compositions was prepared and these coatings were fused under conditions where the entire fusion treatment was in a helium atmosphere to maintain close control over the composition. In addition to extensive evaluation under cyclic exposure conditions at 2600° F, 10 torr (1700° K, 13.33 hN/m^2), additional exposures were conducted at 2600° F, 0.1, 0.5, and 0.75 torr (1700° K, 0.13, 0.65, and 0.98 hN/m^2), and at 2800° F, 0.1 and 10 torr (1811° K, 0.13 and 13.33 hN/m^2). Some studies were conducted using specimens having oversprayed edges because it was noted that when coating wearout did occur, it was initially in the edge regions. In addition to these process variables, coating thickness was considered. Thicknesses of 0.002 and 0.004 in. (0.005 and 0.010 cm) were evaluated, and the thicker coating appeared to be more effective.

The additional MnTiSi compositions that were evaluated are shown in the ternary phase diagram presented in Figure 31. The results of cyclic exposure evaluations, shown in Table 8 , indicate that a large range of compositions in this system have the capability for long lifetimes.

The shaded area of the ternary diagram represents compositions that are effective in protecting Ta-10W. Within the shaded area, the higher manganese levels lead to increased softening of the protective layer, whereas at lower manganese levels the protective layer is more viscous. On the silicon-rich side of the shaded area, the flow improves during fusion, compared with the behavior of compositions on the silicon-lean side of the shaded region.

Within this shaded area, the service requirements for the coating should dictate the exact coating composition. For high-temperature applications, compositions along the manganese-lean side of this region should be selected so that the coating will be resistant to high flow-rate environments. For lower temperature applications, compositions should be selected in regions richer in manganese, where the protective layer has a lower temperature softening point. For example, tantalum wire hooks coated with 8Mn-31Ti-61Si were used to support specimens from a water-cooled copper holder in this program. The hooks were exposed to a broad temperature gradient, from a few hundred degrees to over 2600° F (1700° K), at pressures ranging from 0.1 to 10 torr (0.13 to 13.33 hN/m^2). This coating, high in manganese content, was effective in protecting the hooks for long times – in some cases for several hundred cycles.

The structure of the 8Mn-31Ti-61Si coating is shown in Figure 32 in the as-coated condition and after 111 cycles at 2600° F (1700° K), 10 torr (13.33 hN/m^2). The as-coated structure is uniform, with a M_5Si_3 zone at the coating/substrate interface that is thick enough to arrest hairline fissures. In the outer portion is a sound layer of mixed silicides. After exposure, the M_5Si_3 layer has grown as the result of interdiffusion with the substrate, and a substantial region of mixed silicides remains. An oxide layer on the outer surface has effectively covered the entire coating, including regions having hairline fissures.

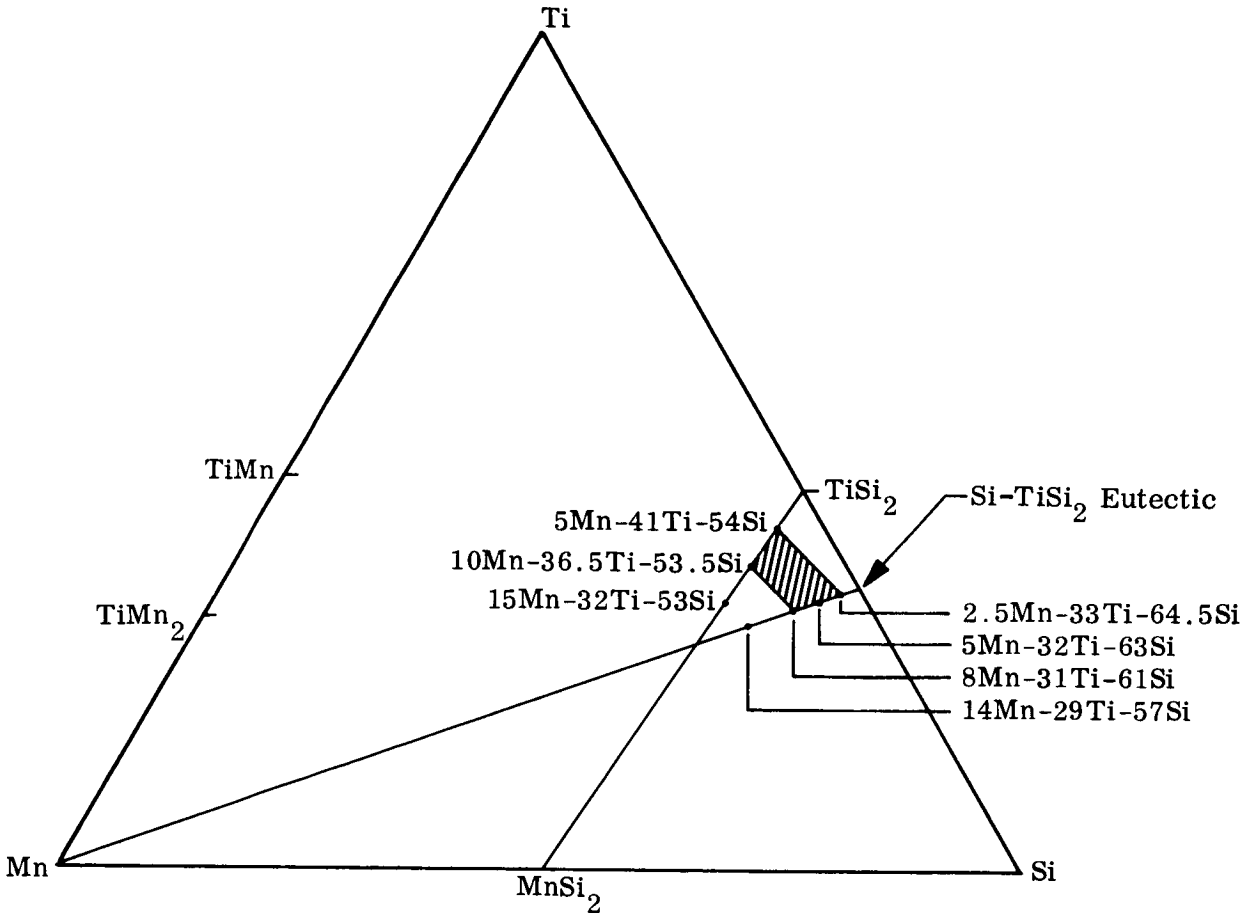

Figure 31 Mn-Ti-Si Ternary Diagram. Shaded area represents compositions that are effective coatings for Ta alloys

Because the objective of this program was to develop coatings for use at high temperatures [2600 to 2800° F (1700 to 1811° K)] that would be practical for complex parts, attention was directed toward the 5Mn-32Ti-63Si and 2.5Mn-33Ti-64.5Si compositions. These coatings are relatively lean in manganese and rich in silicon and therefore have both performance and application capabilities commensurate with the program objectives.

Both coating compositions had lifetimes greater than 100 cycles at 2600° F (1700° K), 0.1 and 10 torr (0.13 and 13.33 hN/m^2). It should be pointed out, however, that, as will be discussed in greater detail later in the report, 0.1 torr (0.13 hN/m^2) is very close to the active-passive transition pressure at this temperature; and the long lifetimes at this pressure may reflect slight pressure fluctuations during exposure.

At 2800° F (1811° K), 10 torr (13.33 hN/m^2), lifetimes of 29 to 52 cycles were observed, with coating wearout occurring at edges. Because of the initial wearout at the edges,

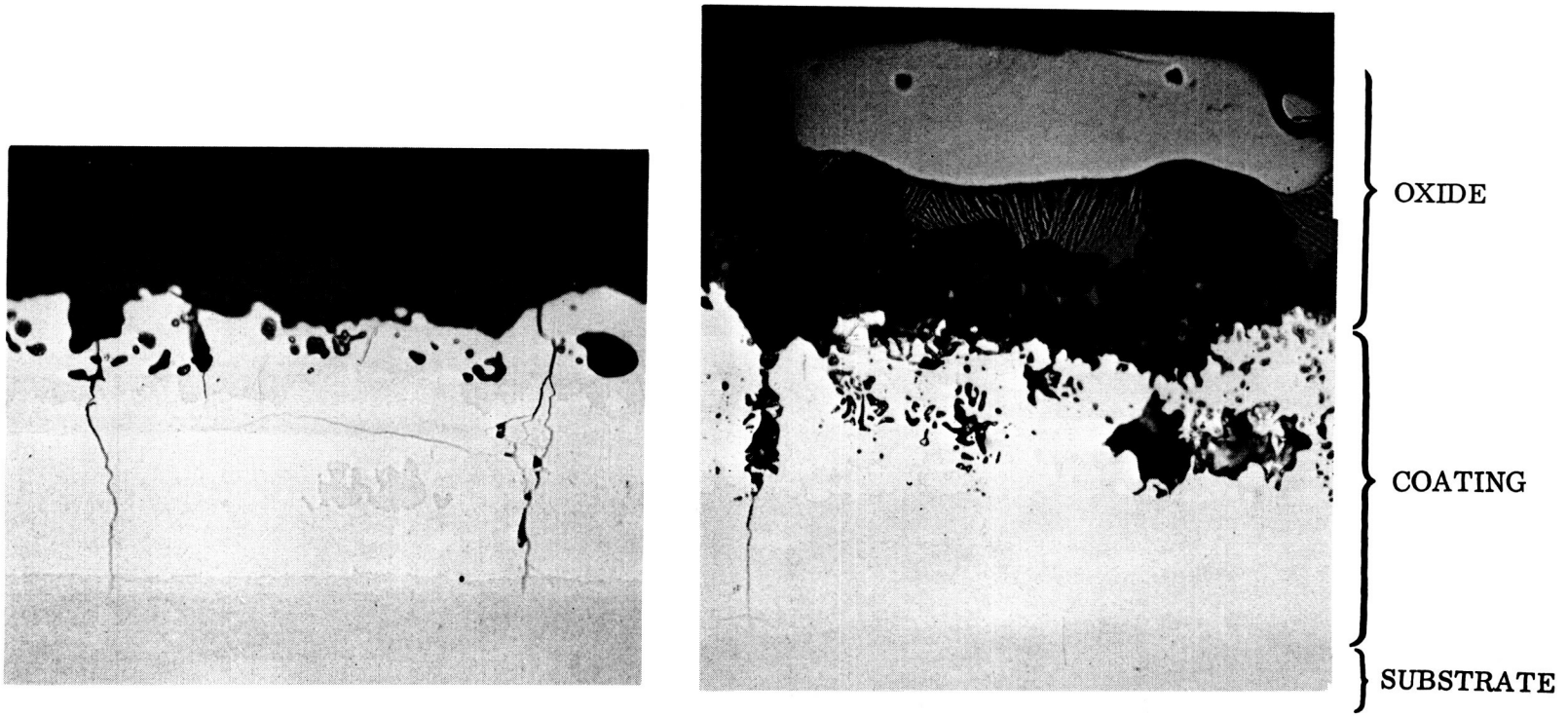

B3161

(a) As-Coated

B3162

(b) 2600° F (1700° K), 10 Torr (13.33 hN/m^2), 111 Cycles

Figure 32 Structure of 8Mn-31Ti-61Si Coating, Not Etched, 500×.

attention was given to overspraying edges to develop a thicker coating at the edges. The edges of four specimens were oversprayed, but this overspraying had no effect on performance. The lifetimes at 2800° F (1811°K), 10 torr (13.33 hN/m^2) were in the same range as for specimens without oversprayed edges.

At 2800° F (1811°K) the oxide layer of these coatings appeared to be more refractory than at 2600° F (1700°K). This is believed to be due to loss of manganese to the environment. In order to maintain the appropriate viscosity of the oxide layer, cobalt was added; the objective was to form CoO in the oxide layer and to compensate for the loss of manganese. A composition of 2.5Co-2.5Mn-32Ti-63Si was selected to retain a similar level of silicon concentration and about the same titanium : silicon ratio as in the MnTiSi coatings.

Studies were conducted to determine the best combination of process variables for application of the CoMnTiSi composition. The same fusion treatment as used for the MnTiSi coatings [5 min to 2552° F (1673°K) and 1 hr at this temperature] was found to produce an excellent, uniform coating.

Cyclic exposures at various temperatures and pressures were conducted using this composition, and lifetimes in excess of 100 cycles were observed at 2600° F (1700°K) 10 torr (13.33 hN/m^2). Furthermore, improved lifetimes were realized at 2800° F (1811°K), 10 torr (13.33 hN/m^2). At lower pressures the lifetimes were comparable to those of the MnTiSi coatings. The results of cyclic exposure evaluations of this system are also presented in Table 8.

- Selection of Two Best Coating Compositions

An analysis was made of the performance of all the developmental coating compositions studied, with the objective of selecting the two best coating compositions for extensive characterization as improved coatings for tantalum alloys. Compositions within the CoTiSi system, while showing promise in coating ability, were inconsistent in behavior. Good protection was afforded by the MnZrSi system coatings, but the oxide layer that formed on these coatings during exposure was considered insufficiently viscous to resist high-flow environments. In addition, the oxide layer tended to spall under cyclic temperature exposure.

The MnTiSi and CoMnTiSi coatings clearly offered the greatest potential for effective protection of Ta-10W under the conditions of interest in this program. In the MnTiSi system, the 2.5Mn-33Ti-64.5Si composition was favored over the composition containing 5-percent manganese because the lower manganese content provides a more suitable oxide layer for service at 2800° F (1811°K). Therefore, the 2.5Mn-33Ti-64.5Si composition was selected as one of the two best coating compositions for further characterization. Because of the indications of a greater potential at a temperature of 2800° F (1811°K), the 2.5Co-2.5Mn-32Ti-63Si composition was selected as the other coating for extensive characterization.

The 2.5Mn-33Ti-64.5Si composition was designated the "MTS" coating and the 2.5Co-2.5Mn-32Ti-63Si composition was designated the "CMTS" coating. The as-coated structures of these coatings are shown in the photomicrographs of Figures 32a and b. Detailed analyses of their performance and the properties of the substrate as a function of oxidation exposure, as well as analyses of coating structures, will be presented in subsequent sections of the report.

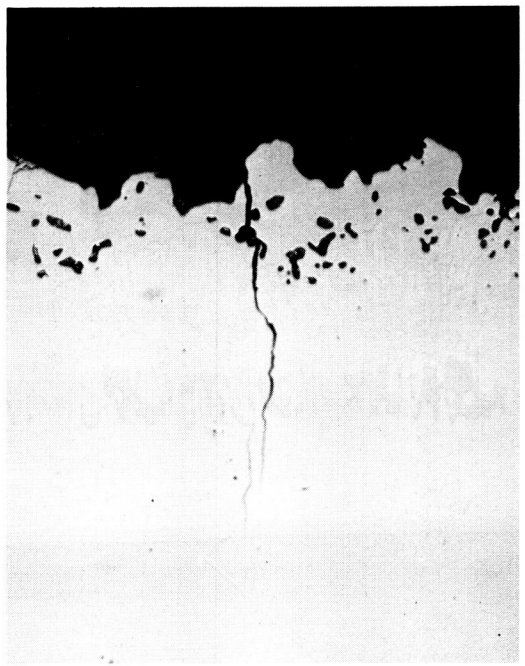

B3244

(a) MTS-31 mg/cm^2

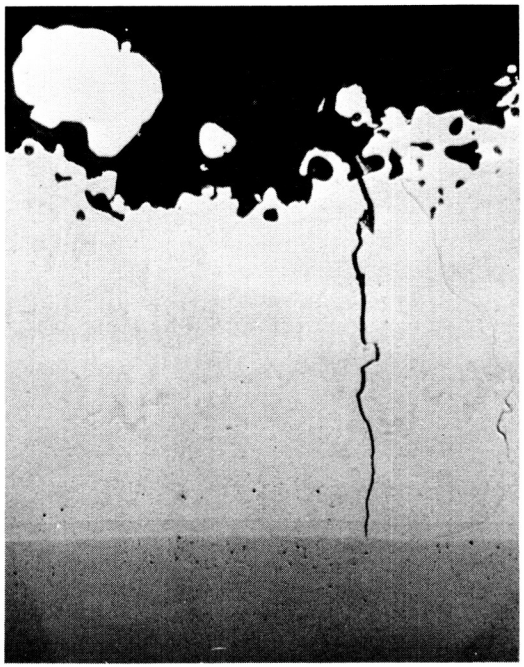

B3247

(b) CMTS-30 mg/cm^2

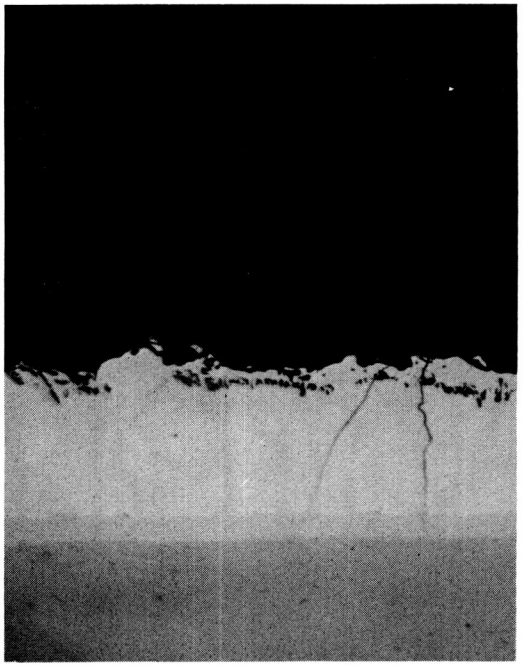

B3285

(c) CMTS-20 mg/cm^2

Figure 32a Structure of Best Coating Systems, Flat Surfaces As-Coated, Not Etched, 500×.

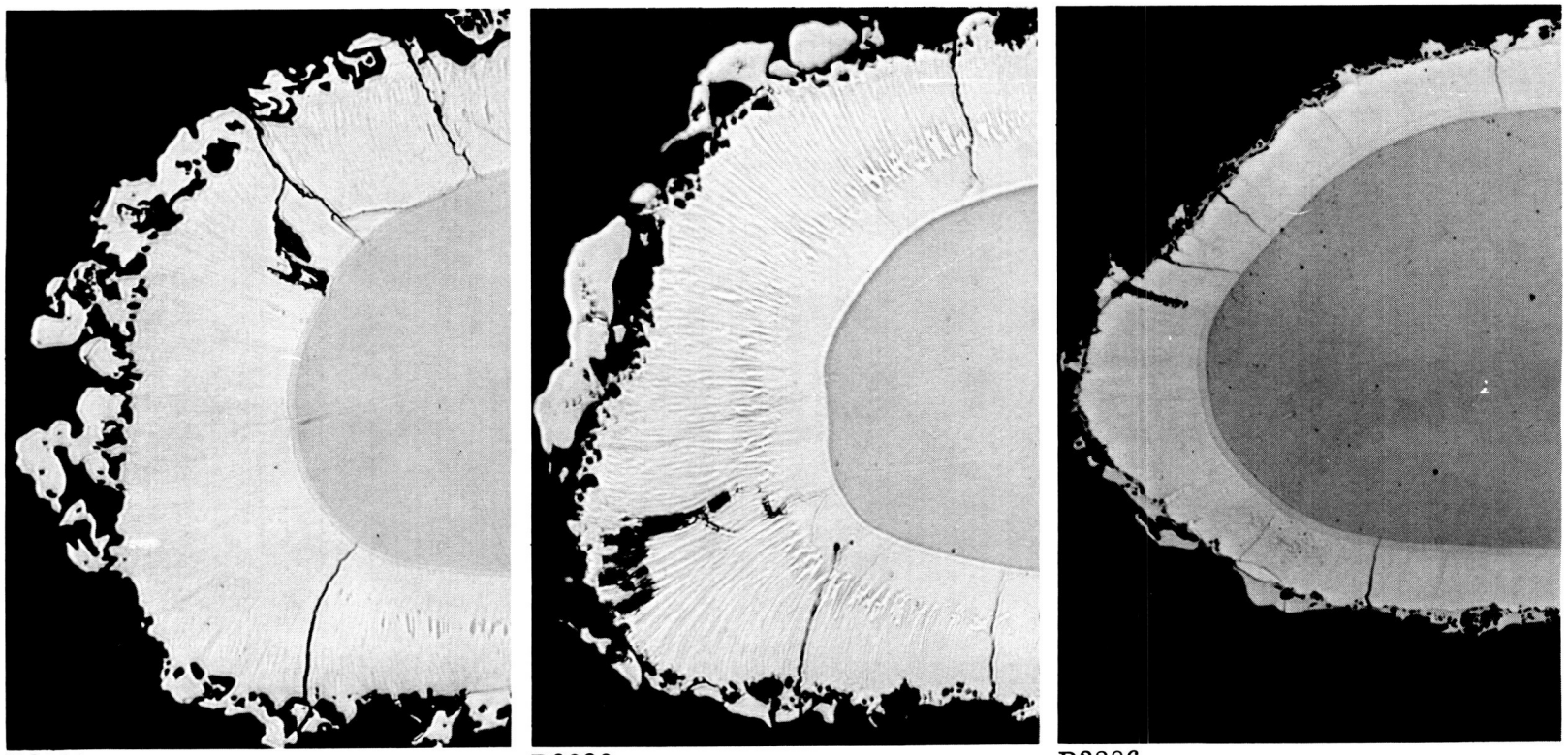

B3239 B3238 B3286

(a) MTS-31 mg/cm^2 (b) CMTS-30 mg/cm^2 (c) CMTS-20 mg/cm

Figure 32b Structure of Best Coating System, Edges As-Coated, Not Etched, 200×.

RESULTS OF TESTS WITH BEST COATINGS

The evaluation of the MTS and CMTS coatings – the two best coatings developed during the program – consisted of characterizing (1) coating lifetime as a function of environmental conditions, (2) coating emittance as a function of exposure time and environmental conditions, (3) coating/substrate composite mechanical properties as a function of exposure time and environmental conditions, (4) resistance to intentional damage, and (5) oxidation behavior under stress. Initially, the coating lifetimes of the two systems were determined under isothermal conditions at 2600°, 2700°, and 2800° F (1700°, 1755°, and 1811° K) at air pressures of 0.1 to 10 torr (0.13 to 13.33 hN/m^2). These experiments were conducted to provide a baseline for performance, i.e., the maximum lifetime for each coating at specific temperature/pressure combinations under noncyclic conditions. Cyclic exposures were conducted at 2600° and 2800° F (1700° and 1811° K) at air pressures of 0.1, 1.0, and 10 torr (0.13, 1.33, and 13.33 hN/m^2) to evaluate the effect of temperature cycling on coating performance as compared with the performance under isothermal conditions. A sufficient number of specimens were tested to provide a statistical interpretation of results of the cyclic tests. Emittance measurements were made with both coatings after various exposure levels at 2600° and 2800° F (1700° and 1811° K) and 0.1, 1.0, and 10 torr (0.13, 1.33, and 13.33 hN/m^2). In addition, the substrate/coating composite bend ductile-brittle transition temperature and tensile properties were determined after various exposure levels at these temperatures and pressures. The tensile properties were determined both at room temperature and at elevated temperatures. Also, creep tests were conducted on specimens coated with both coatings. Coated specimens were intentionally damaged, and their resistance to this damage was evaluated. Microstructures are correlated with coating performance and properties as well as substrate/coating composite properties in the Analysis of Results section. Oxidation behavior under stress is discussed in the Applicability to Structural Components section.

Isothermal Baseline Studies

Isothermal exposures at 2600°, 2700°, and 2800° F (1700°, 1755°, and 1811° K) at pressures of 0.1, 1.0, and 10 torr (0.13, 1.33, and 13.33 hN/m^2) included at least two specimens containing each coating at each of two coating weights, 20 and 30 mg/cm^2 [specimen thickness, 0.002 and 0.004 in. (0.005 and 0.010 cm)]. Additional experiments were conducted on duplicate specimens of both coatings, with the thicker coating at 2600° F (1700° K) at 0.3 and 0.5 torr (0.4 and 0.66 hN/m^2). Exposures of specimens continued until coating wearout occurred, except for cases where the coating lifetime was so great that inordinately long furnace times would have been required to complete the exposures. The results are tabulated in Table 9 and are presented graphically in Figures 33 and 34. In these figures, boundaries are included that show the coating lifetime as a function of pressure at each temperature for each coating.

In general, the thicker coatings provide longer lifetimes for both systems. In some temperature/pressure combinations, the lifetimes of the thick and thin coatings were similar.

TABLE 9. - SUMMARY OF ISOTHERMAL BASELINE STUDIES

Coating system	Specimen No. OT2-	Temperature, °F (°K)	Pressure, torr (hN/m^2)	Coating weight, (mg/cm^2)		Lifetime, hours
				Green	Fused	
MTS	90-11	2600(1700)	0.1(0.13)	29	27	>200
	88-10	↓	↓	30	28	>200
	90-5	↓	↓	21	20	12
	90-6	↓	↓	19	17	12
CMTS	96-1	2600(1700)	0.1(0.13)	29	27	12
	96-2	↓	↓	32	30	12
	94-12	↓	↓	21	19	22
	94-13	↓	↓	20	19	12
MTS	138-4	2600(1700)	0.3(0.4)	30	28	>300
	138-5	↓	↓	31	29	>300
CMTS	137-4	↓	↓	30	28	19
	137-10	↓	↓	31	29	19
MTS	138-2	2600(1700)	0.5(0.66)	29	27	>460
	138-1	↓	↓	30	28	244
CMTS	137-2	↓	↓	30	27	161
	137-1	↓	↓	32	29	74
MTS	88-1	2600(1700)	1(1.33)	30	28	>167
	88-2	↓	↓	31	29	>167
	88-3	↓	↓	32	30	200
	88-4	↓	↓	29	27	>215
	88-11	↓	↓	21	20	>167
	88-12	↓	↓	22	20	>167
	88-13	↓	↓	21	20	>230
	88-14	↓	↓	20	19	>230
CMTS	94-9	2600(1700)	1(1.33)	30	28	>141
	94-14	↓	↓	29	27	140
	94-10	↓	↓	22	20	140
	94-11	↓	↓	21	20	140
MTS	88-5	2600(1700)	10(13.3)	32	30	>72
	88-6	↓	↓	29	27	>72
	88-7	↓	↓	32	30	>310

Table 9. (Cont.)

Coating system	Specimen No. OT2-	Temperature, °F (°K)	Pressure, torr (hN/m^2)	Coating weight, (mg/cm^2)		Lifetime, hours
				Green	Fused	
MTS	88-8	2600(1700)	10(13.3)	30	28	>310
	90-1	↓	↓	21	20	>72
	90-2			19	18	>72
	90-3			19	18	>310
	90-4			20	19	>310
CMTS	92-13	2600(1700)	10(13.3)	30	28	>247
	92-14	↓	↓	31	29	>247
	92-9			21	20	>140
	92-10			19	18	140
MTS	90-15	2700(1755)	0.1(0.13)	28	26	7
	90-16	↓	↓	31	29	6
	98-8			18	–	7
	98-9			20	–	7
CMTS	100-17	2700(1755)	0.1(0.13)	29	–	108
	100-18	↓	↓	30	–	108
	96-11			20	19	7
	96-12			22	21	7
MTS	90-13	2700(1755)	1(1.3)	29	27	10
	90-14	↓	↓	28	27	10
	102-1			20	19	8
	90-7			20	18	12
CMTS	96-5	2700(1755)	1(1.3)	31	29	14
	96-6	↓	↓	31	29	14
	96-9			21	20	8
	96-10			21	19	12
MTS	98-1	2700(1755)	10(13.3)	29	26	72
	98-2	↓	↓	31	25	72
	98-6			20	–	72

Table 9. (Cont.)

Coating system	Specimen No. OT2-	Temperature, °F (°K)	Pressure, torr (hN/m^2)	Coating weight, (mg/cm^2)		Lifetime, hours
				Green	Fused	
MTS	98-7	2700(1755)	10(13.3)	19	–	72
CMTS	96-7	2700(1755)	10(13.3)	31	29	>128
	96-8	↓	↓	32	30	>128
	100-1	↓	↓	20	19	128
	100-2	↓	↓	22	21	72
MTS	111-5	2800(1811)	0.1(0.13)	30	29	18
	111-6	↓	↓	30	28	18
	102-6	↓	↓	20	19	5
	102-7	↓	↓	20	19	5
CMTS	110-5	2800(1811)	0.1(0.13)	30	28	43
	110-4	↓	↓	30	28	43
	110-3	↓	↓	20	19	7
	110-7	↓	↓	21	20	8
MTS	111-3	2800(1811)	1(1.3)	32	30	5
	111-4	↓	↓	29	27	5
	102-4	↓	↓	20	18	5
	102-5	↓	↓	19	18	5
CMTS	110-6	2800(1811)	1(1.3)	31	28	5
	110-8	↓	↓	29	27	5
	100-3	↓	↓	23	21	5
	100-4	↓	↓	22	20	5
MTS	111-1	2800(1811)	10(13.3)	31	29	80
	111-2	↓	↓	30	28	80
	102-2	↓	↓	20	19	69
	102-3	↓	↓	19	18	69
	110-9	2800(1811)	10(13.3)	30	28	80
	110-10	↓	↓	29	27	80
	100-5	↓	↓	20	19	80
	100-6	↓	↓	18	17	80

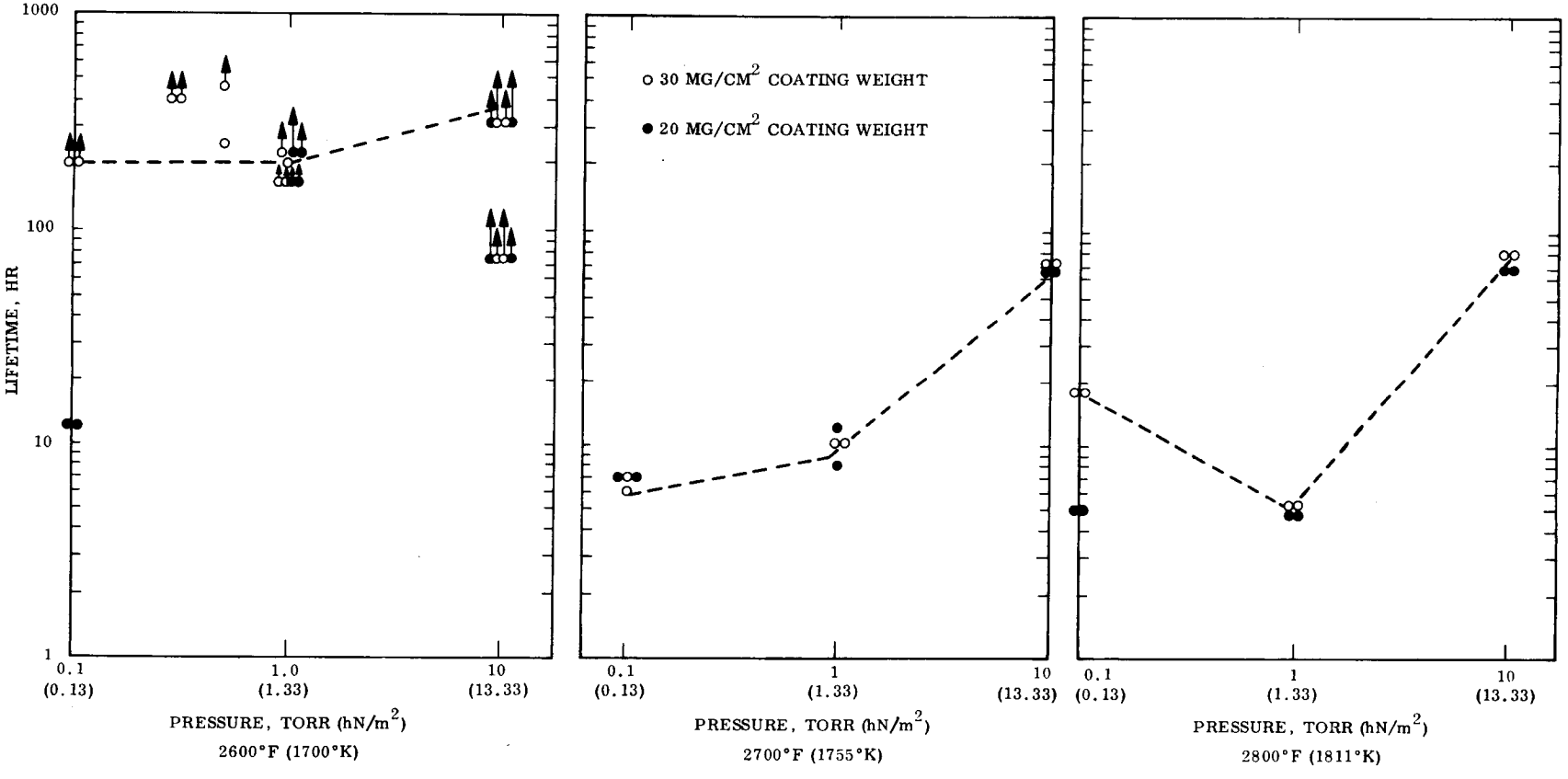

Figure 33. Performance of MTS Coating Under Isothermal Conditions. Dashed lines represent wearout boundary for 30 mg/cm2 coatings.

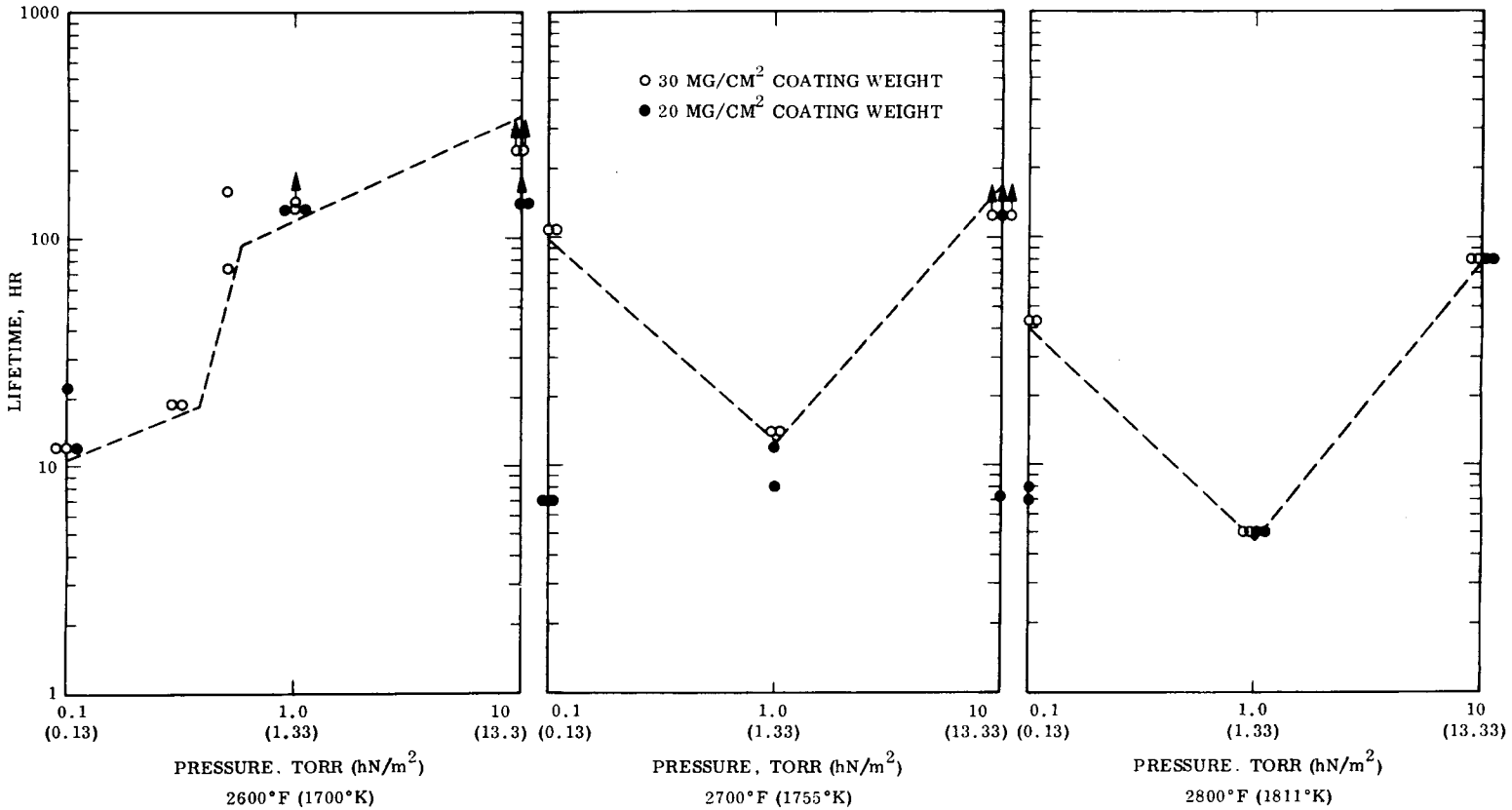

Figure 34. Performance of CMTS Coating Under Isothermal Conditions. Dashed lines represent wearout boundary for 30 mg/cm^2 coatings.

At 2600°F (1700°K) the lifetime of the thick MTS coating was at least 200 hr over the entire pressure range of 0.1 to 10 torr (0.13 to 13.33 hN/cm^2). The lifetime of the CMTS coating decreased with decreasing pressure at pressures lower than about 0.5 torr (0.66 hN/m^2), indicating a passive-to-active transition pressure between 0.1 and 0.5 torr (0.13 to 0.66 hN/m^2).

At 2700° and 2800°F (1755° and 1811°K) the lifetimes of the MTS and CMTS coatings were similar to one another at 1.0 and 10 torr (1.33 and 13.33 hN/m^2), but the lifetime of the CMTS system was greater at 0.1 torr (0.13 hN/m^2) than that of the MTS system. At this pressure, the lifetime of the CMTS system was 108 hr at 2700°F (1755°K) compared with 7 hr for the MTS coating. At 2800°F, 0.1 torr (hN/m^2) the lifetimes of the CMTS and MTS systems were 43 hr and 18 hr, respectively.

The results at 2800°F (1811°K), showing longer lifetimes at 0.1 torr (0.13 hN/m^2) than at 1.0 torr (1.33 hN/m^2), may indicate that the presence of titanium is changing the thermodynamics of the system in such a way that the formation of SiO is not favored. Thus, there is less loss of silicon to the environment. It is also possible that the cobalt has a similar effect at 2700°F (1755°K), in that the lifetimes of the CMTS coating are greater at 0.1 torr (0.13 hN/m^2) than at 1.0 torr (1.33 hN/m^2).

These studies demonstrated the potential of both coatings for long lifetimes at 2600°F (1700°K) over a broad range of pressure and the potential for long lifetimes at pressures near 10 torr (13.33 hN/m^2) at 2700° and 2800°F (1755° and 1811°K). Furthermore, these studies showed that the thicker coating, i.e., 0.004 in. (0.010 cm), provides more effective protection than the thinner coating. On the basis of the results of this study, the thicker coating was selected for use on other test specimens to be evaluated.

Statistical Studies

Cyclic temperature exposures at 2600° and 2800°F (1700° and 1811°K) at 0.1, 1.0, and 10 torr (0.13, 1.33, and 13.33 hN/m^2) included multiple specimens to establish coating lifetimes of the MTS and CMTS coatings on a statistical basis. The results are tabulated in Table 10 for the 2600°F (1700°K) exposures and Table 11 for the 2800°F (1811°K) exposures. The results are also plotted in terms of Weibull statistics (ref. 28) in Figure 35 for 2600°F (1700°K) and in Figure 36 for 2800°F (1811°K). The Weibull analysis was selected because it has been shown to be appropriate for evaluation of the performance of coated refractory metals (refs. 29, 30, and 31).

At 2600°F (1700°K), there was a reasonably good fit of the data to a straight line for the MTS coating and a good straight-line fit for the CMTS coating. At 1.0 torr (1.33 hN/m^2), a mixed distribution with the CMTS coating apparently occurred, since the slope of the curve changed at about 150 cycles. Testing of the MTS system at 1.0 torr (1.33 hN/m^2) was discontinued after 429 cycles. (It should be noted that because of the nature of the Weibull analysis, specimens having identical lifetimes are represented on the Weibull plot as a single data point. Therefore, the number of data points on a Weibull curve is not necessarily indicative of the number of specimens tested.)

At 2800°F (1811°K), there is a good straight-line fit to all the data except for two data points at 10 torr (13.33 hN/m^2). These data points represent two specimens where coating wearout was observed at specimen edges at short lifetimes relative to the remainder of the population tested at this temperature/pressure combination. The cause of the

TABLE 10. – RESULTS OF STATISTICAL STUDIES AT 2600°F (1700°K)

Pressure		Coating system	Specimen Number OT2-	Coating weight, mg/cm^2		Coating lifetime, cycles
torr	hN/m^2			green	fused	
10	13.33	MTS	40-10	33	31	264
			40-17	30	28	259
			40-15	31	30	258
			40-16	32	31	254
			40-9	31	30	248
			40-11	34	33	203
			40-18	32	30	169
			40-14	29	27	158
			40-13	30	28	130
			40-19	32	30	128
			40-20	30	29	125
10	13.33	CMTS	36-25	31	29	312
			36-26	32	30	278
			48-5	32	30	269
			48-3	34	32	259
			48-2	33	32	248
			48-1	33	31	243
			48-4	32	30	230
			48-6	33	31	220
			48-7	33	30	206
			48-8	34	33	206
			48-12	28	26	159
1.0	1.33	MTS	62-1	31	29	>403
			62-2	29	27	>429
			62-3	31	29	>429
			62-5	32	30	>429
			62-6	31	29	>429
			62-7	33	31	>429
			62-9	33	31	>429
			62-10	32	30	>429
			62-11	31	29	>429
			62-12	29	28	>429
			62-13	29	27	>429
			62-14	29	27	>429
			62-15	31	29	>429
		CMTS	64-15	31	29	>374
			64-2	32	31	334
1.0	1.33	CMTS	64-8	29	27	242
			64-7	31	29	210
			64-9	31	29	210
			64-10	28	26	210
			64-4	31	29	194
			64-5	29	27	194
			64-6	30	28	194
			64-11	29	27	194
			64-12	31	30	194
			64-13	31	29	194
			64-14	32	30	190
0.1	0.13	MTS	54-8	32	30	42
			54-2	32	31	41
			54-4	30	28	39
			54-1	31	29	34
			54-7	31	29	33
			54-6	28	26	25
			54-9	32	30	24
			54-10	30	28	23
			54-5	30	28	21
			54-11	32	30	20
			54-12	30	29	19
0.1	0.13	CMTS	60-10	31	29	15
			60-11	31	29	15
			60-9	29	27	14
			60-6	30	28	14
			60-1	29	27	14
			60-2	29	27	13
			60-5	28	26	13
			60-13	31	30	13
			60-14	29	27	13
			60-15	29	27	13
			60-3	28	26	12
			60-7	30	28	12
			60-12	32	30	12
			60-4	27	25	11
			60-8	29	27	11

TABLE 11. – RESULTS OF STATISTICAL STUDIES AT 2800° F (1811° K)

Pressure		Coating system	Specimen Number OT2-	Coating weight, mg/cm^2		Coating lifetime, cycles
torr	hN/m^2			green	fused	
10	13.33	MTS	116-1	28	26	104
			116-5	29	27	104
			116-7	28	26	103
			116-2	28	26	102
			116-4	30	28	92
			116-2	30	28	80
			116-9	29	28	78
			116-8	32	31	76
			111-10	31	29	67
			116-14	30	27	63
			116-13	29	27	60
			116-3	29	26	58
			112-13	28	26	55
			116-10	31	29	15
			116-11	30	28	10
10	13.33	CMTS	100-16	31	29	139
			115-14	29	27	124
			115-13	29	26	120
			115-9	31	28	112
			115-12	30	28	110
			115-8	30	28	99
			115-6	29	27	98
			115-7	31	29	96
			115-1	30	28	96
			115-5	33	30	90
			115-11	31	29	88
			115-10	32	30	85
			115-4	30	28	79
			115-2	30	28	78
			115-3	33	31	74
1.0	1.33	MTS	111-9	33	31	8
			112-5	29	27	7
			112-6	28	27	7
			112-9	29	27	7
			112-12	31	29	7
			112-1	32	30	6
			112-2	30	28	6
			112-4	29	28	6
			112-7	31	29	6
			112-9	29	27	6
			112-11	28	27	6
			111-8	29	27	6
			112-3	30	28	5
			112-10	31	29	5
			111-7	29	27	4

Pressure		Coating system	Specimen Number OT2-	Coating weight, mg/cm^2		Coating lifetime, cycles
torr	hN/m^2			green	fused	
1.0	1.33	CMTS	100-14	34	32	104
			100-15	30	28	70
			100-13	33	32	70
			113-11	31	29	19
			113-10	32	30	17
			113-9	33	31	13
			113-8	32	30	13
			113-4	32	30	12
			113-3	35	33	12
			113-5	33	31	8
			113-2	31	29	8
			113-7	33	36	6
			113-12	31	29	5
			113-6	31	29	5
			113-1	33	31	5
0.1	0.13	MTS	117-6	31	29	17
			117-8	30	27	16
			111-11	32	30	15
			117-7	32	30	15
			117-9	32	30	15
			117-12	31	29	15
			117-13	31	29	15
			117-3	28	26	14
			117-5	30	28	14
			117-11	32	30	14
			112-14	31	29	13
			117-2	28	26	13
			117-4	30	28	13
			117-10	29	27	13
			117-1	28	27	12
0.1	0.13	CMTS	118-7	30	28	15
			118-10	28	27	15
			118-11	30	28	15
			118-13	30	28	15
			118-14	30	28	14
			113-14	29	27	12
			118-2	30	28	12
			118-3	29	27	12
			118-4	29	27	12
			118-5	30	27	12
			118-8	29	27	12
			118-9	30	28	12
			118-6	29	27	11
			118-1	29	27	10
			118-12	28	26	10

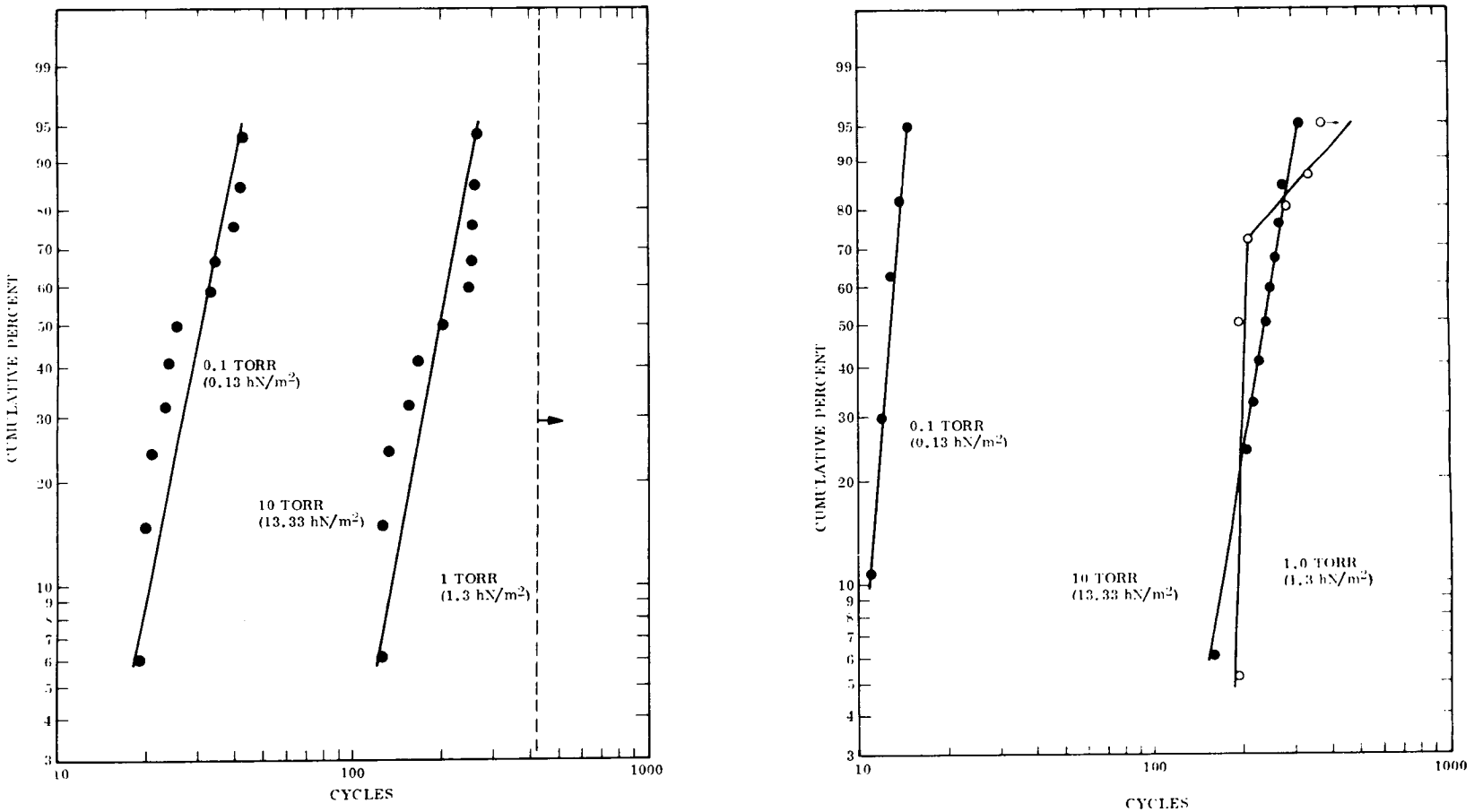

(a) MTS

(b) CMTS

Figure 35 Weibull Plot of MTS and CMTS Coating Performance at 2600°F (1700°K)

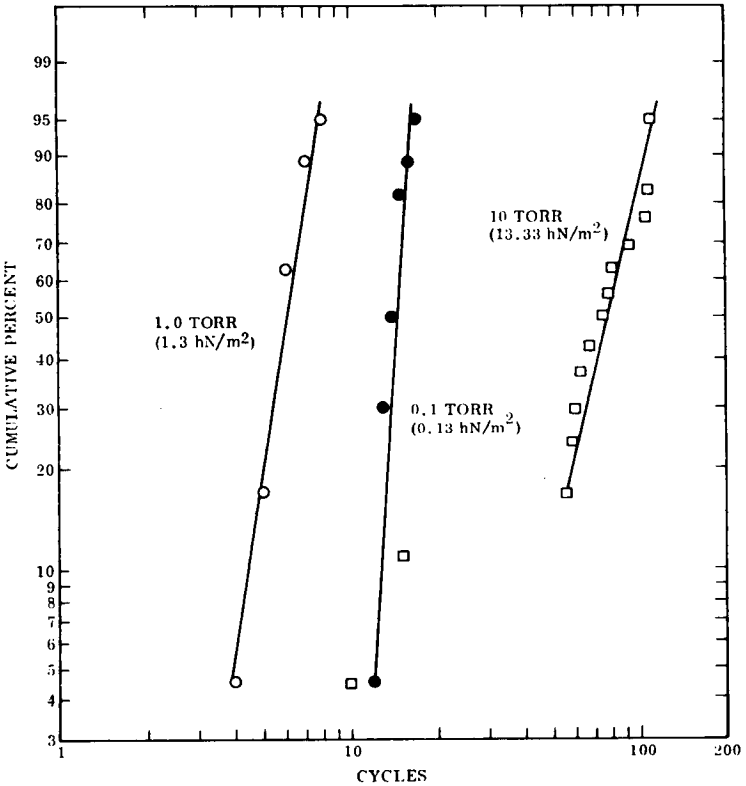

(a) MTS

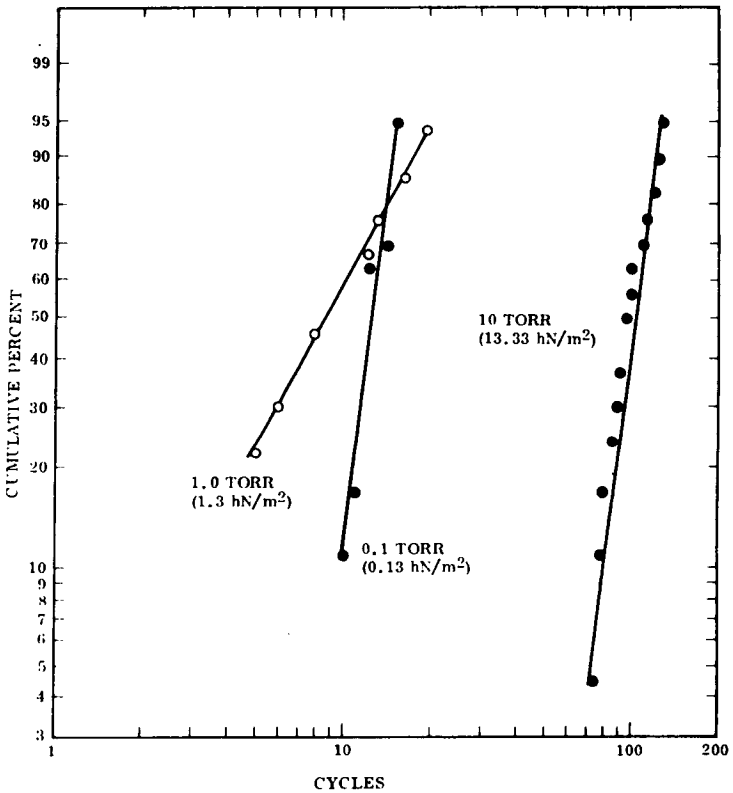

(b) CMTS

Figure 36 Weibull Plot of MTS and CMTS Coating Performance at 2800°F (1811°K)

premature wearout in these specimens was believed to be improper preparation of the substrate edges before coating application. At 1.0 torr (1.33 hN/m^2) the lifetime of three specimens with the CMTS coating far exceeded the distribution shown in the Weibull plot. The lifetime of two specimens was 70 cycles and that of the third was 104 cycles. Because these specimens had a somewhat different appearance after fusion from that of the other specimens, they were not included in the statistical population; however, they do show the potential for longer lifetimes than that indicated by the Weibull plots.

The statistical tests showed the lifetime potential of each coating at various temperature/pressure combinations and provided a basis for predicting coating lifetime. The exposure schedule for emittance, tensile, and bend specimens at each temperature/pressure condition was based on the results of the statistical analyses.

Emittance Measurements

The normal spectral emittance at a wavelength, λ, of 0.65 μm, was determined for the MTS and CMTS coatings after various exposure levels at 2600° and 2800°F (1700° and 1811°K), 0.1, 1.0, and 10 torr (0.13, 1.33, and 13.33 hN/m^2). For conditions where the coating lifetime was 100 cycles or greater, the emittance was determined using duplicate specimens of each system after 1, 10, 25, 50, and 100 cycles. For conditions where lifetimes were less than 100 cycles, the emittance was determined with duplicate specimens after exposure levels that were corresponding fractions of the coating lifetime established in the statistical tests. For all conditions, specimens for the one-cycle emittance determination were exposed in the emittance test equipment, and emittance was measured as a function of time during the first cycle. In addition, emittance values for the as-coated condition were measured in a helium atmosphere. For the 2600°F (1700°K) exposures, the emittance was determined at 1870°, 2200°, and 2600°F (1294°, 1478°, and 1700°K) on heating and cooling, and for the 2800°F (1811°K) exposures, the emittance was determined at 2000°, 2400°, and 2800°F (1366°, 1588°, and 1811°K) during heating and cooling. Environmental conditions during the emittance determinations were the same as those during cyclic exposure. The results are presented in Tables 12 and 13.

No measurable difference in the emittance of the MTS and CMTS coatings occurred under any conditions. The emittance of the as-coated specimens in helium was 0.5 to 0.7 over the temperature range of interest. Under all environmental conditions, the emittance reached its maximum value of 0.85 to 1.0 at the maximum temperature within 1 min of the first cycle and remained at this value throughout the lifetime of the coating. Emittance values over the temperature range 2200° to 2800°F (1478° to 1811°K) were also high, independent of the exposure level, under all environmental conditions.

The emittance values at 1870° and 2000°F (1294° and 1366°K) were unexpectedly low. To ensure that an artifact in the measurements was not introduced at low temperatures, a series of emittance determinations was made with unpolished molybdenum in vacuum. At temperatures of 1870° to 2800°F (1294° to 1811°K), the molybdenum emittance was in the range 0.5 to 0.6, which is in agreement with published values for the emittance of molybdenum. It was therefore concluded that an artifact was not introduced in the emittance determinations at low temperature.

In addition to the extensive emittance determinations, the room-temperature reflectance of exposed MTS and CMTS coatings was measured in a Cory spectroreflectometer. The reflectance traces are shown in Figures 37 and 38. From the room-temperature

TABLE 12. – NORMAL SPECTRAL EMITTANCE OF COATED Ta-10W EXPOSED AT 2600° F (1700° K)

[MTS = 2.5Mn, 33Ti, 54.5Si. CMTS = 2.5Mn, 2.5Co, 32Ti, 63Si.]

Exposure conditions			Coating system	Sample No. OT2-	Normal spectral emittance[a]				
Pressure		Cycles			Heating			Cooling	
torr	hN/m^2				1870° F (1294° K)	2200° F (1478° K)	2600° F (1700° K)	2200° F (1478° K)	1870° F (1299° K)
–	–	As-	MTS	122-2[b]	0.51	0.60	0.72	0.60	0.51
–	–	coated	CMTS	123-9[b]	0.51	0.67	0.72	0.67	0.51
10	13.33	1	MTS	121-12[c]	–	–	0.94	0.84	0.43
		1		122-1[c]	–	–	0.94	0.96	0.43
		10		88-16	0.37	0.92	0.92	0.92	0.46
		10		88-17	0.62	0.95	0.95	0.95	0.58
		25		121-8	0.67	1.0	1.0	1.0	0.50
		25		121-10	0.37	0.86	0.92	0.92	0.46
		50		72-13	0.58	0.92	1.0	1.0	0.58
		50		72-14	0.41	0.8	0.98	0.82	0.48
		100		72-11	0.58	0.95	0.95	0.95	0.58
		100		72-12[d]	0.62	1.0	0.98	–	–
		1	CMTS	120-1[c]	–	–	1.0	0.82	0.53
		1		120-2[c]	–	–	0.88	0.73	0.43
		10		99-1	0.49	0.82	0.98	0.82	0.49
		10		99-2	0.43	0.86	0.98	0.86	0.37
		25		44-15	0.43	0.86	0.92	0.92	0.43
		25		44-16	0.43	0.82	0.88	0.82	0.43
		50		44-11	0.49	0.78	0.88	0.78	0.43
		50		44-13	0.37	0.73	0.80	0.82	0.43
		115		44-9	0.49	0.82	0.94	0.82	0.49
		115		44-10	0.46	0.86	0.92	0.82	0.49
1.0	1.33	1	MTS	122-7[c]	–	–	0.80	0.73	0.49
		1		122-8[c]	–	–	0.88	0.73	0.46
		10		68-11	0.37	0.82	1.0	0.82	0.37
		10		54-16	0.37	1.0	1.0	0.96	0.49
		25		56-1	0.41	0.82	0.94	0.82	0.37
		25		56-2	0.37	0.73	0.92	0.82	0.43
		50		56-3	0.46	0.78	0.80	0.78	0.43
		50		56-4	0.41	0.73	0.88	0.73	0.49
		100		56-5[e]	–	–	–	–	–
		100		56-6	0.49	0.92	1.0	0.96	0.49
		1	CMTS	120-3[c]	–	–	0.88	0.73	0.43
		1		120-4[c]	–	–	0.88	0.73	0.43
		10		52-19	0.46	0.78	0.88	0.82	0.46
		10		52-20	0.49	0.96	1.0	0.96	0.49
		25		52-17	0.43	0.82	0.88	0.82	0.43
		25		52-18	0.46	0.82	0.88	0.82	0.46
		50		52-15	0.49	0.82	0.92	0.73	0.49
		50		52-16	0.43	0.92	0.98	0.92	0.49
		100		52-13	0.49	0.92	0.98	0.86	0.41
		100		52-14	0.41	0.92	1.0	1.0	0.46
0.1	0.13	1	MTS	122-5[c]	–	–	0.92	0.78	0.37
		1		122-6[c]	–	–	0.84	0.73	0.37
		2		68-9[e]	–	–	–	–	–
		2		68-10	0.43	0.73	0.92	0.73	0.43
		5		68-7	0.43	0.82	0.84	0.82	0.41
		5		68-8	0.46	0.78	0.84	0.78	0.43
		10		46-9	0.43	0.82	1.0	0.92	0.41
		10		56-9	0.43	0.78	0.94	0.82	0.37
		20		56-7	0.49	0.78	0.84	0.78	0.43
		20		56-8	0.43	0.73	0.92	0.82	0.49
		1	CMTS	123-13[c]	–	–	0.88	0.63	0.43
		1		123-14[c]	–	–	0.82	0.82	0.43
		2		58-7	0.46	0.92	1.0	0.92	0.41
		2		58-8	0.46	0.78	1.0	0.78	0.41
		4		58-5	0.43	0.82	0.98	0.82	0.37
		4		58-6	0.43	0.82	0.98	0.86	0.43
		8		70-14	0.49	0.78	0.98	0.82	0.49
		8		70-15[f]	–	–	–	–	–
		10		52-21	0.43	0.82	0.98	0.82	0.43
		10		52-22	0.43	0.82	0.92	0.82	0.43

[a] Accuracy ~ ±10%

[b] Measured in helium.

[c] At 2600° F (1700° K), emittance reached maximum value in <1 min.

[d] Test discontinued because of arcing at the electrode.

[e] Support hook wore out during oxidation exposure.

[f] Coating wore out during oxidation exposure.

TABLE 13. – NORMAL SPECTRAL EMITTANCE OF COATED Ta-10W EXPOSED AT 2800°F (1811°K)

[MTS = 2.5Mn, 33Ti, 64.5Si. CMTS = 2.5Mn, 2.5Co, 32Ti, 63Si.]

Exposure conditions			Coating system	Sample No. OT2-	Normal spectral emittance[a]				
					Heating			Cooling	
Pressure torr	Pressure hN/m^2	Cycles			2000°F (1366°K)	2400°F (1588°K)	2800°F (1811°K)	2400°F (1588°K)	2000°F (1366°K)
–	–	As-	MTS	122-2[b]	0.60	0.63	0.54	0.63	0.60
–	–	coated	CMTS	123-9[b]	0.60	0.63	0.54	0.63	0.60
10	13.33	1	MTS	122-11[c]	–	–	**0.82**	**0.86**	**0.60**
		1		122-12[c]	–	–	**0.86**	**0.73**	**0.56**
		5		109-2	0.67	0.82	1.0	0.82	0.67
		5		109-3	0.80	0.82	1.0	0.90	0.80
		12		109-4	0.67	0.98	1.0	0.90	0.67
		12		109-5	0.75	0.98	0.98	0.90	0.67
		25		109-6	0.75	0.98	1.0	0.98	0.67
		25		109-7	0.67	0.94	0.92	0.94	0.67
		50		109-1[d]	–	–	–	–	–
		50		121-1	0.80	0.86	1.0	0.86	0.72
		1	CMTS	120-7[c]	–	–	**0.80**	**0.90**	**0.67**
		1		120-8[c]	–	–	**0.72**	**0.77**	**0.56**
		7		99-9	0.53	0.80	0.82	0.80	0.53
		7		99-10	0.67	0.77	0.82	0.73	0.60
		17		99-7	0.67	0.86	0.94	0.86	0.67
		17		99-8	0.63	0.86	0.94	0.77	0.60
		35		99-6	0.72	0.94	0.98	0.82	0.63
		35		99-3	0.67	0.82	0.98	0.80	0.67
		70		99-4	0.80	0.90	0.86	0.90	0.72
		70		99-5	0.72	0.86	0.86	0.77	0.67
1	1.33	1	MTS	122-9[c]	–	–	**1.0**	**0.86**	**0.67**
		1		122-10[c]	–	–	**0.82**	**0.73**	**0.56**
		2		109-9	0.72	0.80	0.92	0.86	0.75
		2		109-10	0.67	0.94	0.92	0.86	0.67
		5		109-11	0.75	1.0	0.98	0.90	0.86
		5		109-12	0.63	0.77	0.82	0.80	0.63
		10		109-13[d]	–	–	–	–	–
		10		109-14	0.72	0.86	0.94	0.75	**0.75**
		1	CMTS	120-5[c]	–	–	**0.86**	**0.73**	0.72
		1		120-6[c]	–	–	**0.86**	**0.73**	0.60
		2		58-9	0.63	0.86	1.0	0.82	0.72
		2		58-10	0.60	0.90	1.0	0.94	0.60
		4		99-11	0.60	0.80	0.82	0.86	0.60
		4		99-12	0.72	0.82	0.90	0.82	0.72
		8		99-13	0.63	1.0	1.0	0.94	0.63
		8		99-14	0.63	0.86	0.98	0.86	0.63
0.1	0.13	1	MTS	122-3[c]	–	–	**0.86**	**0.77**	**0.56**
		1		122-4[c]	–	–	**0.86**	**–[e]**	–
		2		121-2	0.72	0.94	0.92	0.86	0.67
		2		121-3	0.56	0.90	0.94	0.86	0.60
		3		121-4	0.56	0.66	0.80	0.73	0.60
		3		121-5	0.53	0.66	0.80	0.73	0.56
		6		121-6	0.63	0.66	0.90	0.73	0.63
		6		121-7	0.53	0.60	0.82	0.80	0.53
		1	CMTS	123-11[c]	–	–	0.82	0.73	0.53
		1		123-12[c]	–	–	**0.94**	**0.86**	**0.63**
		2		123-1	0.72	1.0	0.98	0.90	0.67
		2		123-2	0.67	0.86	0.98	0.90	0.60
		3		123-5	0.60	0.82	0.80	0.80	0.56
		3		123-6	0.60	0.77	0.90	0.77	0.60
		6		123-3	0.63	0.86	0.94	0.82	0.53
		6		123-4	0.75	0.90	0.86	0.82	0.67

[a] Accuracy ~ ±10%

[b] Measured in helium.

[c] At 2800°F (1800°K), emittance reached maximum value in < 1 min.

[d] Coating wore our during oxidation exposure.

[e] Test discontinued because of arcing at the electrode.

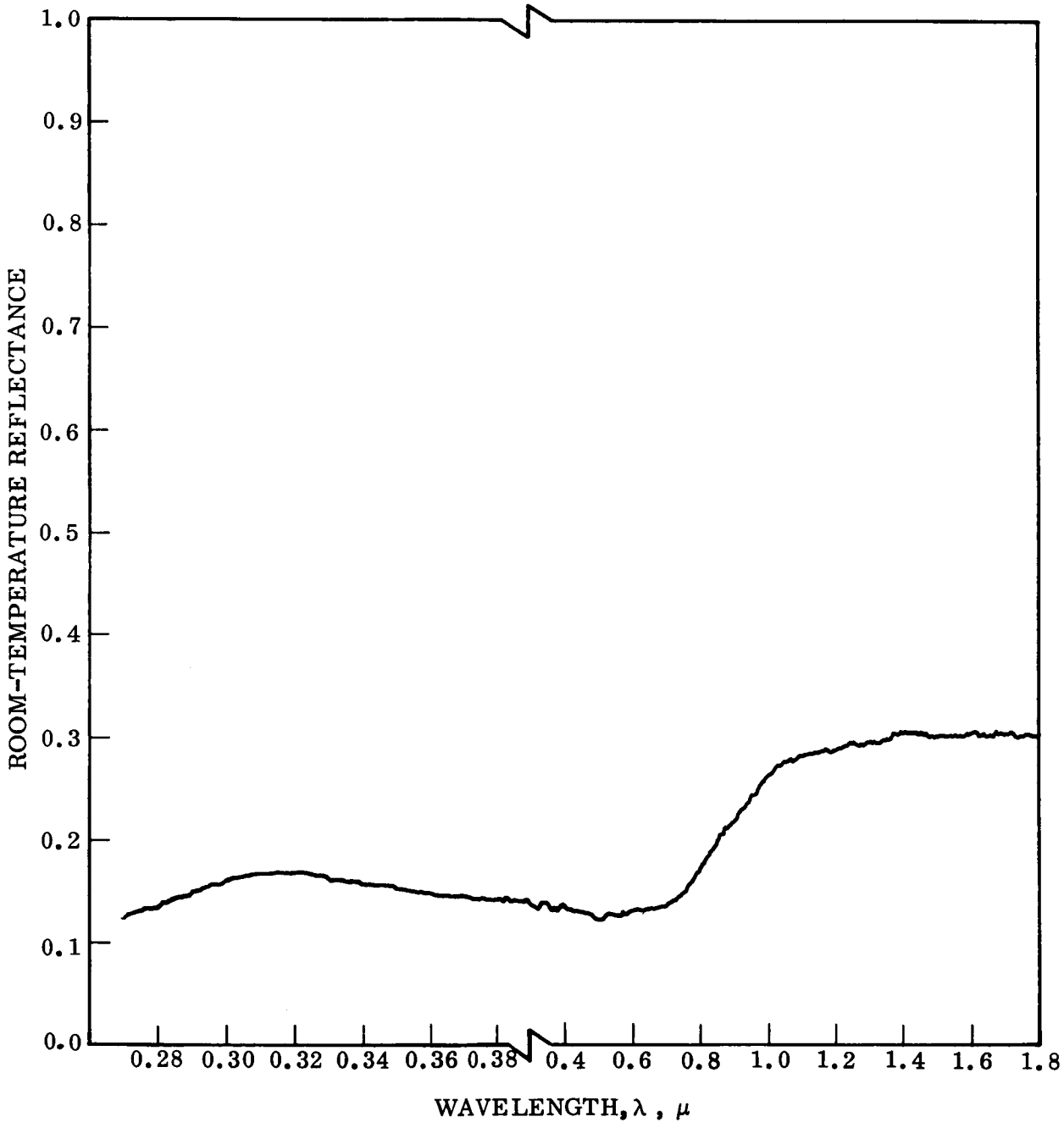

Figure 37 Room-Temperature Reflectance for MTS Coating After Exposure at 2600° F (1700° K), 10 Torr (13.33 hN/m^2), 80 Cycles.

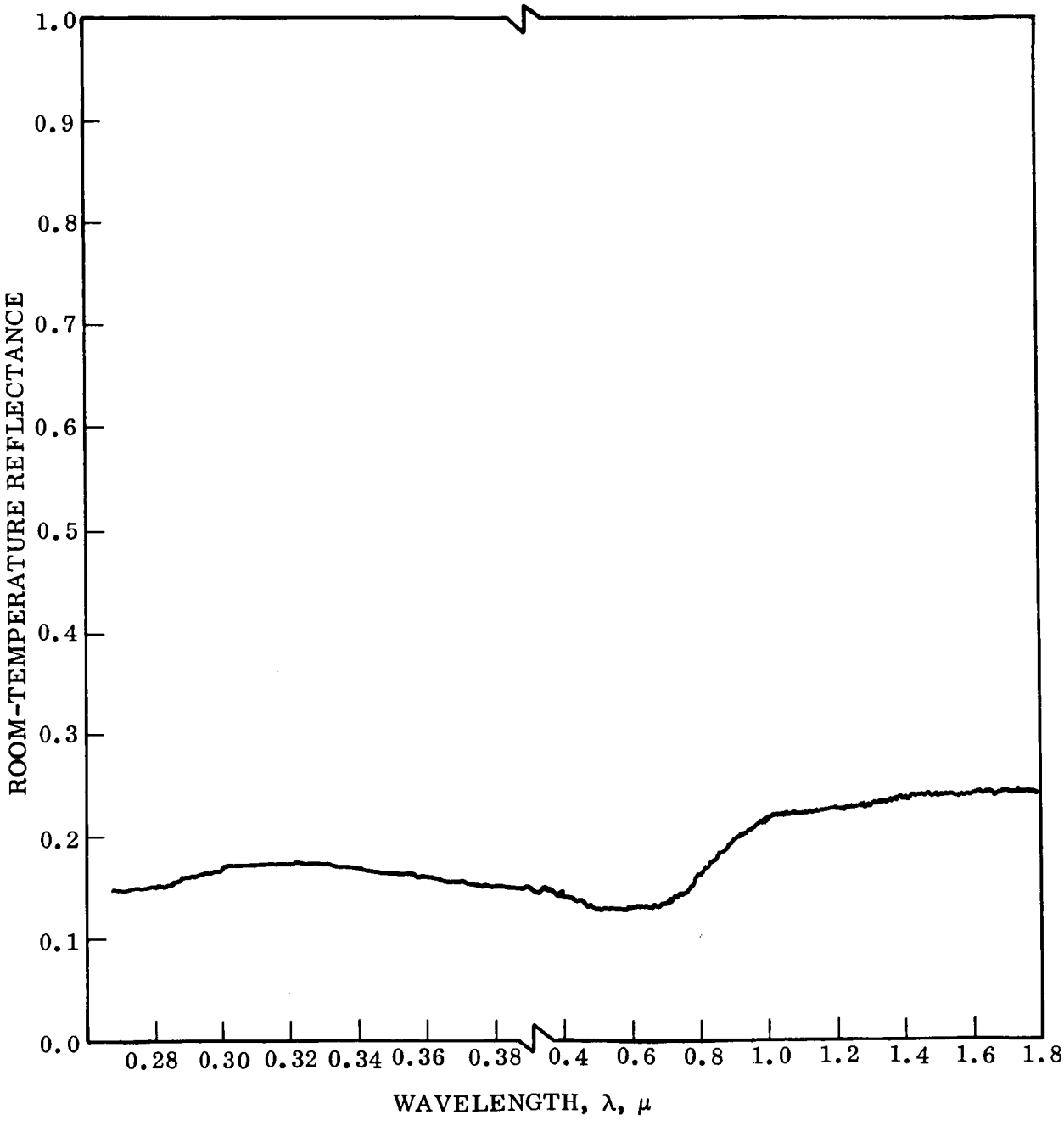

Figure 38 Room-Temperature Reflectance for CMTS Coating After Exposure at 2600° F (1700° K), 10 Torr (13.33 hN/m^2), 100 Cycles.

reflectance data, the elevated temperature normal spectral emittance at a wavelength of 0.65 μm can be inferred to be 0.87 for both coatings.

Mechanical Properties

The MTS (2.5Mn-33Ti-64.5Si) and CMTS (2.5Co-2.5Mn-32Ti-63Si) coatings have been evaluated for bend ductile-to-brittle transition temperature, room temperature, and elevated temperature tensile properties, and creep behavior in the as-coated and cyclic-oxidation exposed conditions (creep tests on as-coated only). Tensile and creep properties were measured for duplicate samples for each different exposure, and the bend DBTT was determined with a single test at each temperature. The exposure conditions are those described at the start of the section on the results of tests with the best coating systems.

- Bend Ductile-to-Brittle Transition Temperature

The 4t-90deg bend ductile-to-brittle transition temperature for MTS- and CMTS-coated Ta-10W is presented in Table 14. Both systems in the as-coated condition are ductile in bending at -321°F (77°K). As shown in Table 14, with two exceptions, all the samples exposed to 2600° and 2800°F (1700° and 1811°K) slow-cycle oxidation at 0.1, 1.0, and 10 torr (0.133, 1.33, and 13.33 hN/m^2) for the minimum cyclic lifetime of the coating also are ductile in bending at -321°F (77°K). Facilities were not available for testing below this temperature, and the DBTT is reported as less than this value.

The CMTS coating exposed for 70 cycles at 2800°F (1811°K) and 10 torr (13.33 hN/m^2) was brittle at liquid nitrogen temperatures [-321°F (77°K)] in two tests but was ductile at room temperature. At -108°F (195°K) the sample was ductile except for one edge crack, indicating that coating wearout had initiated at the edge and that oxygen was leaking through to the substrate. The DBTT is taken to be -108°F (195°K) for this exposure condition. Edge cracks were also formed on CMTS samples bent in liquid nitrogen after 35-cycle exposure (half the minimum lifetime) to this condition and after 4-cycle exposure (half the minimum lifetime) to 2800°F (1811°K), 1.0 torr (1.33 hN/m^2). The MTS coating at 2800°F (1811°K) provides complete protection to the edges and is a better coating in this respect.

The maximum loads during bending are also listed in Table 14. The bending loads are consistent from sample to sample, when they have the same thermal history. The loads decrease with increasing cyclic exposure (time at temperature) as a consequence of coating/substrate interdiffusion, which reduces substrate thickness. Since the coating was removed from the compression side before bending, only the substrate cross-section area governs the bending load. As shown in Table 14, the maximum load is more than doubled if the coating is left on the compressive side. The coating resists compression, and the high compressive strength results in a higher bending strength for the composite. As shown in the section on test procedures, however, when the coating yields on the compression side and spalls from the surface, the load drops immediately to the lower value.

- Tensile Properties

The 0.2-percent offset yield strength, ultimate tensile strength, and total elongation were measured for the MTS and CMTS coating systems at room temperature, 1400°, 2600°, and 2800°F (1033°, 1700°, 1811°K) as-coated and after cyclic exposure at 2600° and 2800°F (1700°, 1811°K).

TABLE 14. – SUMMARY OF BEND DUCTILE-BRITTLE TRANSITION TEMPERATURES TESTS[a]

Exposure Conditions				Cycles	Coating system	Sample number	Test temperature		Bend angle, deg	Maximum load		Comments
Temperature		Pressure										
°F	°K	torr	hN/m²				°F	°K		lb	kg	
2600	1700	10	13.33	25	MnTiSi	OT2-40-3	-321	77	90	17.7	8.0	Ductile
				50		OT2-40-5				16.0	7.3	
				142		OT2-40-7				15.0	6.8	
				25	CoMnTiSi	OT2-36-7				16.5	7.5	
				50		OT2-36-9				15.0	6.8	
				100		OT2-36-10				13.8	6.3	
		1.0	1.33	25	MnTiSi	OT2-72-9				17.5	8.0	
				50		OT2-72-7				17.0	7.7	
				100		OT2-66-16				13.3	6.0	
				100		OT2-62-16				29.5(b)	13.4(b)	
				25	CoMnTiSi	OT2-70-9				16.3	7.4	
				50		OT2-70-7				15.2	6.9	
				100		OT2-70-6				13.8	6.3	
		0.1	0.13	5	MnTiSi	OT2-98-4				19.3	8.8	
				10	MnTiSi	OT2-102-10				17.5	8.0	
				2	CoMnTiSi	OT2-70-13				19.0	8.6	
				4		OT2-70-3				19.2	8.7	
				10		OT2-70-11				17.6	8.0	
2800	1811	10	13.33	12	MnTiSi	OT2-119-3				16.0	7.3	
				25		OT2-119-2				17.2	7.8	
				50		OT2-131-9				14.6	6.6	
				17	CoMnTiSi	OT2-134-3				19.9	9.0	
				35		OT2-96-13A				13.6	6.2	Edge Crack
				35		OT2-96-13B				17.3	7.9	Ductile
				70		OT2-134-1A			20	13.0	5.9	Brittle
						OT2-134-1B	+ 25	273	90	13.0	5.9	Ductile
						OT2-134-2A	-321	77	20	13.2	6.0	Brittle
						OT2-134-2B	-108	195	90	13.6	6.2	Edge Crack
		1.0	1.33	2	MnTiSi	OT2-119-4	-321	77		19.5	8.9	Ductile
				5		OT2-119-6				18.0	8.2	
				8		OT2-131-12				17.5	8.0	
				2	CoMnTiSi	OT2-100-7				20.0	9.1	
				4		OT2-100-8A				18.5	8.1	Edge Crack
				4		OT2-100-8B				17.8	8.1	Edge Crack
				8		OT2-134-11				14.5	6.6	Ductile
		0.1	0.13	2	MnTiSi	OT2-119-7			20	20.2	9.2	
				3		OT2-119-9				18.5	8.4	
				6		OT2-119-8				17.2	7.8	
				2	CoMnTiSi	OT2-100-10				20.3	9.2	
				3		OT2-134-6				16.8	7.6	
				6		OT2-134-4				18.2	8.3	

[a]4t radius, 90 deg bend angle, 1 in. (2.5 cm)/min.
[b]Coating left on compression side of bend sample.

The strength values are reported for four different cross-sectional areas as the basis for calculating stress from load values:

(1) Original substrate thickness before coating
(2) Residual substrate thickness after coating
(3) Total thickness as-coated
(4) Residual substrate thickness after cyclic oxidation exposure

The first method is the one most commonly used in measuring the strength of coated metals. It is based on the assumption that either (1) the substrate loss on coating is negligible and the coating has no strength or (2) the strength added by the coating equals the strength of the metal removed in forming the coating. It is generally believed that this approach gives the best estimate of composite strength. The second and fourth methods, based on the assumption that the coating contributes nothing to strength, are less commonly used. These methods compensate for the substrate material that is removed during formation of the coating and subsequent thermal exposures as a result of coating/substrate interdiffusion. If the coating has significant strength, however, these methods will give inordinately high values, since stress will be calculated on the basis of too small a cross section. The danger in this is that designers may apply the strength data to a larger cross section (based on original thickness), resulting in excessive loads. This is why the more conservative approach, based on original thickness for area calculations, has traditionally been preferred. The third approach, based on the total cross section after coating, will be ultraconservative if the coating is weak in tension relative to the substrate material.

The gage dimensions (thickness and width) of each sample were measured prior to coating to obtain the original cross-section area. The residual substrate thickness after coating versus cyclic exposure was measured directly in the shoulder regions of samples from which the coating had been removed for attachment of support tabs. These values closely matched calculated values based on metallographic measurements of substrate thickness as a function of thermal history; the substrate recession rates were 0.15 and 0.175 mil/cycle$^{1/2}$ (0.381 and 0.445 cm/cycle$^{1/2}$) per side at 2600° and 2800°F (1700° and 1811°K), respectively. These values were used to calculate residual substrate thickness for the room-temperature tensile tests in which the coating was not removed from the shoulder region of samples.

The results listed in Table 15 show that strength values based on total thickness as-coated (coating plus substrate) are roughly half those of the uncoated alloy or of the coated materials, based on original substrate thickness. The values shown indicate that the coating has a low strength relative to that of the metal, based on the full cross section of the coating. These strength data are of little value and were not considered further; the data based on original and residual substrate measurements are more representative of actual strength values and were used in preparing the following summary charts of tensile behavior in Figures 39 through 44.

The plots of yield strength versus exposure at both temperatures indicate an increase in strength with cyclic exposure at 10 torr (13.33 hN/m^2) when samples are tested at room temperature to 2600°F (1700°K). The effect is most pronounced when strength is calculated on the basis of residual substrate thickness. A similar effect is noted for 1 torr (1.33 hN/m^2) cyclic exposure conditions when samples are tested at 1400° to 2600°F (1033° to 1700°F). Tests at 2800°F (1811°K) show no significant changes in yield strength as a function of exposure conditions. In all cases, the effects are the same for both coating systems.

TABLE 15. – TENSILE PROPERTIES OF COATED Ta-10W

Exposure conditions					Test temp.		Coating system	Sample No. OT2-	0.2 Percent yield strength								Ultimate strength								Elongation %
Temp.		Pressure							Original substrate		Coated substrate		As-coated		Residual substrate		Original substrate		Coated substrate		As-coated		Residual substrate		
°F	°K	torr	hN/m^2	Cycles	°F	°K			ksi	MN/m^2	ksi	MN/m^2	ksi	MN/m^2	ksi	MN/m^2	ksi	MN/m^2	ksi	MN/m^2	ksi	MN/m^2	ksi	MN/m^2	
–	–	–	–	–	RT	298	Uncoated	6-3	73.3	505	–	–	–	–	–	–	86.2	594	–	–	–	–	–	–	25.4
–	–	–	–	–	RT	298		104-2	70.5	486	–	–	–	–	–	–	82.8	571	–	–	–	–	–	–	23.6
–	–	–	–	–	1400	1033		AR-5	31.4	216	–	–	–	–	–	–	50.3	347	–	–	–	–	–	–	16.8
–	–	–	–	–	1400	1033		AR-6	29.4	203	–	–	–	–	–	–	51.3	354	–	–	–	–	–	–	17.0
–	–	–	–	–	2600	1700		AR-1	15.1	104	–	–	–	–	–	–	21.5	148	–	–	–	–	–	–	61.4
–	–	–	–	–	2600	1700		AR-2	17.5	121	–	–	–	–	–	–	21.7	150	–	–	–	–	–	–	46.3
–	–	–	–	–	2800	1811		AR-4	16.5	114	–	–	–	–	–	–	17.9	123	–	–	–	–	–	–	59.5
–	–	–	–	–	2800	1811		AR-3	14.8	102	–	–	–	–	–	–	19.0	131	–	–	–	–	–	–	36.9
–	–	–	–	As-coated	RT	298	MTS	135-10	64.9	447	76.6	528	37.1	256	–	–	79.6	549	94.0	648	45.5	314	–	–	15.5
–	–	–	–				MTS	139-9	66.2	456	77.8	536	38.4	265	–	–	79.7	550	93.6	645	46.2	319	–	–	13.5
–	–	–	–				CMTS	105-6	66.4	458	79.0	545	41.1	283	–	–	79.0	545	94.2	649	48.9	337	–	–	15.5
–	–	–	–				CMTS	105-7	68.9	475	82.0	565	40.0	275	–	–	82.8	571	98.7	681	50.3	347	–	–	13.3
–	–	–	–		1400	1033	MTS	132-12	33.3	230	39.4	272	19.3	133	–	–	56.6	390	66.9	461	32.8	226	–	–	13.1
–	–	–	–				MTS	135-9	27.8	192	32.6	225	15.5	107	–	–	44.0	303	51.7	356	24.6	170	–	–	14.7
–	–	–	–				CMTS	79-9	29.4	203	35.0	241	18.4	127	–	–	49.0	338	58.2	401	30.6	211	–	–	12.6
–	–	–	–				CMTS	78-12	30.5	210	37.0	255	18.3	126	–	–	50.6	349	60.1	414	30.3	209	–	–	11.2
–	–	–	–		2600	1700	MTS	135-11	18.5	128	21.8	150	10.4	72	–	–	23.7	163	28.0	193	13.4	92	–	–	29.5
–	–	–	–				MTS	135-10	18.2	125	21.4	148	9.8	68	–	–	24.1	166	28.4	196	13.1	90	–	–	34.8
–	–	–	–				CMTS	44-7	18.0	124	21.4	148	11.5	79	–	–	20.5	141	24.3	168	13.1	90	–	–	35.0
–	–	–	–				CMTS	44-6	18.5	128	22.0	152	12.0	83	–	–	20.9	144	24.8	171	13.5	93	–	–	45.8
–	–	–	–		2800	1811	MTS	135-12	–	–	–	–	–	–	–	–	18.3	126	21.5	148	10.9	75	21.9	151	58.9
–	–	–	–				MTS	139-1	14.9	103	17.5	121	8.8	61	17.6	121	20.7	143	24.2	167	12.2	84	24.4	168	45.3
–	–	–	–				CMTS	136-10	15.0	103	17.6	121	8.7	60	18.2	125	20.7	143	24.3	168	12.0	83	25.2	174	52.9
–	–	–	–				CMTS	136-11	16.7	115	19.7	136	9.7	67	19.9	137	20.6	142	24.3	168	12.0	83	24.5	169	47.0
2600	1700	10	13.33	25	RT	298	MTS	148-12	67.8	467	80.4	554	35.3	243	83.5	576	79.0	545	93.7	646	41.2	284	97.3	671	13.0
				25				82-9[a]	–	–	–	–	–	–	–	–	–	–	–	–	–	–	–	–	–
				50				148-13	64.8	447	77.2	532	35.1	242	83.9	578	74.5	514	88.8	612	40.4	279	96.5	665	14.0
				62				103-1	75.5	521	89.8	619	48.0	331	101.1	697	82.1	566	97.6	673	52.2	360	110.0	758	6.7
				87				74-4	78.5	541	93.0	641	47.4	327	109.5	755	85.8	590	101.8	702	51.9	358	119.7	825	14.4
				88				148-11	70.7	487	72.5	500	34.8	240	99.0	683	78.6	542	80.4	554	38.6	266	110.0	758	9.0
				100				82-10	74.7	515	88.8	612	44.5	307	103.6	714	81.2	560	96.5	665	48.3	333	112.7	777	5.1
				25			CMTS	44-1	73.2	505	87.0	600	44.2	305	94.0	648	80.0	552	95.0	655	48.3	333	102.6	707	11.5
				25				44-2	76.7	529	91.3	629	44.4	306	95.7	660	85.3	588	101.5	700	49.4	341	106.4	734	11.7
				50				44-3	72.5	500	85.2	587	44.2	305	96.0	662	79.6	549	94.6	652	48.7	336	105.5	727	12.8
				50				44-4	73.3	505	87.0	600	46.1	318	97.2	670	79.4	547	94.3	650	49.9	344	105.2	725	7.8
				100				44-5	68.2	470	81.1	559	43.7	301	94.6	652	73.6	507	87.5	603	47.2	325	102.0	703	8.7
				100				44-8	68.9	475	82.2	567	41.3	285	96.3	664	74.3	512	88.7	612	44.5	307	104.0	717	6.0
				50	1400	1033	MTS	82-6	36.1	249	43.0	296	21.4	148	47.8	330	37.8	261	45.0	310	22.5	155	50.1	345	2.6
				50				82-7[b]	36.3	250	43.5	300	21.0	145	46.7	322	36.3	250	43.5	300	21.0	145	46.7	322	Nil
				50				106-1	38.9	268	46.7	322	21.8	150	51.7	356	39.7	274	47.7	329	22.3	154	52.8	364	3.6
				100				103-10	41.3	285	49.0	338	26.8	185	57.6	397	41.4	285	49.1	339	26.9	185	57.8	399	2.8
				100				103-8	40.3	278	48.1	332	22.9	158	52.7	363	43.7	301	52.2	360	24.9	172	57.1	394	3.7
				50			CMTS	80-11	38.6	266	44.7	308	23.2	160	49.5	341	43.7	301	51.8	357	26.2	181	56.1	387	3.8
				50				80-12	35.0	241	41.7	288	20.6	142	46.9	323	39.1	270	46.5	321	23.0	159	52.4	361	3.4
				100				80-7	33.4	230	39.8	274	19.7	136	44.0	303	50.3	347	59.8	412	29.6	204	66.0	455	11.4
				100				80-8	33.5	231	39.9	275	19.8	137	43.8	302	38.5	265	45.8	316	22.7	157	50.5	348	4.4
				25	2600		MTS	82-9	19.9	137	23.7	163	11.7	81	24.2	167	22.2	153	26.5	183	13.0	90	27.0	186	22.6
				61				74-1	19.1	132	27.1	187	11.6	80	21.1	145	21.5	148	25.6	177	13.1	90	23.8	164	2.0
				62				103-3	19.6	135	23.4	161	11.5	79	26.0	179	24.6	170	29.5	203	14.4	99	32.6	225	18.8
				62				103-2	19.0	131	22.6	156	11.6	80	26.3	181	21.1	145	25.1	173	12.8	88	29.1	201	25.3
				100				43-2	17.8	123	21.1	145	11.0	76	21.5	148	21.3	147	25.2	174	13.2	91	25.8	178	29.5
				100				103-9	20.7	143	24.6	170	11.9	82	27.2	188	23.5	162	27.9	192	13.5	93	30.9	213	26.3
				50			CMTS	104-4	19.1	132	22.7	157	13.0	90	25.3	174	21.7	150	25.8	178	14.7	101	28.7	198	26.1
				50				104-1	22.6	156	27.0	186	13.1	90	31.2	215	25.2	174	30.1	208	14.6	101	34.9	241	13.8
				100				80-10	18.8	130	22.3	154	11.4	79	25.6	177	25.0	172	29.7	205	15.2	105	34.2	236	25.4
				100				80-13	19.2	132	22.9	158	11.4	79	27.2	188	22.0	152	26.2	181	13.1	90	31.0	214	10.4
		1	1.33	25	RT	298		74-6	61.9	427	82.9	572	38.1	263	79.3	547	72.1	497	85.7	591	44.4	306	92.5	638	14.7
				25				74-7	58.9	406	72.7	501	35.9	248	75.6	521	69.6	480	86.0	593	42.4	292	89.5	617	13.2
				50				74-10	64.8	447	77.3	533	39.7	274	86.0	593	74.2	512	88.3	609	45.3	312	98.4	678	16.5
				50				74-11	63.3	436	75.1	518	39.0	269	83.8	578	71.7	494	85.1	587	44.1	304	95.0	655	13.8
				100				74-5	58.7	405	70.0	483	35.2	243	81.6	563	66.8	461	79.7	550	40.1	276	93.0	641	13.2
				100				74-9	59.1	407	70.2	484	36.9	254	81.3	561	67.6	466	80.2	553	42.1	290	93.0	641	9.3
				25			CMTS	80-1	69.5	479	82.7	570	43.7	301	88.7	612	79.6	549	94.8	654	50.1	345	101.7	701	12.5
				25				80-6	64.2	443	76.5	527	39.0	269	81.6	563	73.8	509	88.0	607	44.7	308	93.8	647	11.0
				50				104-8	67.0	462	79.4	547	45.0	310	88.3	609	75.5	521	89.5	617	50.7	350	99.5	686	12.2
				50				104-9	63.2	436	74.8	516	37.8	261	83.4	575	71.2	491	84.3	581	42.6	294	93.9	647	13.5

See footnotes at end of table.

TABLE 15 (Cont.)

Exposure conditions					Test temp.		Coating System	Sample No. OT2-	0.2 Percent yield strength								Ultimate strength								Elongation %
Temp.									Original substrate		Coated substrate		As-coated		Residual substrate		Original substrate		Coated substrate		As-coated		Residual substrate		
°F	°K	torr	hN/m^2	Cycles	°F	°K			ksi	MN/m^2	ksi	MN/m^2	ksi	MN/m^2	ksi	MN/m^2	ksi	MN/m^2	ksi	MN/m^2	ksi	MN/m^2	ksi	MN/m^2	
2800	1811	10	13.33	50	1400	1033	CMTS	128-1	38.5	265	45.3	312	23.6	163	51.2	353	41.4	285	48.8	336	25.4	175	55.2	381	2.5
				70	1400	1033	CMTS	108-1[a]	–	–	–	–	–	–	–	–	–	–	–	–	–	–	–	–	–
				25	2800	1811	MTS	124-3	16.9	117	20.1	139	9.4	65	20.7	143	19.7	136	23.4	161	11.0	76	24.1	166	47.0
				25				127-10	14.9	103	17.7	122	8.7	60	19.1	132	18.5	128	21.9	151	10.7	74	23.6	163	35.3
				41				124-1[a]	–	–	–	–	–	–	–	–	–	–	–	–	–	–	–	–	–
				41				124-2	14.5	100	17.2	119	8.0	55	17.5	121	19.0	131	22.5	155	10.4	72	22.9	158	40.5
				35			CMTS	108-3	17.9	123	21.2	146	10.4	72	21.4	148	21.5	148	25.4	175	12.5	86	25.7	177	35.2
				35				128-4	14.1	97	16.7	115	8.8	61	19.0	131	18.0	124	21.2	146	11.1	77	24.2	167	31.6
				70				107-10	16.7	115	19.8	137	10.2	70	22.7	157	20.2	139	24.3	168	12.5	86	27.9	192	32.2
				70				108-2	14.4	99	17.0	117	8.7	60	21.9	151	18.3	126	21.6	149	11.1	77	27.9	192	34.4
		1.0	1.3	2	RT	297	MTS	127-3	64.1	442	76.2	525	36.9	254	77.5	534	75.4	520	89.5	617	43.3	299	91.1	628	11.3
				2				127-4	61.7	425	73.3	505	35.4	244	74.7	515	73.5	507	87.4	603	41.4	285	89.0	614	11.0
				5				106-10	68.7	474	82.2	567	40.9	282	84.3	581	78.0	538	93.3	643	46.5	321	95.8	661	17.5
				5				124-7	69.5	479	82.7	570	38.1	263	84.8	585	79.0	545	94.1	649	43.4	299	96.5	665	16.8
				10				106-9[b]	56.6	390	67.8	467	31.5	217	72.4	499	56.6	390	67.8	467	31.5	217	72.4	499	Nil
				10				106-6[a]	–	–	–	–	–	–	–	–	–	–	–	–	–	–	–	–	–
				2			CMTS	125-1	63.0	434	74.7	515	38.1	263	76.1	525	75.2	518	89.2	615	45.5	314	90.8	626	13.8
				2				125-2	62.5	431	74.4	513	38.2	263	75.8	523	75.0	517	89.2	615	45.8	316	90.9	627	12.3
				4				108-5	61.7	425	73.5	507	36.3	250	75.4	520	71.7	494	85.4	589	42.2	291	87.6	604	14.5
				4				128-12	64.8	447	76.8	530	39.2	270	79.0	545	74.7	515	88.7	612	45.3	312	91.3	629	13.2
				8				108-6	64.6	445	76.9	530	36.8	254	80.8	557	73.3	505	87.3	602	41.7	288	91.7	632	13.2
				8				108-9	63.4	437	75.7	522	35.2	243	79.0	545	72.3	498	86.2	594	40.1	276	90.0	621	16.0
				5	1400	1033	MTS	124-4	29.0	200	34.3	236	15.5	107	34.7	239	52.8	364	62.5	431	28.2	194	63.1	435	11.2
				5				124-8	32.0	221	38.2	263	17.7	122	36.4	251	53.0	365	63.0	434	29.3	202	60.2	415	12.7
				10				124-5	33.4	230	39.8	274	8.9	61	39.8	274	35.0	241	41.7	288	19.7	136	41.7	288	3.2
				10				124-6	33.0	228	39.1	270	18.2	125	37.7	260	55.6	383	65.7	453	30.7	212	63.4	437	12.2
				4			CMTS	128-11	30.2	208	35.5	245	18.1	125	36.6	252	51.4	354	60.4	416	30.8	212	62.3	430	12.9
				4				128-13	283	195	33.4	230	17.7	122	35.7	246	45.2	312	53.3	367	28.3	195	56.9	392	11.0
				8				108-7[c]	30.1	208	35.7	246	16.5	114	38.2	263	>39.8	274	>47.1	325	>21.8	150	50.5	348	>3.8
				8				128-7	32.0	221	37.7	260	19.5	134	40.7	281	52.7	363	62.0	427	32.0	221	66.9	461	11.2
				5	2800	1811	MTS	124-9	15.6	108	18.6	128	8.5	59	18.6	128	19.3	133	23.0	159	10.5	72	23.0	159	62.2
				5				124-10	17.1	118	20.3	140	9.8	68	20.7	143	20.8	143	24.6	170	12.0	83	25.2	174	57.6
				10				106-7	15.5	107	18.4	127	8.8	61	19.0	131	20.3	140	24.1	166	11.5	79	24.8	171	19.8
				10				106-8	15.0	103	17.9	123	8.5	59	18.2	125	19.3	133	23.1	159	10.9	75	23.5	162	33.3
				4			CMTS	128-9	14.1	97	16.5	114	8.5	59	18.5	128	18.3	126	21.5	148	11.1	77	24.0	165	35.3
				4				128-10	14.5	100	17.1	118	8.7	60	18.7	129	18.8	130	22.1	152	11.2	77	24.2	167	63.2
				8				108-8[e]	–	–	–	–	–	–	–	–	19.9	137	23.7	163	11.1	77	26.3	181	13.1
				8				128-8	13.4	92	15.8	109	8.4	58	16.9	117	18.5	128	21.8	150	11.6	80	23.3	161	47.0
		0.1	0.13	2	RT	297	MTS	132-6	67.7	467	80.5	555	39.7	274	82.1	566	78.5	541	93.5	645	46.0	317	95.2	656	16.3
				2				132-7	66.0	455	77.0	531	39.3	271	78.4	541	76.3	526	89.0	614	45.4	313	90.6	625	14.8
				3				132-1	65.6	452	78.0	538	38.7	267	80.3	554	74.5	514	88.5	610	43.9	303	91.1	628	13.6
				3				132-2	64.0	441	76.5	527	36.4	251	78.5	541	73.4	506	87.7	605	41.8	288	90.0	621	15.5
				6				132-3	66.3	457	78.9	544	38.2	263	81.9	565	73.9	510	87.8	605	42.5	293	91.1	628	11.7
				6				132-4	61.2	422	72.2	498	36.8	254	75.1	518	71.2	491	84.0	579	41.6	287	87.3	602	11.6
				2			CMTS	133-1	67.7	467	80.7	556	41.0	283	82.1	566	77.8	536	92.8	640	47.2	325	94.4	651	19.0
				2				133-2	65.7	453	80.2	553	40.9	282	82.5	569	76.5	527	93.3	643	47.6	328	96.0	662	15.0
				3				125-9	62.5	431	74.4	513	38.5	265	76.3	526	72.8	502	86.6	597	44.8	309	89.0	614	14.8
				3				125-10	69.3	478	82.3	567	42.8	295	84.5	583	77.5	534	91.9	634	47.8	330	94.5	652	12.5
				6				125-3	63.0	434	74.8	516	38.1	263	78.6	542	73.2	505	87.0	600	44.3	305	91.5	631	20.3
				6				125-4	69.2	477	82.4	568	42.6	294	86.2	594	77.9	537	92.7	639	47.9	330	97.0	669	13.7
				3	1400	1033	MTS	132-8	30.9	213	36.8	254	18.0	124	35.7	246	51.8	357	61.8	426	30.4	210	60.0	414	12.7
				3				132-9	32.1	221	38.2	263	18.6	128	37.9	261	53.0	365	63.0	434	30.7	212	62.6	432	13.2
				6				132-5	30.8	212	36.6	252	18.3	126	35.9	248	48.3	333	57.4	396	28.7	198	56.3	388	10.0
				6				127-11	31.2	215	37.1	256	18.0	124	36.7	253	51.4	354	61.2	422	29.6	204	60.5	417	12.9
				3			CMTS	133-3	31.1	214	37.1	256	18.7	129	36.3	250	51.8	357	62.0	427	31.2	215	62.0	427	13.2
				3				133-4	31.7	219	37.8	261	19.0	131	35.1	242	53.2	367	63.3	436	31.9	220	58.8	405	13.5
				6				125-5	31.2	215	38.2	263	19.6	135	36.2	250	51.4	354	60.9	420	31.3	216	57.8	399	11.9
				6				125-6	27.5	190	32.7	225	16.2	112	31.4	216	45.0	310	53.5	369	26.5	183	51.5	355	13.0
				3	2800	1811	MTS	132-10	13.8	95	16.3	112	8.3	57	15.9	110	18.0	124	21.2	146	10.9	75	20.7	143	61.1
				3				132-11	14.7	101	17.5	121	8.4	58	17.9	123	17.8	123	21.2	146	10.2	70	21.8	150	59.1
				6				127-12[e]	–	–	–	–	–	–	–	–	20.7	143	24.6	170	12.1	83	25.0	172	60.5
				6				127-13	14.0	97	16.5	114	8.5	59	17.3	119	18.6	128	22.0	152	11.3	78	23.0	159	47.2
				3			CMTS	133-5	14.5	100	17.1	118	8.6	59	19.1	132	17.4	120	20.4	141	10.2	70	22.8	157	54.1
				3				133-6	14.2	98	16.9	117	8.2	57	17.1	118	17.8	123	21.3	147	10.3	71	21.5	148	64.4
				6				125-7	14.4	99	17.1	118	8.7	60	17.1	118	16.9	117	20.1	139	10.2	70	20.1	139	45.2
				6				125-8	14.4	99	17.2	119	8.8	61	17.2	119	16.6	114	19.8	137	10.1	70	19.8	137	51.7

[a] Coating wore out during oxidation exposure.
[b] Specimen fractured on loading to yield.
[c] Specimen fractured in tab section.
[d] No elongation value because of dial gage malfunction.
[e] No yield data because of transducer malfunction.

TABLE 15 (Cont.)

Exposure conditions					Test temp.		Coating system	Sample No. OT2-	0.2 Percent yield strength								Ultimate strength								Elongation %
Temp.		Pressure							Original substrate		Coated substrate		As-coated		Residual substrate		Original substrate		Coated substrate		As-coated		Residual substrate		
°F	°K	torr	hN/m^2	Cycles	°F	°K			ksi	MN/m^2	ksi	MN/m^2	ksi	MN/m^2	ksi	MN/m^2	ksi	MN/m^2	ksi	MN/m^2	ksi	MN/m^2	ksi	MN/m^2	
2600	1700	1	1.33	100	RT		CMTS	80-2	61.3	423	72.7	501	38.2	263	84.5	583	68.7	474	81.4	561	42.7	294	94.5	652	9.3
				100	RT		CMTS	80-5	63.3	436	75.5	521	39.9	275	87.7	605	70.9	489	84.5	583	44.7	308	98.1	676	15.0
				50	1400	1033	MTS	106-2	31.4	216	38.9	268	17.4	120	41.0	283	46.2	319	57.1	394	23.6	163	60.3	416	8.0
				50				106-3	32.3	228	38.4	265	18.3	126	43.6	301	47.0	324	56.0	386	26.7	184	63.5	438	10.5
				100				103-6	37.8	261	45.1	311	23.9	165	51.9	358	50.6	349	60.4	416	31.9	220	69.5	479	7.7
				100				103-7	32.9	227	39.1	270	19.4	134	44.5	307	48.0	331	57.0	393	28.2	194	64.9	447	9.8
				50			CMTS	80-3	30.3	209	36.0	248	19.1	132	41.1	283	42.0	290	50.0	345	26.5	183	57.0	393	7.4
				50				80-4	34.7	239	41.3	285	21.4	148	45.6	314	47.0	324	56.0	386	29.0	200	61.9	427	8.1
				100				104-2	31.6	218	37.7	260	19.7	136	41.6	287	43.8	302	52.2	360	27.3	188	57.7	398	7.1
				100				104-3[c]	34.2	236	40.5	279	22.2	153	44.8	309	>37.9	261	>44.8	309	>24.6	170	>49.6	342	>2.8
				50	2600	1700	MTS	106-4	20.8	143	24.8	171	11.5	79	28.7	198	22.9	158	27.2	188	12.7	88	31.5	217	18.3
				50				106-5[a]	–	–	–	–	–	–	–	–	–	–	–	–	–	–	–	–	–
				100				103-4	21.3	147	25.4	175	12.3	85	28.1	194	24.7	170	29.4	203	14.3	99	32.5	224	16.1
				100				103-5[a]	–	–	–	–	–	–	–	–	–	–	–	–	–	–	–	–	–
				50			CMTS	104-7	20.8	143	25.7	177	13.3	92	29.0	200	24.0	165	29.6	204	15.3	105	33.6	232	28.8
				50				104-10	20.0	138	23.7	163	11.6	80	27.7	191	22.8	157	27.1	187	13.3	92	31.5	217	17.8
				100				104-5	20.7	143	24.6	170	12.8	88	28.8	199	22.8	157	27.1	187	14.1	97	31.6	218	21.9
				100				104-6	19.6	135	23.3	161	12.0	83	27.4	189	22.5	155	26.7	184	13.7	94	31.5	217	32.2
		0.1	0.13	5	RT	298	MTS	135-1	63.1	435	74.4	513	37.6	259	76.5	527	74.8	516	88.2	608	44.5	307	90.7	625	21.2
				5				135-2	63.0	434	74.2	512	36.7	253	76.1	525	74.9	516	88.1	607	43.7	301	90.4	623	21.0
				10				135-5	63.1	435	74.2	512	37.4	258	80.3	554	73.7	508	86.7	598	43.7	301	97.7	674	22.8
				10				74-14	63.6	439	75.6	521	38.0	262	79.1	545	74.0	510	87.8	605	44.1	304	91.9	634	17.3
				15				74-15	63.0	434	74.8	516	37.7	260	78.5	541	73.3	505	86.9	599	43.8	302	91.2	629	17.5
				15				74-12	61.5	424	73.0	503	35.9	248	77.5	534	72.0	496	85.5	590	42.0	290	90.8	626	17.0
				2			CMTS	78-6	62.5	431	74.3	512	37.6	259	75.7	522	76.0	524	90.3	623	45.6	314	91.1	628	16.7
				2				78-7	62.2	429	73.8	509	38.7	267	75.3	519	74.2	512	88.1	607	46.2	319	89.8	619	12.2
				5				78-5	62.6	432	76.7	529	37.6	259	77.8	536	72.6	501	89.0	614	43.6	301	91.5	631	10.0
				5				78-8	62.5	431	74.6	514	38.0	262	76.7	529	76.0	524	88.0	607	43.7	301	90.3	623	14.3
				8				107-4	69.8	481	83.1	573	43.8	302	86.5	596	78.8	543	93.7	646	49.5	341	97.5	672	15.8
				10				107-6	69.0	476	82.0	565	41.5	286	85.9	592	77.5	534	92.0	634	46.5	321	96.4	665	18.0
				5	1400	1033	MTS	82-2	28.2	194	33.4	230	16.6	114	34.4	237	44.3	305	52.5	362	26.0	179	54.1	373	12.3
				10				135-7	28.6	197	32.6	225	16.3	112	35.7	246	47.5	328	54.1	373	27.0	186	59.3	409	11.7
				10				82-1[c]	–	–	–	–	–	–	–	–	–	–	–	–	–	–	–	–	–
				10				135-8	26.8	185	31.4	216	15.3	105	33.5	231	35.8	247	42.1	290	20.5	141	44.9	310	5.1
				20				135-3	26.9	185	31.6	218	16.0	110	34.0	234	44.3	305	52.1	359	26.4	182	>56.0	386	14.7
				4			CMTS	107-1	29.5	203	35.0	241	17.7	122	36.0	248	47.4	327	56.2	387	28.5	197	57.8	399	10.8
				5				133-9	30.2	208	35.8	247	18.0	124	36.5	252	52.6	363	62.4	430	31.4	216	63.5	438	11.8
				8				107-3	29.8	205	35.4	244	18.5	128	36.1	249	50.0	345	59.5	410	31.2	215	60.6	418	12.5
				10				133-7[c]	30.9	213	36.9	254	18.4	127	37.2	256	>40.4	279	>48.2	332	>24.0	165	48.7	336	4.6
				2	2600	1700	MTS	82-3	21.8	190	25.9	179	12.8	88	25.4	175	23.3	161	27.7	191	13.7	94	27.2	188	28.6
				7				82-4	18.3	188	21.8	150	10.4	72	22.4	154	20.3	140	24.2	167	11.6	80	24.9	172	34.6
				10				135-6	15.7	108	18.5	128	9.2	63	19.2	132	19.7	136	23.2	160	11.6	80	24.0	165	62.7
				15				74-13	15.7	108	18.7	129	9.0	62	19.6	135	19.2	132	22.9	158	24.0	165	11.0	76	9.3
				20				135-4[a]	–	–	–	–	–	–	–	–	–	–	–	–	–	–	–	–	–
				4			CMTS	107-2	19.0	131	22.5	155	11.3	78	22.9	158	21.6	149	25.6	177	12.9	89	26.1	180	50.0
				5				133-10	14.8	102	17.5	121	8.7	60	17.8	117	20.2	139	23.9	165	11.9	82	24.4	168	64.5
				10				107-5	17.7	122	21.1	145	10.9	75	21.2	146	22.6	156	26.9	185	14.0	97	27.1	187	52.2
				10				133-8	16.8	116	20.0	138	9.8	68	20.4	141	19.4	134	23.2	160	11.4	79	23.6	163	7.7
2800	1811	10	13.33	12	RT	297	MTS	127-8	65.8	454	78.3	540	39.1	270	82.8	571	74.0	510	88.0	607	43.9	303	93.0	641	7.5
				12				127-9	65.3	450	77.0	531	39.0	269	81.4	561	74.6	514	88.0	607	44.6	308	93.0	641	9.6
				25				127-7	74.4	513	88.2	608	44.6	308	96.1	663	82.3	567	97.5	672	49.3	340	106.3	733	12.5
				25				127-6	70.4	485	83.3	574	43.7	301	90.8	626	77.8	536	92.2	636	48.2	332	100.3	692	10.5
				41				126-2[a]	–	–	–	–	–	–	–	–	–	–	–	–	–	–	–	–	–
				41				126-1	69.8	481	83.0	572	39.6	273	92.5	638	76.4	527	90.8	626	43.4	299	101.3	698	8.7
				17			CMTS	128-5	70.6	487	83.3	574	42.0	290	88.9	613	78.0	538	92.0	634	46.4	320	98.2	677	6.7
				17				128-6	71.3	492	83.8	578	45.0	310	89.3	616	79.4	547	93.2	643	49.3	340	99.3	685	8.3
				35				107-7	68.0	469	80.8	557	39.6	273	88.7	612	77.0	531	91.5	631	44.8	309	100.4	692	13.3
				35				108-4	71.0	490	84.8	585	40.9	282	93.6	645	78.0	538	93.1	642	44.9	310	102.8	709	9.7
				70				107-8	67.8	467	81.0	558	41.5	286	94.8	654	74.4	513	88.8	612	45.5	314	103.9	716	11.2
				70				107-9	68.4	472	81.4	561	40.5	279	94.9	654	73.7	508	87.7	605	43.6	301	102.1	704	5.0
				25	1400	1033	MTS	127-1	37.4	258	44.2	305	22.1	152	48.2	332	58.8	405	69.5	479	34.9	241	76.0	524	(d)
				25				127-2	36.9	254	43.7	301	21.2	146	45.3	312	59.3	409	70.3	484	34.1	235	72.8	502	11.6
				41				126-3[a]	–	–	–	–	–	–	–	–	–	–	–	–	–	–	–	–	–	–
				41				126-4[a]	–	–	–	–	–	–	–	–	–	–	–	–	–	–	–	–	–	–
				35			CMTS	108-2	33.1	228	39.4	272	19.4	134	39.7	274	41.7	288	49.6	342	24.5	169	50.0	345	4.9
				35				128-3	36.7	253	43.3	299	21.8	150	47.2	325	50.4	347	59.5	410	30.0	207	64.7	446	6.7

See footnotes at end of table.

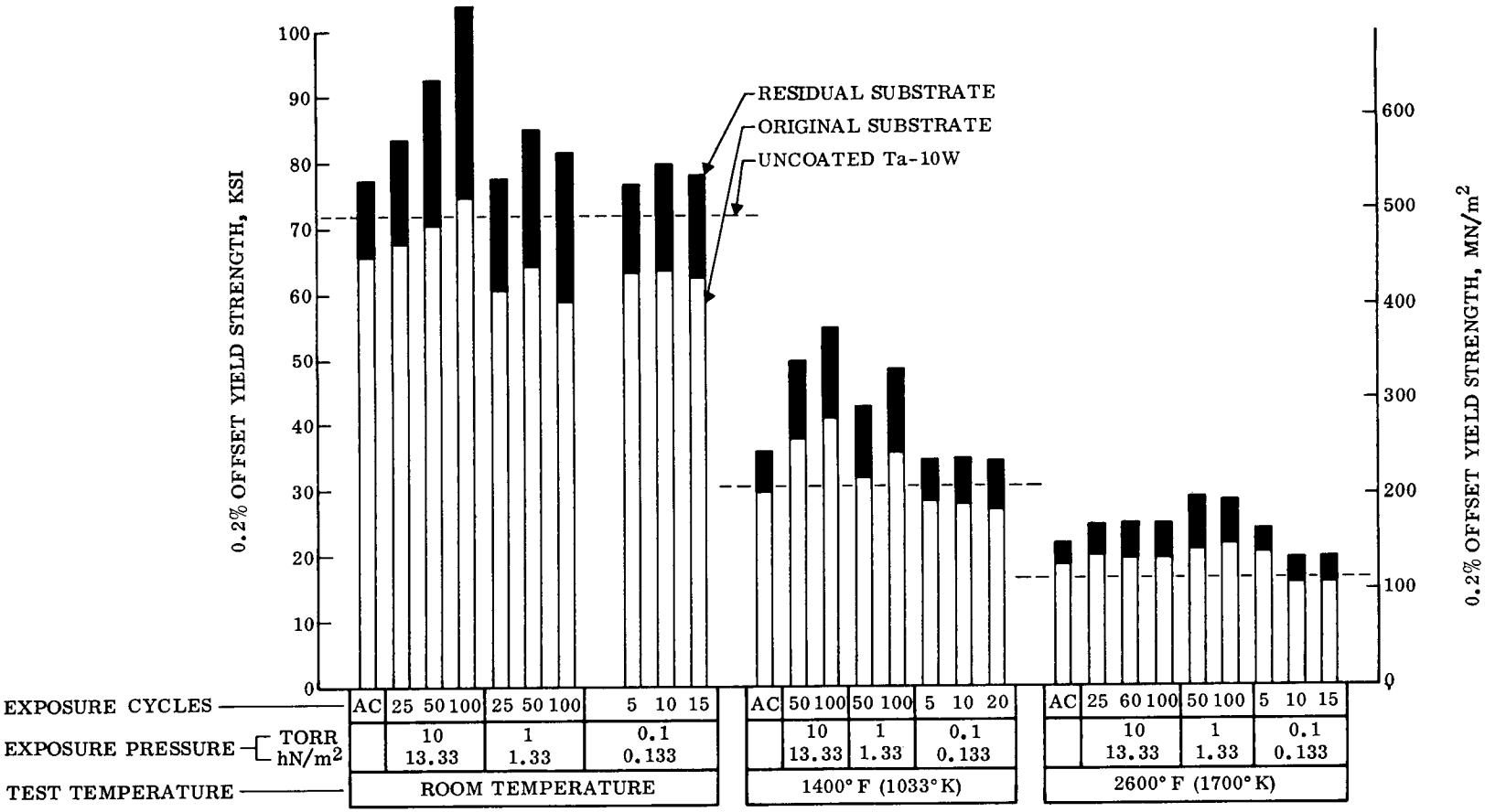

Figure 39. Effect of 2600° F (1700° K) Cyclic Exposure on Yield Strength of Ta-10W/MTS.

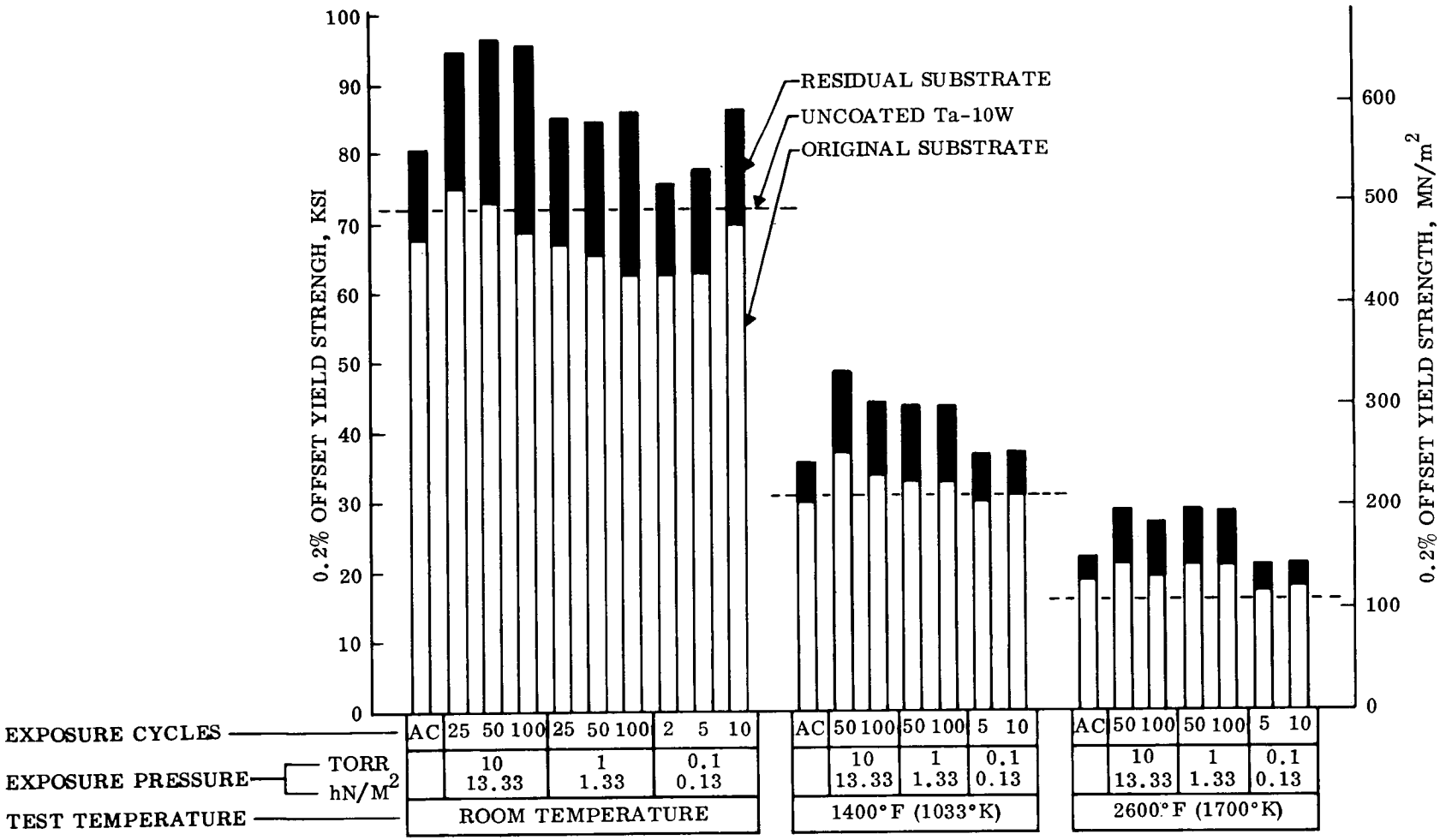

Figure 40. Effect of 2600° F (1700° K) Cyclic Exposure on Yield Strength of Ta-10W/CMTS.

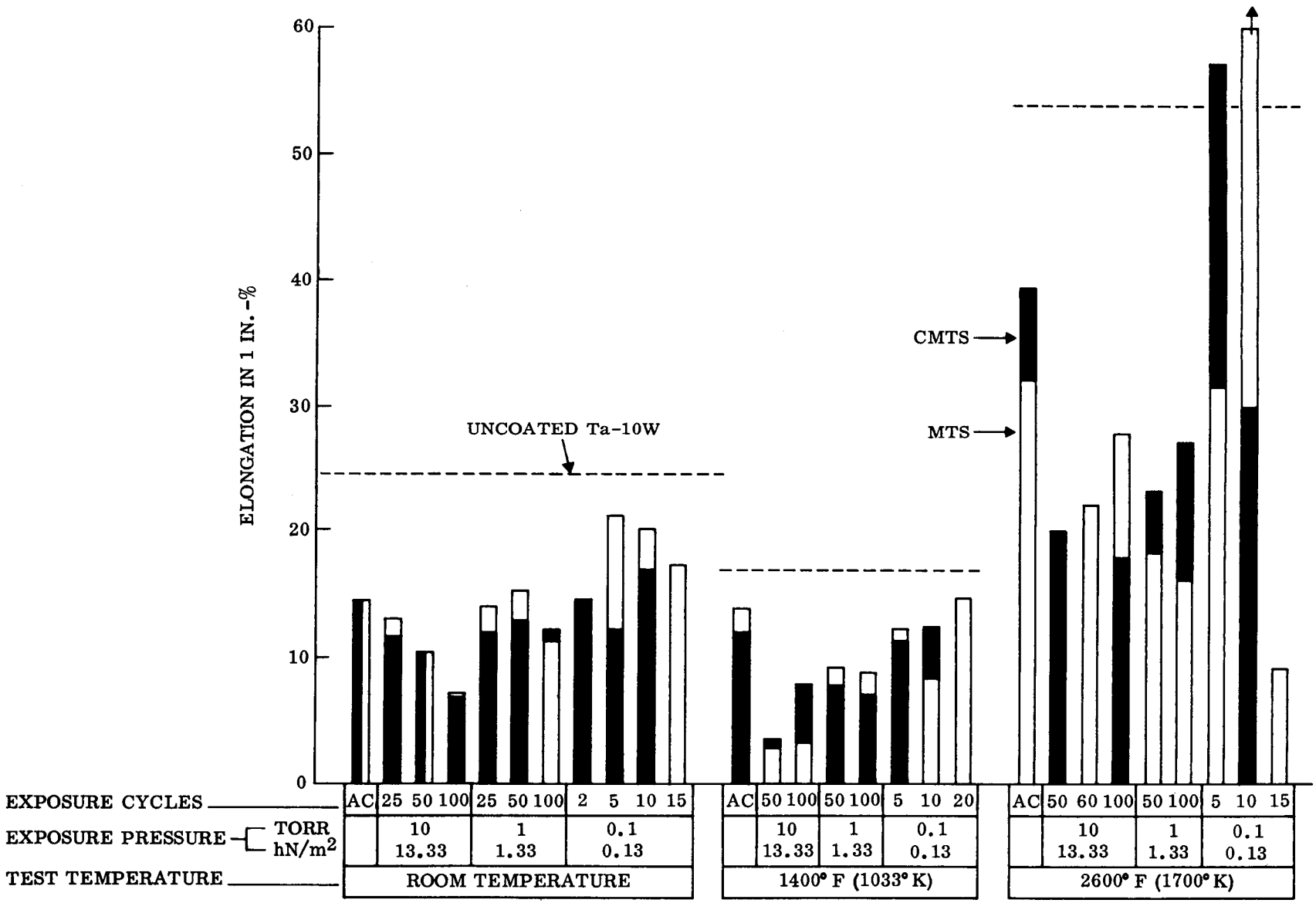

Figure 41. Effect of 2600° F (1700°K) Cyclic Exposure on Tensile Ductility of Coated Ta-10W.

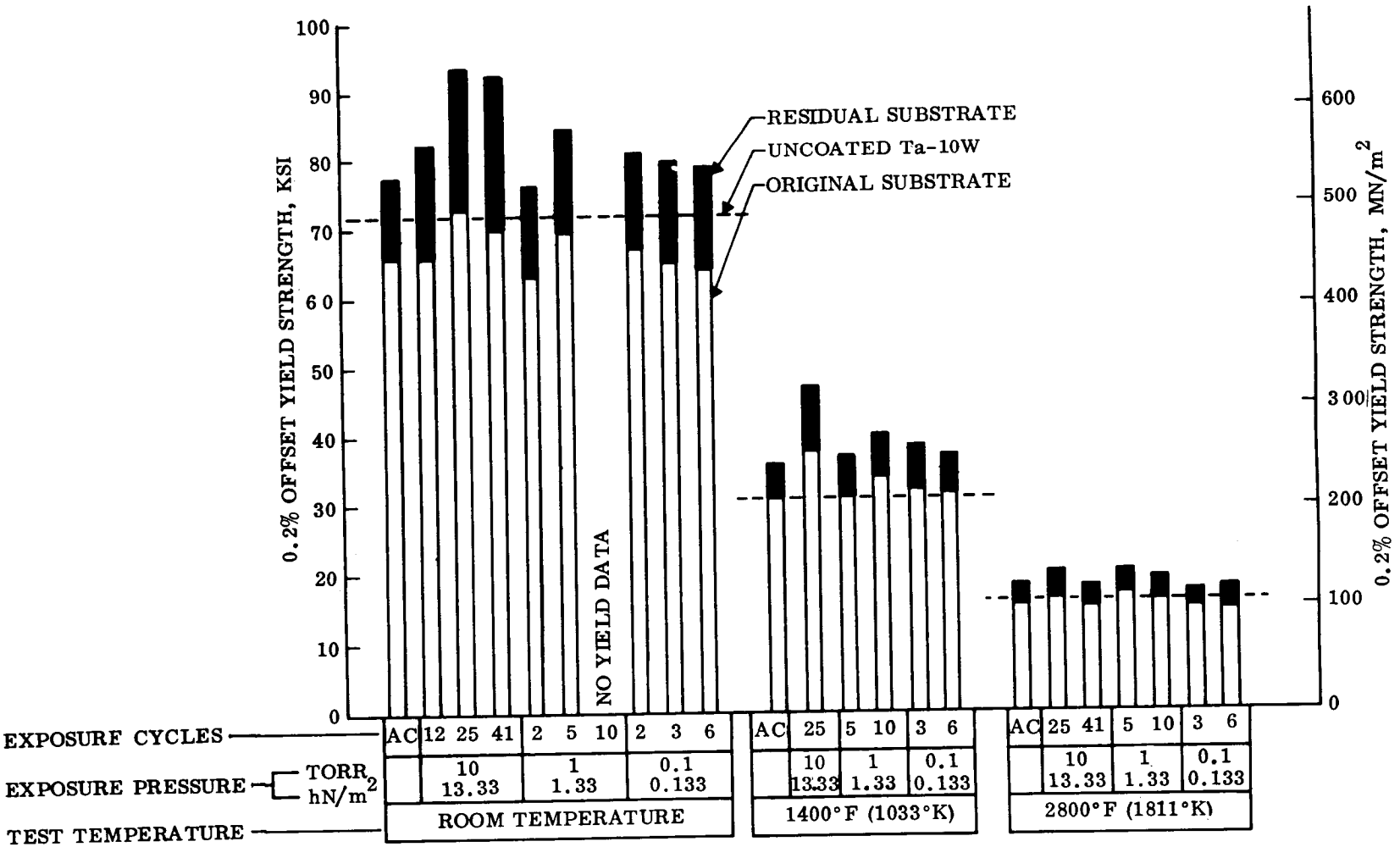

Figure 42. Effect of 2800° F (1811° K) Cycle Exposure on Yield Strength of Ta-10W/MTS.

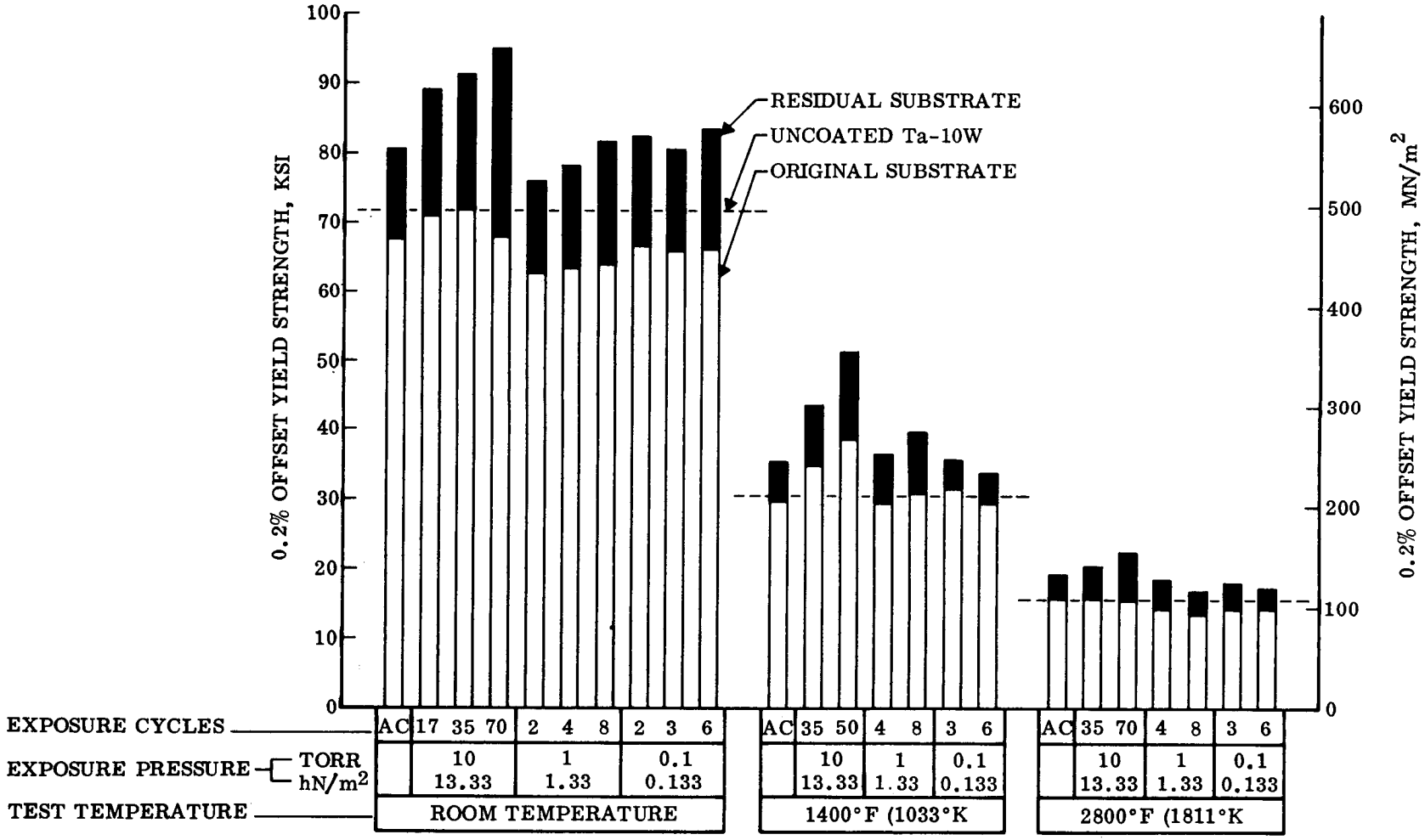

Figure 43. Effect of 2800° F (1811° K) Cyclic Exposure on Yield Strength of Ta-10W/CMTS.

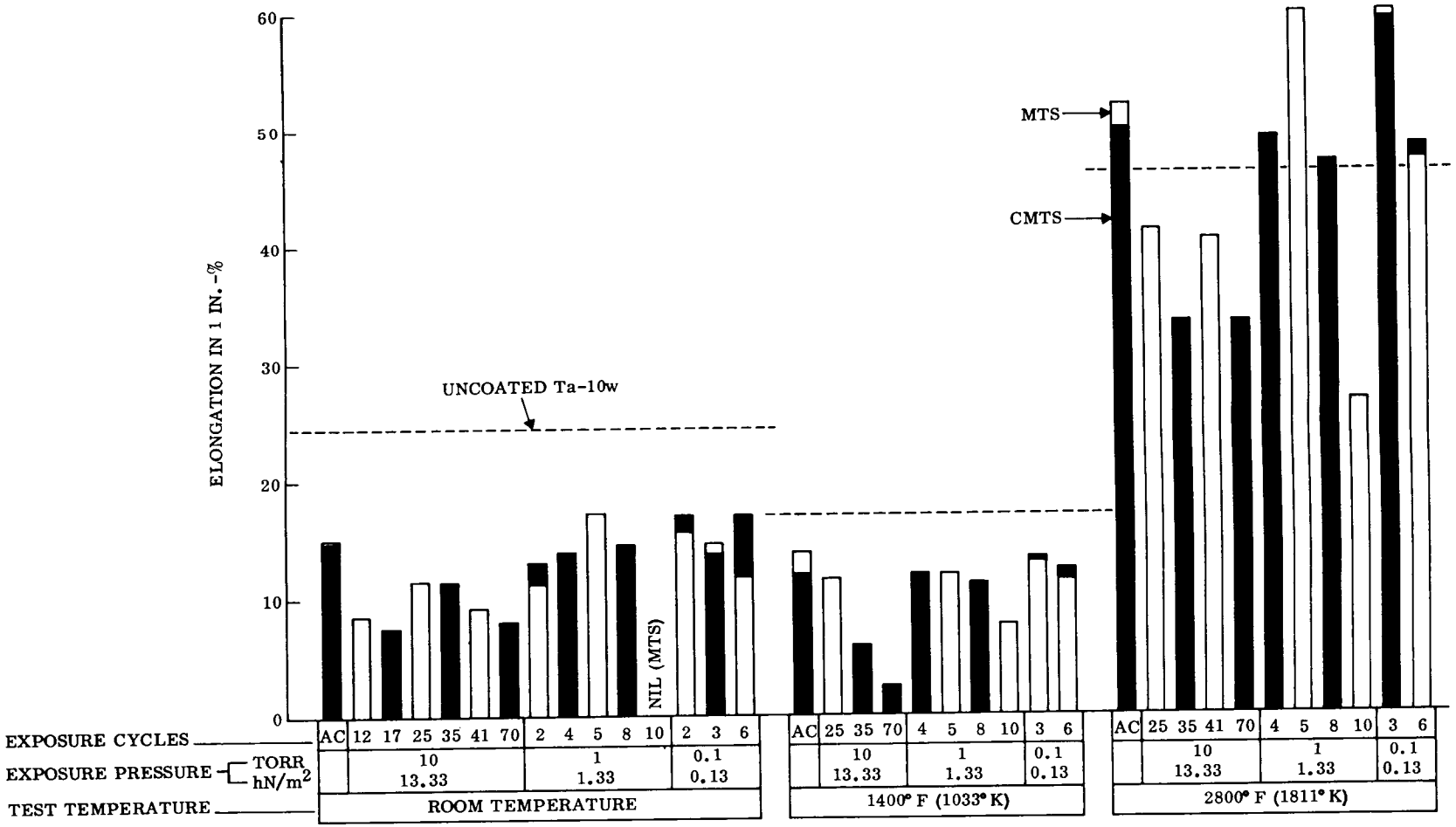

Figure 44. Effect of 2800° F (1811° K) Cyclic Exposure on Tensile Ductility of Coated Ta-10W.

The plots of tensile ductility show that the increased yield strength is accompanied by a decrease in tensile elongation, particularly at 1400°F (1033°K), where Ta-10W already has a ductility minimum. The maximum increase in strength and reduction in ductility appears to occur during the first few cycles of exposure, although in some cases ductility decreases with continued cycling to full lifetime. With two exceptions, the ductility at room temperature to 1400°F (1033°K) is above 5-percent elongation at all times and the metal is not embrittled (i.e., no ductility) until actual wearout of the coating is indicated by visible oxidation of the substrate. The exceptions are for the CMTS coating, which has significant loss of ductility or embrittlement after extended cycling at 2800°F (1811°K) in air at 1 and 10 torr (1.33 and 13.33 hN/m^2). A decrease in bend ductility, as previously noted, occurred under the same exposure conditions.

The simultaneous increase in yield and decrease in ductility is due to the diffusion of either coating elements or oxygen into the substrate during cyclic exposure. Since the effect is more pronounced at 10 torr than at 1 torr (13.33 to 1.33 hN/m^2) for the same thermal history, reaction with oxygen appears to be responsible; and since the effect is noted early in cycling, it would appear that some leakage of oxygen through the coating does occur during the first few cycles, while the protective oxide film is being developed. Once a stable film has been formed, the substrate is protected more completely and the mechanical properties reach a fairly stable value.

In all cases [except the CMTS coating at 2800°F (1811°K)] where the cyclic exposure is within the minimum coating lifetime as established by visual appearance on a statistical basis from Weibull plots, the tensile strength and ductility are considered to be very good. The yield strength is, for all practical purposes, the same as that for uncoated Ta-10W, and the tensile elongation is about half that of Ta-10W from room temperature to 2800°F (1811°K). At 2800°F exposure, the MTS coating provides better protection at edges, with better retention of tensile properties.

The significance of these data and the interpretation of strength values calculated from different area considerations are discussed in the section on analysis of results.

- Creep Properties

Representative creep curves for the MTS and CMTS coating systems on Ta-10W in air at 2600° and 2800°F (1700° and 1811°K) are shown in Figures 45 and 46.. Curves for uncoated Ta-10W in vacuum are included for comparison. The creep curves for these coating systems in vacuum and in air were shown previously, in the section on creep testing procedures (Figure 9). The creep data obtained from the tests in both vacuum and air are presented in Table 16.

All tests were run at constant load calculated to give an initial stress of 6 ksi, based on residual substrate thickness after coating. This assumes no strength contribution from the coating. As shown in Figure 45 and Table 16, the creep resistance of the coated alloy is superior to that of the uncoated alloy at 2600°F (1700°K), indicating that the coating makes a significant strength contribution to the composite coated metal at this temperature. At 2800°F (1811°K) the creep properties of coated and uncoated samples are nearly the same, indicating a lesser contribution of the coating to creep strength. This behavior is consistent with the yield strength data at 2600° and 2800°F (1700° and 1811°K), which indicates the same relative influence of the coatings on tensile strength as a function of temperature. This significant aspect of coating behavior will be discussed in detail in the section on analysis of test results.

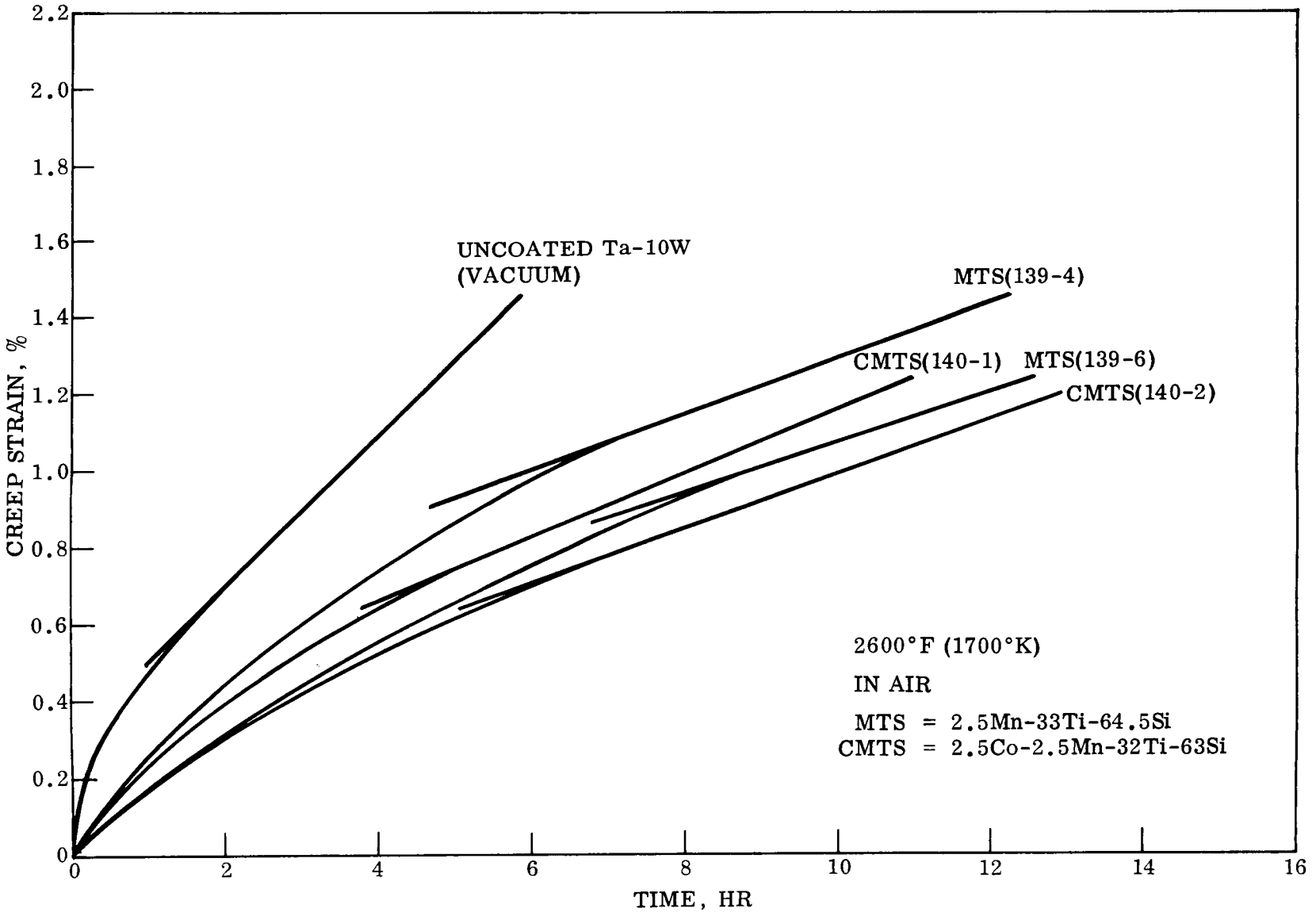

Figure 45. Creep Curves in Air at 2600°F (1700°K).

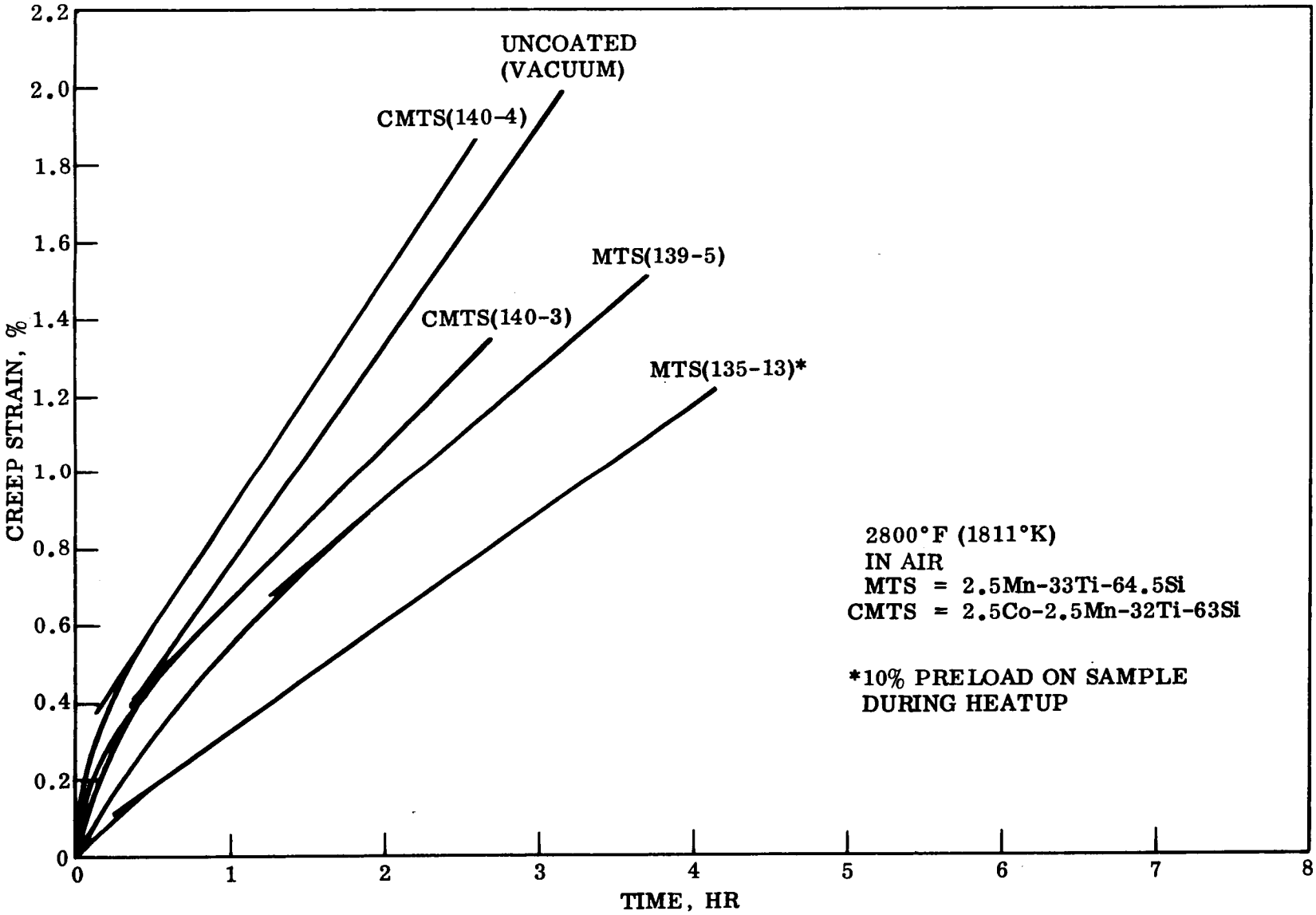

Figure 46. Creep Curves in Air at 2800°F (1811°K).

TABLE 16. – RESULTS OF CREEP TESTS

Sample number	Coating system[a]	Heating method	Atmosphere	Temperature		Time to		Primary strain (ϵ_p), %	Steady state creep rate ($\dot{\epsilon}$), hr^{-1}
				°F	°K	1% ϵ hr	Steady state, hr		
AR-2	Uncoated	Radiation	Vacuum	2600	1700	3.55	2.00	0.70	1.95×10^{-3}
OT2-139-2	MTS	↓	↓	↓	↓	5.90	>12	>1.5	Primary to 12 hr
OT2-105-5	CMTS	↓	↓	↓	↓	8.40	6.00	0.88	0.8×10^{-3}
OT2-139-4	MTS	Resistance	Air	↓	↓	6.35	7.00	1.07	0.69×10^{-3}
OT2-139-6	MTS	↓	↓	↓	↓	9.00	8.50	0.97	0.65×10^{-3}
OT2-140-1	CMTS	↓	↓	↓	↓	8.10	4.80	0.72	0.83×10^{-3}
OT2-140-2[b]	CMTS	↓	↓	↓	↓	10.20	7.00	0.77	0.72×10^{-3}
AR-1	Uncoated	Radiation	Vacuum	2800	1811	1.40	0.50	0.46	5.70×10^{-3}
OT2-139-7	MTS	↓	↓	↓	↓	1.03	0.75	1.44	5.60×10^{-3}
OT2-105-4	CMTS	↓	↓	↓	↓	1.20	1.00	0.87	6.00×10^{-3}
OT2-139-5	MTS	Resistance	Air	↓	↓	2.20	2.05	0.95	3.40×10^{-3}
OT2-139-13[c]	MTS	↓	↓	↓	↓	3.40	0.40	0.16	2.85×10^{-3}
OT2-140-3	CMTS	↓	↓	↓	↓	1.83	0.82	0.60	4.07×10^{-3}
OT2-140-4	CMTS	↓	↓	↓	↓	1.15	0.40	0.53	6.1×10^{-3}

[a]MTS = 2.5Mn-33Ti-64.5Si.
CMTS = 2.5Co-2.5Mn-32Ti-63Si.
[b]Tested to rupture – 35.6 hr. 3% strain.
[c]10% [3.2 lb (1.45 kg)] preload during heatup and equilibration.

The creep tests revealed that both the MTS and CMTS coatings afford excellent protection to Ta-10W during creep in air. Total creep strains as great as 2 percent were sustained while retaining full protective capability of the coatings. No significant difference between the two systems were detected.

Data that characterize the transition from primary to steady-state creep also are included in Table 16. The total creep strain at this transition point and the time to reach steady-state creep are given. Both coated and uncoated materials have a large primary creep region at these temperatures. This is normal behavior for fully recrystallized high-purity Ta-10W. The total primary creep strain is between 0.7 and 1.0 percent in the majority of tests. In one case (OT 2-139-13) a small (10 percent) preload was left on the specimen during heatup and equilibration. The primary strain, which is measured from the time of application of the major load, was reduced significantly – to 0.16 percent. The steady-state creep rate also was reduced. In all tests but this one, care was taken to assure that no load was on the specimen for any extended period of time during heating or equilibration. With thin sheet specimens such as this, the mere weight of pull rods and assemblies on the sample during this period was sufficient to cause a significant change in creep behavior. Extensive tests with other alloys at LMSC have shown that primary creep is particularly sensitive to operator variables, and slight variations in procedure can introduce significant scatter into test results.

Intentional Damage Studies

The tolerance of intentional damage was studied with the MTS and CMTS coatings as well as the Sylvania-coated R512-A, C, and K coatings at 2600° and 2800°F (1700° and 1811°K), 10 torr (13.33 hN/m^2) air pressure. Damage to the coatings was introduced in the form of 1/2, 2, and 4t (where t = substrate thickness) holes through the coating and 4t holes through the entire coated specimen.

In one series of experiments, the damage was introduced to the specimens in the as-coated condition; the specimens were exposed for one cycle; and the effects of the damage on the specimen were evaluated. In another series of experiments, the specimens were exposed (specimens with MTS and CMTS coatings for 25 cycles, and specimens with R512 coatings for 10 cycles); the damage was introduced; the specimens were exposed for an additional cycle; and the effects were evaluated. Specimens with the MTS and CMTS coatings after exposure at 2600°F (1700°K) are shown in Figure 47. Where the damage penetrated the entire coating, a hole through the specimen formed. To show these holes more clearly, the reverse sides of the specimens with the oxide removed are also shown. The condition of the R512 coatings exposed at 2600°F (1700°K) is shown in Figure 48. The condition of the MTS, CMTS, and R512 coatings after exposure at 2800°F (1811°K) is shown in Figure 49. As would be expected, there is a greater degree of reaction at 2800°F (1811°K) than at 2600°F (1700°K).

In further studies, 4t holes through the coating only and through the specimen were produced in MTS and CMTS specimens in the as-coated condition, and in specimens that had been exposed for 70 hr at 2600°F (1700°K), 10 torr (13.33 hN/m^2). These specimens were exposed at 2600°F (1700°K), 10 torr (13.33 hN/m^2) for 5 cycles and the amount of oxidation was measured. It was found that the substrate oxidizes at a rate of about 0.1 in. (0.3 cm) per cycle. This rate is similar to that observed earlier with other coatings.

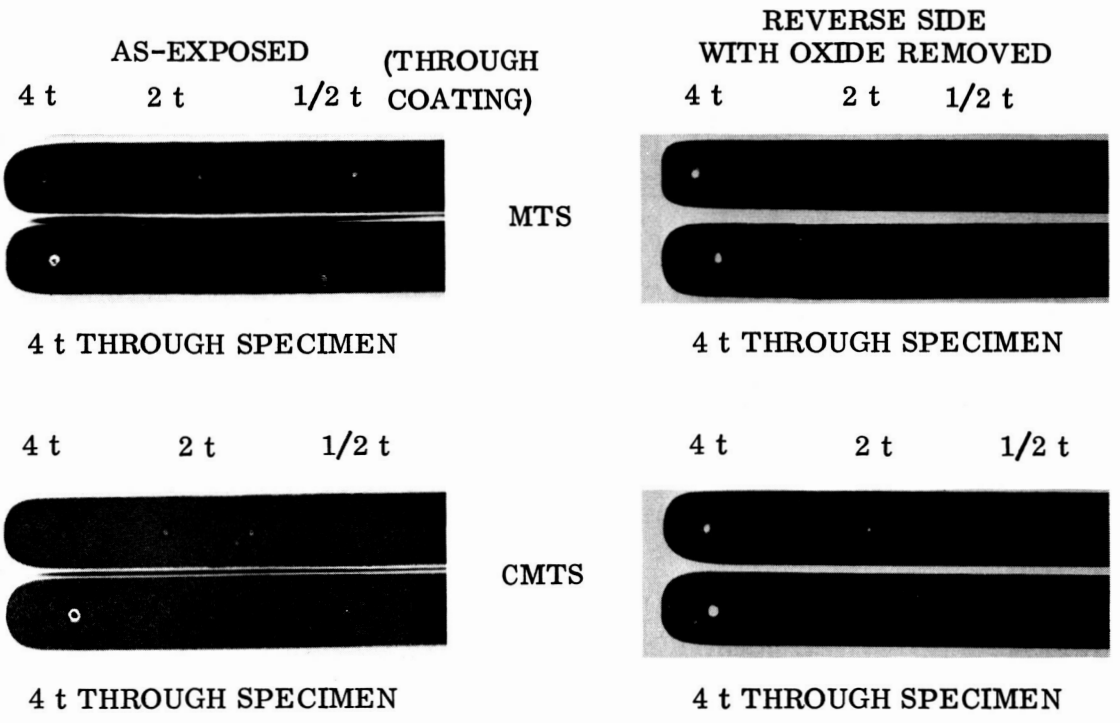

(a) Intentionally Damaged and Exposed for 1 Cycle (t = Substrate Thickness)

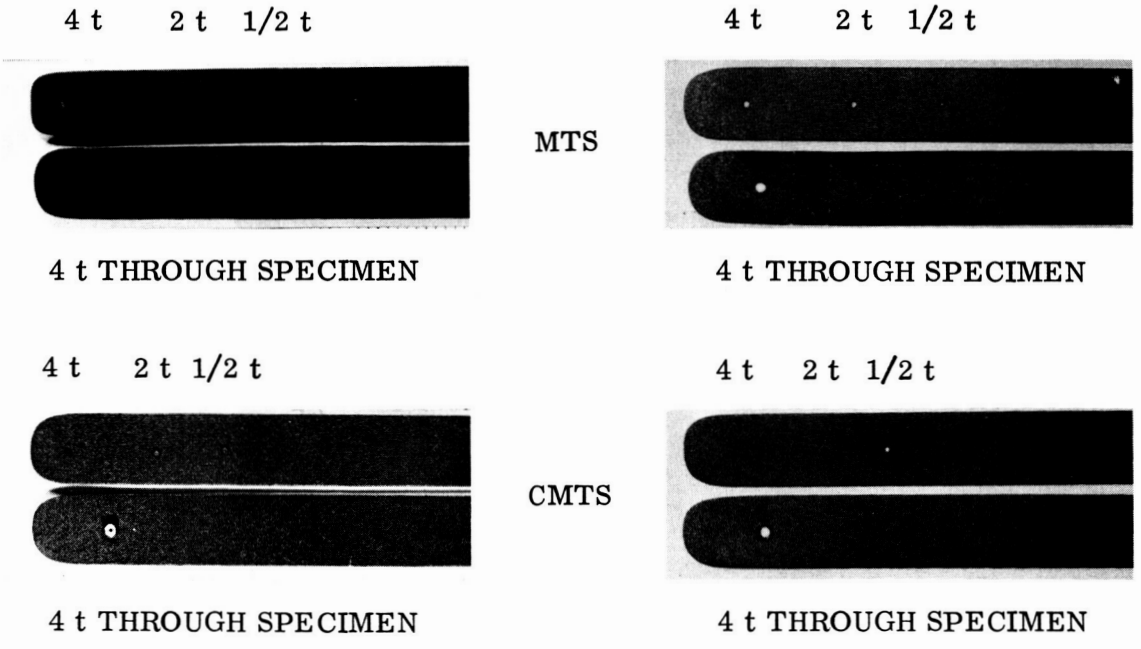

(b) Exposed for 25 Cycles, Intentionally Damaged, and Exposed for 1 Cycle

Figure 47 Condition of Intentionally Damaged Coated Ta-10W After Exposure at 2600° F (1700° K), 10 Torr (13.33 hN/m^2), 3/4×. There was incomplete penetration of the coating in damage sites where there is no reaction.

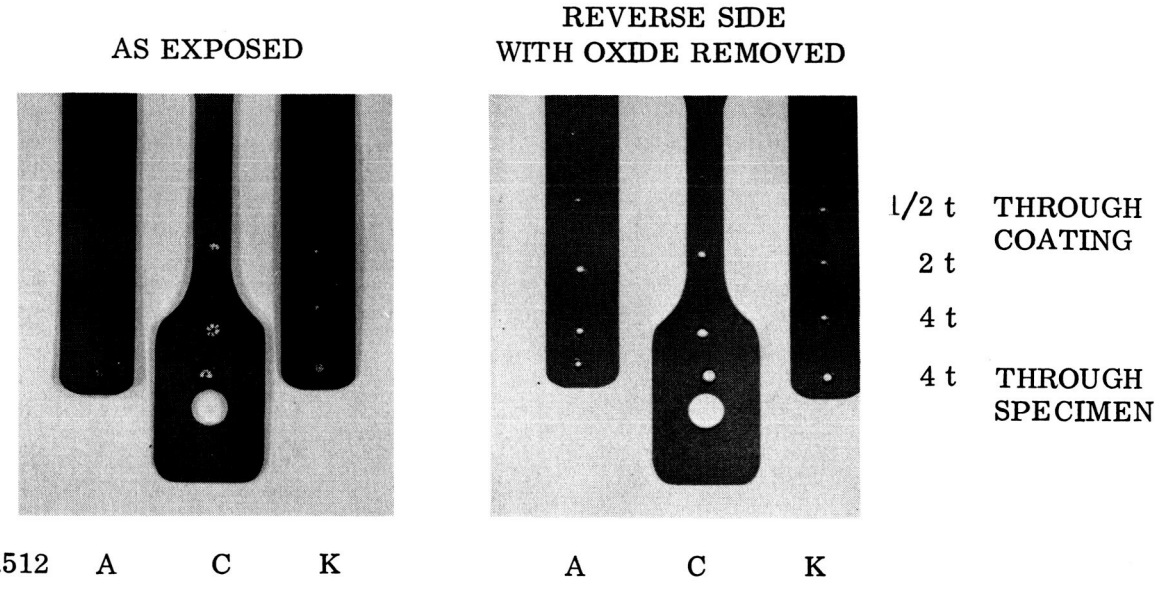

(a) Intentionally Damaged and Exposed for 1 Cycle (t = Substrate Thickness)

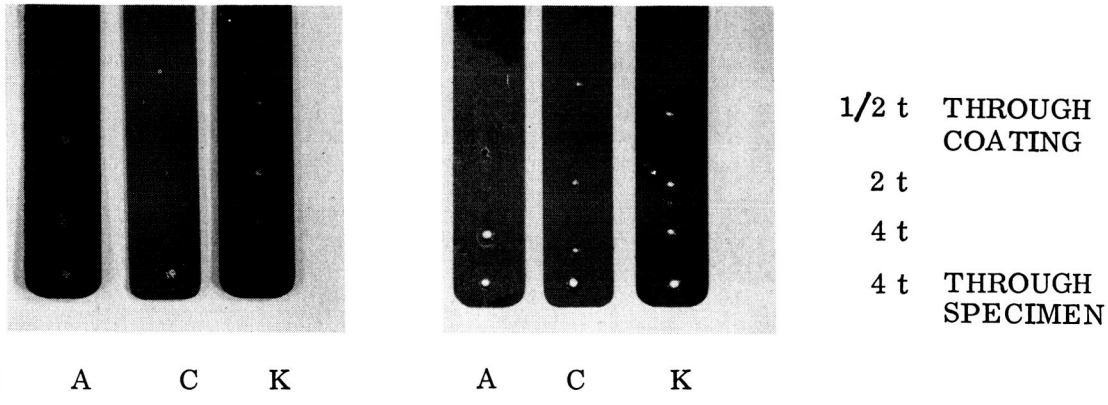

(b) Exposed for 10 Cycles, Intentionally Damaged, and Exposed for 1 Cycle

Figure 48 Condition of Intentionally Damaged R512-Coated Ta-10W After Exposure at 2600° F (1700° K), 10 Torr (13.33 hN/m^2), 3/4×. There was incomplete penetration of the coating in damage sites where there was no reaction.

Values at sides of photos are holes through coatings unless otherwise noted.

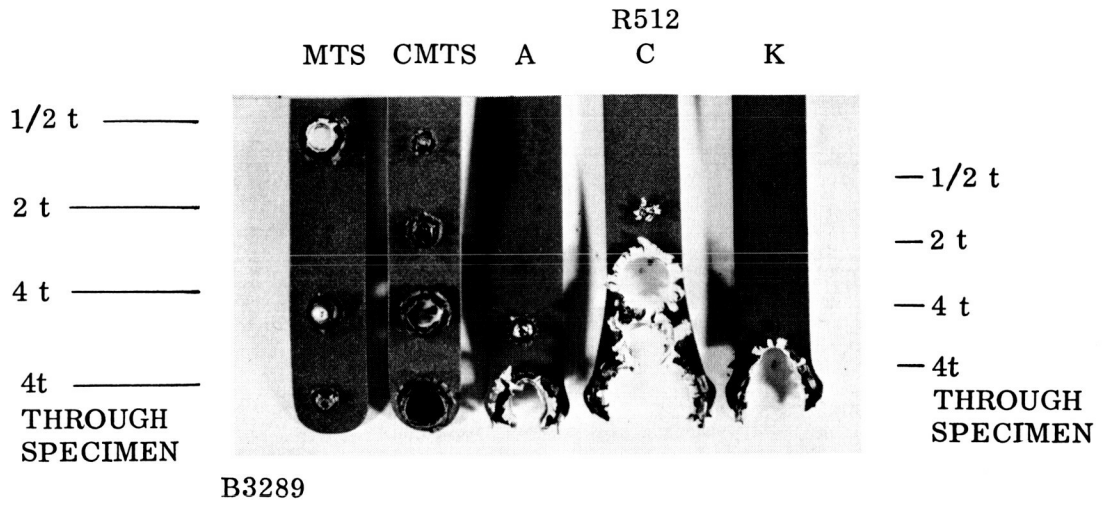

B3289

(a) Intentionally Damaged and Exposed for 1 Cycle (t = Substrate Thickness)

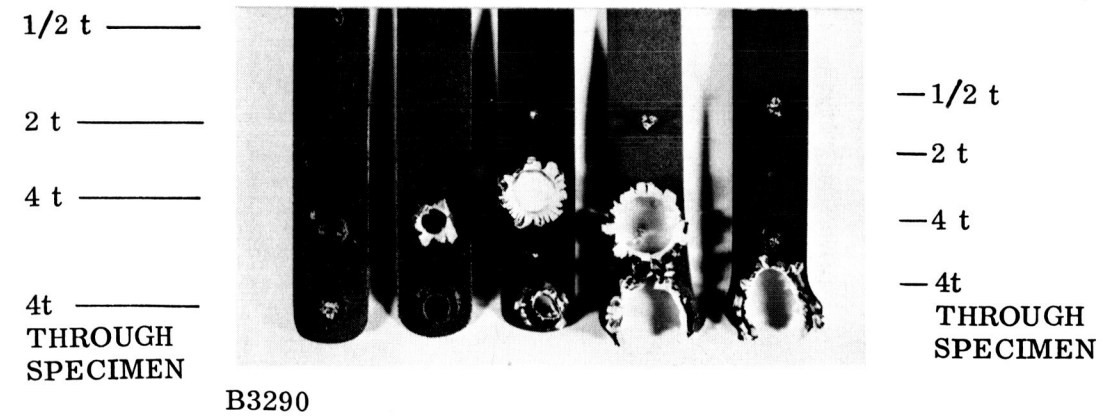

B3290

(b) Exposed for 25 Cyles, Intentionally Damaged, and Exposed for 1 Cycle (R512 Exposed for 10 Cycles)

Figure 49 Condition of Intentionally Damaged Coated Ta-10 W Specimens After Exposure at 2800° F (1811° K), 10 Torr (13.33 hN/m^2) 3/4×. There was incomplete penetration of the coating in damage sites where there was no reaction.

The conclusions were reached that (1) the MTS and CMTS coatings have similar tolerance of intentional damage and (2) during the first cycle after damage the growth of the damaged region is less than that in specimens coated with other systems. After the first cycle, however, the rate of growth during subsequent cycles is similar to that of other coatings.

ANALYSIS OF TEST RESULTS

Coating Structure and Composition

- MTS and CMTS Coatings

Metallographic, electron microprobe, and x-ray diffraction studies were conducted to characterize the structure and composition of the coatings in the as-coated condition and after exposure to environmental conditions. Photomicrographs and corresponding electron microprobe traces are shown in Figures 50 and 51 for the MTS and CMTS coatings. In each figure, the structure and composition are shown for the coating in the as-coated condition and after 100 cycles at 2600°F (1700°K), 10 torr (13.33 hN/m^2). In the as-coated specimens, the silicon level increases sharply at the substrate/coating interface to an intermediate level across the thin layer in the coating at the interface and then increases to a higher level in the outer portion of the coating. Titanium is present throughout the coating, and there are concentration peaks at zones intermediate within the coating and near the outer surface. The manganese and cobalt (in the CMTS coating) are concentrated within these same zones. Both tantalum and tungsten are present within the coating. Concentration plateaus of these elements occur at decreasing concentration levels with increasing distances from the interface. (The decreases in the tantalum and tungsten concentration profiles within the substrate are artifacts resulting from the microprobe geometry.)

On the bases of the electron microprobe studies and light microscopy analyses, the phase distributions within the coatings were defined. These distributions are shown in the photomicrographs of Figure 52. The MTS and CMTS coatings are similar except for the presence of cobalt within the complex disilicide zone and within the complex lower silicide zone near the surface of the coating. In the outer portion, the coatings are generally (Ti, Ta, W) Si_2, with zones of (Ti, Mn)Si_2 and (Ti, Mn)$_5Si_3$ in the MTS coating and (Ti, Co, Mn)Si_2 and (Ti, Co, Mn)$_5Si_3$ in the CMTS coating. In the inner portion, there is a thin (Ta, W)$_5Si_3$ zone at the interface and a larger zone of (Ta, W)Si_2.

After 100 cycles at 2600°F (1700°K), 10 torr (13.33 hN/m^2), there was growth of the (Ta, W)$_5$ Si_3 zone resulting from interdiffusion between the coating and the substrate. The silicon profile changed, showing a high plateau at the outer surface of the coating which reflected the formation of a layer of silica. The titanium, manganese, and cobalt have new peaks associated with the metal-oxide layer that formed on the outer surface of the silica. The titanium peak is relatively high in the oxide layer, and virtually all the manganese and some of the cobalt have moved to areas near the outer surface. There is also an indication that some tantalum and tungsten have moved to the metal-oxide layer.

The metal-oxide layer was analyzed using x-ray diffraction. The diffraction results indicated a strong TiO_2 pattern for both coatings, as well as a weak $MnO \cdot TiO_2$ pattern for the MTS coating and a weak $CoO \cdot TiO_2$ pattern for the CMTS coating. The conclusion was reached that the metal-oxide layer was mainly (Ti, Mn) O_2, with trace amounts of $MnO \cdot TiO_2$ and $CoO \cdot TiO_2$, respectively, in the MTS and CMTS coatings.

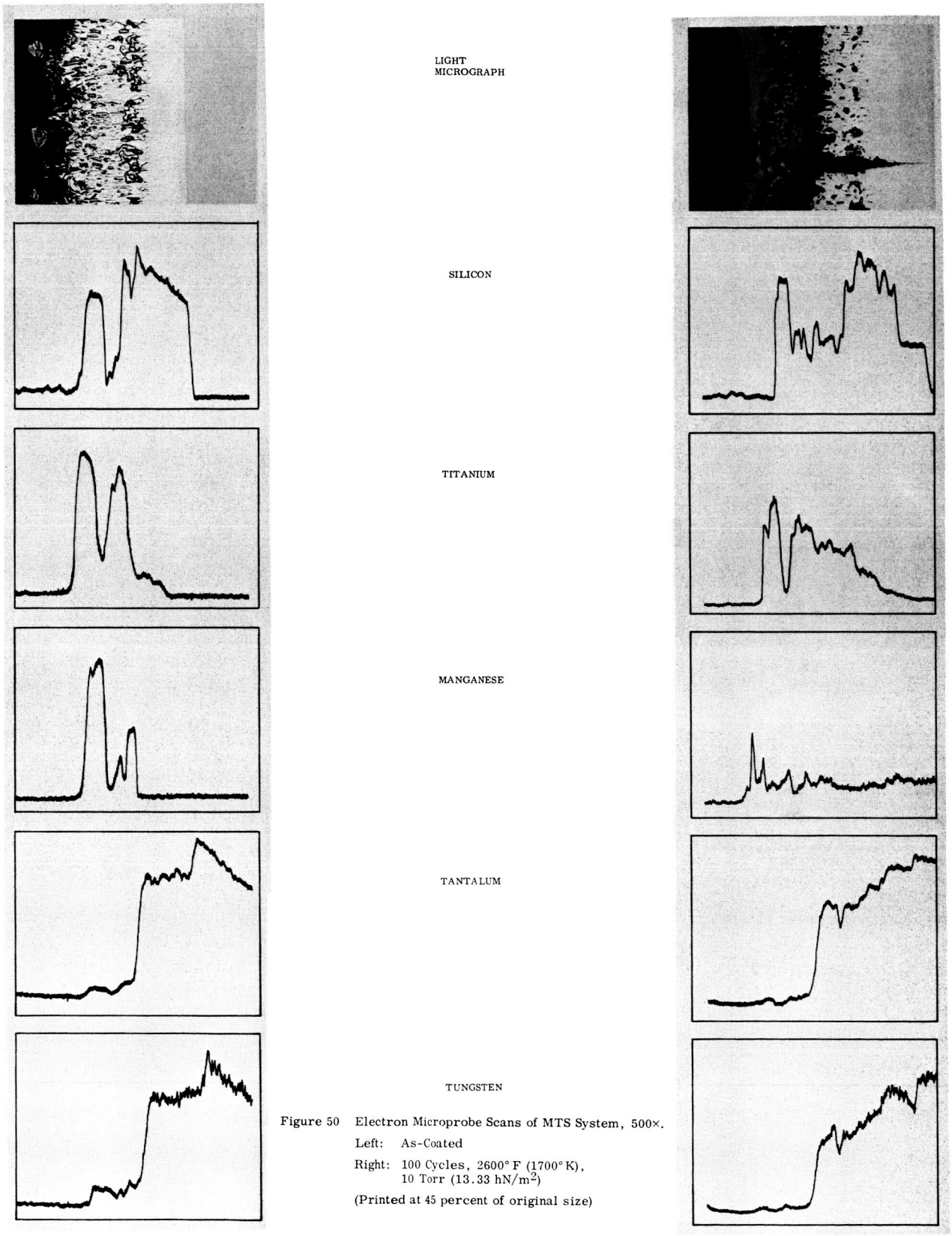

Figure 50 Electron Microprobe Scans of MTS System, 500×.

Left: As-Coated

Right: 100 Cycles, 2600° F (1700° K), 10 Torr (13.33 hN/m^2)

(Printed at 45 percent of original size)

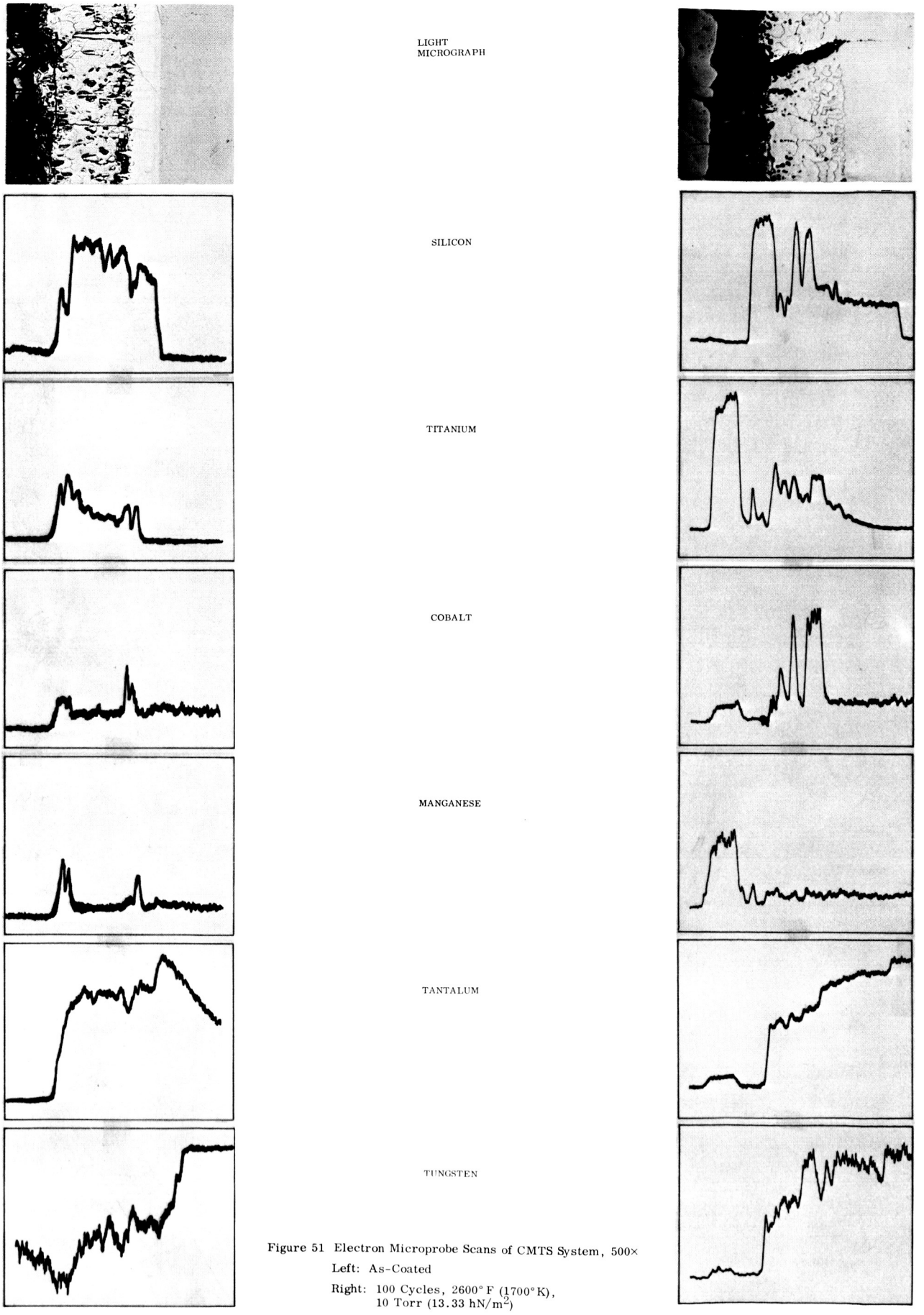

Figure 51 Electron Microprobe Scans of CMTS System, 500×

Left: As-Coated

Right: 100 Cycles, 2600° F (1700° K), 10 Torr (13.33 hN/m^2)

(Printed at 45 percent of original size)

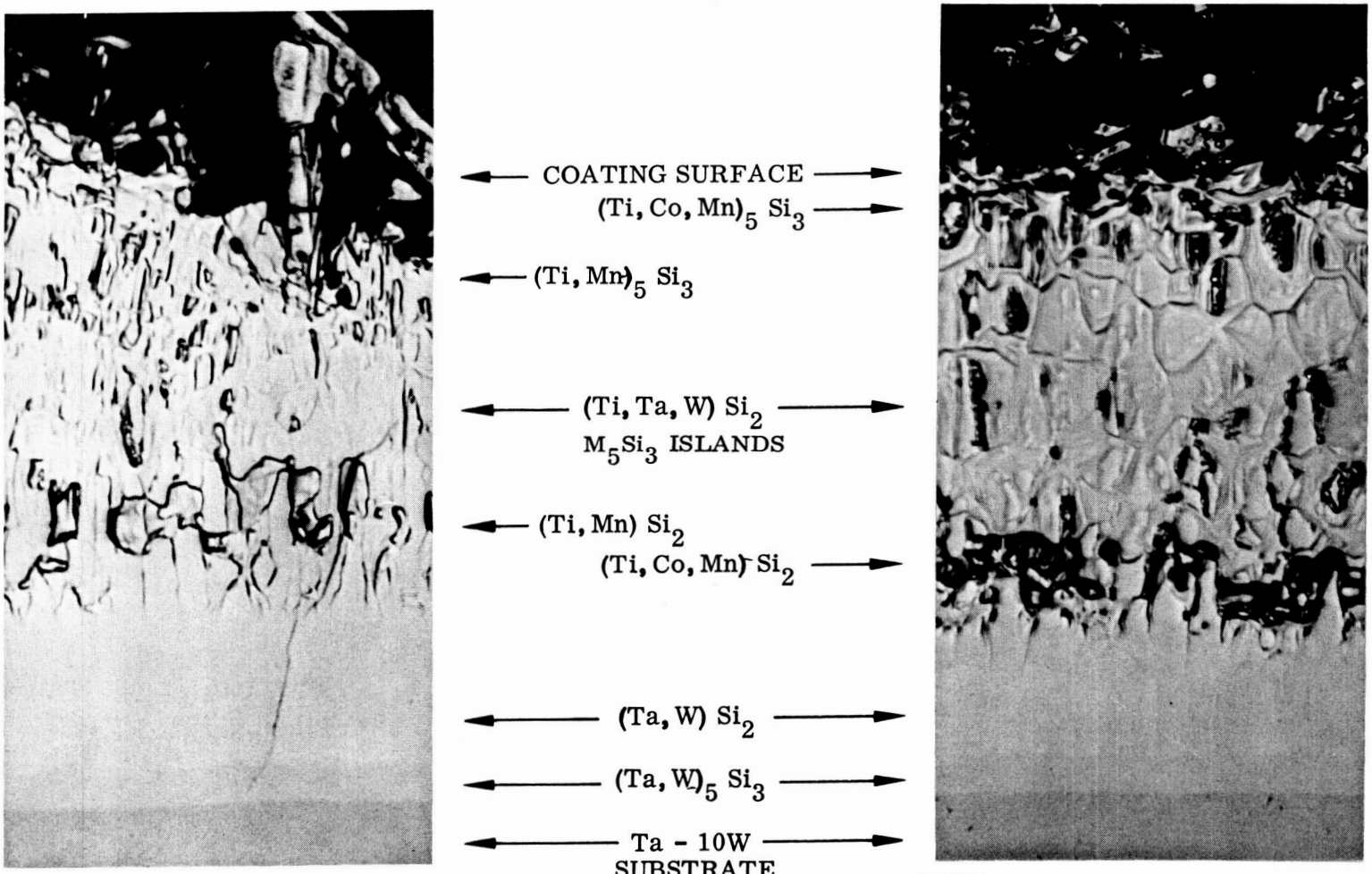

(a) MTS

(b) CMTS

Figure 52 Distribution of Constituents in MTS and CMTS Coating Structures, Etched, 1000×.

The phase distribution in the MTS coating after exposure at the site of an edge fissure is shown in Figure 53. In this figure, the MTS structure is compared with the structure of a simple $TaSi_2$ coating on tantalum that has been exposed to an oxidizing environment. In the $TaSi_2$ structure, there is no metal-oxide layer, and the silica layer is much less continuous than the silica on the MTS coating. From those photomicrographs, it is clear that the MTS coating forms oxide layer structures that are much more effective in protecting the coating and the substrate than the $TaSi_2$ coating.

- Differences Between Silicon-Eutectic Coatings and Metal-Eutectic Coatings

The MTS and CMTS coatings are formed by the fusion of silicon or by the eutectic melting of silicon with elements in the coating or substrate. They contain an excess of silicon over that which could combine with the coating elements to form silicides. The excess silicon will react with the substrate, and all elements in the substrate will appear in the final coating. As shown in Figures 50 and 51, the substrate elements are found throughout the coatings in varying concentrations. The highest concentrations are in the denser inner region of the coating, formed by dissolution of 0.5 to 1.0 mil (0.00127 – 0.00254 cm) of the substrate during melting of the coating constituents. As previously discussed, many of the developmental coatings studied in this program are formed by eutectic melting between metallic constituents in the coating. These coatings fuse below the melting point of silicon or silicon eutectics with the substrate elements and do not contain an excess of silicon above that required to form silicides with the coating elements. It was postulated that such coatings would dissolve less of the substrate and have a more closely controlled composition, relatively free of substrate elements. Electron microprobe studies made with a 24Co-24Ti-52Si coating fused at two different temperatures below the melting point of silicon indicate that such coatings do behave in this manner. As shown in Figure 54, substrate elements are found in a high concentration in the inner one-third of the coating which appears to have formed by substrate dissolution. The outer two-thirds of the coating, however, is free of substrate elements. As shown in Figure 54, variations in fusion temperature below the melting point of silicon had little effect on the distribution of elements in the coatings.

Protective Mechanism

The discussion in the section on Coating Development indicates a complex protective mechanism for silicide coatings. Two regions of active behavior exist – one associated with concurrent oxidation of both the metal and the silicon constituents of the silicide, and the other associated with the formation of volatile SiO. In between these lies a broad region of passive behavior associated with the formation of protective silica films. It was the aim of this program to develop an improved silicide coating for tantalum by modification of the silica film to broaden the temperature/pressure range for passive oxidation behavior. This was to be accomplished by the addition of elements such as zirconium, hafnium, iron, chromium, aluminum, and yttrium to form double oxides or spinels, or cobalt and manganese to control the softening point and viscosity of the silica film.

As shown in the Coating Development section, only the latter approach was successful in significantly improving the performance of silicide coatings on tantalum. Eight of 10 experimental coatings formulated with cobalt and manganese had cyclic lifetimes in excess of 30 cycles as 2600°F (1700°K), 10 torr (13.33 hN/m^2). Three of these met or exceeded the program target of 100 cycles. This is to be compared with 5 to 25 cycles for coatings formulated with the other additives.

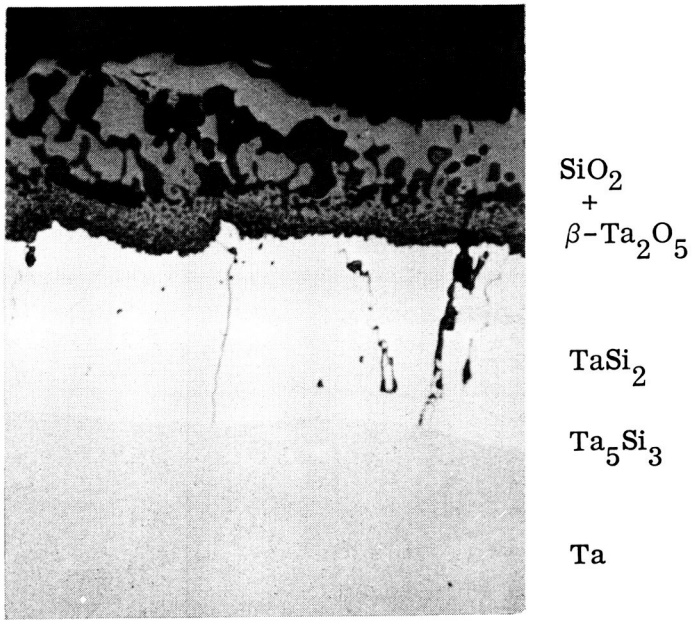

P746 500×

(a) $Ta/TaSi_2$, 2800° F(1811° K)-Air (1 atm)

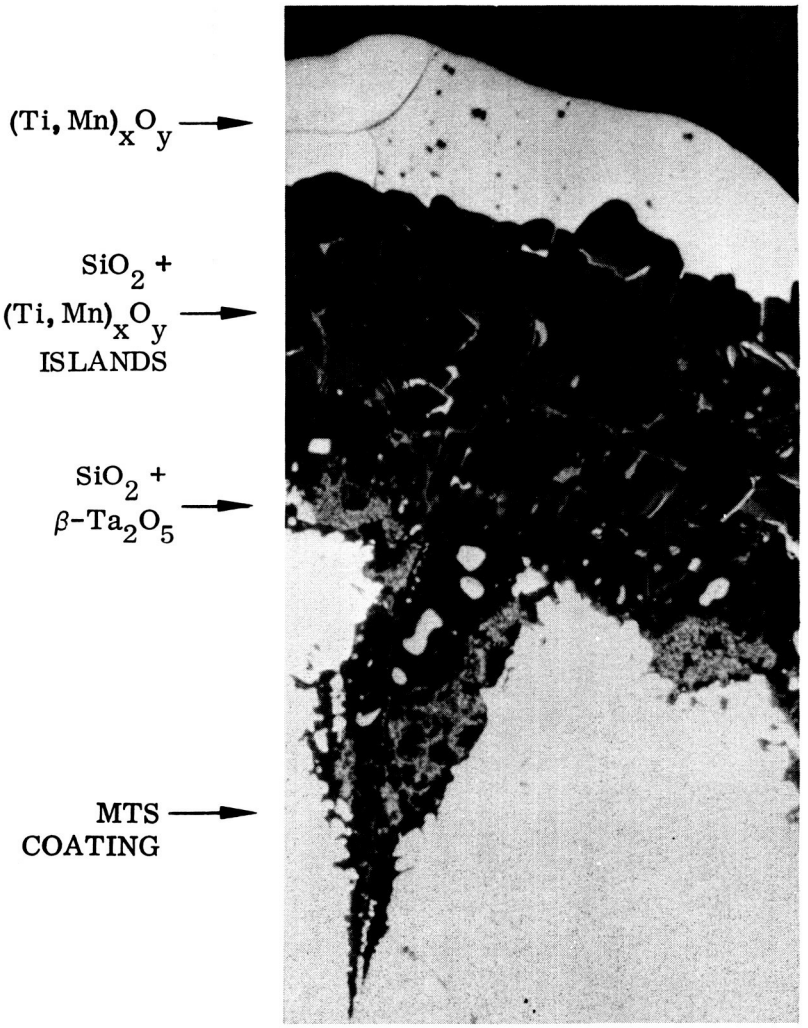

A9633 100×

(b) Ta-10W/MTS, 2600° F (1700° K) 10 Torr (13.33 hN/m^2)

Figure 53 Structure and Distribution of Constituents in Oxide Layer Formed During Oxidation Exposure.

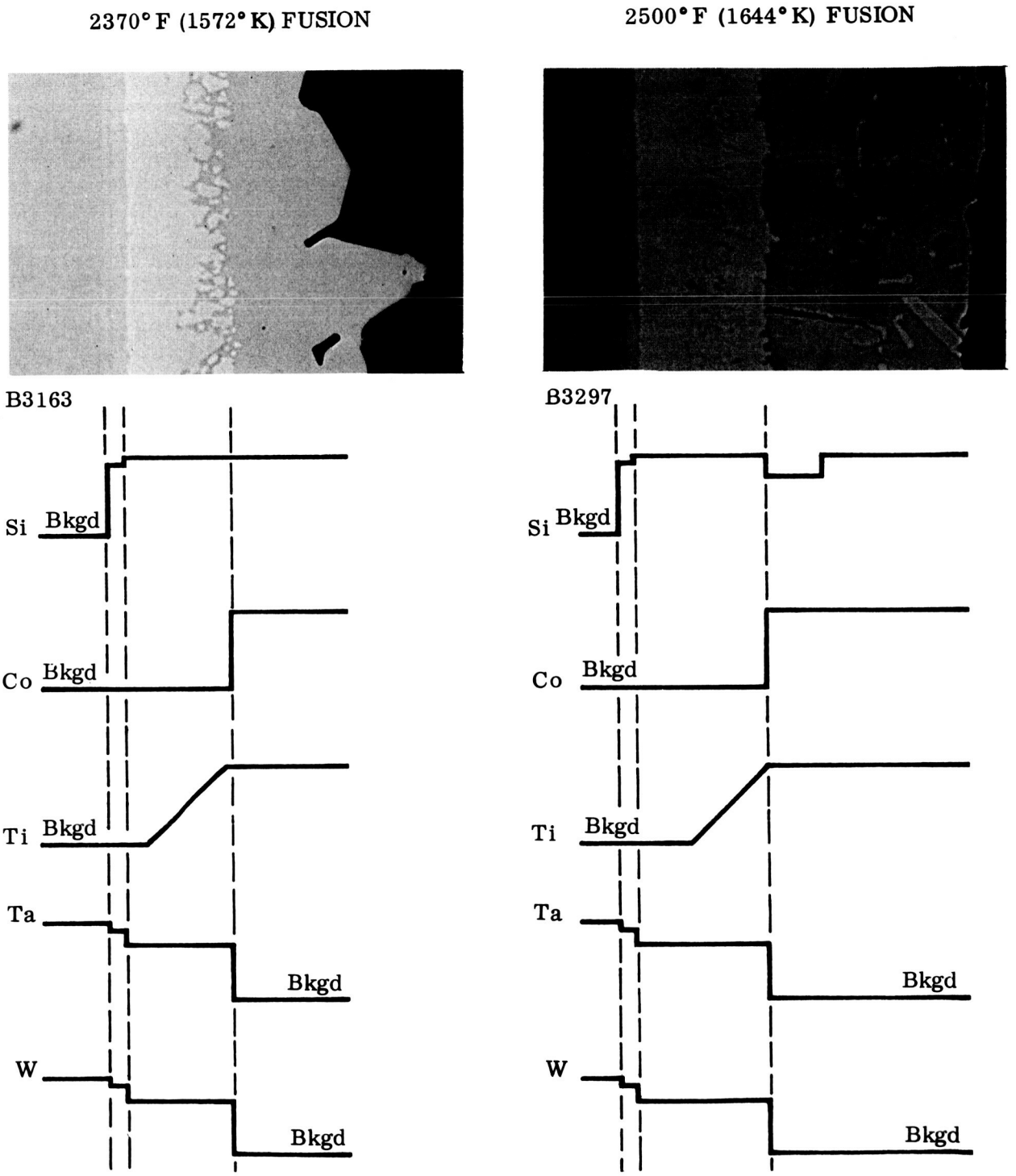

Figure 54 Qualitative Representation of Electron Microprobe Traces Across 24Co-24Ti-52Si Coating.

Metallographic studies of the best manganese- and cobalt-modified coatings (MTS and CMTS) clearly reveal the mechanism by which these elements have produced this significant improvement in performance: As shown in Figure 55, a protective oxide coating, 0.5 to 2 mils thick (0.001 to 0.005 cm), forms on the surface in one cycle of exposure. This represents a total of 30 min at 2600°F (1700°K),10 torr (13.33 hN/m^2). The oxide-forming capability of this coating in air at reduced pressures is vastly superior to that of any silicide coatings for the refractory metals that have been studied to date. As shown previously, in Figure 19f, a standard 22 Ti-78 Si coating without manganese forms a thin, porous oxide less than half a mil (0.00127 cm) thick after 10 cycles of exposure. The MTS coating, on the other hand, forms a dense oxide film, 1 to 1.5 mils thick (0.003 to 0.004 cm) after 6 cycles (Figure 55b).

As discussed in the analysis of coating structure and composition, the outermost layer of the MTS coating is a $(Ti,Mn)_5Si_3$ type of compound. This material appears to be easily oxidized and is capable of generating a large volume of oxide in a short time at high temperature, even with limited availability of oxygen. As shown in Figure 55, small pieces of unoxidized coating have been trapped in the oxide film in the process of reacting to form additional oxide.

The gray-colored portion of the oxide at the surface, and also dispersed in the silica, is $(Ti,Mn)O_2$. It is believed that the presence of manganese in the $(Ti,Mn)_5Si_3$ layer contributes to the ease with which this compound can be oxidized to form a large volume of oxide. A larger proportion of the $(Ti,Mn)O_2$ phase occurs in the oxide film during the first few cycles of exposure. The addition of cobalt to the CMTS coating serves the same function.

The dense oxide film protects the coating from further oxidation and extends lifetime by two different means. First, the film restricts the access of oxygen to the surface and stabilizes the thickness of the coating. Virtually no surface recession occurs after the first few cycles when the oxide film has formed a stable thickness. As shown in Figures 55 c and d, the oxide film thickness is the same at 26 and 125 cycles and in fact, remains the same with continued exposure to 300 cycles. This behavior is illustrated for both the MTS and CMTS coatings in Figures 56 and 57, respectively. Virtually no change occurs in the thickness and structure of the oxide nor in the outer portions of the coating, including the enlarged fissure region from 100 to 300 cycles. The only change is a thickening of the intermediate $(Ta, W)_5 Si_3$ layer as a result of diffusion to the interface and a slight coarsening of the $Ta_5 Si_3$ islands in the outer portion of the coating as a result of depletion of silicon. No significant differences are evident in the structure or in the behavior of the two coating systems. Coating thickness is about 4 mils (10.16 cm), and the oxide thickness is 2 mils (5.08 cm) at 245 to 312 cycles. The coating, in turn, actually increases in thickness with exposure, as a result of silicon diffusion to the substrate and formations of $(Ta, W)_5 Si_3$ at this interface. The system reaches a stable state with respect to oxidation of the surface within the first 10 cycles and is truly passive beyond this point at 2600°F (1700°K), 10 torr (13.33 hN/m^2).

The second mechanism by which these modified silica films greatly increase coating life is related to the healing of coating fissures and surface irregularities. No surface irregularities – particularly at the site of coating fissures – protrude through the oxide film. The surface coverage is complete and continuous at high temperatures. At temperature, the oxide film effectively excludes oxygen from preexisting coating fissures, and the fissures heal by diffusion. Traces of preexisting fissures that have healed and no longer exist can be seen in each of the four pictures in Figure 55. These prior fissure sites are outlined as vertical arrays of small black dots, which are either voids or small oxide particles.

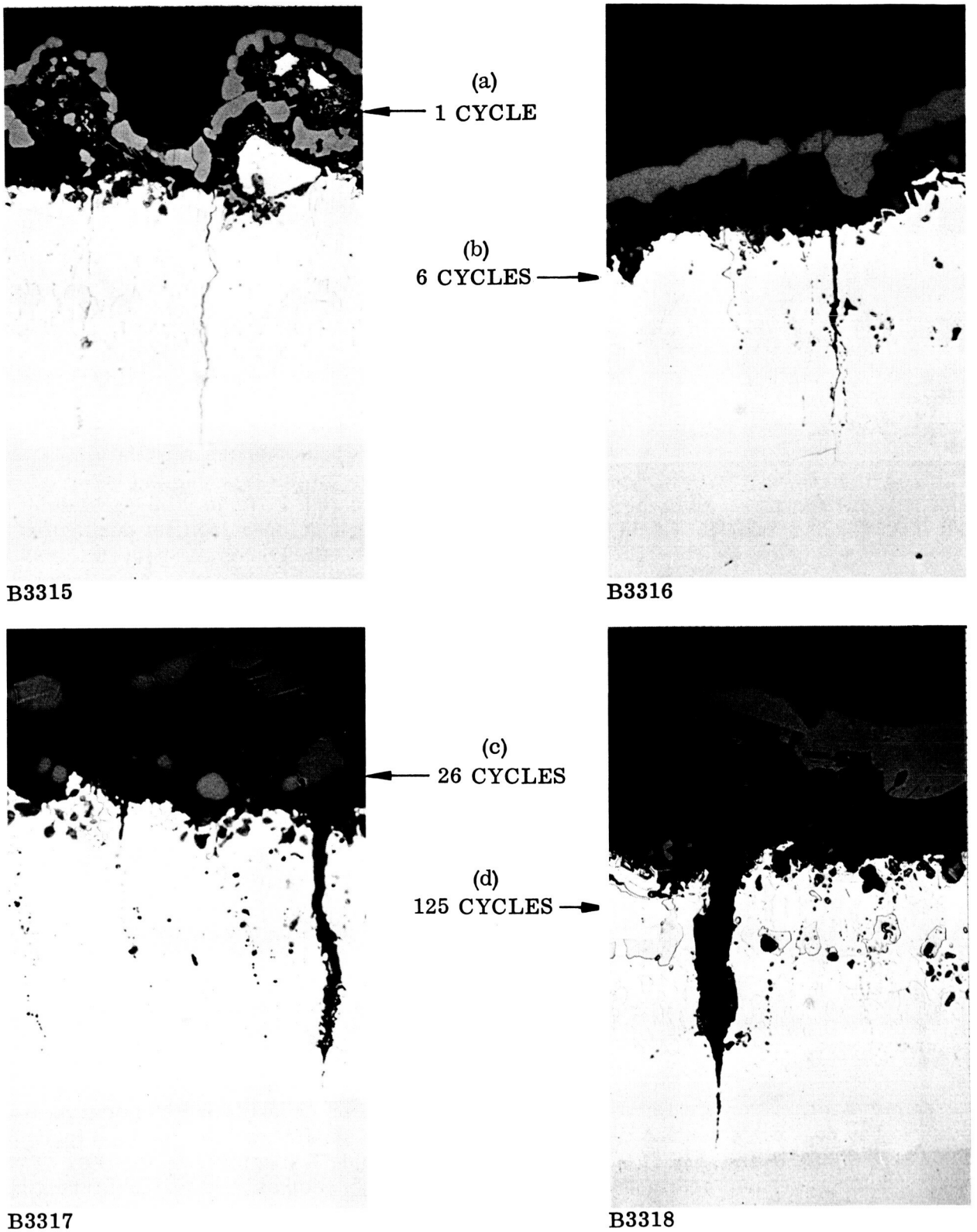

Figure 55 Effect of Cyclic Exposure on Oxide Formation and Growth of Hairline Fissures in the MTS Coating at 2600° F (1700° K), 10 Torr (13.33 hN/m^2), Not Etched, 500×.

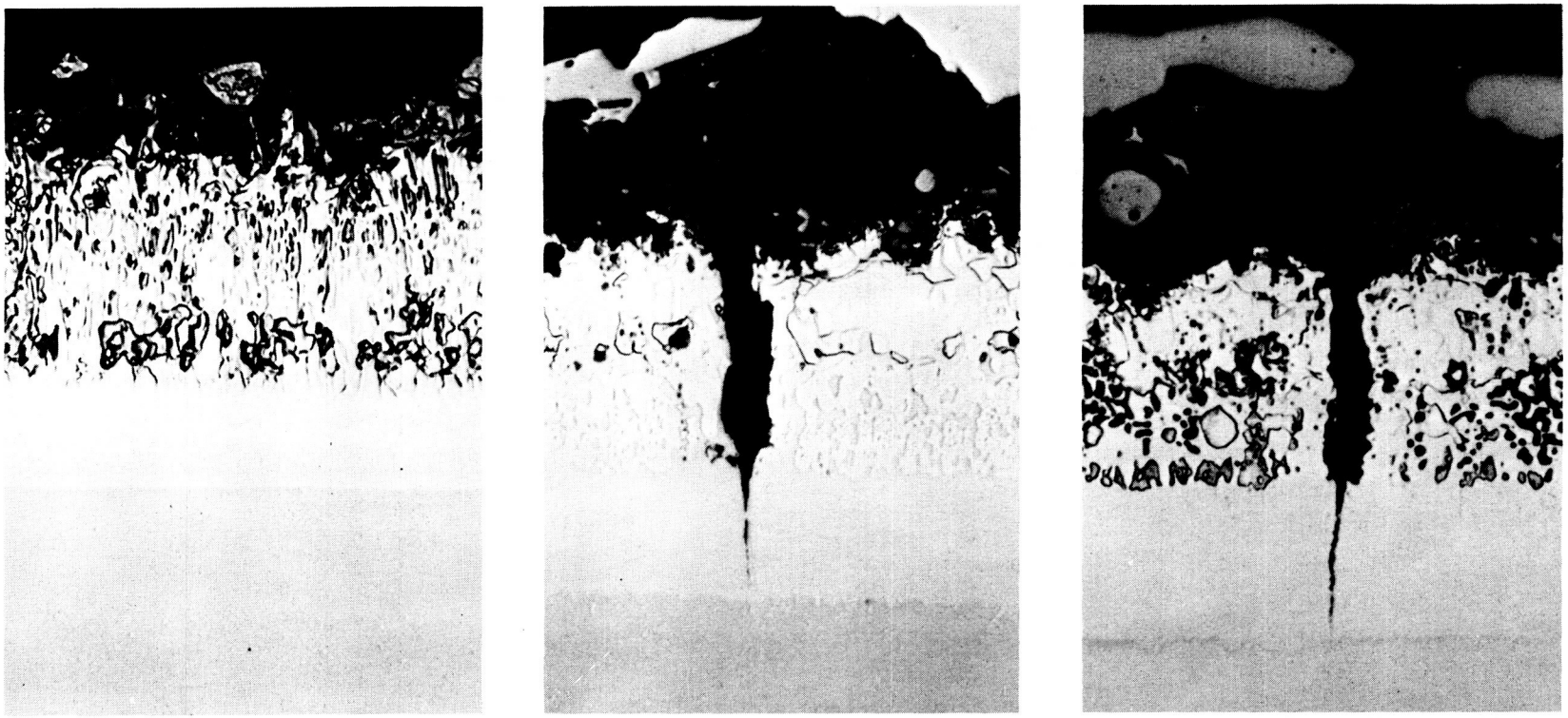

A9975 (a) As-Coated

A9980 (b) 125 Cycles

A9682 (c) 245 Cycles

Figure 56 Effect of Cyclic 2600° F (1700° K), 10 Torr (13.33 hN/m^2) Exposure on Structure of MTS Coating, Etched, 500×.

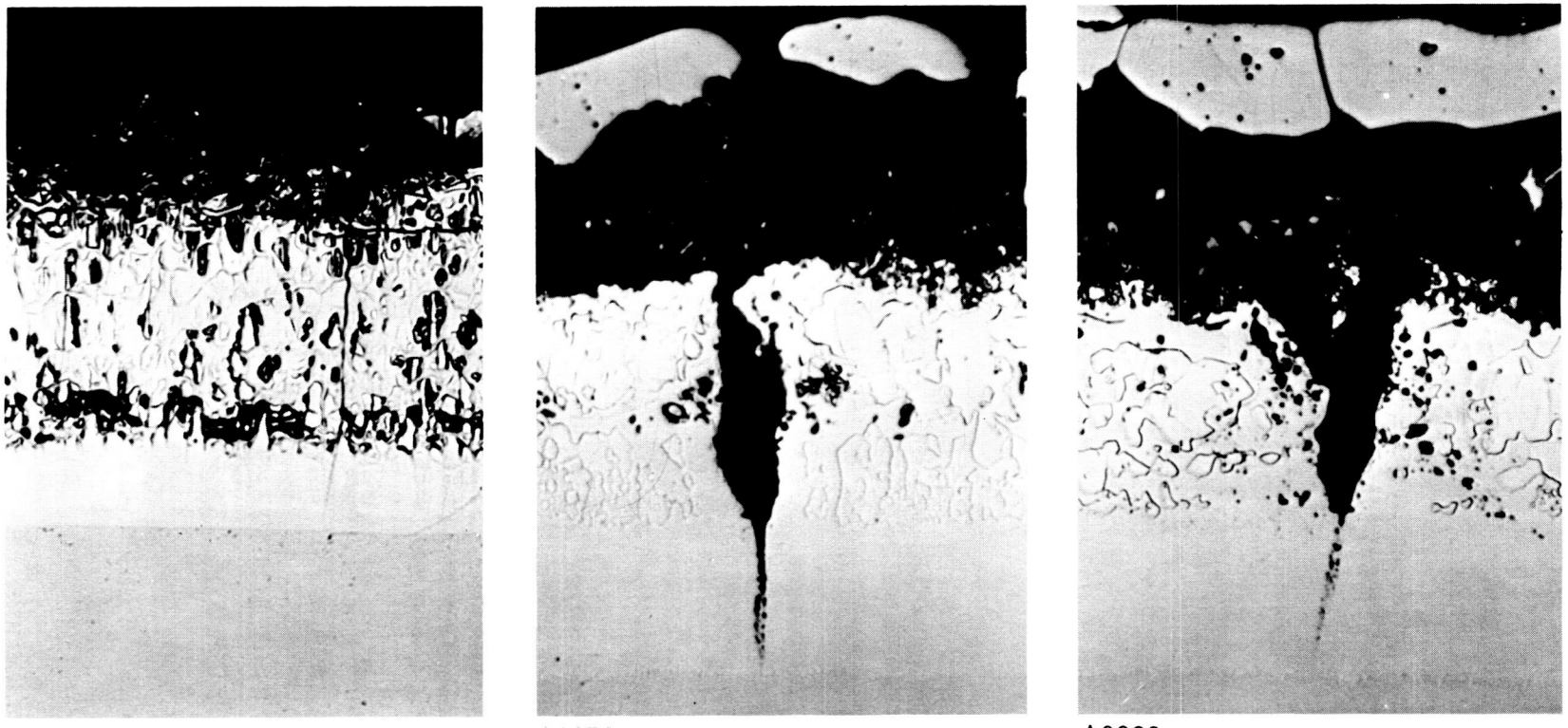

A9973 (a) As-Coated

A9979 (b) 100 Cycles

A9988 (c) 312 Cycles

Figure 57 Effect of Cyclic 2600° F (1700° K), 10 Torr (13.33 hN/m^2) Exposure on Structure of CMTS Coating, Etched, 500×.

On cooling, new fissures, or in some cases preexisting fissures, open to relieve tensile stresses resulting from the higher thermal expansion coefficient of the coating relative to that of the substrate. The oxide film also is placed in tension, and the fissures extend through to the surface. When the sample is reheated, oxygen will have access to the coating until the fissures in either the coating or the oxide is healed by expansion and interdiffusion. Manganese and cobalt in the oxide lower the softening point and accelerate the healing reaction during heating. This protects the fissures in the coating from further oxidation and permits them to heal by diffusion. The large number of healed traces in the coating indicates that this phenomenon happens many times in localized regions.

Eventually, some of the fissures become oxidized and cannot heal by diffusion. These will continue to widen with each cycle of exposure (as shown in Figure 55) and constitute the sites at which the initial wearout of the coating will occur at all pressure levels. The manganese- and cobalt-modified oxides do not prevent this process from occurring; they do, however, slow down the rate of fissure oxidation. The amount of widening of the fissures in the MTS or CMTS coatings that occurs in 100 to 200 cycles is observed to occur in 10 to 25 cycles for other coating systems. As shown in Figures 58 and 59, the fissures in 20Ti-10Mo-70Si (R512C) and 20Cr-10Fe-70Si coatings on Ta-10W are widened to the point of wearout in 15 and 25 cycles, respectively. These structures are typical at the maximum life for these materials. The fissures in the MTS coating at 125 cycles (Figure 56) are about as wide, but the coating has at least 100 more cycles of use before wearout. The fissures are well healed by the protective oxide, and their rate of growth is very slow.

Environmental Effects

The introductory discussion on the fundamentals of coating systems showed how changes in temperature and pressure can alter the protective capabilities of oxide films. The results of oxidation tests with the best coating systems in this program indicate a general trend of increased coating life with decreasing temperature or increasing pressure. In addition, at 2600°F (1700°K) the life under isothermal conditions tends to exceed that under cyclic conditions, whereas at 2800°F (1811°K) the isothermal and cyclic lifetimes are similar. Comparing the two coating systems, the MTS system has better overall performance at 2600°F (1700°K), whereas both systems are very similar at 2800°F (1811°K). Metallographic studies have been made to determine the structural factors and protective mechanisms governing these aspects of behavior in relation to the fundamentals of coating systems.

- Effect of Pressure

The changes in structure of the coating and oxidation products as a function of pressure during cyclic exposure at 2600°F (1700°K) are shown in Figures 60, 61, and 62. At 1 torr (1.33 hN/m^2) the protective oxide film is about half the thickness of that formed at 10 torr (13.33 hN/m^2) (Figures 60 and 61). The oxide is dense and continuous and appears to be just as protective as that formed at the higher pressure. There appears to be a slightly higher ratio of the $(Ti,Mn)O_2 : SiO_2$ in the oxide formed at the lower pressure. The oxide developed a stable thickness in as little as 18 cycles and showed no major change out to 426 cycles. Fissures in the coating widened, and the growth rate was comparable to that observed at 10 torr (13.33 hN/m^2). These features of the structure indicate that no major decrease in performance occurs at the lower pressure levels, which is in agreement with the experimental results of cyclic oxidation tests. In fact, the MTS coating has a much greater cyclic life at 1 torr (1.33 hN/m^2) than at 10 torr (13.33 hN/m^2).

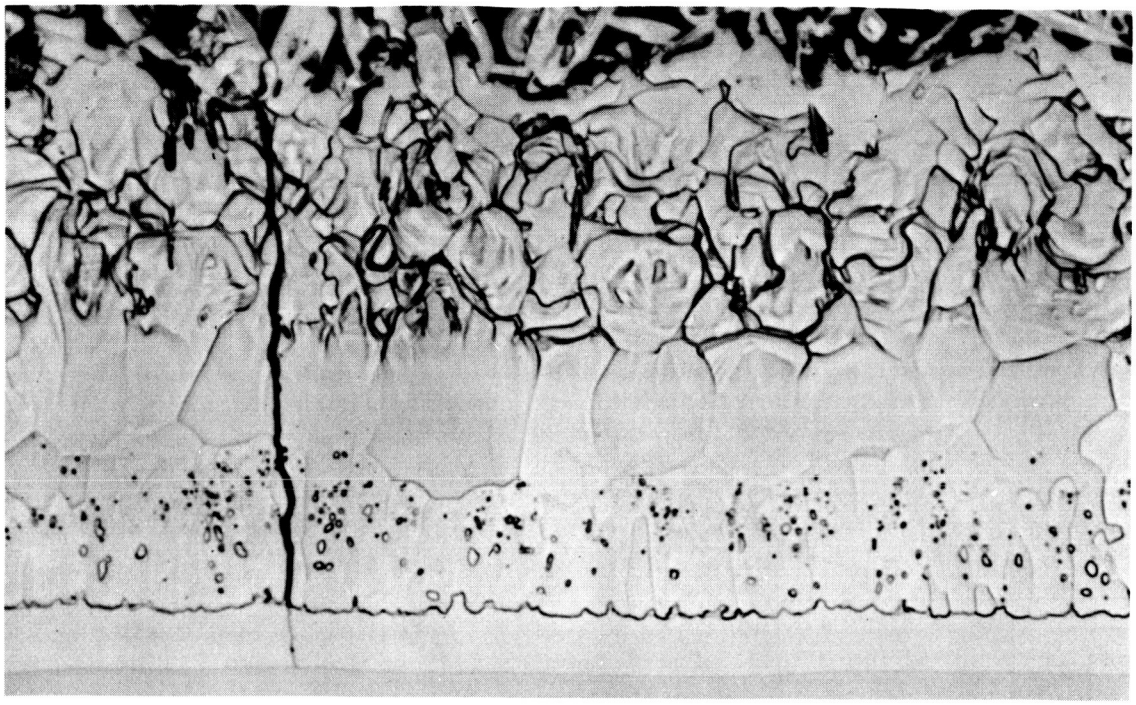

A2572 1000×

(a) As-Coated

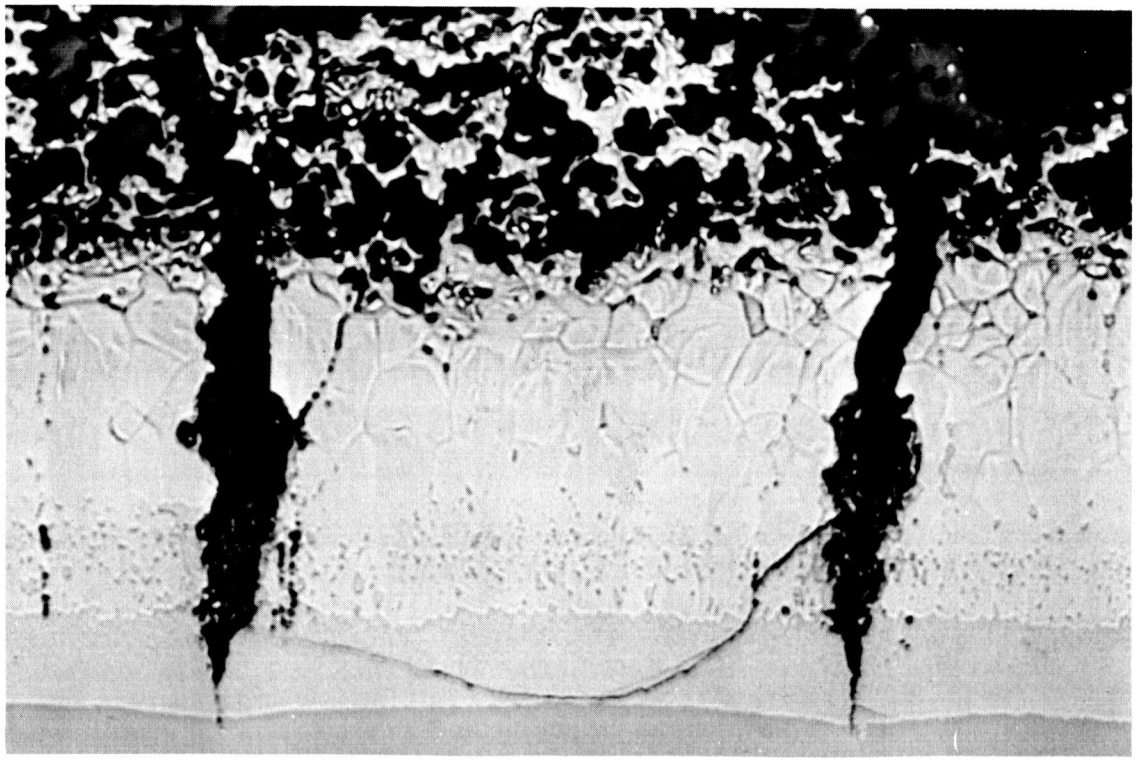

A4394 600×

(b) 15 Cycles at 2600° F (1700° K), 10 Torr (13.33 hN/m^2)

Figure 58 Effect of Cyclic Oxidation on Structure of R512C (Si-20Ti-10Mo), Etched.

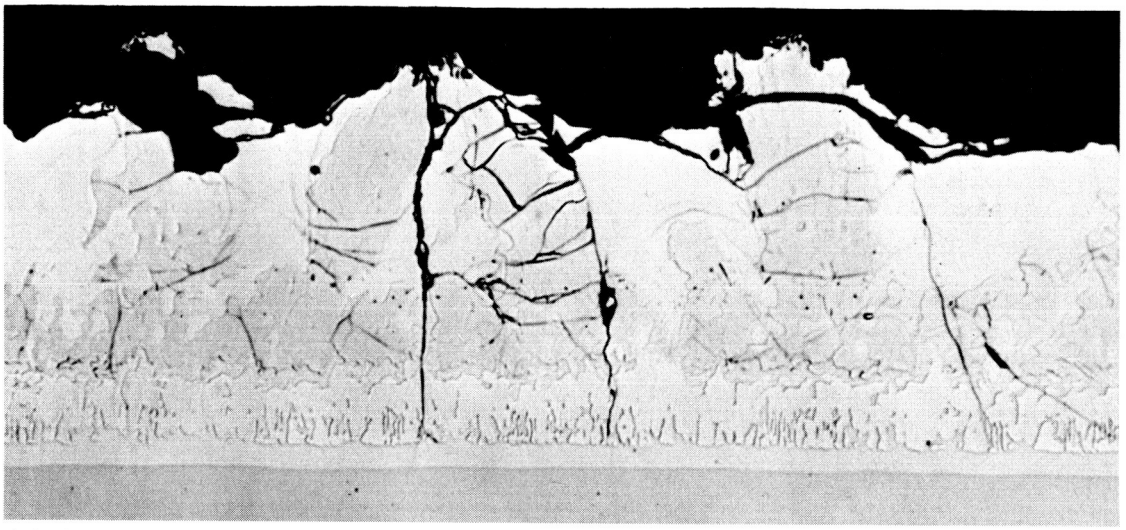

A4210

(a) As-Coated

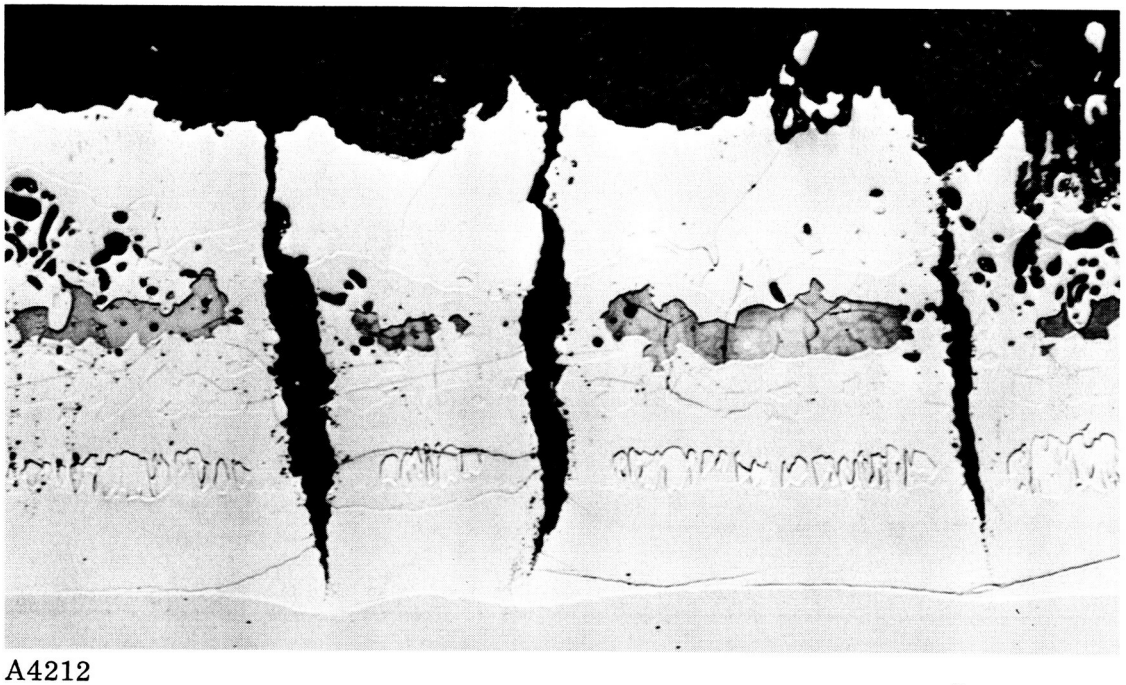

A4212

(b) 23 Cycles, 2600° F (1700°K), 10 Torr (13.33 hN/m^2)

Figure 59 Effect of Cyclic Oxidation on Structure of Coating 11, Si-20Cr-10Fe, Etched, 500×.

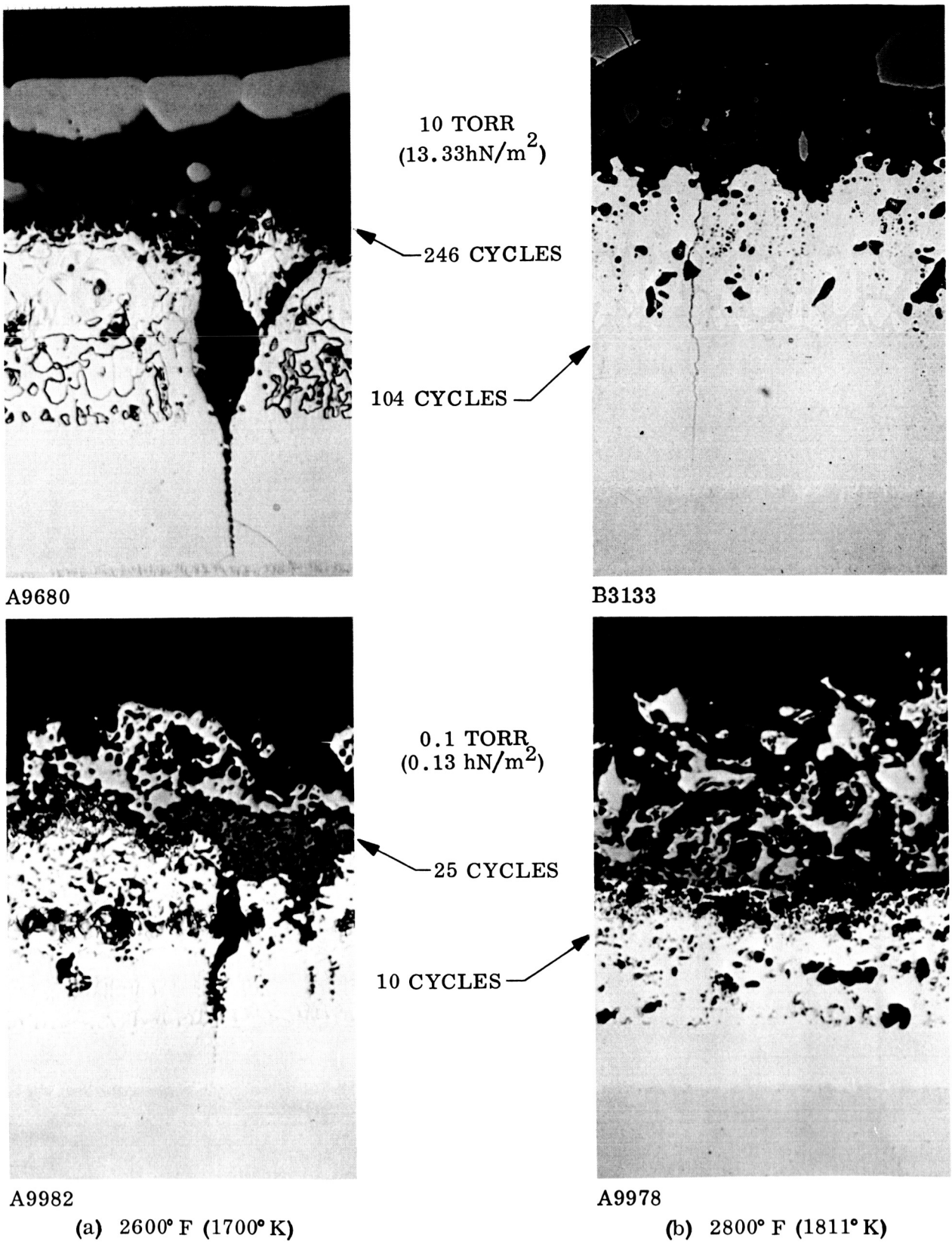

Figure 60 Effect of Temperature and Pressure on Structure of MTS Coating, Cyclic Exposure, Etched, 500×.

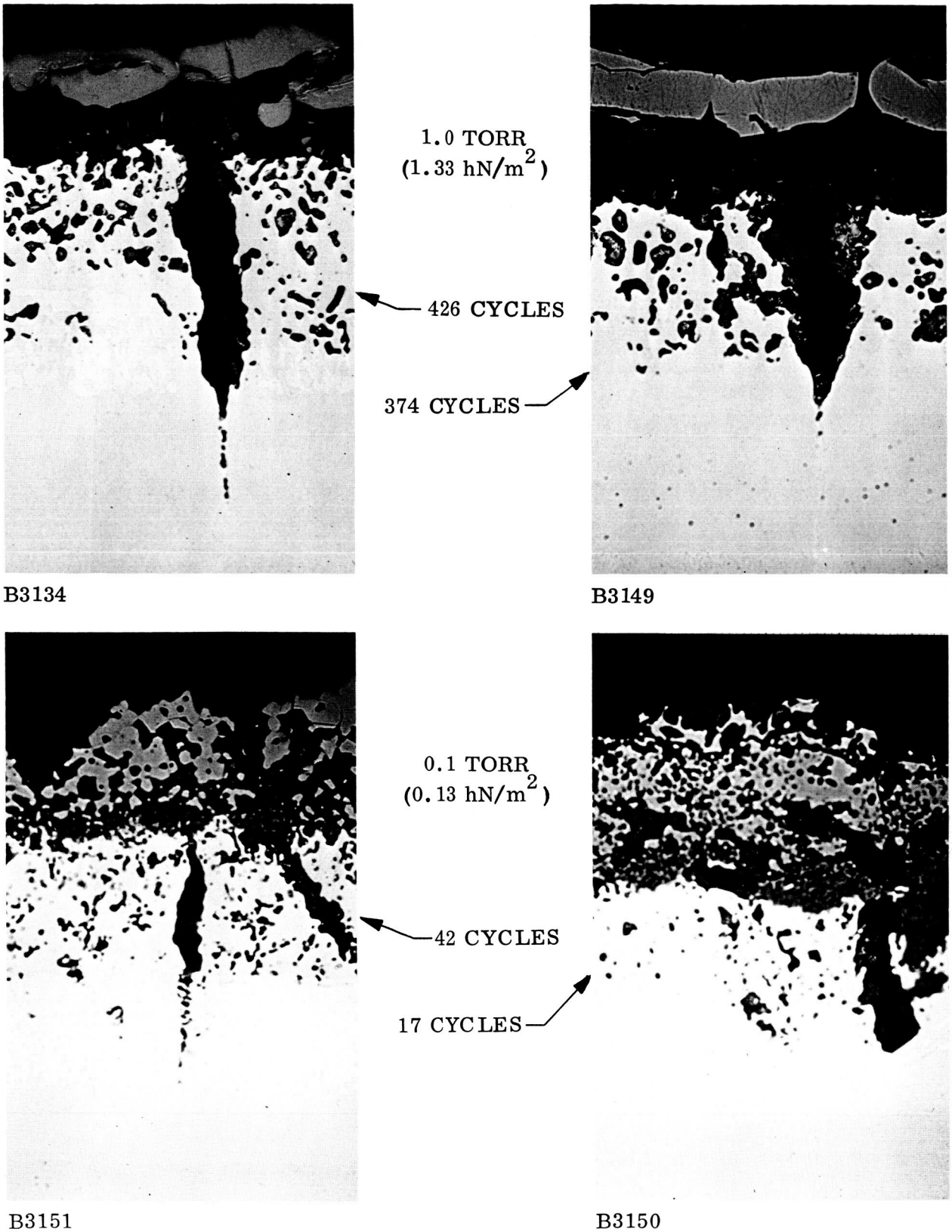

Figure 61 Structure of MTS and CMTS Coatings After Cyclic Exposure at 2600° F (1700° K), Not Etched, 500×.

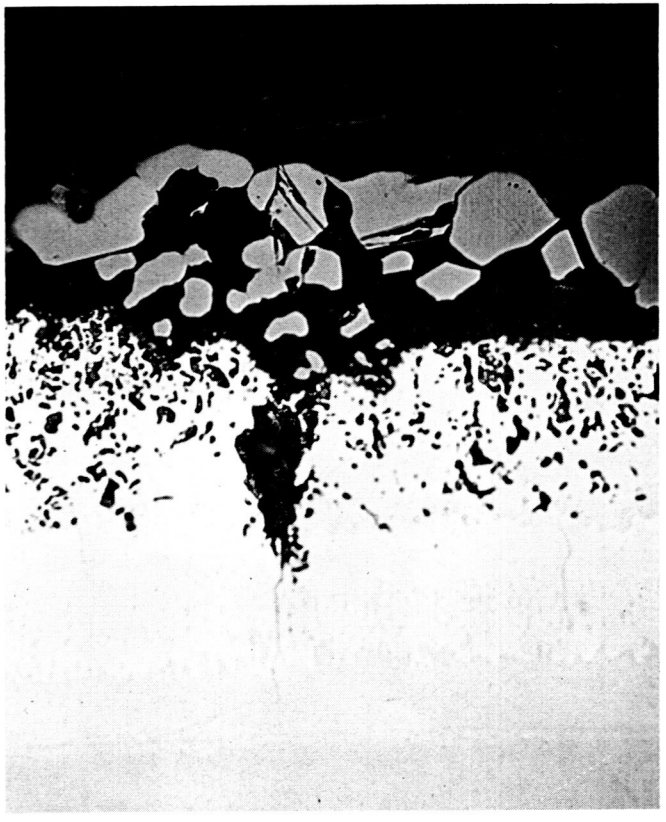

B3136

(a) 18 Cycles

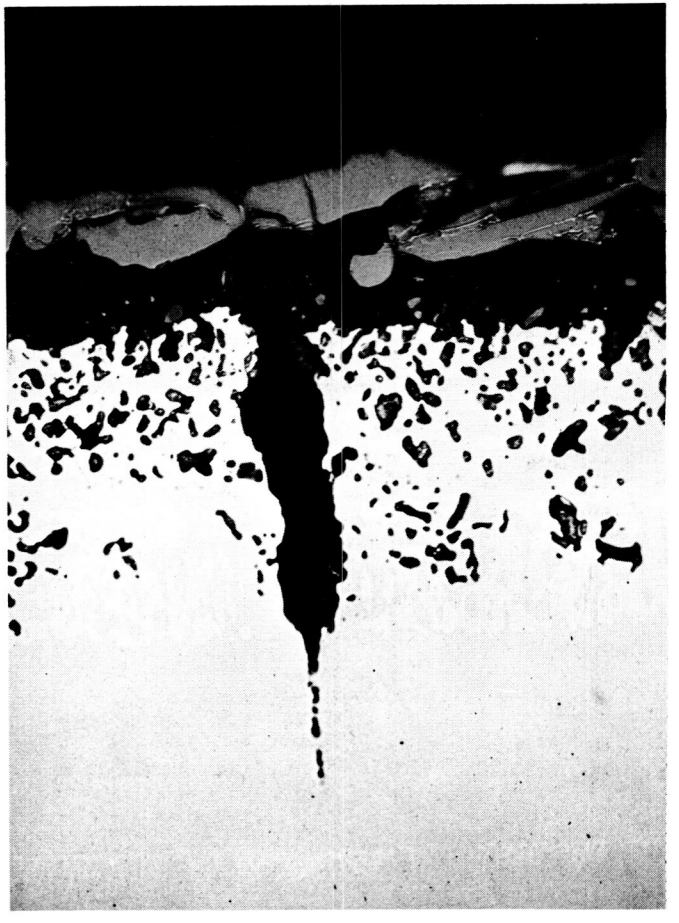

B3134

(b) 426 Cycles

Figure 62 Effect of Cyclic 2600° F (1700° K), 1.0 Torr (1.33 hN/m^2) Exposure on Structure of MTS Coating, Not Etched, 500×.

The outer one-third of the MTS coating is porous after exposure to 2600° F (1700° K), 1 torr, for as little as 18 cycles, as shown in Figure 62a. This fact, coupled with the lower silica content of the oxide and the thinner oxide layer, suggests that silicon is being lost to the atmosphere, probably as SiO. Much of this loss appears to occur very early, probably as the protective oxide is being formed. The pores coalesce and grow in size with time, and the volume-percent of pores in the coating also increases. These pores, however, do not appear to have caused reduced performance. The improved performance at 1 torr (1.33 hN/m^2), in fact, may be due to the lower silicon content of the coating (lower activity) or to the higher metal oxide content of the glass, both of which would tend to stabilize the coating with respect to continued high rates of SiO formation.

A marked change in both the coating and the oxide film occurs as the pressure is reduced to 0.1 torr (0.13 hN/m^2). As shown in Figure 60a, the silica content of the coating has been reduced considerably and a dense, continuous film no longer forms. A layer of Ta_2O_5 crystals is present beneath the oxide film. Accelerated oxidation of the outer region of the coating is evident. These structures indicate extensive loss of silicon to the atmosphere as SiO. Coating lifetime should be decreased and, in fact, is only a fraction of that observed at higher pressures. The MTS and CMTS coatings exhibit the same behavior and microstructural features at 0.1 torr (0.13 hN/m^2).

Bulk silicides and coatings have a transition from passive (protective) to active oxidation behavior with decreasing pressure, as a result of the formation of SiO, a volatile oxide (ref. 17). As discussed previously, the location of the temperature/pressure boundary for this transition can be estimated from free energy or heat of reaction data for individual silicides. The boundaries for $TaSi_2$ and Ta_5Si_3 estimated by Bartlett et al. are shown in Figure 63. To the left of these boundaries, a protective film of SiO_2 is formed on the surface by selective oxidation of silicon. To the right of these boundaries, SiO vapor is formed by the reaction of the SiO_2 film with silicon in the silicide as follows:

$$Si_{(s)} + SiO_{2(s)} \rightarrow 2SiO_{(g)} \uparrow$$

Silica may or may not be a condensed phase in this region, depending on the relative rates of formation of SiO_2 by oxidation and of SiO by reaction with the silicide. Exposure to this temperature/pressure region results in high rates of oxidation of silicon from the coating and should reduce coating life.

Samples from isothermal, cyclic, and heat-shield panel oxidation tests were examined to determine if passive or active oxidation of the coating had occurred. Passive oxidation is defined as the formation of a dense silica film with no evidence of reaction in the film to form SiO. This type of oxidation was invariably accompanied by a long isothermal or cyclic life. Active oxidation is that in which the silica film shows definite signs of breakdown and evaporation. This type of oxidation was invariably accompanied by a shorter coating life. Examples of the oxide film structures for the active and passive states of oxidation are shown for the MTS coating after isothermal exposure at 2700° F (1755° K) in Figure 64a. At 10 torr (13.33 hN/m^2), a thick, dense silica film with islands of $(Ti,Mn)O_2$ on the surface has formed. There is no porosity or evidence of reaction with the silicide in this passive state. It is significant that, unlike the 2600° F (1700° K) cyclic specimens, there is no widening of fissures by oxidation during isothermal exposure. The fissures all healed at temperature, and new fissures just like those in the original coating formed on cooling. This condition is typical of isothermal exposures at all pressures and

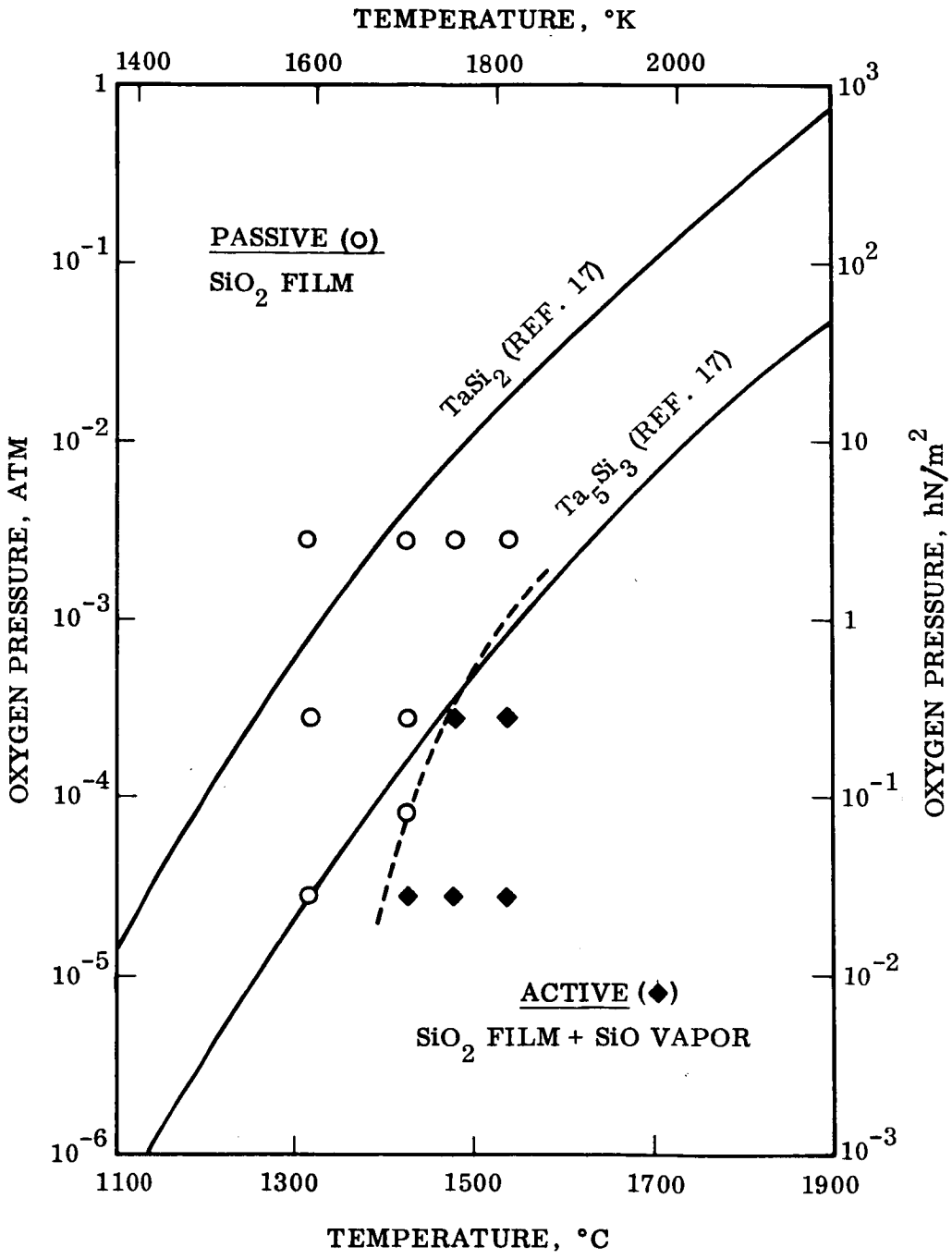

Figure 63. Active-to-Passive Transition for MTS Coating in Air Compared With Theoretical Boundaries for Tantalum Silicides.

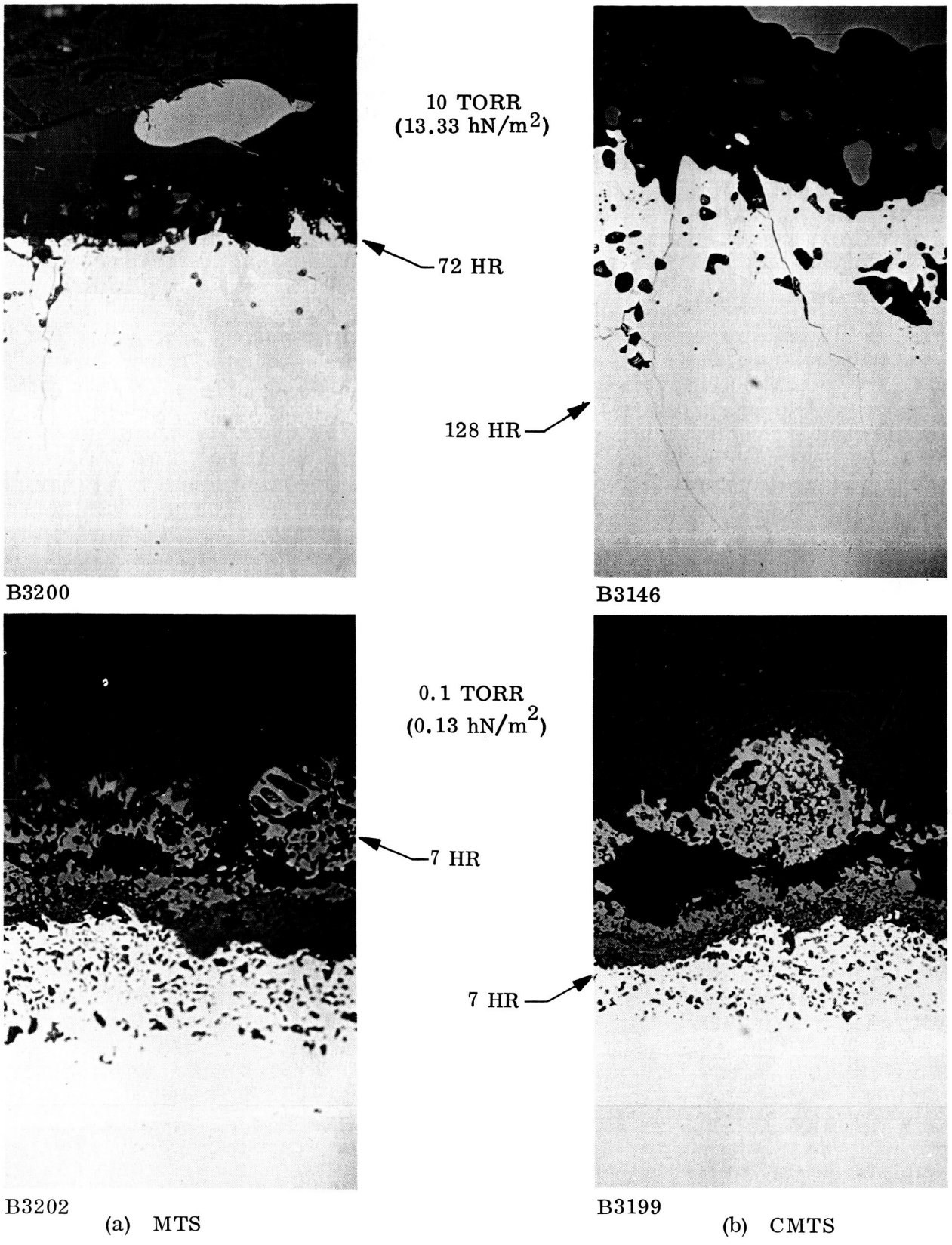

Figure 64 Structure of MTS and CMTS Coatings After Isothermal Exposure at 2700° F (1755° K), Not Etched, 500×.

temperatures. At 0.1 torr, a porous film of silica and $(Ti,Mn)O_2$ with a much lower ratio of Si to $(Ti,Mn)O_2$ has formed on the surface. Many voids have developed within the outer layer of the silicide coating, probably as the result of more rapid oxidation of silicon, which is volatilizing as SiO. This oxide film is still protective, however, and there is no evidence of rapid oxidation of the bulk coating as such. Only the rate of selective oxidation of the silicon has increased. Depletion of the silicon reservoir in the coating is accelerated, and coating life is shortened as a result. The coating eventually wears out, when local regions are so depleted in silicon that oxidation of the bulk coating material occurs. As shown in Figure 64a, the coating lifetime under the passive condition is 72–128 hr, compared with 7 hr under the active condition at the same temperature but a lower pressure.

The data from these tests converted from air pressure to equivalent oxygen pressure have been plotted with the active/passive transition curves for tantalum silicides in Figure 63. The open circles represent passive behavior; the diamonds represent active behavior based on metallographic examination and coating life data. The dashed line, which represents the active/passive transition boundary for the MTS coating, crosses the theoretical boundary for Ta_5Si_3. As previously noted, after oxidation the surface layers of this coating are rich in titanium, tantalum, and tungsten and have a silicon content lower than that of the core of the coating. This layer from qualitative microprobe data was designated to be $(Ti,Ta,W)_5Si_3$. The agreement between the boundary for this coating and the calculated boundary for Ta_5Si_3 indicates that this coating may have approached a theoretical limit with respect to its performance capabilities in air at reduced pressure.

- Effect of Temperature

The effect of increasing temperature at any pressure is, first, to increase the kinetics of all reactions. The growth of M_5Si_3 silicide layers at the substrate interface and the oxidation and vaporization reactions at the coating/oxide and oxide/gas interfaces will proceed more rapidly. It can be seen in Figure 63 that the passive-to-active transition temperature at any pressure level can be approached and crossed with increasing temperature. The result on coating structure and life will be the same as if the pressure had been reduced at constant temperature, except that reaction kinetics will be increased and coating life will be decreased significantly. For example, crossing the boundary by decreasing pressure from 1 to 0.1 torr (1.33 to 0.133 hN/m^2) at 2600°F (1700°K) reduces the isothermal life of the CMTS coating from 140 to 12 hr. Crossing the boundary at 1 torr (1.33 hN/m^2) by increasing the temperature to 2800°F (1811°K) decreases the life from 140 to 5 hr.

Increasing temperature within the active region should increase the rate of SiO formation and reduce life. At 0.1 torr (0.13 hN/m^2), however, the life of the CMTS coating increases from 12 to 43 hr when the temperature is increased from 2600° to 2800°F (1700° to 1811°K). As the silica content of the oxide film is decreased by SiO evaporation, the metal oxide content $(Ti,Mn,Co)O_2$ is increased. It appears that, in this case, a continuous metal oxide film is forming to protect the coating (Figure 64b). The effect is not observed at 1 torr (1.33 hN/m^2) nor is it as great with the MTS coating. More definitive studies are needed to clarify several aspects of the anomalous behavior.

The effect of increasing temperature within the passive (protective) region on coating life depends on two factors – rate of oxidation and rate of interdiffusion with the substrate. The rates of diffusion of oxygen or silicon and other metal atoms through the oxide and the

rates of diffusion of silicon to the substrate to form M_5Si_3 at the interface would both increase. If the latter increases more rapidly, silicon depletion of the coating would be accelerated and coating life would be decreased. However, the isothermal data show that thick and thin coatings have the same lifetime at all temperatures under passive oxidation conditions at all temperatures. This clearly indicates that reactions in the oxide or the oxide/metal interface and not reactions at the coating/metal interface govern life. Thus, decreased lifetime with increased temperature, as observed in these tests, is the result of increased coating oxidation rates.

The effect of increasing temperature on coating structure in the passive (10 torr, 13.33 hN/m^2) and active (0.1 torr, 0.13 hN/m^2) regions is shown in Figure 60. The increased rate of oxidation in the passive state at 2800°F (1811°K) is indicated by the appearance of additional metal-oxide particles in the silica film and by the formation of voids within the outer portion of the coating. At the low pressure, the amount and size of voids in the coating increases with increasing temperature. The voids are formed by coalesence of vacancies as a result of silicon diffusion to the surface where it is oxidized to form SiO and SiO_2. The oxide also contains a large amount of metal oxide at the higher temperatures. It should be noted that this sample had less than half the cyclic exposure of the 2600°F (1700°K) sample, further illustrating the accelerated rates of oxidation with increased temperature in this active oxidation region.

One very significant feature distinguishes the 2600°F (1700°K) from the 2800°F (1811°K) samples. At the lower temperature, the hairline fissures have been widened as a result of oxidation. At 2800°F, the hairline fissures after 104 cycles of exposure look no different from those in the coating as deposited. This is true at all pressure levels. The 2800°F (1811°K) cyclic samples have a coating structure that is identical to that of samples which have been exposed under isothermal conditions (Figure 64).

The hairline fissures in the coating are perfectly healed during cyclic exposure to all pressures at 2800°F (1811°K). This unique aspect of behavior explains the reasonably good agreement between cyclic and isothermal coating lifetimes at this temperature. The fissures form on each cool-down part of the cycle but are sealed and diffusion bonded together on reheating. A large number of healed fissure traces can be seen in the structure of these samples.

Wearout Modes

The MTS and CMTS coatings wear out as the result of oxidation reactions that deplete the reservoir of silicon required to form protective oxide films. At some critical metal : silicon ratio in the coating, the passive-to-active transition boundary will be crossed and both the metal and silicon constituents of the coating will be oxidized. Tantalum silicides in the coating are oxidized, and oxides of tantalum appear in the reaction products. The film is less protective and the rate of oxidation increases, culminating in exposure and oxidation of the substrate.

Tantalum oxide in the protective film triggers a rapid oxidation process. This effect appears to be mechanical rather than chemical. The oxide of tantalum (Ta_2O_5) occupies a much larger volume than the metal or compound from which it was formed. The voluminous nature of the oxide is responsible for its reduced protective capabilities and, hence, for the high rate of oxidation of uncoated tantalum and its alloys. When this oxide begins to appear in the protective oxide film on a silicide coating, it creates a mechanical

disruption at the oxide/coating interface. The protective film is forced away from the coating and bulges out at the surface. This breaks down the protective capabilities in a local region, and rapid oxidation of the coating follows.

The start of such a process is shown in Figure 65. The widened fissure in the lower left corner is filled with Ta_2O_5 as a result of concurrent oxidation of all elements in the coating at this site. The protective oxide film has broken away from the surface at this point and is bulged out. A new protective film has formed beneath the original disrupted film. Wearout in this area is imminent. The process is just beginning in the fissure at the upper left, and not enough Ta_2O_5 has formed at this point to disrupt the original oxide layer.

When this oxidation process progresses to the tantalum substrate, the oxidation process will proceed along the coating/substrate interface as well as into the substrate. Formation of Ta_2O_5 at the interface will separate the coating from the substrate and cause the affected area to enlarge. As mentioned in the section on intentional damage studies, the rate of progression of the oxidized region, once the substrate has been exposed, is 0.1 in. (0.254 cm) per cycle for the 2600°F (1700°K), 10 torr (13.33 hN/m^2) exposure conditions.

The mode and location of wearout varies as a function of the environmental exposure conditions. With isothermal exposure at all temperatures and pressures and with 2800°F (1811°K) cyclic exposure at 0.1 to 1.0 torr (0.13 to 1.33 hN/m^2), wearout occurs by the coalescence of vacancies and growth of voids in the outer half of the coating. This is the result of diffusion of silicon away from this area to the surface, where it is converted to SiO_2 and SiO. The voids increase in size and eventually trigger the internal oxidation and accelerated wearout of the coating. This process occurs at variable rates in random locations over the entire surface and at edges. The reactions are not necessarily related to preexisting fissures in the coating, although at very low pressures some preference for more rapid oxidation in these regions is evident. Samples exposed to these environments tend to wear out initially on flat surfaces. The area is much greater than that at edges and, hence, the probability for wearout is greatest on the flat surfaces. Edge wearout can and does occur; however, edges are not the predominant sites for initial wearout under isothermal conditions.

Cyclic exposure at 2600°F (1700°K) at all pressures results in wearout by widening of the fissures in the coating, as previously noted. Cyclic exposure at 2800°F (1811°K) and 10 torr (13.33 hN/m^2) also results in wearout by widening of fissures, but only at the edges. Fissures on the flat surfaces are healed and show no trace of internal oxidation. The mode of wearout on flat surfaces at 2800°F (1811°K), 10 torr (13.33 hN/m^2) is by vacancy coalescence and growth of voids, as previously discussed. Widening of fissures is more pronounced at the edges of 2600°F (1700°K) samples. As shown in Figure 65, the two fissures at the edge are widened more than those on the flat surfaces. As a result, in cyclic exposures at 2600°F (1700°K) at all pressures and at 2800°F (1811°K), 10 torr (13.33 hN/m^2), the initial wearout locations are predominantly at edges. This is the result of a mechanical limitation imposed by the configuration at the edge of coated thin-gage sheet and is not the result of coating deficiencies (such as thin spots or V-shaped fissures) at the edges.

The structure of as-deposited CMTS coating on the edge of 13 mil (0.033 cm) thick Ta-10W sheet is shown in Figures 66a and b. These edges are typical of inadequately radiused edges that normally produce large V-shaped fissures in other silicide-base coatings. (See Figures 21c and d.) Even with sharp or chiseled edges, the MTS and CMTS coatings give a

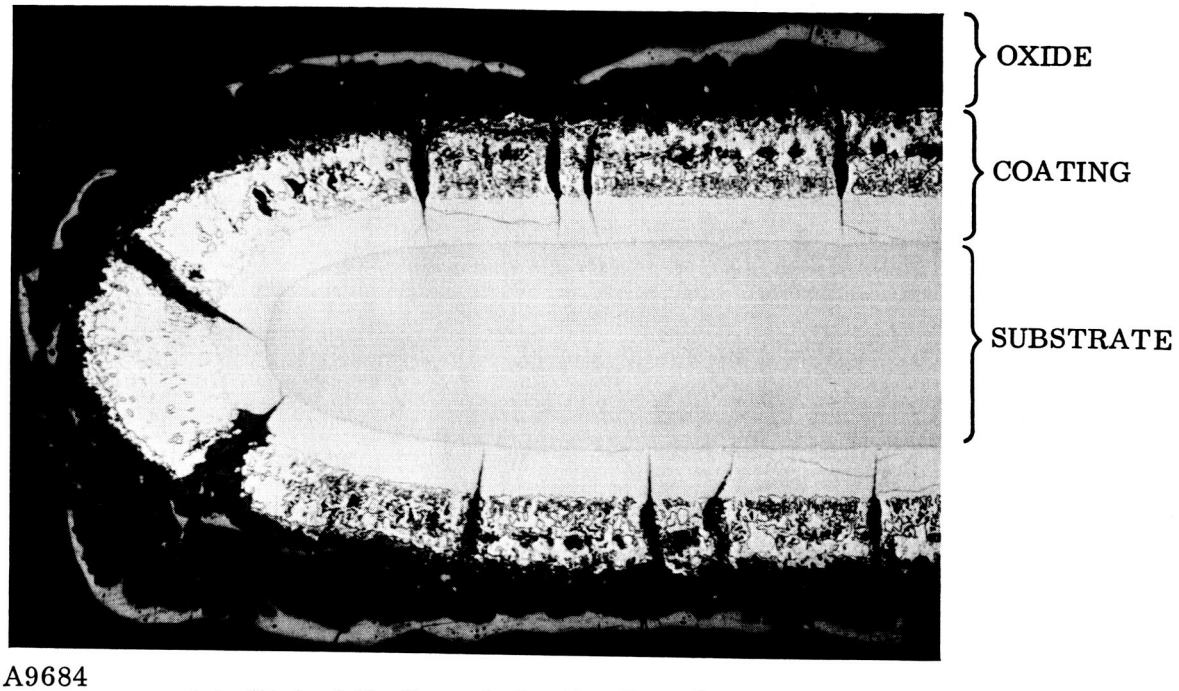

A9684

(a) Etched To Reveal Coating Details

A9639

(b) Printed To Reveal Oxide Details (Not Etched)

Figure 65 Structure of MTS Coating and Surface Oxides After 203 Cycles at 2600° F (1700° K), 10 Torr (13.33 hN/m^2), 100×.

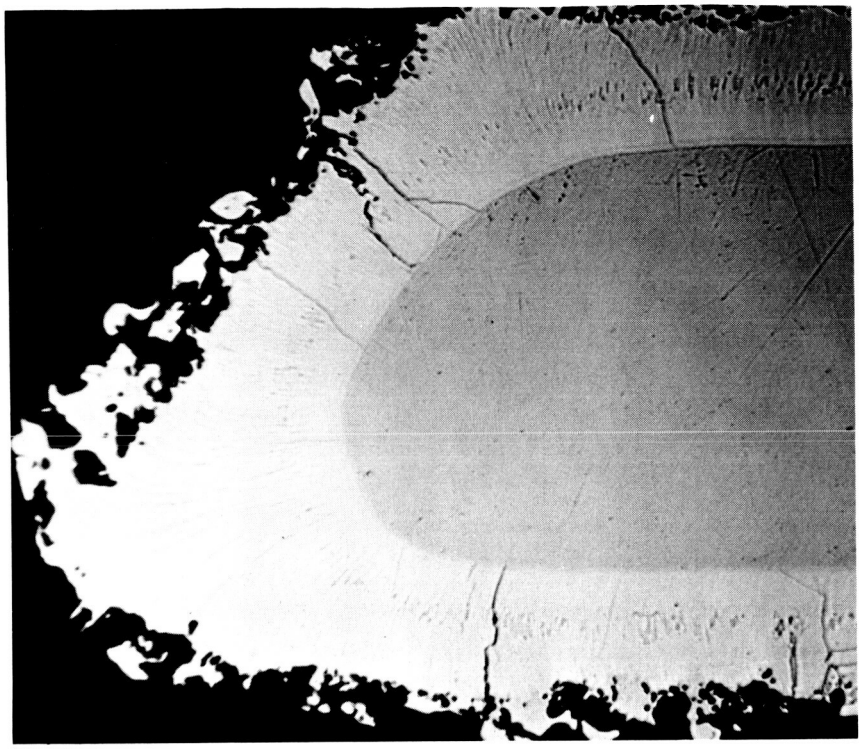

B3288

(a) Chisel Edge on Panel Rib

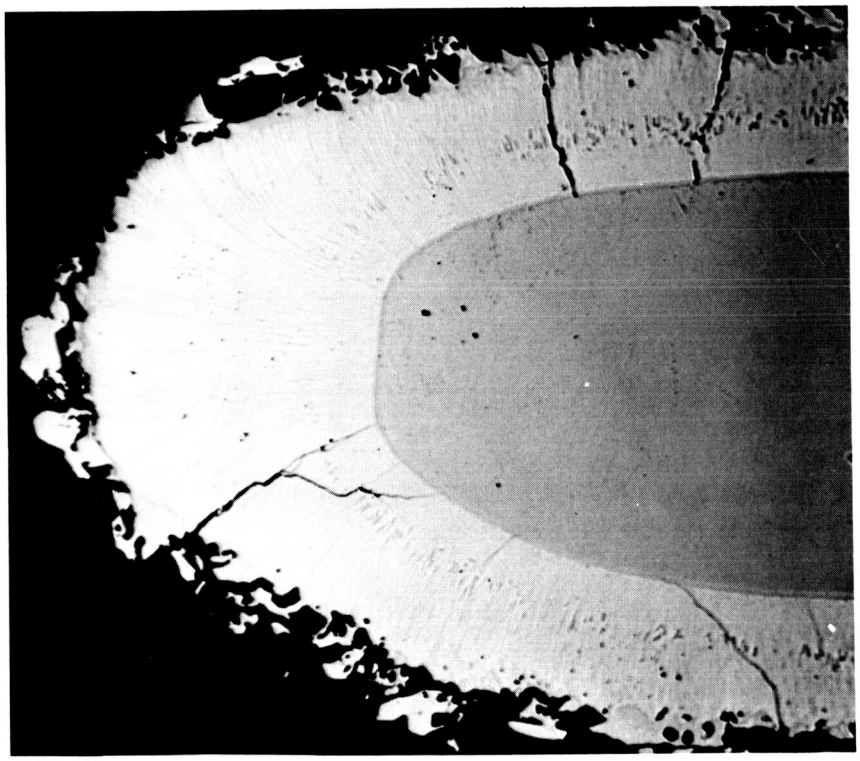

B3287

(b) Sharp Edge on Panel Tab

Figure 66 Effect of Variations in Edge Radius on CMTS Coating Structure, Miniature Panels, Not Etched, 200×.

dense, thick, and complete coverage to edges. These edges have not been striped or oversprayed, and coating application was the same as on flat surfaces. The MTS and CMTS coatings do not require special processing to give excellent edge coverage and protection. No thin spots or V-shape defects are formed.

Variations in edge radius affect only the amount of coating buildup on edges. During fusion, surface tension effects tend to draw the liquid alloy to sharp edges, resulting in an excessive coating thickness (Figure 66). With a uniformly radiused edge, only a minor amount of flow to the edge occurs and thickness is comparatively uniform, as shown in Figure 65. Even here, however, it can be seen that the coating at the very end is about 36-percent thicker than that on flat surfaces [4.75 versus 3.5 mils (0.0121 versus 0.0089 cm)].

The reason that wearout predominates at edges during cyclic exposure at 2600°F (1700°K) and at 2800°F (1811°K), 10 torr (13.33 hN/m^2) is the increased width of fissures initially developed at three unique locations at edges during cooling from high temperatures. As previously mentioned, the coating has a high coefficient of thermal expansion relative to that of the substrate and is placed in tension on cooling. Tensile stresses exceed the fracture strength of the coating at room temperature, and hairline cracks are formed normal to the surface. On flat surfaces, these appear as very fine hairline fissures. They come together on reheating and are healed by diffusion if protected from oxidation by the silicon film on the surface. New fissures open on cooling back to room temperature.

At edges, however, the surface area is greater than the substrate area and the total expansion or contraction of the coating is greater at the surface than at the interface. The volume-to-surface ratio of the coating also increases at edges, which adds further to this differential expansion and contraction; and coating buildup at sharp corners adds still more to the differential. The net result is that the fissures formed on cooling in the end regions are slightly wider than those formed on the flat surfaces.

These wider fissures generally occur in three unique positions – one on each side near the junction of the radius of the edge curvature and the flat surface, and one near the mid-radius position parallel to the plane of the sheet. Typical examples are shown in Figure 66. More than one wide fissure may be formed in any of these regions. At times, only two fissures form at 45 deg to the plane of the sheet, as shown in Figure 65. These fissures are difficult to heal on reheating and are oxidized on the internal surfaces before a protective film can be formed to close the gap at the surface. The difficulty in sealing these fissures is shown by the 2800°F (1811°K) test, in which the surface fissures healed completely on cyclic exposure and the end fissures did not. On cooling, they once again open wider than the fissures on flat surfaces. The net result is an increased rate of oxidation in cyclic exposure at these unique edge locations. The fissures widen more rapidly than those on flat surfaces and thus are the sites at which the initial wearout of the coating occurs. This behavior is a consequence of the geometry of coated thin sheet and is not a limitation in the coating. The coating, in fact, with its excellent ability to form a thick, protective oxide film on the first cycle does a far better job of healing fissures in this region than any formulations previously developed. The high cyclic lifetimes exhibited by both the MTS and CMTS coatings attest to this fact.

Comparative Evaluation of Best Coatings

- Oxidation Behavior

A comparative evaluation of the MTS and CMTS coatings includes analyses of their performance under isothermal and cyclic environmental exposures. A comparison of the performance of the two coatings under cyclic conditions is shown in Figure 67. The median of the probability distribution determined on the basis of the Weibull analysis of cyclic life is shown in this figure. A comparison of the lifetimes of the MTS and CMTS coatings under both cyclic and isothermal conditions is shown in Table 17. The cyclic life is represented in this table in terms of total cumulative hours at maximum temperature to provide a convenient comparison with lifetimes under isothermal conditions. On the basis of the data shown in Figure 67 and Table 17, the performance of the two coatings under each set of conditions was compared, and for each set the coating with the better performance was noted. The criteria for performance evaluation were based on visual examination of the specimens for evidence of substrate oxidation. These comparisons are summarized in Table 18. On the basis of this table, the MTS coating would be favored at 2600° F (1700° K), whereas at 2800° F (1811° K) the CMTS coating would be slightly favored. However, bend ductile-brittle transition temperature tests showed that after cyclic exposure at 2800° F (1811° K), 10 torr (13.33 hN/m^2) and 1 torr (1.33 hN/m^2) the CMTS edges were embrittled. The MTS coating provided better protection of the edges under all conditions of exposure and is a better coating, both at 2600° and at 2800° F (1700° and 1811° K), based on bend ductility as a performance criterion.

The structure of the two coatings was similar over the temperature and pressure ranges studied. Examples of the structural similarity presented in Figures 68 and 69 show the same coating and oxide layer thicknesses for both coatings after similar exposures. In addition, the degree of fissure-widening at 2600° F (1700° K) is similar. For example, in Figures 68a and b the entire structure, including the nature of the fissures, is similar after long exposures — 426 cycles for the MTS coating and 374 cycles for the CMTS coating. At 2800° F (1811° K) (Figure 69b), there is no widening of the fissures in either of the coatings at 1.0 torr (1.33 hN/m^2), and the structures are similar at 0.1 torr (0.13 hN/m^2) although the MTS coating is near wearout.

Nondestructive testing measurements based on eddy current techniques were the same for the MTS and CMTS coatings, in both the green and the fused condition. These NDT techniques were useful in controlling the thickness and uniformity of the coatings on all specimens. The reproducibility in the application of coatings resulting from the use of NDT techniques was reflected in the slopes of the Weibull curves. The steep slopes of these curves indicated a high consistency in the performance of the coatings, which, in turn, reflected a high consistency in the application of the coatings.

- Mechanical Properties

The mechanical properties of the MTS and CMTS coating systems as measured by bend ductile-to-brittle transition temperature, room-temperature, and elevated-temperature tests, and creep tests in air and vacuum are comparable in most respects. As-coated samples, as well as those exposed for up to 100 cycles at 2600° F (1700° K) at 1 — 10 torr (1.33 to 13.33 hN/m^2), are ductile in bending (90 deg - 4t bend) at liquid nitrogen temperatures. The MTS samples exposed for the minimum cyclic life, as established by the

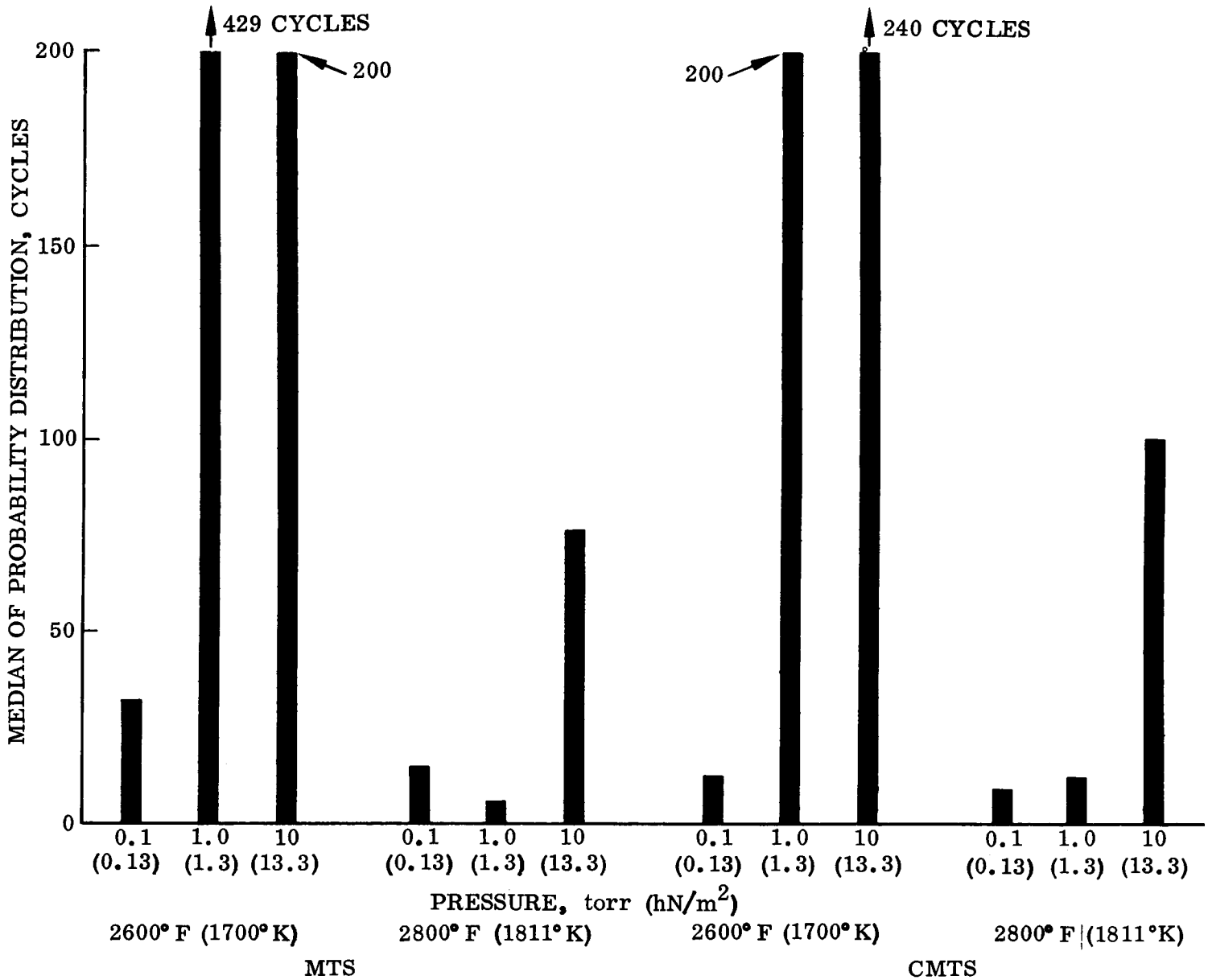

Figure 67 Median of Probability Distribution for Cyclic Life of MTS and CMTS Coatings at 2600° and 2800° F (1700° and 1811°K), 0.1, 1.0, and 10 Torr (0.13, 1.3, 13.33 hN/m^2).

TABLE 17. – COMPARISON OF COATING LIFETIMES UNDER ISOTHERMAL AND CYCLIC OXIDATION EXPOSURE CONDITIONS

Coating	Temperature °F (°K)	Type of Exposure	Lifetime, hr[a]		
			Pressure		
			0.1 Torr (0.13 hN/m^2)	1.0 Torr (1.33 hN/m^2)	10 Torr (13.33 hN/m^2)
MTS	2600 (1700)	Isothermal[b]	>200, >200	>167, >167, >200, >215	>310, >310
		Cyclic[c]	13 20 26	>270 >270 >270	79 125 162
CMTS		Isothermal[b]	12, 12	>141, 140	>247, >247
		Cyclic[c]	8 9 10	56 125 >230	100 150 200
MTS	2800 (1811)	Isothermal[b]	18, 18	5, 5	80, 80
		Cyclic[c]	8 9 11	3 4 5	35 48 75
CMTS		Isothermal[b]	43, 43	5, 5	80, 80
		Cyclic[c]	6 8 10	4 6 13	46 63 80

[a]Cyclic life is the total cumulative time at temperature, based on an effective time of 37 min at maximum temperature during each cycle.

[b]Lifetimes are for individual specimens.

[c]Lifetimes are as follows: Lowest cyclic life; median cyclic life from Weibull plots; highest cyclic life.

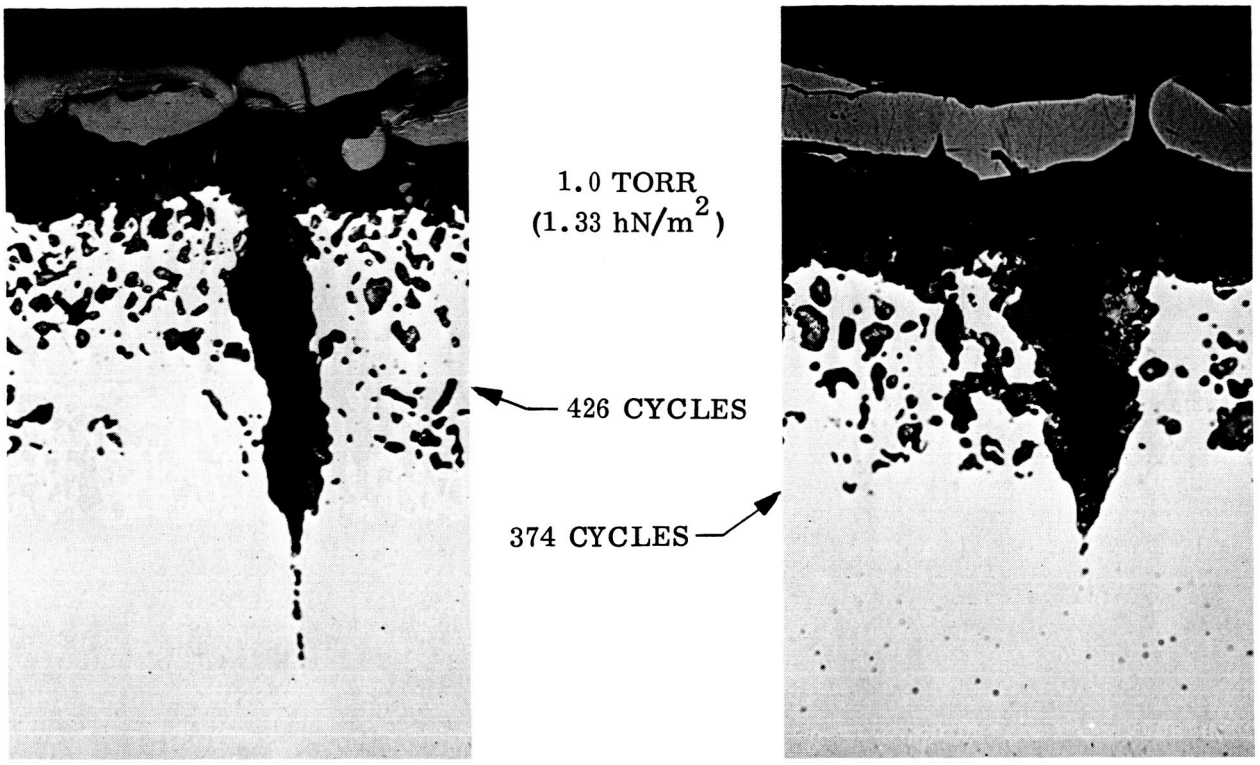

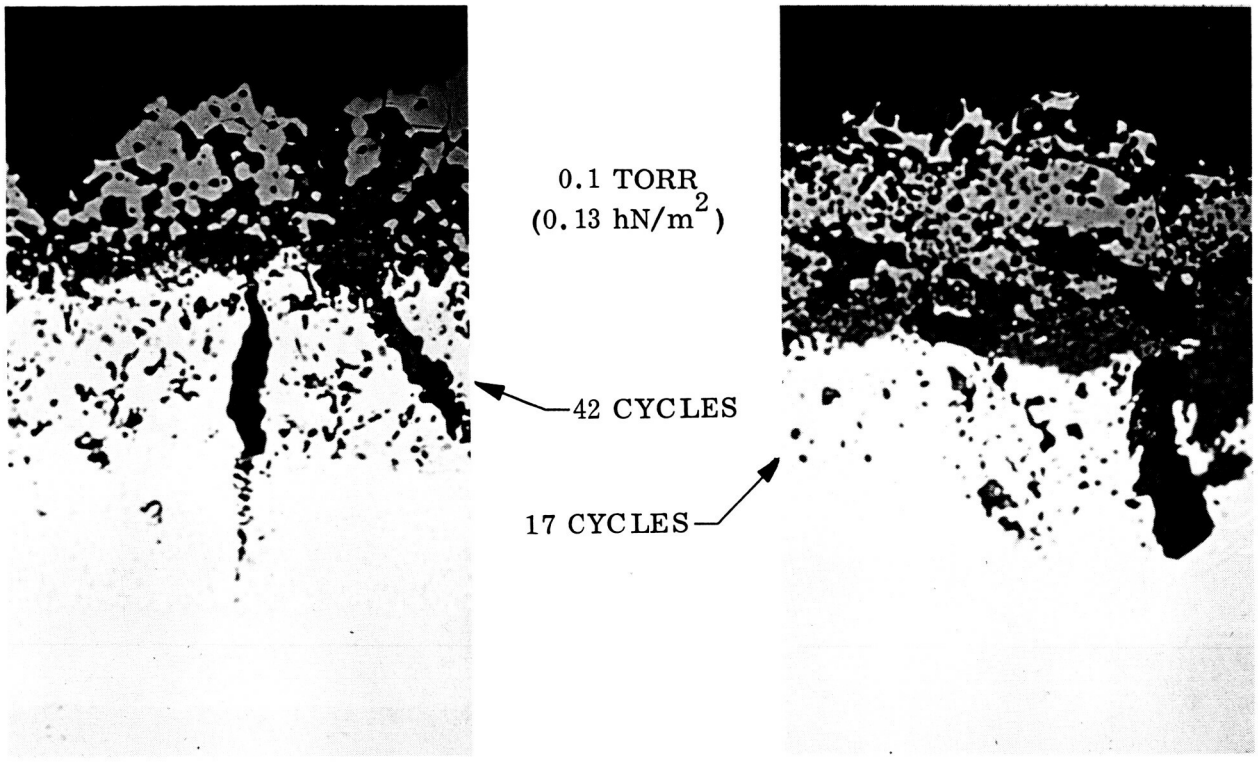

(a) MTS (b) CMTS

Figure 68 Structure of MTS and CMTS Coatings After Cyclic Exposure at 2600°F (1700°K). Not Etched, 500×

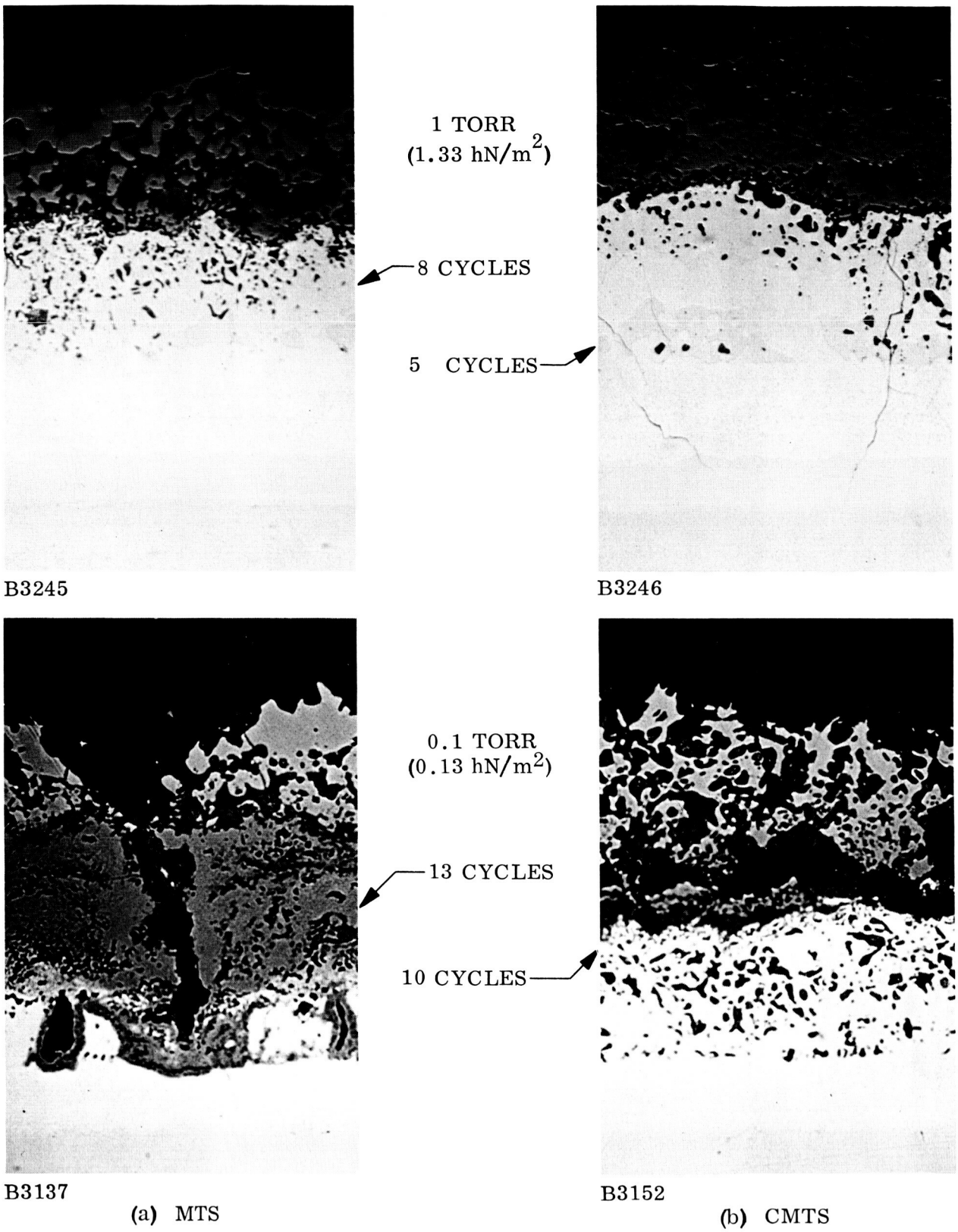

Figure 69 Structure of MTS and CMTS Coatings After Cyclic Exposure at 2800° F (1811° K), Not Etched, 500×.

TABLE 18. – SUMMARY OF MTS AND CMTS COATING PERFORMANCE COMPARISONS

Temperature, °F (°K)	Pressure, torr (hN/m^2)	Type of exposure	Coating[a]	
			MTS	CMTS
2600 (1700)	0.1 (0.13)	Isothermal	X	
		Cyclic	X	
	1.0 (1.33)	Isothermal	X	
		Cyclic	X	
	10 (13.33)	Isothermal	X	
		Cyclic		X
2800 (1811)	0.1 (0.13)	Isothermal	–	X
		Cyclic	–	–
	1.0 (1.33)	Isothermal	–	–
		Cyclic		X
	10 (13.33)	Isothermal	–	–
		Cyclic		X

(a) X = Better performance.
– = Equivalent performance.

Wiebull distribution, at 2800° F (1811°K), 10 torr (13.33 hN/m^2) and 1 torr (1.33 hN/m^2) also are ductile in bending at -321° F (77°K). The CMTS samples, on the other hand, exposed for half- and full-minimum cyclic lifetimes at 10 torr (13.33 hN/m^2) and half the minimum cyclic lifetime at 1 torr (1.33 hN/m^2) edge cracked on bending in liquid nitrogen. Edge cracking in bending indicates that wearout has been initiated at the edges and the sample is contaminated with oxygen in a local region. No visual evidence of wearout exists on the surface. This coating does not provide as good protection to edges at 2800° F (1700°K) as does the MTS coating.

The tensile elongation from room temperature to 1400° F (1033°K) averages 15 percent, which is about two-thirds that of uncoated sheet for both systems. The elongation at 2600° – 2800° F (1700° – 1811°K) is between 35 and 55 percent as-coated. The two systems have equally good ability to retain high ductility after cyclic exposure to air at high temperatures and reduced pressures.

The yield and ultimate strengths are comparable for the two systems and are in good agreement with the values for uncoated Ta-10W at all temperatures after a wide range of cyclic exposures. A comparison of the as-coated yield strengths at four different temperatures is given in Figure 70. The strength values for the coated samples are shown for two different methods of stress calculations for the yield strength – one based on cross-sectional area of the sheet before coating and the other based on residual cross-sectional area of the sheet after coating. The first method assumes that the strength contributed by the coating just equals the strength of the metal removed in applying the coating; the second method assumes that the coating has no strength and does not carry any portion of the load. The two values for each system are compared with the strength of uncoated Ta-10W.

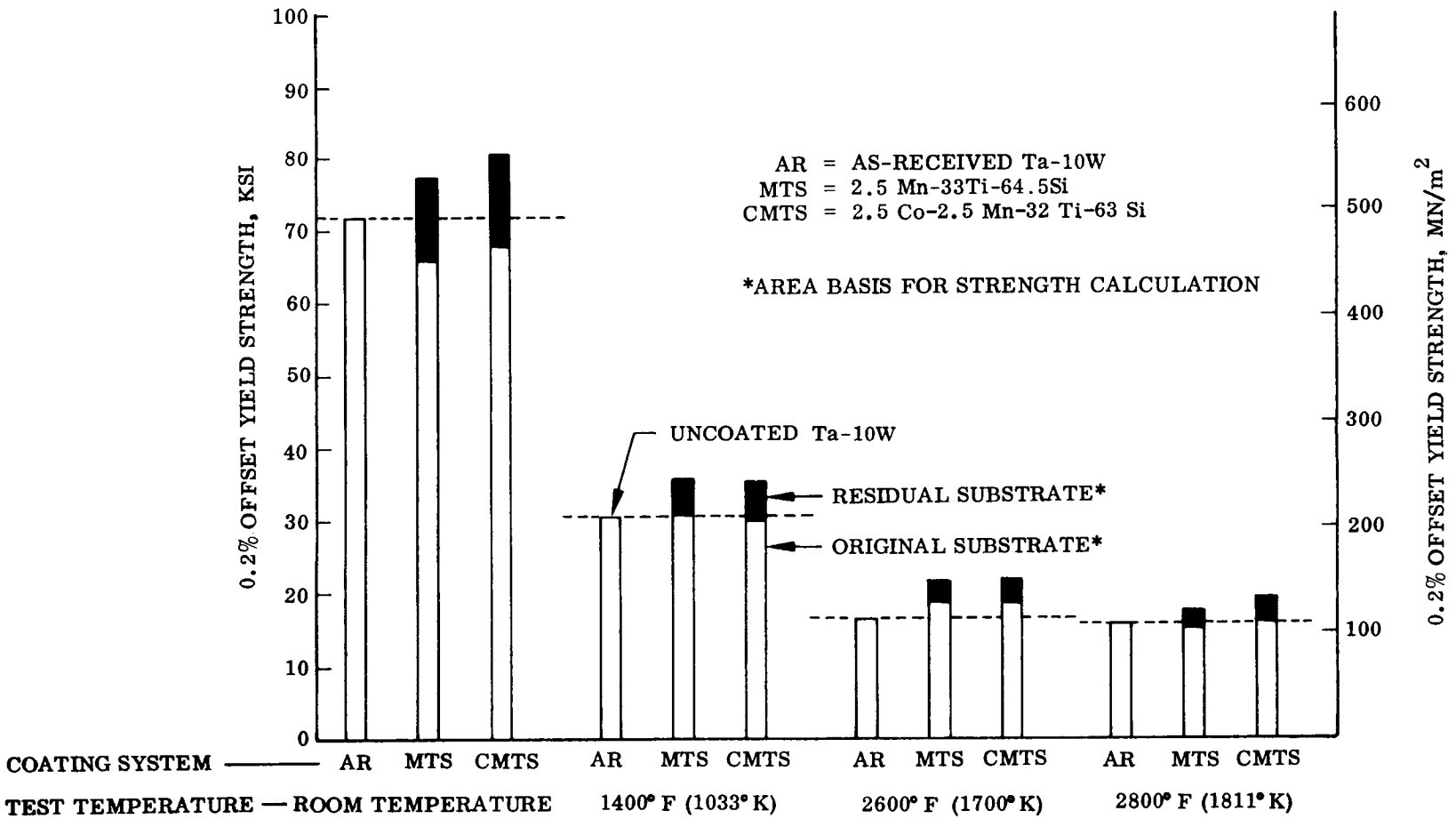

Figure 70. Effect of Coatings on Yield Strength of Ta-10W.

As shown in Figure 70, strength calculations based on residual substrate are much higher than those of Ta-10W, clearly indicating that the coatings do carry a significant amount of load at all temperatures and contribute to the strength of coated thin-gage sheet. Coated sheet is a true composite material at all temperatures. Compared with the values for Ta-10W, the strength values calculated on the basis of original sheet thickness before coating are lower at room temperature; equal at 1400° F (1033° K); higher at 2600° F (1700° K); and lower at 2800° F(1811° K). This indicates that the contribution of the coating to the strength of the composite varies with temperature, reaching a maximum at 2600° F (1700° K). In comparing both systems, the CMTS coating appears to be slightly stronger than the MTS coating at room temperature, but the two coatings are comparable in strength at elevated temperatures.

Since the strength of the substrate is known as a function of temperature, and the residual cross-sectional area of the substrate is known, an estimate can be made of the actual coating strength. The substrate strength times the residual substrate area gives the total load at yield for the substrate at any temperature. Subtracting this value from the total measured load of the composite at yield gives the load actually carried by the coating. If the effective cross-sectional area of the coating is known, this load can be converted to coating strength in pounds per square inch (MN/m^2).

At present, the effective thickness of a coating with respect to its load-carrying ability is not known. Coatings tend to have layered structures, with a wide range of compositions and structures in each layer. The representative structures for the as-coated MTS and CMTS coatings are shown in Figure 52 (in the section on coating structure and composition). Total coating thickness averages from 3.5 to 4.0 mils (0.0089 to 0.0102 cm). The outer surface is uneven, and the net coating thickness is about 3 mils (0.0076 cm). The inner third of this is a fully dense, fine-grain, uniform deposit of (Ta, W) Si_2 with a thin, dense interface layer of $(Ta, W)_5 Si_3$. The outer two-thirds of the coating is a mixed structure of tantalum, tungsten, titanium, manganese, and cobalt silicides of the M_5Si_3 and MSi_2 type. Many phase boundaries and microcracks exist in this region. For the purpose of these calculations, it has been assumed that only the inner 1 mil (0.00254 cm) of the coating is truly effective in carrying load. The actual effective coating cross section would have to be determined experimentally by physically removing successively greater amounts of coating until the total load at yield begins to decrease.

Using the simplifying assumption that only the inner 1 mil (0.00254 cm) of the coating contributes significantly to strength, the coating strength was estimated from load measurements of the composite at yield by subtracting the portion of the load that is actually carried by the substrate. The results of these calculations are presented in Figure 71. Based on these assumptions, the coating strength is about 30 ksi (207 MN/m^2) from room temperature to 2600° F (1700° K) and is 10 to 15 ksi (69 to 103 MN/m^2) at 2800° F (1811° K). The CMTS coating appears to have a higher strength at room temperature than the MTS coating and comparable strengths at elevated temperatures.

These values are in excellent agreement with the tensile yield strength of bulk disilicides, as shown in Table 19.

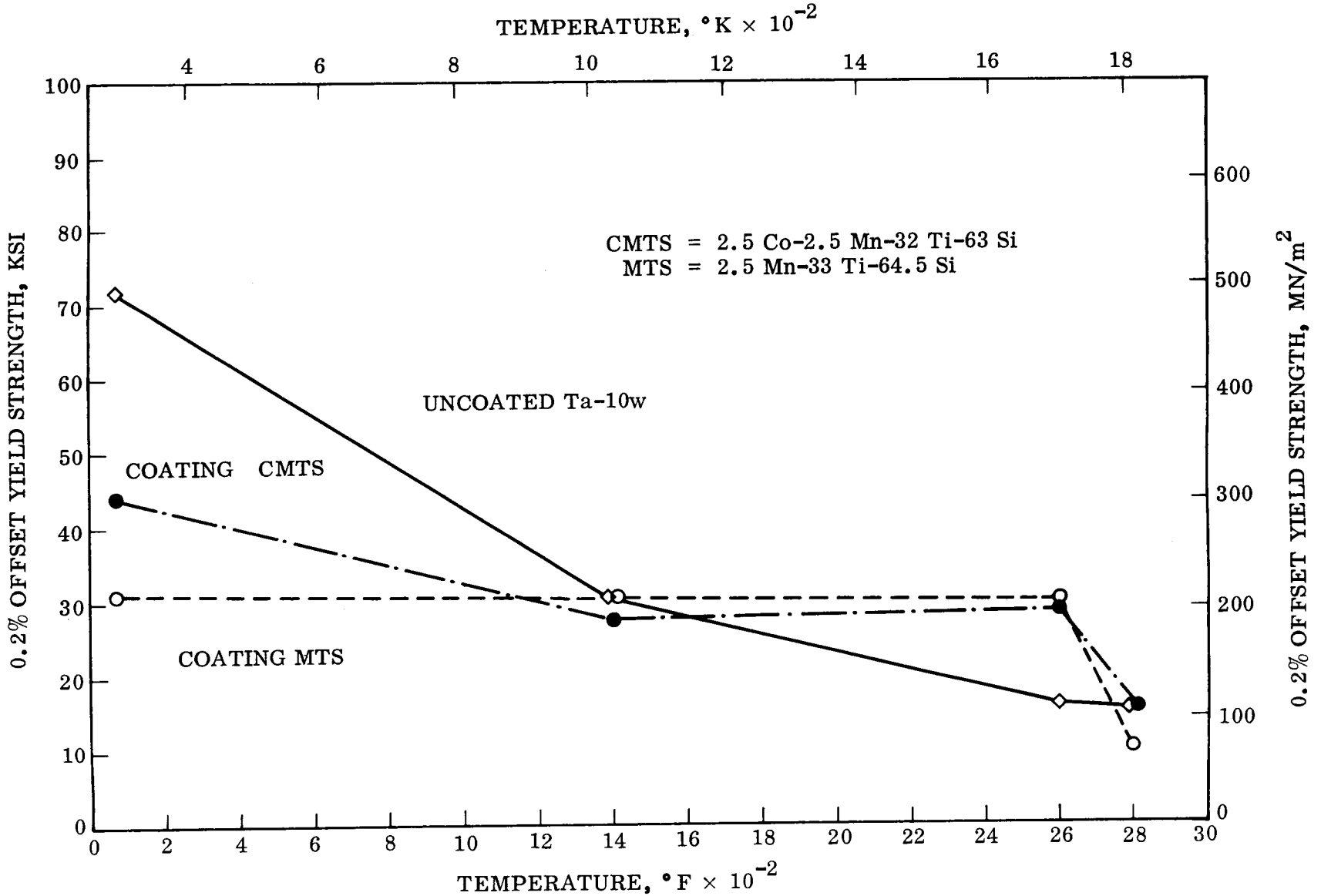

Figure 71 Calculated 0.2-Percent Offset Yield Strength of MTS and CMTS Coatings as a Function of Temperature.

TABLE 19. – TENSILE YIELD STRENGTH OF HOT-PRESSED SILICIDES

Silicide	Temperature Range °C	Temperature Range °K	Yield Strength ksi	Yield Strength MN/m^2	Reference
$MoSi_2$[a]	980 – 1300	1253 – 1573	40 – 43	276 – 298	32
$MoSi_2$[b]	20	293	27 – 29	186 – 260	32
	982	1255	39 – 40	269 – 276	32
	1093	1366	39 – 43	269 – 298	32
	1204	1477	37	255	32
	1316	1589	22 – 23	152 – 159	32
$MoSi_2$[c]	1093	1366	20	138	32
	1204	1477	25 – 26	173 – 180	32
	1316	1589	22	152	32
$TiSi_2$	25	298	21.5	159	33

[a] Fine, nonuniform powder.
[b] Fine, uniform powder.
[c] Coarse powder.

$MoSi_2$ has a yield strength in the range of 30 to 40 ksi from room temperature to 2200° F (1477° K). Strength seems to increase slightly with increased temperature and is probably the brittle fracture stress since the compound has little ductility in this range. Above 2200° F (1477° K) the silicide becomes ductile at low strain rates and the strength decreases with increasing temperature.

The significance of this behavior is that although the strength of the substrate alloy decreases with increasing temperature, the strength of the coating remains the same. Thus, the coating contributes more to the strength of the composite as temperature is increased. Finally, a temperature is reached at which the coating softens and its contribution to strength declines as the metal once again becomes the stronger of the two components in the composite. The data for the MTS coating show that the coating strength is greater than that of the metal from 1400° to 2600° F (1033° – 1700° K) but that the metal is stronger at 2800° F (Figure 71).

These calculations indicate that current methods of computing the strength of coated metals on the basis of cross section before coating will give strength values that are too low at low temperatures and too high at high temperature. On the other hand, strengths calculated on the basis of residual substrate will be too high at all temperatures, since this ignores any contribution from the coating. Of the two approaches, the use of original substrate thickness before coating gives the more reasonable estimate of composite strength, since it is the more conservative of the two values. The best approach – and the one that should be used in the design of any coated structure – is to determine the effective cross section and strength of the coating as a function of temperature and then treat the coated structure as a true composite material in calculating its strength. This is important, of course, only in the use of structures of thin-gage sheet, where the coating represents a reasonable fraction (10 percent or more) of the total thickness.

In addition to their effect on strength, the MTS and CMTS coatings have a significant effect on deformation behavior at elevated temperatures. At room temperature, the coating will spall from the surface when large amounts of plastic strain occur after the yield point is passed. The deformation behavior is not unlike that of the uncoated substrate. The stress-strain curves are similar in shape, including the presence of an upper and lower yield strength and a pronounced yield drop. At elevated temperatures, however, the coating does not spall on straining and large amounts of plastic deformation can be accommodated. In creep, strains greater than 2 percent have been obtained at 2600° to 2800°F (1700 to 1811°K) in air without rupture of the coatings or disturbance of their protective mechanisms. In tests of commercial silicide coatings on columbium alloys under independent studies at the Lockheed Palo Alto Research Laboratory, creep strains of up to 20 percent have been sustained at 2800°F (1811°K) without coating breakdown.

Coated samples tested in tension at elevated temperatures have very high, uniform elongation, whereas uncoated Ta-10W deforms locally and develops a marked necked-down region at fracture. This behavior is shown in Figure 72. Uncoated Ta-10W tested in tension at 2600°F (1700°K) necked down in the center and fractured with a total elongation of 46 percent. The width at the fracture is 0.19 in. (0.482 cm). The MTS coated sample, on the other hand, elongated 35 percent and did not develop a necked-down region. Width at the fracture is 0.23 in. (0.584 cm). The initial width in each case is a nominal 0.25 in. (0.635 cm).

A longitudinal cross section through the test region (Figure 72c) shows that the sample deforms by local straining of the substrate just below the fissures in the coating. A series of small local necks is developed at regular intervals along the deformed section. The substrate material, which has continuous blocks of coating on either side, is uniformly strained, but to a much lesser extent.

The development of local necked regions in the substrate at coating fissures is clearly shown by scanning electron micrographs of the edge (Figure 73). This figure also shows two different sets of fissures in the coating. The original coating fissures prior to straining are generally parallel and are perpendicular to the stress direction (specimen axis). A second set of fissures appears on the surface at a 45-deg angle to the stress axis. Clearly, these fissures were formed by the shear of the coating during straining, as a result of tensile stresses in the coating. Scanning electron micrographs reveal various width and degrees of local deformation beneath the fissures over the entire surface. The fissures appear to have formed at different times. Had they developed simultaneously at some critical stress level, the deformation at each fissure should be more or less uniform.

These observations indicate that the metal is strengthened as a composite material by intact blocks of coating on the surface. Where cracks or fissures exit, the coating contributes no strength, and deformation will occur in these regions upon application of a tensile load. The strength of Ta-10 W increases with increased strain. For example, at 2600°F (1700°K) the flow stress increases from 12 ksi (82.7 MN/m^2) at 0.2-percent strain to 18.5 ksi (127 MN/m^2) at 1.2-percent strain. As the resistance to straining increases, the fracture stress in some areas of the coating is exceeded and new cracks develop. Deformation then shifts to these areas, which are now reduced in strength, and a new region of local strain develops. This process keeps repeating, with a resultant high, uniform elongation and no areas of excessive local deformation. This explains why many samples tested at 2800°F (1811°K) had 60- to 65-percent uniform elongation compared with 45- to 50-percent for uncoated tantalum, which necked at the ultimate load. Both the MTS and CMTS coatings had a similar behavior.

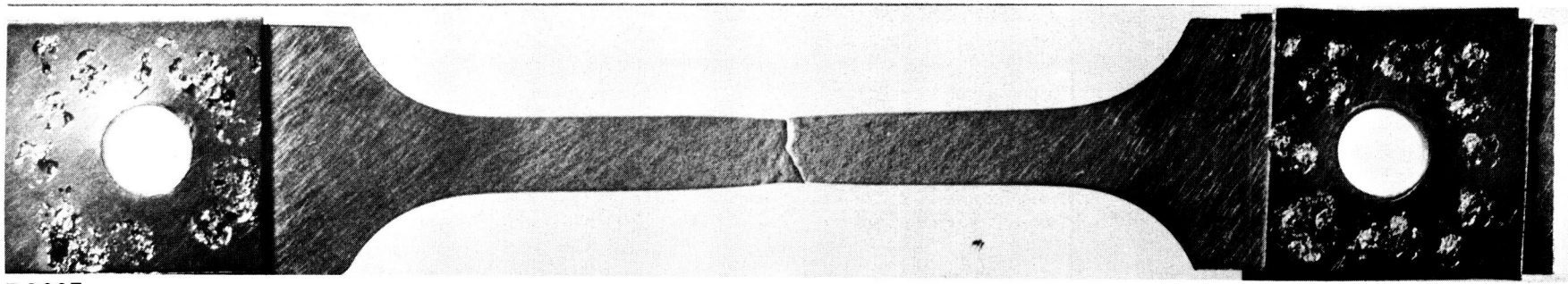

B2007 2×

(a) Uncoated Ta-10W, Localized Deformation

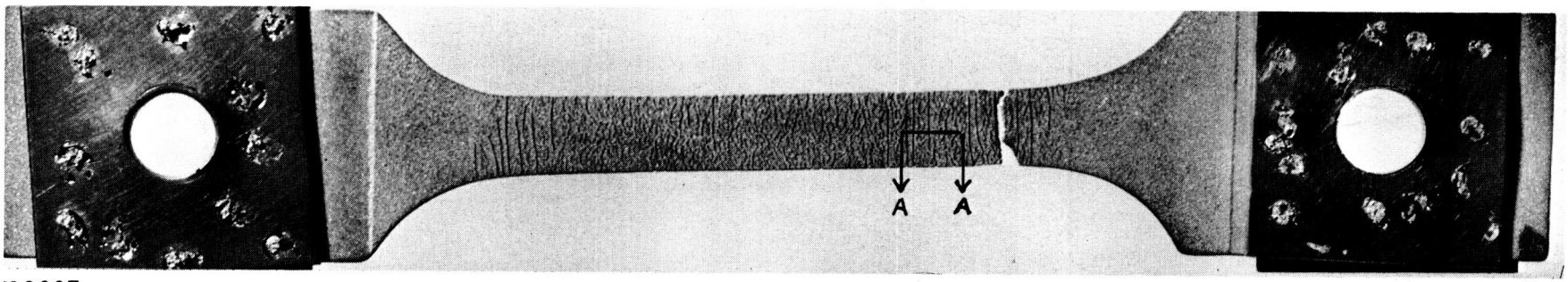

B2007 2×

(b) Ta-10W/MTS, As-Coated, Uniform Elongation

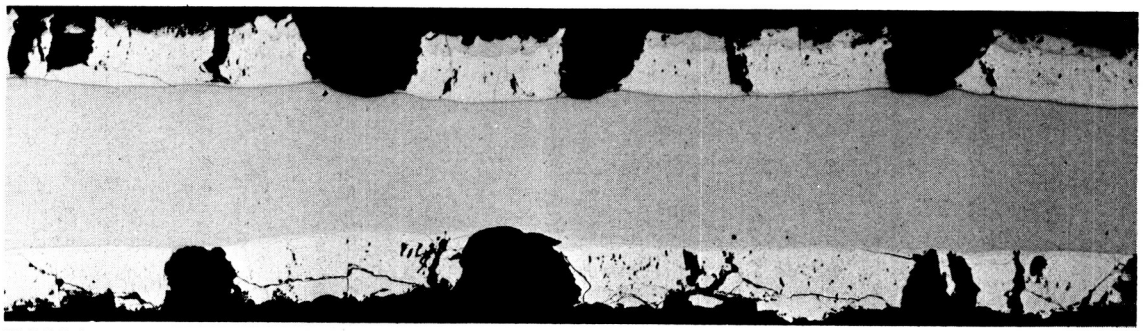

B2024 100×

(c) Longitudinal Cross Section A-A

Figure 72 Effect of Surface Coating on Deformation Behavior During Tensile Test at 2600° F (1700° K).

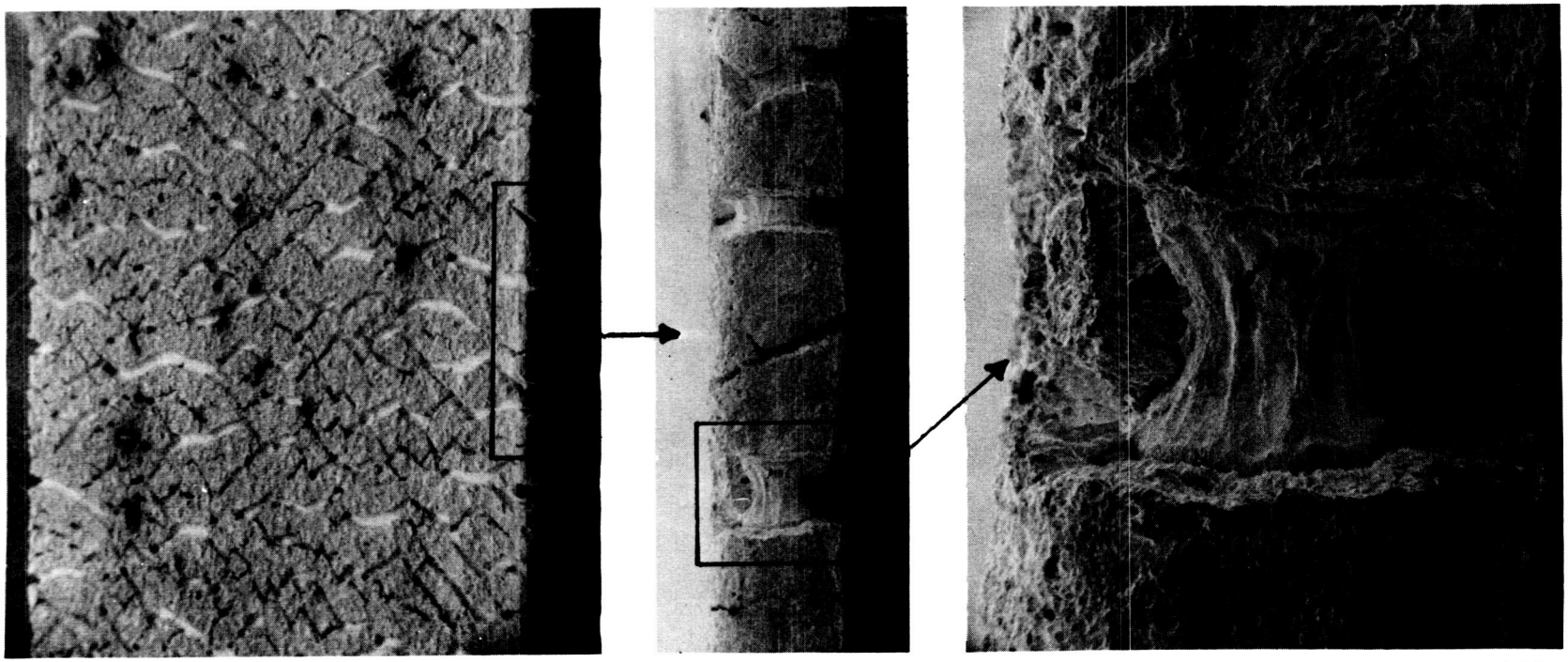

Figure 73 Scanning Electron Micrographs of MTS-Coated Ta-10W Tested in Tension to 46-Percent Elongation at 2600° F (1700° K).

- Emittance

The normal spectral emittance at a wavelength of 0.65 μm was similar for both coatings at all combinations of environmental conditions and exposed levels. The emittance of both coatings reached a high value within a minute of reaching maximum temperatures. The similarity in emittance properties can be related to the similarity in the oxide layer that forms very rapidly upon exposure.

For comparative purposes, the emittance of Sylvania-coated R512 coatings was determined after exposures of 1 and 10 cycles at 2600°F (1700°K), 10 torr (13.33 hN/m^2). The results are presented in Table 20. The values determined for the MTS and CMTS coatings were higher than those for the R512 coatings. At this temperature and pressure, the emittance of the MTS and CMTS coatings was from 0.85 to 1.0.

TABLE 20. – SUMMARY OF NORMAL SPECTRAL EMITTANCE MEASUREMENTS OF R512 COATINGS

[2600°F (1700°K), 10 torr (13.33 hN/m^2)]

Coating	Cycles at 2600°F (1700°K), 10 torr (13.33 hN/m^2)	Temperature, °F (°K)				
		Heating			Cooling	
		1870 (1294)	2200 (1478)	2600 (1700)	2200 (1478)	1870 (1294)
R512A	1	–	–	0.84	0.67	0.62
	–	–	–	0.84	(a)	–
	10	0.46	0.67	0.72	0.67	0.46
R512C	1	–	–	0.72	0.67	0.49
	1	–	–	0.72	0.67	0.49
	10	(b)	–	–	–	–
R512K	1	–	–	0.77	0.73	0.37
	1	–	–	0.75	0.67	0.37
	10	0.49	0.78	0.80	0.73	0.43

[a]Test discontinued because of arcing at the electrode.

[b]Coating wore out during oxidation exposure.

APPLICABILITY TO STRUCTURAL COMPONENTS

Coating of Complex Parts

During the course of this program, complex configurations coated included miniature rib-stiffened heat-shield panels for simulated reentry environmental testing as well as 16 similar panels and 24 plasma-arc test samples for delivery to NASA. (Drawings of these parts are presented in the section entitled "Materials and Test Specimens.")

Both coatings have an excellent capability for convenient applicability and effective protection of structural components having complex configurations. They can be applied by either dipping or spraying to form a sound, uniform coating. When practical, spraying is the preferable means of application because it provides somewhat better control over coating thickness. This method was used during the program for coating of complex parts. Upon fusion, the coatings flow well into regions such as corners and low reentrant angles forming a uniform coating having the same thickness as that in more readily accessible regions. An as-coated miniature heat-shield panel representative of the panels tested in simulated reentry environments is shown in Figure 74.

A sound, continuous coating was produced in all portions of the panel, including the restricted region between the tab and the panel facing sheet. The only difficulties encountered involved the preparation of edges. Because of the way in which these panels were fabricated, it was not possible to detail the edges before welding, and the channel region under the tabs was too small for the relatively large alumina shapes to be effective in vibratory finishing. The edges, therefore, were hand-finished, and some edge locations had limited accessibility. This would not be a problem in production components, however, as the fabrication procedure could be designed to include edge finishing before welding. The effect of inadequate edge preparation on coating structure is shown in Figure 66. In Figure 66(a) the substrate edge was chisel-shaped and there was a sharp edge on the substrate, as shown in Figure 66(b). In both cases, an altered coating volume-to-substrate area ratio led to a somewhat different coating structure and a change in the stresses in the coating that are the result of differences in thermal expansivity.

A metallographic analysis was conducted with a CMTS-coated panel in the as-coated condition, and photomicrographs are shown in Figures 75 and 76. The low-magnification photomicrograph in Figure 75(a) shows both the quality of the electron-beam welded joint and the coating uniformity in the weld region. The coating at the top of the photomicrograph is on the panel facing sheet, and the coated areas in the lower part of the photomicrograph are within the restricted area between the tab and the panel facing sheet. These areas were the more difficult to coat, but, as can be seen, an excellent coating was produced. In Figure 75(b), the coating on a well-rounded rib edge is shown. Again, a uniform coating was produced along the surface and around the edge. The structure of the CMTS coating on the inside and outside of the panel facing sheet is shown in Figure 76. At the panel center, the thicknesses of the coating on the inside and outside of the facing sheet are comparable. The inside coating in the area opposite the tab is somewhat thinner than the outside coating; however, a sound coating was produced in all locations.

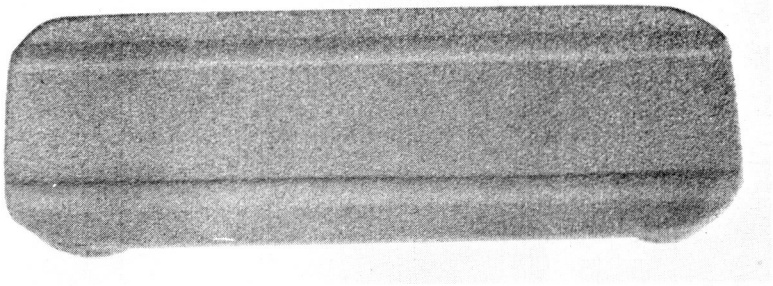

B2054 (a) Top 1.7×

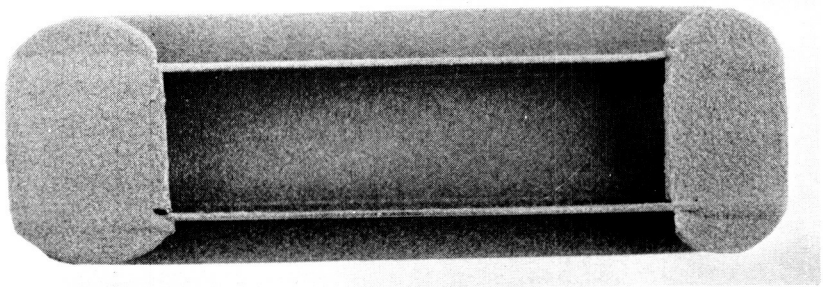

B2053 (b) Bottom 1.7×

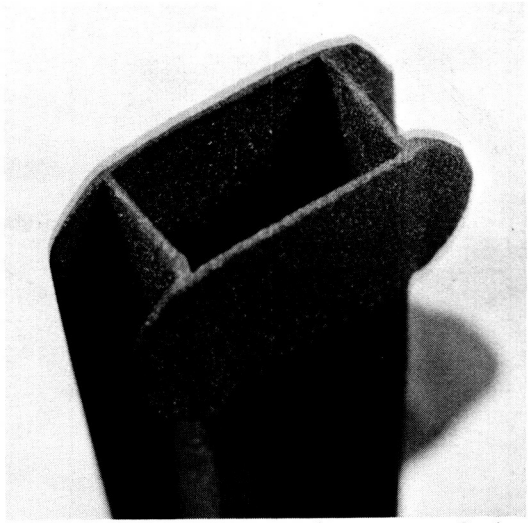

B2055 (c) End 2.4×

Figure 74 As-Coated Miniature Rib-Stiffened Heat Shield Panel

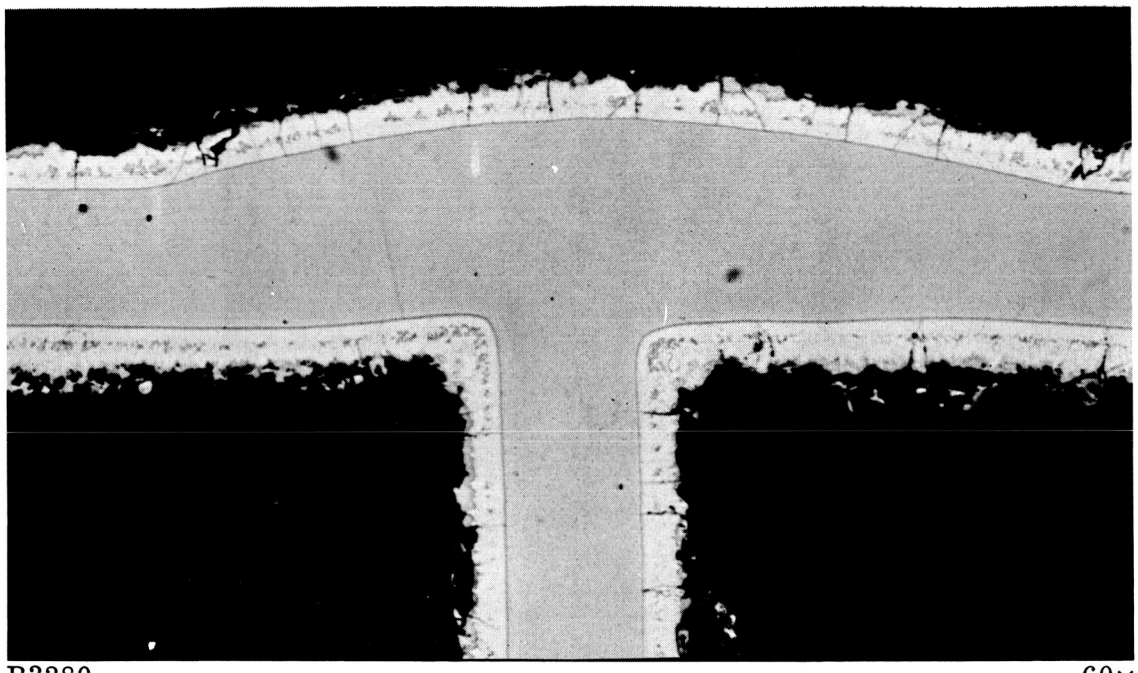

B3280 (a) EB Weld Joint 60×

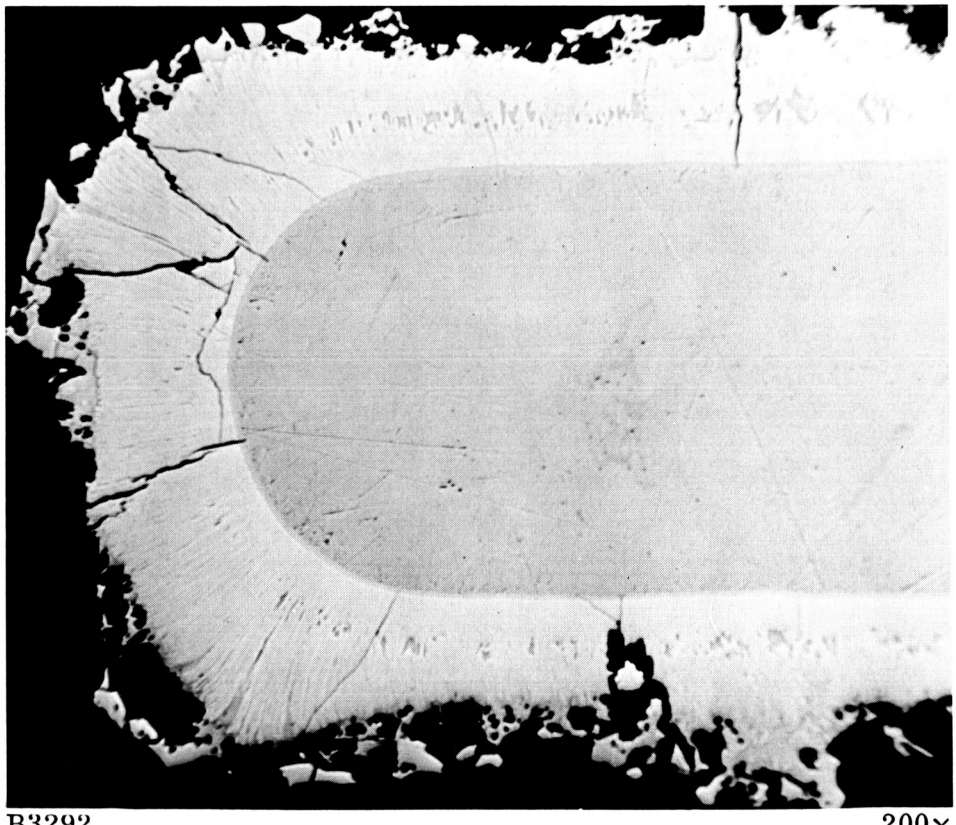

B3292 (b) Rib Edge 200×

Figure 75 CMTS Coating on Miniature Heat Shield Panels, Not Etched. The specimen in (b) was damaged during metallographic preparation.

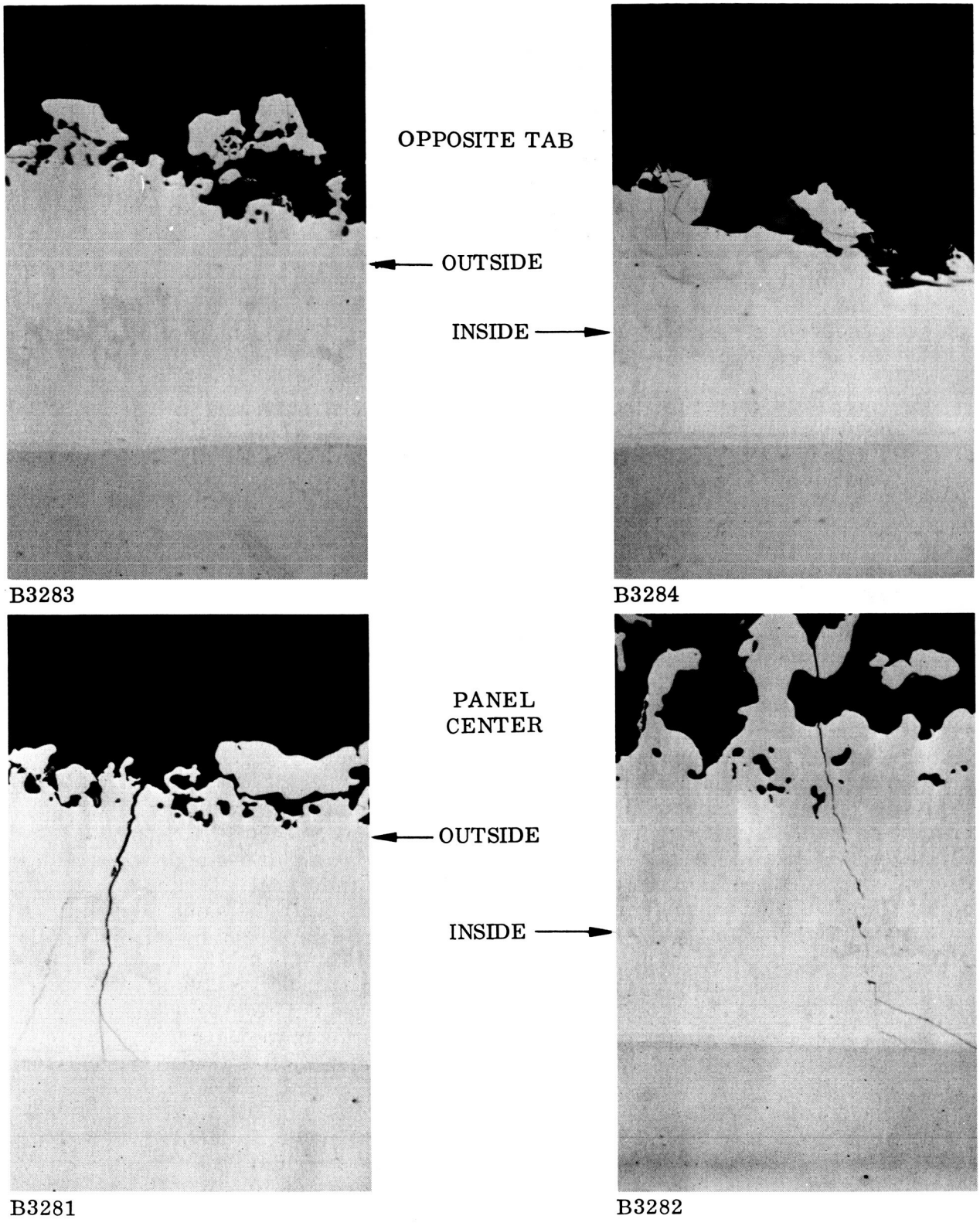

Figure 76 Structure of CMTS Coating on Flat Surfaces of Facing Sheet of Miniature Heat Shield Panels, Not Etched, 500×.

Simulated Reentry Environmental Testing of Panels

Simulated reentry environmental tests were conducted to evaluate the performance of both the MTS and CMTS coatings on structural components under conditions of cyclic stress and temperature at two pressure levels. The temperature/stress schedule for these studies is shown in Figure 77. The stress levels shown represent the stresses in the outer fibers of the ribs. These tests were conducted at 0.1 and 10 torr(0.13 and 13.33 hN/m^2). The test fixture with a panel in place is shown in Figure 78. The loads that were applied to produce appropriate stresses were determined on the basis of the stress analysis presented in the Procedures section of the report.

Eighteen panels were evaluated under the simulated reentry environmental conditions. The results of these experiments are presented in Table 21.

The life-controlling factor for the coatings was coating wearout near the ends of the panels in locations where the edges were not properly prepared. The performance of the coatings was not affected by the cyclic stress conditions and was in reasonably good agreement with the performance of the simple tab-type specimens evaluated earlier in the program. Similar to the results of the earlier evaluations, lifetimes at 2600° F (1700°K), 0.1 torr (0.13 hN/m^2) were limited by oxidation of the coating and silicon loss to the environment. The results indicate that the MTS coating is more tolerant of improperly prepared edges than the CMTS coating.

No deformation occurred in any of the panels, except in two cases where the support and loading fixture was misaligned. The absence of any deformation and the effectiveness of the coatings can be seen in Figure 79. The distortion of one panel caused by misaligned supports and the localized deformation in another panel caused by the load pin bearing directly on the panel can be seen in Figure 80. The deformation in the panels did not affect the coating performances; the coating remained protective.

Panels with each coating were metallographically evaluated after exposure. The structure of the MTS coating after 112 simulated reentries at 2400°F (1584°K), 0.1 torr (0.13 hN/m^2) is shown in Figure 81. The ability of the coating to protect shapes with low reentrant angles is shown in the photomicrograph of the weld joint. During fusion, the coating flowed well into these regions, producing a coating with the same structure as that on flat surfaces. In Figure 81, the effective protection provided by the oxide layer around a tab edge is shown. The oxide layer at 2400°F (1584°K), 0.1 torr (0.13 hN/m^2) is similar to the oxide layer that forms with this coating at 2600°F (1700°K), 1.0 torr (1.33 hN/m^2). This is consistent with conclusions reached earlier regarding the temperature/pressure boundary for the passive-to-active transition in the behavior of this coating; that is, at a lower temperature, there is a lower passive-to-active transition pressure.

Figure 82 shows the structure of the MTS coating at a weld joint and a tab edge after 100 simulated reentries at 2600°F (1700°K), 10 torr (13.33 hN/m^2). In this case, the coating was protective in an edge region where there was a very irregular, chisel-shaped edge, although the coating structure at the edge is different from that along the flat surfaces. The CMTS coating structure after 36 simulated reentries at 2600°F (1700°K), 0.1 torr (0.13 hN/m^2) is shown in Figure 83. The coating is uniform and effective at the weld joint. At the sharp tab edge, however, there is some variation in coating structure and the coating is approaching wearout. The structures of the MTS and CMTS coatings on the outside and inside of the facing sheet after simulated reentry testing at 2600°F (1700°K) are shown in Figure 84. At 0.1 torr (0.13 hN/m^2) the structure of the CMTS coating is

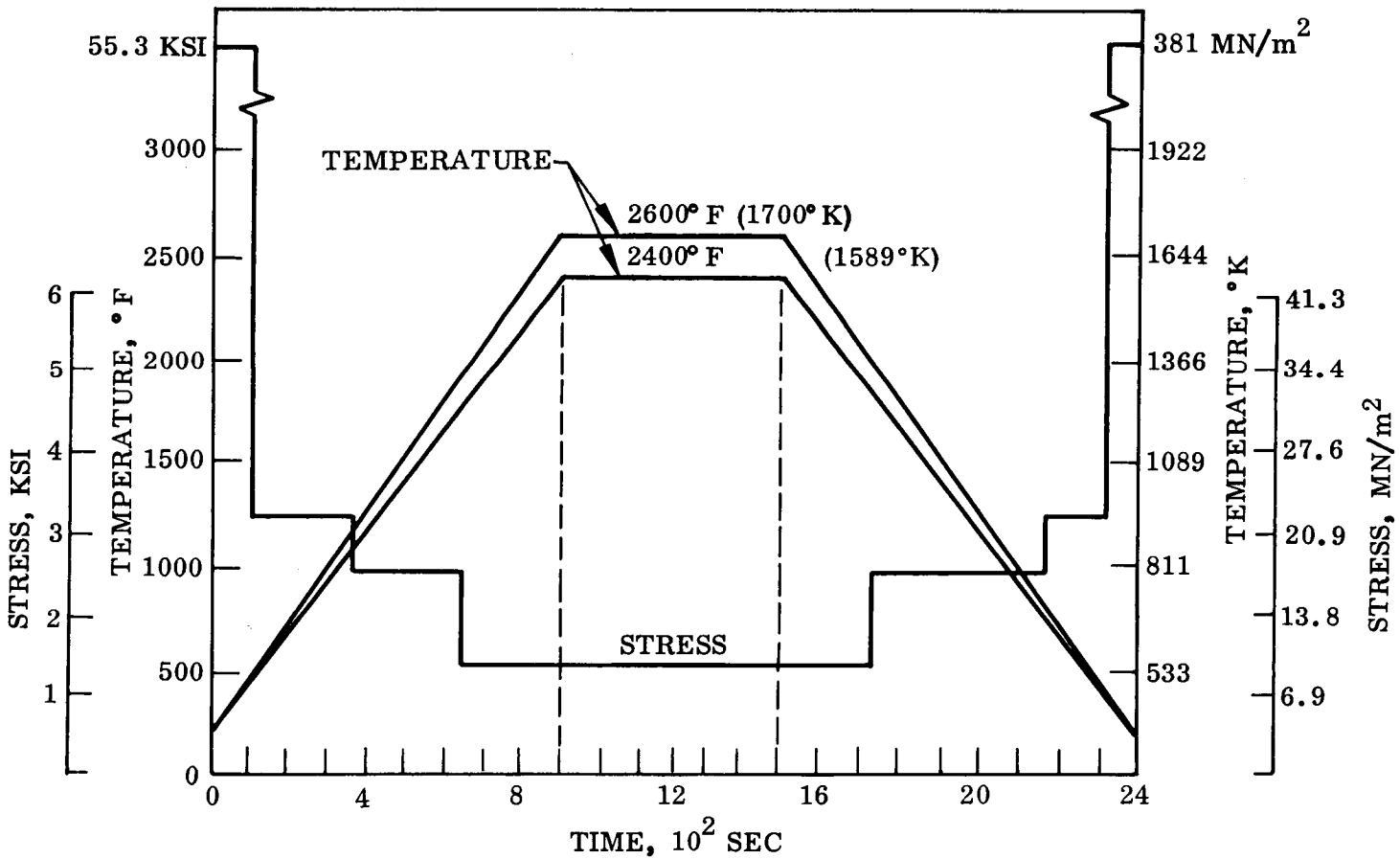

Figure 77 Temperature/Stress Schedule for Simulated Reentry Environmental Testing.

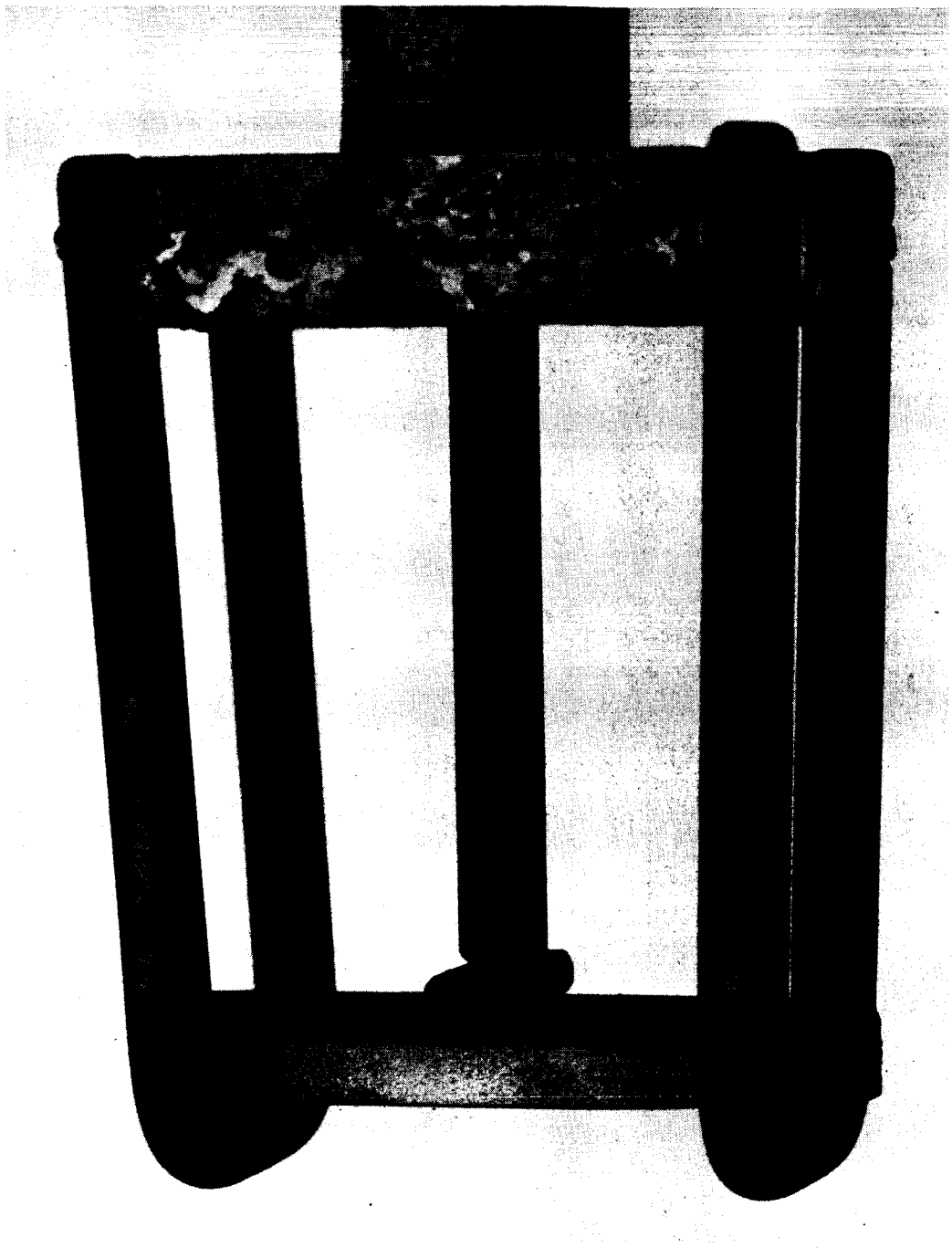

B3093 2×

Figure 78 Test Fixture for Miniature Heat Shield Panel Testing

TABLE 21. – SUMMARY OF SIMULATED REENTRY ENVIRONMENTAL TESTING RESULTS

Temperature		Pressure		Lifetime , Cycles	
°F	°K	Torr	hN/m^2	MTS coating	CMTS coating
2400	1589	10	13.00	> 100 , 20 ,	67 , 52, 45
2400	1589	0.1	0.13	> 112 , 105	67 , 40
2600	1700	10	13.33	100 , 4 [a]	> 100 , 52 , 40
2600	1700	0.1	0.13	15 , 13	36 , 8

[a] Misaligned specimen support resulted in uneven loading and distortion of the specimen; panel removed from test. There was no measurable deformation in the other panels.

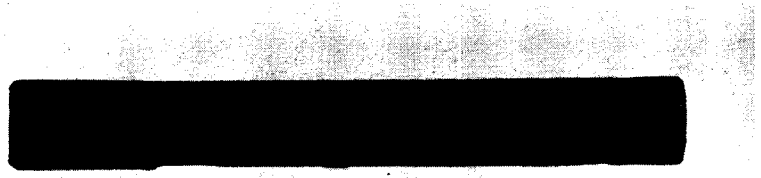

B3083 Side 1.6×

B3082 Top 1.6×

B3081 Bottom 1.6×

(a) CMTS Coating – 112 Cycles, 2400° F (1584° K), 0.1 Torr (0.13hN/m^2)

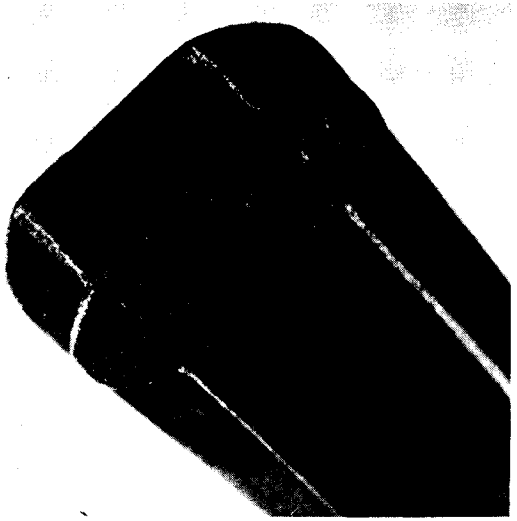

B3217 3×

B3216 1.6×

(b) MTS Coating – 100 Cycles, 2600° F (1700° K), 10 Torr (13.33 hN/m^2)

Figure 79 Miniature Heat Shield Panels After Simulated Reentry Tests

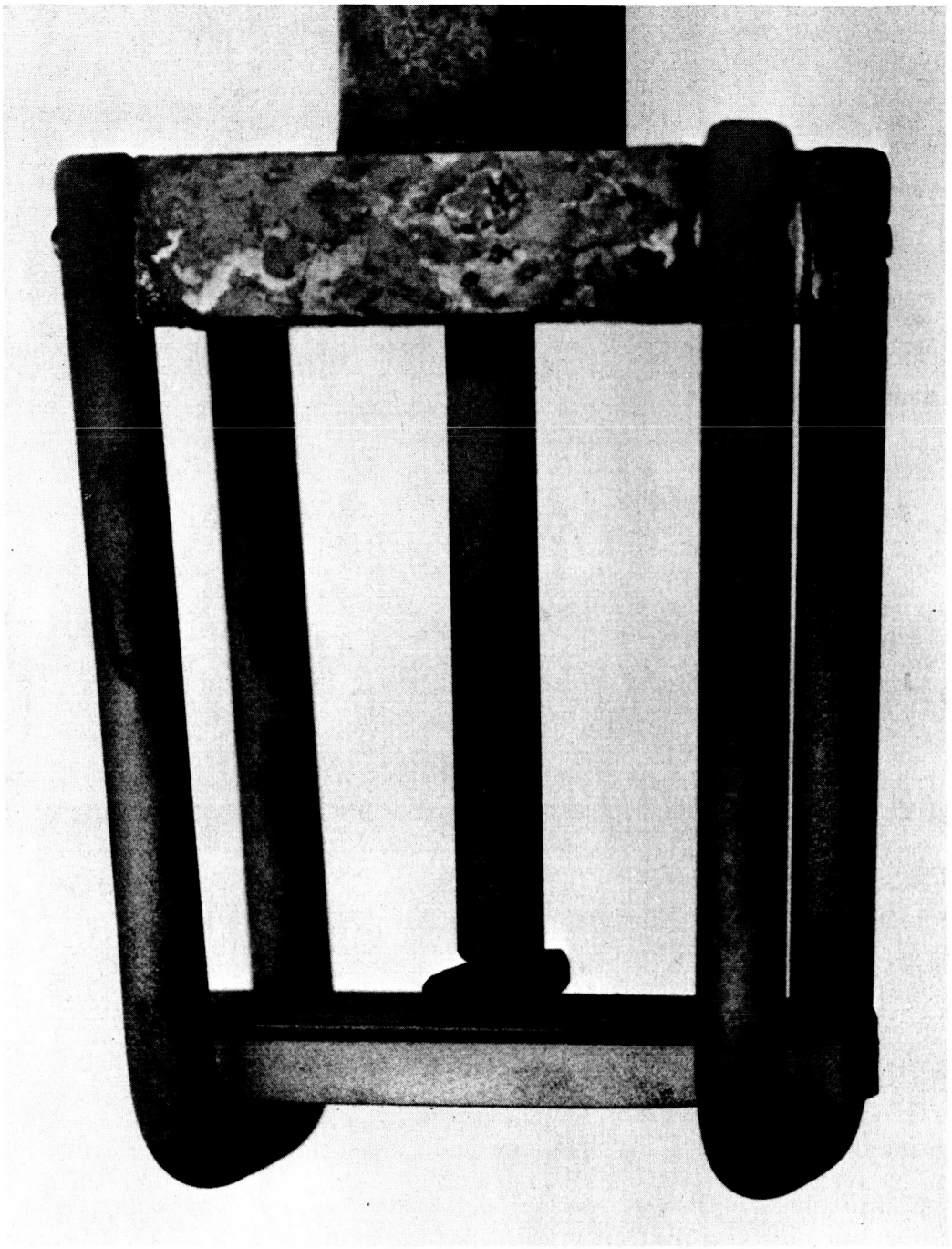

B3093 2×

Figure 78 Test Fixture for Miniature Heat Shield Panel Testing

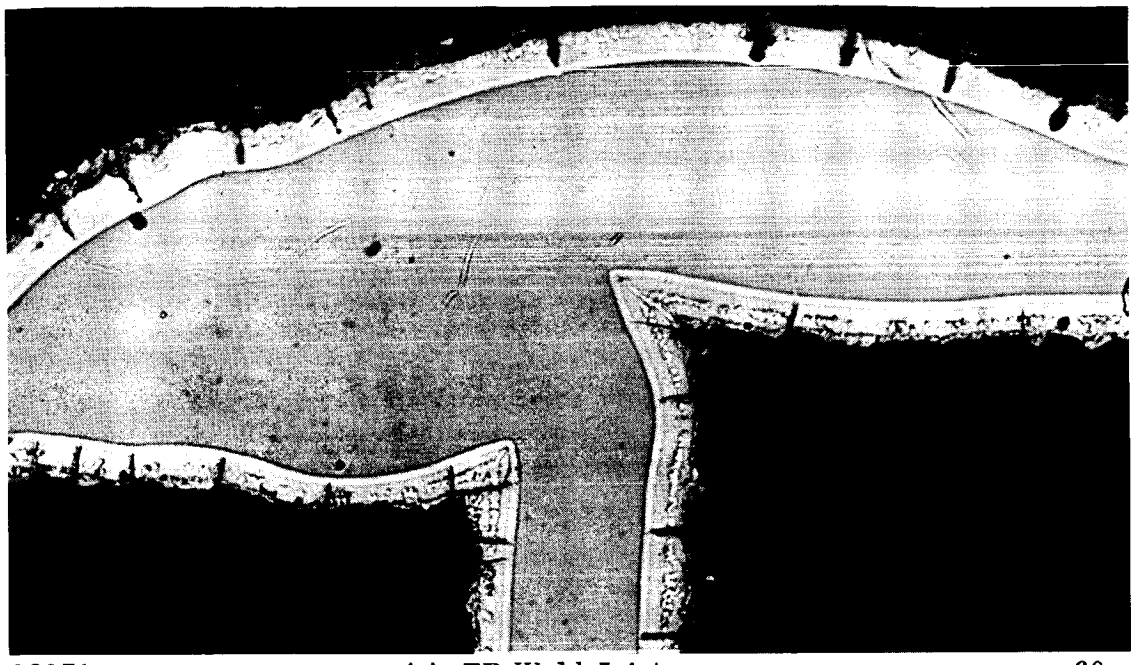

B3271 (a) EB Weld Joint 60×

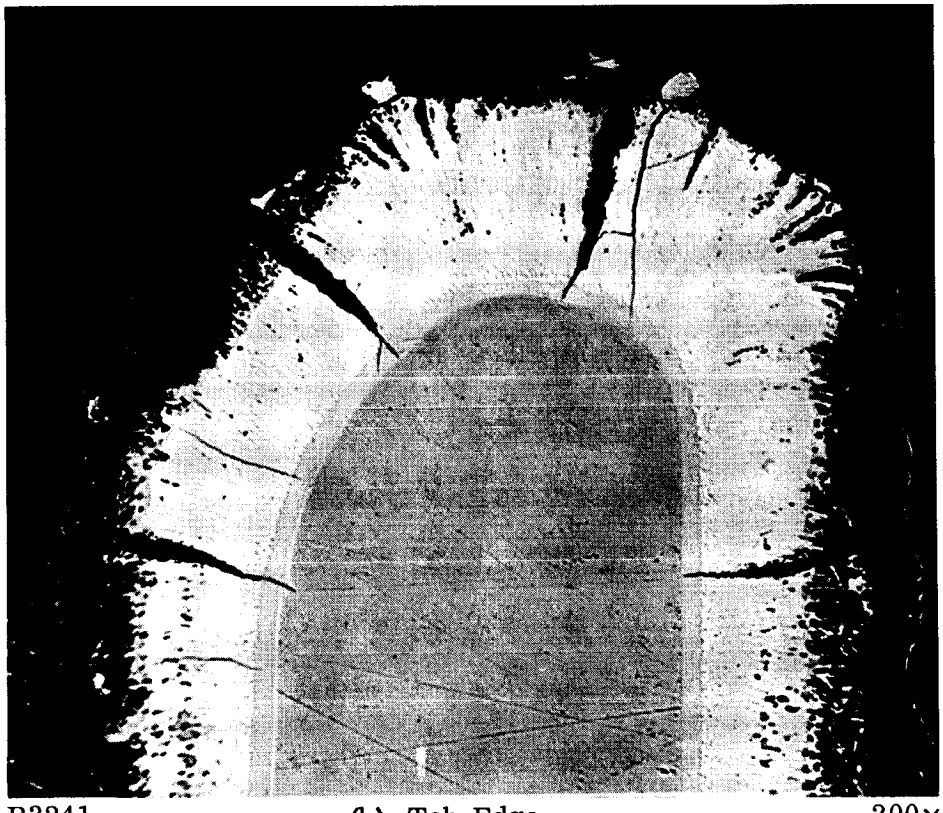

B3241 (b) Tab Edge 200×

Figure 81 MTS-Coated Panel After 112 Simulated Reentries, 2400° F (1584° K), 0.1 Torr (0.13 hN/m^2) Cycle, Not Etched.

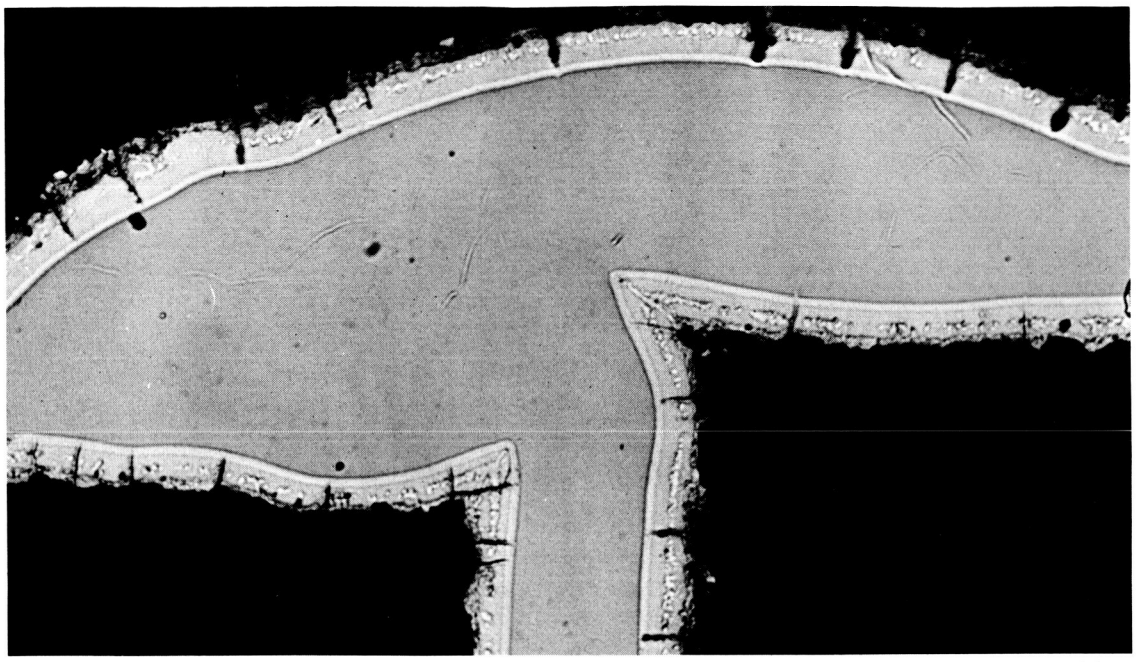

B3271 (a) EB Weld Joint 60×

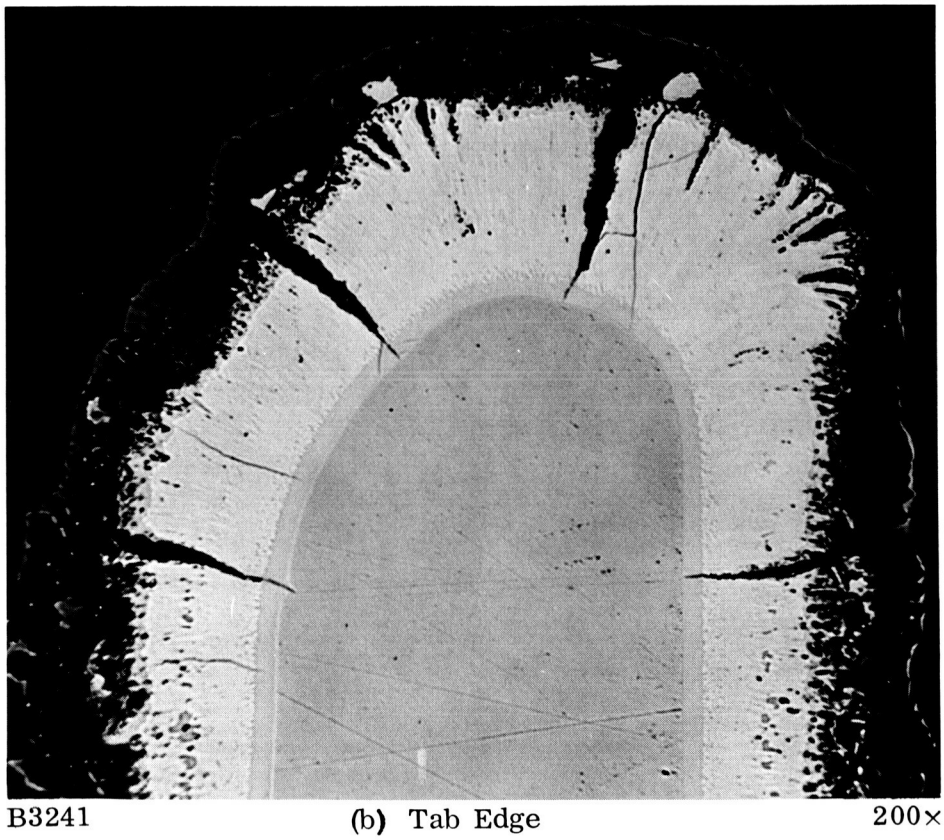

B3241 (b) Tab Edge 200×

Figure 81 MTS-Coated Panel After 112 Simulated Reentries, 2400° F (1584° K), 0.1 Torr (0.13 hN/m^2) Cycle, Not Etched.

B3215 Side 1.6×

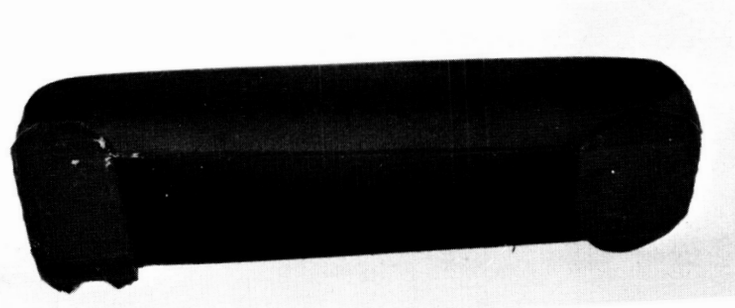

B3214 Bottom 1.6×

(a) Deformation Caused by Nonparallel Alignment of Panel Supports

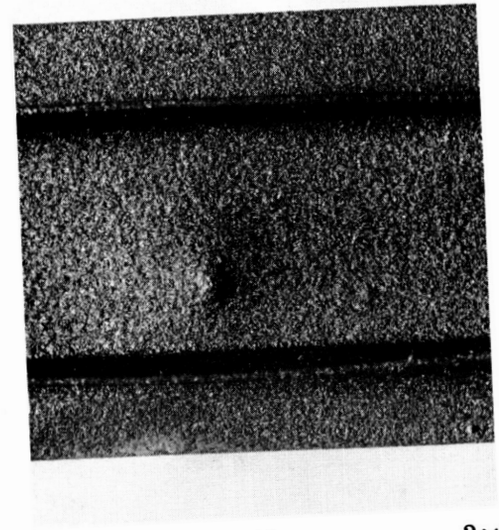

B3218 Bottom 3×

(b) Dimple Caused by Load Pin Bearing Directly on Panel

Figure 80 Panel Distortion Resulting From Misaligned Loading Fixture

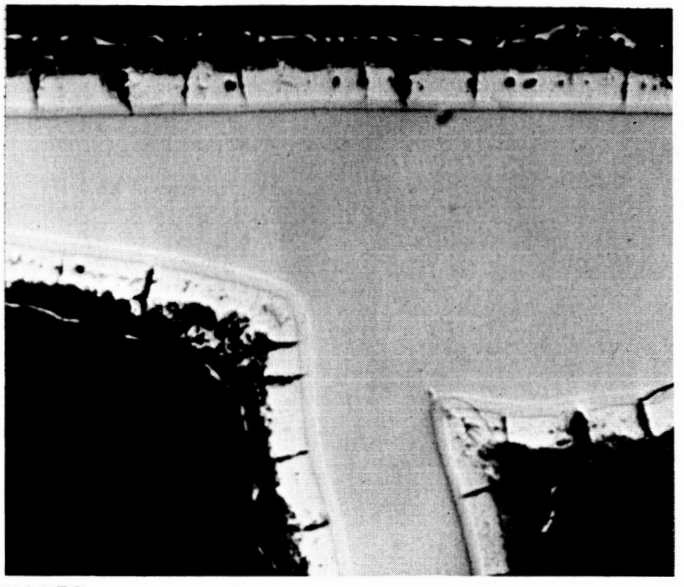

B3252 (a) EB Weld Joint 60×

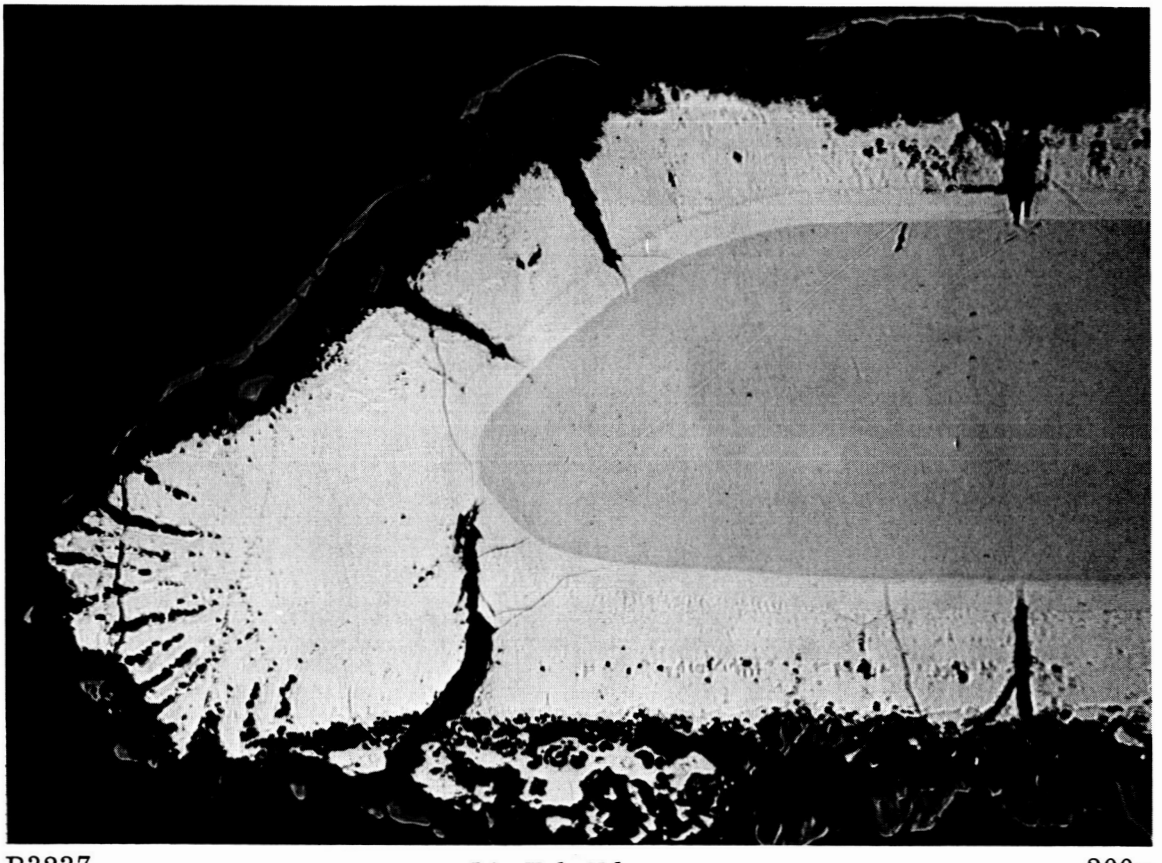

B3237 (b) Tab Edge 200×

Figure 82 MTS-Coated Panel After 100 Simulated Reentries, 2600° F (1700° K), 10 Torr (13.3 hN/m^2) Cycle, Not Etched.

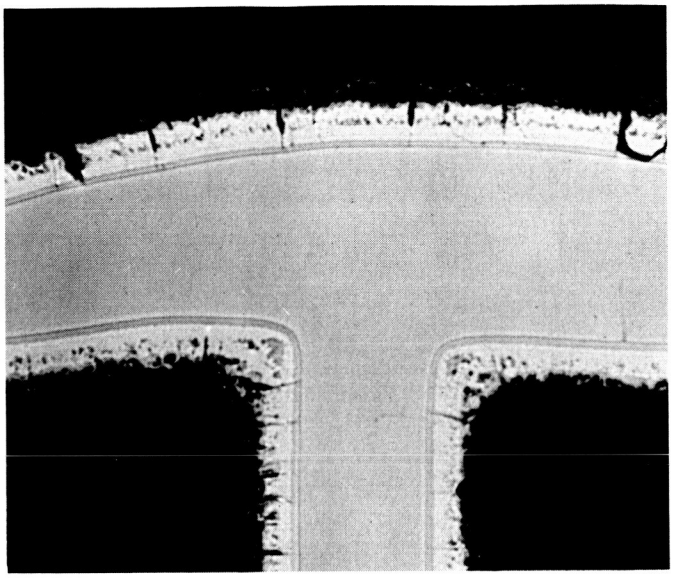

B3248 (a) EB Weld Joint 60×

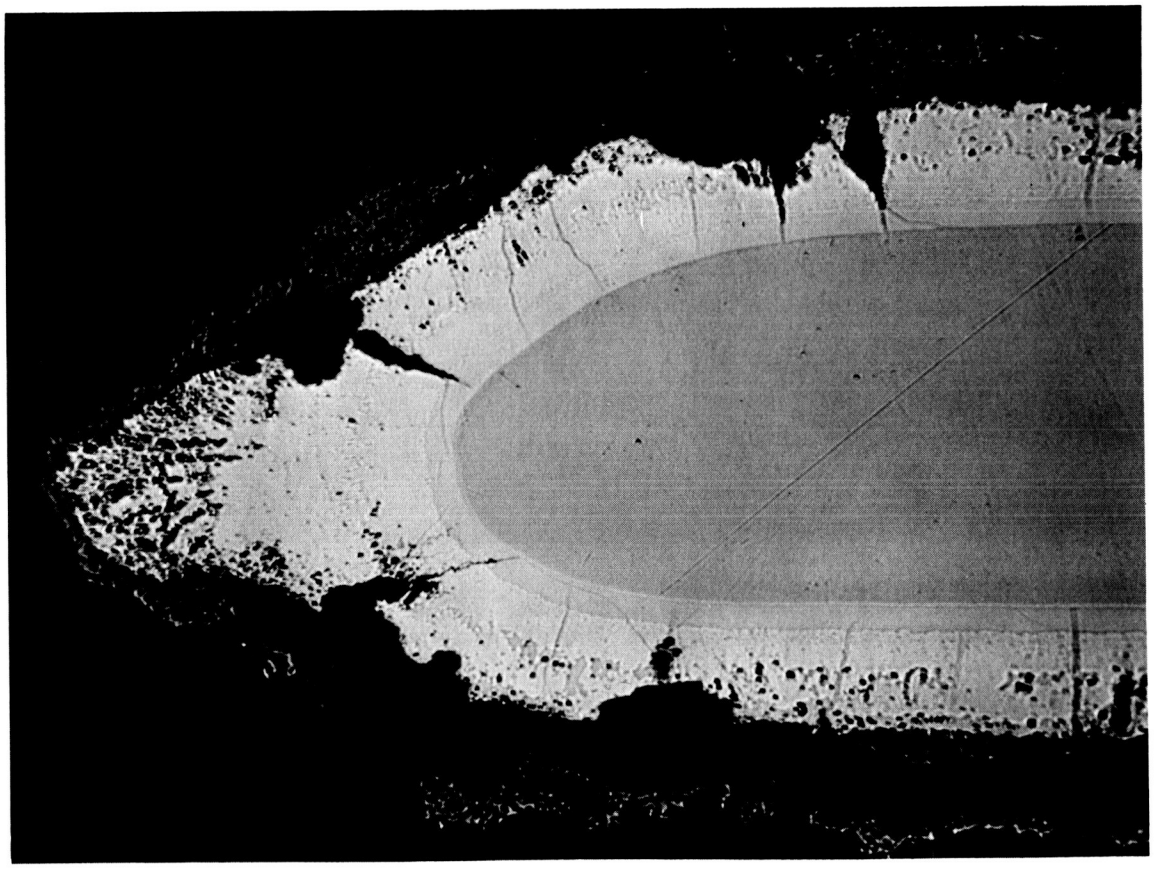

B3236 (b) Tab Edge 200×

Figure 83 CMTS-Coated Panel After 36 Simulated Reentries, 2600° F (1700° K), 0.1 Torr (0.13 hN/m^2) Cycle, Not Etched.

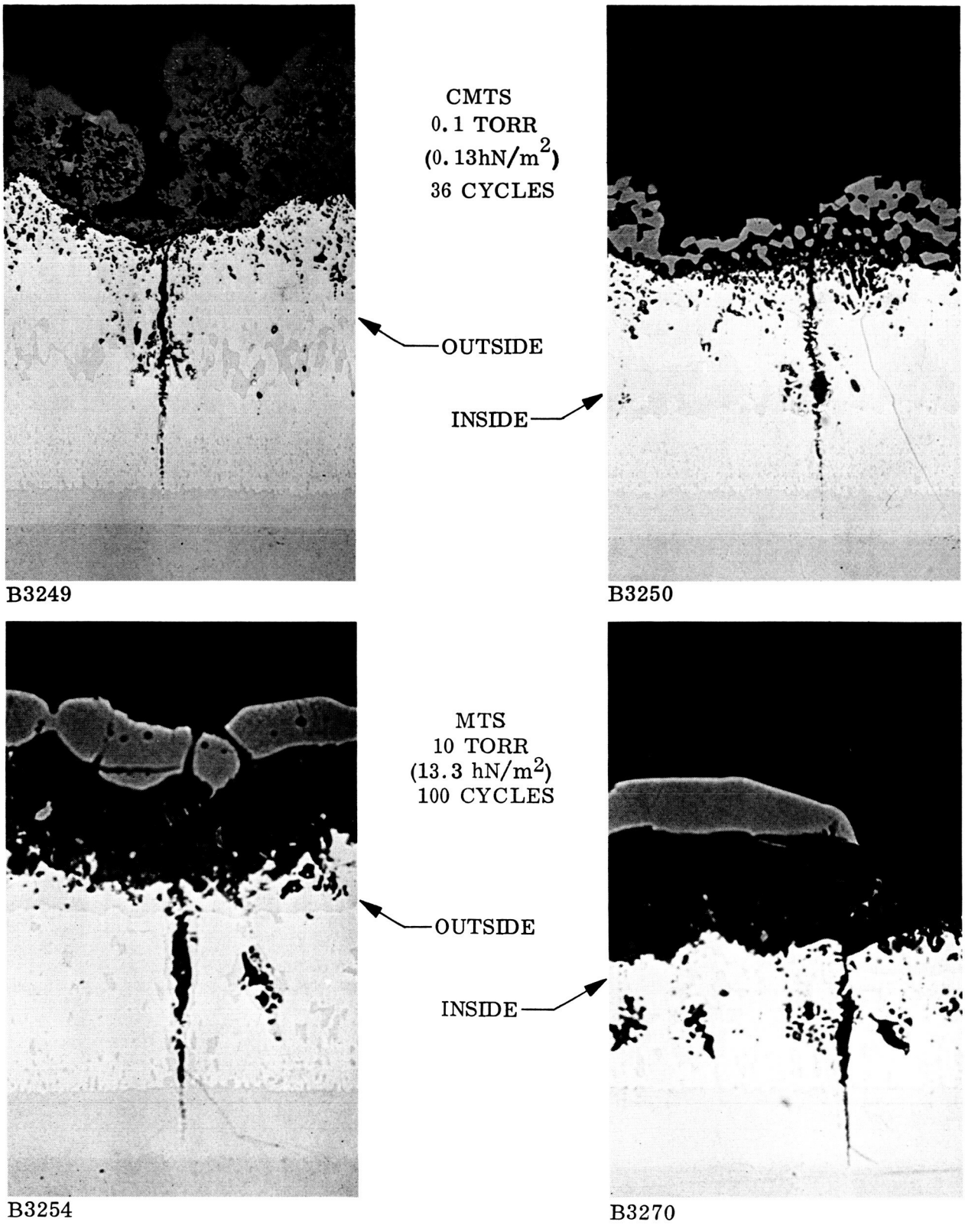

Figure 84 Structure of MTS and CMTS Coatings on Facing Sheet Opposite Tab After Simulated Reentry Testing, 2600°F (1700°K) Cycle, Not Etched, 500×.

similar on the inside and outside of the facing sheet, but there are some differences in the oxide layer structure. These differences may reflect the effect of a somewhat different environment within the channel region between the facing sheet and the tab. At 10 torr (13.33 hN/m^2) the MTS structure is similar on the outside and the inside except that the inside coating is thinner.

These studies show that (1) both of the coatings can be applied effectively to structural components, and (2) coating lifetimes comparable to those with simple shapes can be realized. Furthermore, cyclic stresses in components do not affect coating performance. In addition, edges should be finished before fabrication to ensure adequate edge preparation.

CONCLUSIONS

(1) Two fused slurry silicide coatings for tantalum alloys were developed that have excellent potential for use in atmospheric reentry thermal protection systems at temperatures up to 2800° F (1811° K.) The coatings were consistently effective for more than 100 one-hour cycles (37 min at maximum temperature) at 2600° F (1700° K), 1.0 and 10 torr (1.33 and 13.33 hN/m^2). These coatings are 2.5Mn-33Ti-64.5Si, designated the MTS coating, and 2.5Co-2.5Mn-32Ti-63Si, designated the CMTS coating.

(2) Thorough characterization of isothermal and cyclic temperature lifetimes – as well as substrate/coating composite mechanical properties, and emittance as influenced by environmental exposure – revealed that the MTS coating is the more reliable and effective of the two. At 2600° F (1700° K), 1.0 torr (1.33 hN/m^2), the lifetime of 13 out of 13 MTS-coated Ta-10W test specimens exceeded 400 cycles. Increased temperature or decreased pressure resulted in more limited lifetimes. The coating has a high stable emittance of 0.85 – 0.95 at 2600° to 2800° F (1700° to 1811° K) under all conditions of exposure.

(3) The MTS coating provides the substrate with absolute protection from oxygen contamination embrittlement as measured by room-temperature tensile elongation and bend ductile to brittle transition temperature up to the time of the first appearance of substrate oxide on the surface of the coating at wearout sites. The significant aspect of behavior permits visual inspection for worn-out parts, since good mechanical properties are maintained until visible signs of coating wearout occur.

(4) The initial wearout of the MTS coating occurs predominantly at the edges of thin-gage coated sheet during cyclic exposure to air at high temperature and low pressure. This is the result of a geometric constraint in coated thin sheet and is not indicative of any discontinuities or nonuniformity in the MTS coating at edges. This coating provides complete, uniform coverage of edges with a thickness equal to or greater than that on flat surfaces without the need for special edge treatments (i.e., overspraying or striping) during application of the coating. The MTS coating provides the best edge protection and is more tolerant of inadequate edge preparation than any of the other coatings evaluated in this program.

(5) The MTS composition can be applied conveniently as a uniform coating, in a single-step process, to complex structural components fabricated from thin-gage sheet metal. This coating exhibits the same reliable performance on structural components under cyclic temperature and stress during simulated reentry environmental exposure as it does in cyclic oxidation tests with simple specimens.

(6) Conventional fusion coating equipment and procedures can be used in the application of the MTS and CMTS coatings. Limited process development work will be required for scale-up to full-size structural components. Since manganese has a high vapor pressure, the coating must be fused in an inert atmosphere at a pressure of about 600 torr (800 hN/m^2) to ensure a controlled, reproducible composition.

(7) The bend ductile-to-brittle transition behavior, tensile strength at room and elevated temperatures, and creep resistance of Ta-10W with the MTS coating are equal to or better than the properties of uncoated sheet. Tensile elongation is half that of uncoated sheet but is more than adequate for reliable structural applications. The high mechanical properties of the coated sheet are retained during cyclic exposure to air at high temperature and low pressure.

(8) Silicide coatings on Ta-10W wear out by silicon depletion, as a result of the selective oxidation of silicon, to form protective silica films and SiO vapor. Interdiffusion with the substrate is not a life-controlling factor.

(9) The cyclic lifetime of silicide-coated Ta-10W is controlled by oxidation and vaporization reactions at the surface or along coating fissures. Thick, dense, uniform films of silica must be formed on the surface by selective oxidation of silicon in the coating during the early stages of environmental exposure to provide the maximum resistance to cyclic oxidation.

(10) In this program, titanium, cobalt, and manganese were found to be the most effective additions to silicide coatings for controlling the properties of natural oxide films on the surface. These elements regulate the amount, stability, and plasticity of the protective oxides formed. They are readily oxidized to form thick, dense, and uniform layers of silica at 2000° to 2800° F (1366° to 1811° K) in air at 1 to 10 torr (1.33 to 13.33 hN/m^2) pressure. The oxides have remarkable stability in air at low pressures as the result of formation of (Ti, Mn)O_2 and (Ti, Co)O_2 over the surface of a silica underlayer. The metal-oxide outer layer also results in a high value of emittance, 0.85 to 0.95, in this temperature and pressure range.

(11) Coating compositions containing 2.5 to 15 percent manganese, 29 to 41 percent titanium, and 53 to 63 percent silicon have the most promise for effective and reliable oxidation protection of Ta-10W during cyclic exposure to air at low pressure. The two compositions that provide the best protection are 8Mn-31Ti-61Si and 2.5Mn-33Ti-64.5Si. Both coatings consistently protect the substrate for over 100 cycles of exposure at 2600° F (1700° K) in air at 1 to 10 torr (1.33 – 13.33 hN/m^2) pressure. The 2.5Mn-33Ti-64.5Si coating has a broader temperature range for service and is considered to have the greater potential. The addition of 2.5 percent cobalt to this composition for additional stabilization of the oxide films did not improve its overall performance.

(12) Silicide-base coatings have significant strength in tension at room and elevated temperatures and appear to be stronger than the substrate at 1400° to 2600° F (1033° – 1811° K). They contribute materially to the high-temperature strength and creep resistance of coated thin-gage sheet. Present methods of calculating strength parameters on the basis of original substrate thickness before coating are conservative. However, these give the best estimate of the strength of the composite substrate/coating system, particularly at elevated temperatures, in the absence of more precise determinations of actual strength values for the coating material.

RECOMMENDATIONS

The 2.5Mn-33Ti-64.5Si (MTS) coating has many unique and desirable features which indicate that it could be developed to serve as a good general-purpose oxidation-resistant coating for tantalum alloys. It is recommended that the oxidation behavior and overall performance of this coating be evaluated on Ta-10W and T-222 alloy over a broad range of environmental exposure conditions. The use of the coating in other applications, such as rocket propulsion and flight-control systems, and gas turbine engine components, should be given serious consideration.

REFERENCES

1. C. Krier, Coatings for the Protection of Refractory Metals From Oxidation, DMIC Report 162, Nov 1961

2. W. Klopp et al., Development of Protective Coatings for Ta Base Alloys, ASD-TR-62-676, Mar 1962

3. A. Stetson, H. Cook, and V. Moore, Development of Protective Coatings for Tantalum Base Alloys, AFML TR-65-205, Part I, Jun 1965; ML TDR-64-294, Task II, Jan 1965; ML TDR-64-294, Part II, Nov 1965

4. O. Stansfield, R. Wimber, and A. Stetson, Development of Coatings for Tantalum Alloy Nozzle Vanes, NASA CR-54529, Jul 1967

5. H. Shoemaker and A. Stetson, Silicide Coatings for Tantalum and Columbium Alloys, NASA CR-72519, Aug 1969

6. T. Roach and E. Gowen, Jr., Structural Fasteners for Extreme Elevated Temperatures, AFFDL-TR-66-107, Sep 1966

7. S. J. Klach and M. H. Ortner, Development of Protective Coatings for Tantalum T-222 Alloys, NASA CR 54578, Dec 1966

8. S. J. Klach and M. H. Ortner, Optimization and Evaluation of Electrophoretic Protective Coatings for Tantalum T-222 Alloys, NASA CR 72358, Dec 1967

9. D. D. Lawthers and L. Sama, High Temperature Oxidation Resistant Coatings for Tantalum-Base Alloys, ASD-TR-61-233, 1961

10. L. Sama, High Temperature Oxidation Resistant Coatings for Tantalum-Base Alloys, ASD-TDR-63-160, 1963

11. S. Priceman and L. Sama, Development of Slurry Coatings for Tantalum, Columbium, and Molybdenum Alloys, AFML TR-65-204, 1965

12. S. Priceman and L. Sama, Development of Fused Slurry Silicide Coatings for the Elevated-Temperature Oxidation Protection of Columbium and Tantalum Alloys, AFML-TR-68-210, Dec 1968

13. D. Lawthers and L. Sama, Development of Coatings for Protection of High-Strength Tantalum Alloys in Severe High-Temperature Environments, AFML TR-67-374, Nov 1967

14. V. Hill and J. Rausch, Protective Coatings for Tantalum-Base Alloys, AFML-TR-64-354, Part III, Sep 1966

15. Committee on Coatings, National Materials Advisory Board, High-Temperature Oxidation-Resistant Coatings, Washington, D.C., 1970 (Library of Congress No. 78-606278)

16. J. B. Berkowitz-Mattuck and R. R. Dils, "High-Temperature Oxidation. II. Molybdenum Silicides," J. Electrochem. Soc., Vol. 112, 1965, p. 583

17. R. Bartlett et al., Investigation of Mechanisms for Oxidation Protection and Failure of Intermetallic Coatings for Refractory Metals, ASD-TDR-63-753, Part I, 1963; Part II, 1964; Part III, 1965

18. H. W. Lavendel et al., Investigation of Modified Silicide Coatings for Refractory Metal Alloys With Improved Low-Pressure Oxidation Behavior, AFML TR-65-344, Aug 1965

19. R. P. Elliott, Constitution of Binary Alloys, 1st Supplement, McGraw-Hill, New York, 1965

20. R. Perkins, "Coatings for Refractory Metals: Environmental and Reliability Problems," Materials Science and Technology for Advanced Applications, Vol. II, Trans. ASM Golden Gate Metals Conference, 1964

21. R. Perkins, "Status of Coated Refractory Metals," J. Spacecraft & Rockets, Vol. 2, No. 4, 1965, p 520 – 523

22. Bureau of Mines Bulletin No. 605, 1963

23. R. A. Perkins and C. M. Packer, Coatings for Refractory Metals in Aerospace Environment, AFML-TR-65-351, 1965

24. R. T. Wimber and A. R. Stetson, Development of Coatings for Ta Alloy Nozzle Vanes, NASA-CR-54529, Jul 1967

25. R. A. Jeffreys and J. D. Gadd, Development and Evaluation of High-Temperature Protective Coatings for Columbium Alloys, ASD-TR-61-66, Parts I and II, May 1961

26. H. A. Kmieciak and J. D. Gadd, Development and Characterization of High-Temperature Coatings for Tantalum Alloys, AFML-TR-69-195, Dec 1969

27. J. J. English, Binary and Ternary Phase Diagrams of Columbium, Molybdenum, Tantalum, and Tungsten, DMIC Report 183, Defense Metals Information Center, Battelle Memorial Institute, Columbus, Ohio, 7 February 1963

28. W. Weibull, "A Statistical Theory of the Strength of Material," Ing. Vetenskaps Akad. Handl., Vol. 151, Stockholm, 1939, p. 15

29. J. C. Wurst et al., The Evaluation of High-Temperature Materials, MLDTR-64-62, 1964 (AD 601638)

30. J. D. Gadd, Advancement of Protective Coating Systems for Columbium and Tantalum Alloys, AFML-TR-203, 1965

31. J. C. Wurst, Weibull Analyses of the Oxidation Resistance of Coated Refractory Metals, M. S. Thesis, University of Dayton, 1968

32. R. A. Long, Fabrication and Properties of Hot-Pressed $MoSi_2$, NACA Report RME50F22, 1950

33. R. A. Long, Metals Progress, Vol. 68, 1955, p. 123

Appendix A

PROCESS SPECIFICATION FOR APPLICATION OF MTS AND CMTS COATINGS TO TANTALUM ALLOYS

1. SCOPE

This specification covers the application of the MTS (2.5Mn-33Ti-64.5Si) and the CMTS (2.5Co-25Mn-32Ti-63Si) fused slurry silicide coatings to tantalum alloys.

2. MATERIALS

2.1 Silicon metal powder, -325 mesh, 99.8% pure

2.2 Titanium hydride powder, -325 mesh, 98% pure

2.3 Manganese metal powder, -325 mesh, 99.9% pure

2.4 Cobalt metal powder, -325 mesh, 99.9% pure

2.5 Raffi and Swanson L-18 Lacquer

2.6 Baker MPA 60 Mineral Spirits

3. COATING COMPOSITIONS

3.1 MTS Coating

Silicon – 64.5 wt %
Titanium – 33 wt %
Manganese – 2.5 wt %

3.2 CMTS Coating

Silicon – 63 wt %
Titanium – 30 wt %
Cobalt – 2.5 wt %
Manganese – 2.5 wt %

4. SLURRY PREPARATION

4.1 To prepare a slurry containing 100 g of metallic powders, pour the following quantities of powder into the vessel of a planetary ball mill (or equivalent blender):

MTS	CMTS
Silicon – 64.5 g	Silicon – 63 g
Titanium Hydride – 34.3 g	Titanium Hydride – 33.3 g
Manganese – 2.5 g	Manganese – 2.5 g
	Cobalt – 2.5 g

4.2 Add 60 g of L-18 lacquer if the slurry is to be sprayed; add 50 g if the slurry is to be applied by dipping.

4.3 Add 2 g of MPA 60.

4.4 Blend slurry for 1 hr in planetary ball mill or equivalent blender.

4.5 Measure slurry viscosity at 70° to 75°F (294° to 297°K).

4.6 Required Slurry Viscosity

4.6.1 For spraying: 900 – 1100 cps (0.9 – 1.1 Nsec/m^2)

4.6.2 For dipping: 3500 – 5000 cps (3.5 – 5 Nsec/m^2)

5. SUBSTRATE PREPARATION

5.1 Prepare all corners and edges to eliminate sharp corners and to remove flaws such as burrs caused by machining.

5.2 Finish the surface using a vibratory finisher (or equivalent). Finishing time required: 8 hr.

5.3 Degrease part.

5.4 Etch in 2 parts HNO_3, 2 parts H_2SO_4, 1 part HF for 1–2 min at 75°F (297°K).

5.5 Weigh part.

6. SLURRY APPLICATION

6.1 Spraying

6.1.1 Using compressed gas spray gun, spray slurry uniformly on all surfaces. Make 4 to 6 passes per side.

6.1.2 Weigh part and calculate coating weight per unit area.

6.1.3 Make a sufficient number of additional passes to increase coating thickness such that coating weight is 30 ± 3 mg/cm^2 [for a coating thickness of 0.003 in. (0.008 cm)].

6.1.4 Air-dry.

6.2 Dipping

6.2.1 Immerse part in slurry and withdraw at a rate of 5 in./min (127 cm/min).

6.2.2 Weigh part and calculate coating weight per unit area.

6.2.3 If coating weight is not 30 ± 3 mg/cm^2, remove slurry, using acetone, and recoat, adjusting withdrawal rate to apply appropriate coating thickness.

6.2.4 Air-dry.

7. NDT INSPECTION

7.1 Measure coating uniformity using eddy current instrument which is calibrated with coated standards.

7.2 If coating is not uniform, remove slurry and recoat.

8. FUSION/DIFFUSION TREATMENT

8.1 Heat to 900° to 1000°F (773° to 811°K) in vacuum [$<10^{-4}$ torr (1.3×10^{-4} hN/m^2)] to remove organic volatiles and to dissociate TiH_2.

8.2 Introduce dry helium at a pressure of 2/3 to 3/4 atm.

8.3 Heat to 2552° ± 10°F (1673° ± 6°K) in 5 min.

8.4 Hold at temperature for 1 hr.

8.5 Furnace-cool.

9. INSPECTION

9.1 Inspect part for defects.

9.2 Check for coating uniformity using eddy current instruments.

9.3 Weight part. Coating weight shall be 28 ± 3 mg/cm^2.

Distribution List for NASA CR-120877

Contract NAS3-14316

(The number in parentheses shows how many copies if more than one are to be sent to an address.)

Mr. G. C. Deutsch/RW
NASA Headquarters
600 Independence Avenue
Washington, D.C. 20546

Mr. J. Maltz/RWM
NASA Headquarters
600 Independence Avenue
Washington, D.C. 20546

Dr. A. O. Tishler/RP
NASA Headquarters
600 Independence Avenue
Washington, D.C. 20546

Mr. N. Peil (MN)
NASA Headquarters
600 Independence Avenue
Washington, D.C. 20546

Mr. D. Gilstad (RV-2)
NASA Headquarters
600 Independence Avenue
Washington, D.C. 20546

NASA Representative (2)
Scientific and Technical
Information Facility
Box 33
College Park, MD 20740

Library (2)
MS 60-3
NASA Lewis Research Ctr
21000 Brookpark Road
Cleveland, OH 44135

Mr. J. Gangler/RWM
NASA Headquarters
600 Independence Avenue
Washington, D.C. 20546

Mr. F. J. Demeritte/RV-1
NASA Headquarters
600 Independence Avenue
Washington, D.C. 20546

Mr. M. Rosch/RV-2
NASA Headquarters
600 Independence Avenue
Washington, D.C. 20546

Mr. J. Malament (MTG)
NASA Headquarters
600 Independence Avenue
Washington, D.C. 20546

National Technical (10)
Information Service
Springfield, VA 22151

Contracts Section B
MS 500-313
NASA Lewis Research Ctr
21000 Brookpark Road
Cleveland, OH 44135

Patent Counsel
MS 500-311
NASA Lewis Research Ctr
21000 Brookpark Road
Cleveland, OH 44135

Report Control Office
MS 5-5
NASA Lewis Research Ctr
21000 Brookpark Road
Cleveland, OH 44135

Mr. G. M. Ault
MS 3-13
NASA Lewis Research Ctr
21000 Brookpark Road
Cleveland, OH 44135

Mr. J. P. Merutka (BAL)
MS 49-3
NASA Lewis Research Ctr
21000 Brookpark Road
Cleveland, OH 44135

Mr. J. C. Freche
MS 49-1
NASA Lewis Research Ctr
21000 Brookpark Road
Cleveland, OH 44135

Mr. W. D. Klopp
MS 105-1
NASA Lewis Research Ctr
21000 Brookpark Road
Cleveland, OH 44135

Mr. W. Reihl
S&E-ASTN-MX Bldg. 4612
Marshall Space Flight Ctr
Huntsville, AL 35812

Mr. B. Stein MS 188-A
NASA
Langley Research Ctr
Langley Field, VA 23365

Mr. C. E. Cataldo S&EASTN-M
NASA
Marshall Space Flight Ctr
Huntsville, AL 35812

Technology Utilization
MS 3-19
NASA Lewis Research Ctr
21000 Brookpark Road
Cleveland, OH 44135

Mr. S. S. Manson
MS 49-1
NASA Lewis Research Ctr
21000 Brookpark Road
Cleveland, OH 44135

Mr. R. W. Hall
MS 105-1
NASA Lewis Research Ctr
21000 Brookpark Road
Cleveland, OH 44135

Mr. S. J. Grisaffe
MS 49-3
NASA Lewis Research Ctr
21000 Brookpark Road
Cleveland, OH 44135

Mr. N. T. Saunders
MS 105-1
NASA Lewis Research Ctr
21000 Brookpark Road
Cleveland, OH 44135

Dr. J. Buckley MS206
NASA
Langley Research Ctr
Langley Field, VA 23365

Dr. R. A. Anderson MS188
NASA
Langley Research Center
Langley Field, VA 23365

Library-22-3.Reports
NASA
Ames Research Ctr
Moffett Field, CA 94035

Library
NASA
Goddard Space Flight Ctr
Greenbelt, MD 20771

Library/Acquisitions
Jet Propulsion Lab
4800 Oak Grove Drive
Pasadena, CA 91102

Technical Library, Code JM6
NASA
Johnson Spacecraft Ctr
Houston, TX 77058

Mr. E. Bartlett
Battelle Memorial Inst.
505 King Street
Columbus, OH 43201

Mr. N. Geyer
AFML/LLP
Headquarters
Wright Patterson AFB, OH 45433

Mr. Wendell Emde
Space Division
North American Rockwell 1
12214 Lakewood Blvd
Downey, CA 90241

Mr. J. R. Williamson
AFM/LLP
Wright-Patterson AFB, OH 45433

Mr. R. A. Nau
General Dynamics Corp.
P.O. Box 1128
San Diego, CA 92112

Library
NASA Flight Research Ctr
P.O. Box 273
Edwards, CA 93523

Library M.S.185
NASA
Langley Research Ctr
Langley Field, VA 23365

Library
NASA
Marshall Space Flight Ctr
Huntsville, AL 35812

Mr. R. Perkins
Lockheed Palo Alto R. Lab.
3251 Hanover Street
Palo Alto, CA 94304

Mr. E. F. Styer MS/8K-93
The Boeing Company
P.O. Box 3999
Seattle, WA 98124

Mr. B. Black M7 641-30
Convair Aerospace Div.
General Dynamics Corp.
P.O. Box 1128
San Diego, CA 92112

Mr. S. Musikant, U1237
General Electric Co.
P.O. Box 8555
Philadelphia, PA 19101

Dr. J. Colwell
Aerospace Corporation
P.O. Box 95085
Los Angeles, CA 90045

Mr. L. Mead
Grumman Aerospace Corp.
Plant 25
Bethpage, NY 11714

Mr. C. S. Deneen
Martin Marietta Corp.
815 Connecticut Ave. NW
Washington, D.C. 20006

Mr. H. K. Larson, MS 234-1
NASA
Ames Research Ctr
Moffett Field, CA 94035

Mr. W. H. Goesch
AFDL, Code FDTS
Wright Patterson AFB, OH 45433

Mr. T. P. Brooks (E-231)
McDonnell Douglas Corp.
P.O. Box 516
St. Louis, MO 63166

Mr. L. Sama
HITEM Co.
A. Dewiant Company
70 Cantiague Road
Hicksville, NY 11801

Mr. S. J. Gerardi, Coat. Engr.
VAC-HYD Processing Corp.
928 Engracia Avenue
Torrance, CA 90501

Mr. V. Hackworth
Materials Res. Dept. C-48
Bell Aerospace Co.
P.O. Box One
Buffalo, NY 14240

Mr. L. A. Harris
Space Division
N. American Rockwell
12214 Lakewood Blvd.
Downey, CA 90241

Mr. L. G. St. Leger, ES-8
Bldg. 13, Room 116
NASA
Johnson Spacecraft Ctr
Houston, TX 77058

Mr. G. M. Ecord
SMD-Material Tech.
NASA
Johnson Spacecraft Ctr
Houston, TX 77058

Mr. C. E. Tharratt
Crysler-Space Division
P.O. Box 29200
New Orleans, LA 70129

Mr. B. Fitzgerald
McDonnell Douglas, East
McDonnell Douglas Corp.
St. Louis, MO 63166

Dr. C. C. Ong
Bellcomm Inc.
955 L-Enfant Plaza
North, S.W.
Washington, D.C. 20024

Mr. G. G. Schurr
Mail Code 041-AC25
North American Rockwell
12214 Lakewood Boulevard
Downey, CA 90241

Mr. K. H. Holko
ROHR Industries
Dept. 405 MZ29T
P.O. Box 878
Chula Vista, CA 92011

Mr. B. N. Thomson
Research Liaison Engr.
United Aircraft Rea. Lab.
East Hartford, CO 06108

Mr. C. Panzera
Technical Products Div.
Brunswick Corporation
45 Woodmont Road
Milford, CO 06460

Mr. R. Penty
Fiber Materials Inc.
Bitterford Ind. Park
Bitterford, MA 04005

Mr. A. Stetson
Solar Division
Int. Harvester Co.
2200 Pacific Highway
San Diego, CA 92112